

Instytut Chemii i Techniki Jądrowej

Szkoła Doktorska ICHTJ-NCBJ

Rozprawa Doktorska:

**Radiacyjna degradacja wybranych nowo odkrytych
zanieczyszczeń chloroorganicznych w roztworze wodnym
pod wpływem wiązki przyspieszonych elektronów**

Mgr Stephen Ochieng Kabasa

Promotor:

dr hab. Yongxia Sun, Prof. ICHTJ

Praca przedłożona Radzie Naukowej Instytutu Chemii i Techniki Jądrowej w celu uzyskania
stopnia Doktora Nauk Chemicznych



Warszawa 2024

Institute of Nuclear Chemistry and Technology

Szkoła Doktorska ICHTJ-NCBJ

Ph.D. Thesis:

**Radiation-Induced Degradation of Selected Chlorinated
Emerging Organic Pollutants in Aqueous Solution Under
Electron Beam Irradiation**

M.Sc. Stephen Ochieng Kabasa

Supervisor:

D.Sc. Yongxia Sun, Professor ICHTJ

Thesis submitted to the scientific committee of the Institute of Nuclear Chemistry and
Technology for the award of Doctoral degree in natural sciences in the discipline of chemical
sciences



Warsaw 2024

“Where wast thou when I laid the foundations of the earth? declare, if thou hast understanding.

Who hath laid the measures thereof, if thou knowest? or who hath stretched the line upon it?

Whereupon are the foundations thereof fastened? or who laid the corner stone thereof;

When the morning stars sang together, and all the sons of God shouted for joy?

Or who shut up the sea with doors, when it brake forth, as if it had issued out of the womb?

When I made the cloud the garment thereof, and thick darkness a swaddling band for it,

And brake up for it my decreed place, and set bars and doors,

And said, hitherto shalt thou come, but no further: and here shall thy proud waves be stayed?”

Job 38:4-11

DEDICATION

I wish to dedicate this work to my late father who earnestly believed in the value of education and endeavored to improve his community. Regrettably, he did not live to see this achievement but I wish to commemorate his hard work, resilience, and commitment to bettering the lives of his family and society. This work testifies that “where there is a will, there is a way” and the pursuit of knowledge and understanding is commendable

ACKNOWLEDGMENTS

First and foremost, I express my gratitude and appreciation to my supervisor Professor Dr. Yongxia Sun (ICH TJ) for availing the opportunity, resources, and guidance to pursue my PhD dissertation. Furthermore, I extend my gratitude for her continuous support, persistent, and valuable input during my PhD studies.

I thank my colleagues and staff at the Institute of Nuclear Chemistry and Technology; M.Sc. Sylwester Bulka, Mr. Dariusz Pujdak, and M.Sc. Marcin Sudlitz for their technical support in the electron beam accelerator experiments. Additionally, I extend my utmost gratitude to Dr. Ewalina Chajduk for availing resources in her laboratory to facilitate the experimental portions of this work. I wish to extend my thanks to M.Sc. Yingying Dong for her input on the production and application of catalysts during her Erasmus+ exchange program as well as the ECOSAR evaluation.

I acknowledge the financial support offered through the Institute of Nuclear Chemistry and Technology and IAEA CRP F23034 (Contract no. 23165) to facilitate the research and participation in international conferences invaluable in the dissemination of this work. Similarly, I appreciate the Erasmus+ program that supported my mobility with the University of Nairobi, Kenya.

Last but not least I thank my family and friends for their unwavering belief and support as I pursue my dreams. Their patience and encouragement have sustained me through this period.

ENGLISH ABSTRACT

Emerging organic pollutants pose a substantial risk to the environment and living things owing to their high production volumes, consumption, recalcitrance, toxicity, mutagenic, and carcinogenic properties, and limited knowledge of their fate in the environment. These pollutants are infrequently regulated in wastewater and water treatment, especially in domestic wastewater discharge, and therefore are released into the aquatic ecosystem. Conventional water and wastewater treatment are inadequate in the removal of these pollutants leading to their detection in treated water. Additionally, water and wastewater treatment that utilize phase transfer such as adsorption and filtration lead to secondary pollution from adsorbent and filtration byproducts that necessitate costly post-treatment of adsorbents. Similarly, other processes utilizing chemical additives are of concern due to the quantities of chemicals used and their effects on the environment. Radiation technologies are versatile in the removal of many pollutants in the aqueous phase without additional chemical additives or post-treatment processing. Additionally, radiation technologies are proposed as promising alternatives for pre and post-treatment of polluted water.

In this study, the radiation-induced degradation of chloroquine (CQ) and hydroxychloroquine (HCQ) was investigated as model halogenated emerging organic pollutants. CQ and HCQ are quinoline derivatives prominently used as antimalarials with further applications in rheumatoid arthritis treatment, cancer therapy, inflammatory arthritis, systemic lupus erythematosus (quinacrine), rheumatoid arthritis, dermatological, immunological, infectious diseases, and most recently proposed for treatment of SARS-Covid 19. However, their use is associated with retinal retinopathy, cardiac arrhythmia, and as well toxicity. The therapeutic administration of these pharmaceuticals leads to the release of CQ, HCQ, and their metabolites into wastewater, wastewater treatment plants, and eventually the aquatic systems. Varying concentrations of CQ and HCQ were irradiated under an electron beam at absorbed doses ranging from 0.5 kGy to 7

kGy. The initial concentrations of CQ and HCQ decreased with increasing absorbed dose and the removal efficiency decreased with increasing concentration of CQ and HCQ synonymous with pseudo-first-order degradation kinetics. The degradation of CQ and HCQ was further studied under conditions that promote the selective generation of $\bullet\text{OH}$, e_{aq}^- , and $\text{H}\bullet$, in addition to aerated and Ar purged solutions. The degradation of CQ and HCQ was higher under $\bullet\text{OH}$ compared to $\text{H}\bullet$ and e_{aq}^- . The lower removal efficiency for CQ and HCQ under e_{aq}^- was attributed to the limited reactions involving e_{aq}^- compared to $\bullet\text{OH}$. However, the reactions of e_{aq}^- contributed to a greater extent to the degradation of CQ compared to HCQ. This was attributed to the significantly higher reaction rate constants of the e_{aq}^- with CQ. Aerated solutions (DO between 5-10mg/L) had a higher removal efficiency for CQ and HCQ compared to the Ar purged solution (DO<1mg/L). In aerated solutions, the formation of $\text{HO}_2\bullet$ could positively influence the degradation of CQ and HCQ. The initial pH of the solutions was not found to significantly affect the removal efficiency. However, acidic pH between 2 to 4 favored the removal of CQ and HCQ and the removal efficiency decreased with increasing pH

The degradation of CQ and HCQ was further studied in the presence of selected inorganic ions, and humic acid commonly found in natural water as well as in the presence of H_2O_2 and $\text{S}_2\text{O}_8^{2-}$ that promote the production of $\bullet\text{OH}$ and $\text{SO}_4\bullet^-$, respectively. The presence of CO_3^{2-} , HCO_3^- , NO_3^- , Fe^{2+} , humic acid, and H_2O_2 had a deleterious effect on the degradation of CQ and HCQ under EB processing. These components competitively scavenge the $\bullet\text{OH}$ in addition to the e_{aq}^- and reduce the removal efficiency of the target pollutant. Additionally, higher concentrations of Fe^{2+} , and humic acid cause turbidity. The presence of NO_3^- greatly influenced the degradation of CQ compared to HCQ where the CO_3^{2-} influence was more prominent. The NO_3^- scavenges e_{aq}^- which contribute more to the degradation of CQ than HCQ in addition to the scavenging of the $\bullet\text{OH}$ radicals by NO_2^- formed in the reduction of NO_3^- . However, the presence of $\text{S}_2\text{O}_8^{2-}$ increased the removal efficiency of CQ and HCQ with increasing

concentrations of $S_2O_8^{2-}$ and absorbed dose. Under EB irradiation, the $S_2O_8^{2-}$ was converted to the strongly oxidizing $SO_4^{\bullet-}$. Additionally, $\bullet OH$ radicals are formed that further enhance the efficiency. In tert-BuOH/ $SO_4^{\bullet-}$ solutions, the improvement in efficiency was attributed to the $SO_4^{\bullet-}$.

Several physical-chemical properties were utilized to assess the degradation of CQ and HCQ under the EB process. Chloride ions were released with increasing absorbed doses which is consistent with dechlorination of chlorinated organic compounds under EB processing. Additionally, nitrification an important process in the treatment of nitrogen-containing organic compounds was achieved evidenced by the decreasing concentration of total Kjeldahl nitrogen and increasing concentrations of NO_3^- , and NH_4^+ with increasing irradiation dose. The reduced removal efficiency for CQ and HCQ at higher doses was attributed to the formation of NO_3^- that scavenges the e_{aq}^- and $\bullet OH$ by resultant NO_2^- . However, total mineralization of CQ and HCQ was not achieved according to the results of total organic carbon and chemical oxygen demand obtained in this study. However, the degradation of CQ and HCQ led to the production of lower molecular weight organic compounds. The changes in pH from a slightly acidic pH of 5.5 to a pH of 3.5 were attributed to the formation of organic acids. Results showed increasing concentrations of organic acids with increasing absorbed dose during the EB treatment of CQ and HCQ. Similar changes in pH have been reported in the degradation of CQ and HCQ under electro Fenton oxidation which was attributed to the formation of oxalic and oxamic acids. Other studies also allude to the formation of aldehydes and ketones in the degradation of organic compounds.

Fenton-assisted EB process (EB-F) was investigated to improve the removal efficiency of CQ and HCQ. Preliminary Fenton experiments attained a higher removal of CQ and HCQ when the H_2O_2 concentration was five times ($5\times$) the Fe^{2+} and increased with increasing H_2O_2 concentration from 0.1 to 2 mM. However, when the ratio of H_2O_2 was further increased ($10\times$

to 20×) the removal efficiency decreased owing to the scavenging of •OH radicals. Similar reductions in removal efficiency due to scavenging were observed when the proportions of Fe²⁺ were higher (0.5× and 0.2×). Therefore, the molar ratio of H₂O₂:Fe²⁺ significantly influences the Fenton processes. The molar ratios further influenced the Fenton-assisted EB (EB-F) process. The removal efficiency for CQ and HCQ increased with increasing H₂O₂ concentration from 0.1 to 2 mM. However, contrary to the Fenton process, the removal efficiency for CQ and HCQ was high in excess H₂O₂ (20×). This was attributed to sustained reactions of the H₂O₂ with the reconstituted Fe²⁺ during the synergistic Fenton-assisted EB (EB-F) process. The removal efficiency under EB-F was observed to improve by ≈10% at 7 kGy applied irradiation dose with 2mM H₂O₂ and 20 times the Fe²⁺ volume compared to the EB process. However, the improved removal efficiency was higher at lower doses between 0.5 kGy and 2kGy. Additionally, dechlorination and nitrification were higher under the EB-F compared to the EB process. Similar observations were made for the total organic carbon and chemical oxygen demand reduction. Therefore, the EB-F process improves the overall removal efficiency of CQ and HCQ.

Mathematical simulations using CHEMSIMUL software were performed to further investigate the degradation of CQ and HCQ under EB and EB-F processes. Using available information from pulse radiolysis studies of CQ and HCQ in addition to water radiolysis studies the degradation of CQ and HCQ was investigated and compared to the experimental results. The degradation of CQ and HCQ was faster in simulated conditions compared to the experimental conditions. This was attributed to the inability to simulate the effects of the degradation products on the removal efficiency. Complete removal of CQ and HCQ was achieved at less than 2 kGy under simulations. However, similar to the experimental conditions, the removal efficiency of CQ and HCQ decreased with increasing concentration under different absorbed doses. Additionally, the contribution of the •OH radicals was higher than e_{aq}⁻ to the degradation

of CQ and HCQ. Furthermore, e_{aq}^- contributed more to the degradation of CQ than HCQ which is attributed to the higher rate constants of e_{aq}^- with CQ. However, though the rate constant for e_{aq}^- with CQ was higher than $\bullet\text{OH}$, $\bullet\text{OH}$ contribution to CQ degradation was still higher. Similar observations were made in the laboratory experiments. This was attributed to the $\bullet\text{OH}$ radicals having more sites for attack compared to the e_{aq}^- . Additionally, in the experimental conditions, the e_{aq}^- is scavenged by the products of degradation such as NO_3^- . The rate constants for e_{aq}^- scavenging by NO_3^- are much higher and this will reduce the contribution of the e_{aq}^- to CQ degradation. The contribution of e_{aq}^- and $\bullet\text{OH}$ to the degradation of CQ and HCQ was influenced by the initial pH. The contribution of $\bullet\text{OH}$ decreased with increasing pH whereas those of the e_{aq}^- increased with increasing pH. The pH influences the generation of $\bullet\text{OH}$ and e_{aq}^- under EB and therefore affects the removal efficiency. These observations in simulations explain the observation made in experimental results. Similarly, both experiments and simulations show agreement in the diminished removal efficiency of CQ and HCQ in strongly alkaline conditions ($\text{pH} > 10$). In these conditions, reactions of $\bullet\text{OH}$ with OH^- lead to a reduction in available $\bullet\text{OH}$, additionally the increased concentration in e_{aq}^- causes the recombination reactions of the e_{aq}^- to dominate and lead to reduced degradation.

The degradation products of CQ and HCQ were further determined using LCMS and this information was used to propose a degradation mechanism for CQ and HCQ. The results indicated that the degradation of CQ and HCQ is mediated by reactions with $\bullet\text{OH}$ radicals and e_{aq}^- . Reactions of $\bullet\text{OH}$ radicals were prominent through the addition to the aromatic and pyridine rings. Additionally, N-dealkylation reactions and dechlorination contributed to the degradation of CQ and HCQ. Several degradation intermediates have been proposed. Furthermore, the formation of NO_3^- , NH_4^+ , Cl^- , and organic acids, and the reduction in TOC and COD attest to the mineralization of CQ and HCQ. However, from the results of TOC and COD, complete mineralization was not achieved. From the experiments and simulation results,

EB treatment initiates the degradation of CQ and HCQ in aqueous solutions and the efficiency of the process is affected by the absorbed dose, the initial concentration of the target pollutants, the initial pH of the solutions, irradiation conditions that selectively generate radicals, the presence of inorganic ions, and organic acids. The EB-F process has a higher removal efficiency for both CQ and HCQ with higher release of Cl^- , NO_3^- , NH_4^+ , and reduction of TOC and COD. Overall, the removal efficiency for CQ was improved by up to 37% at 0.5 kGy, and 10% at 2kGy for both CQ and HCQ. The Ecological Structure Activity Relationship (ECOSAR) analysis of CQ, HCQ, and their degradation products showed that the degradation of CQ and HCQ resulted in less toxic products.

STRESZCZENIE

Zanieczyszczenia związkami organicznymi stanowi poważne zagrożenie dla środowiska i organizmów żywych ze względu na dużą skalę produkcji tych związków a także ich znaczne zużycie, trwałość, toksyczność, właściwości mutagenne i rakotwórcze oraz ograniczoną wiedzę na temat ich losów w środowisku. Obecność tych zanieczyszczeń w ściekach i oczyszczaniu wody, zwłaszcza w ściekach bytowych jest rzadko uwzględniana a zatem są one uwalniane do ekosystemu wodnego. Konwencjonalne metody oczyszczania wody i ścieków są niewystarczające w usuwaniu tych zanieczyszczeń, co prowadzi do ich obecności w uzdatnionej wodzie. Ponadto uzdatnianie wody i ścieków, które wykorzystują metody takie jak adsorpcja i filtracja, prowadzą do wtórnego zanieczyszczenia z adsorbentu i produktów ubocznych filtracji, które wymagają kosztownej obróbki końcowej adsorbentów. Podobnie inne procesy wykorzystujące dodatki chemiczne budzą obawy ze względu na ilość stosowanych chemikaliów i ich wpływ na środowisko. Technologie radiacyjne są wszechstronnie wykorzystywane w usuwaniu wielu zanieczyszczeń w fazie wodnej bez dodatkowych dodatków chemicznych lub obróbki końcowej. Ponadto technologie te są proponowane jako obiecujące alternatywy dla wstępnego i końcowego procesu uzdatniania zanieczyszczonej wody.

W prezentowanych badaniach zbadano wywołaną promieniowaniem jonizującym degradację chlorochiny (CQ) i hydroksychlorochiny (HCQ) jako modelowych halogenowanych związków organicznych stanowiących zanieczyszczenia. CQ i HCQ to pochodne chinoliny, które są powszechnie stosowane jako leki przeciwmalaryczne z dalszymi zastosowaniami w leczeniu reumatoidalnego zapalenia stawów, raka, zapalnego zapalenia stawów, toczenia rumieniowatego układowego (chinakryna), reumatoidalnego zapalenia stawów, chorób dermatologicznych, immunologicznych, zakaźnych, a ostatnio zaproponowane w leczeniu SARS-Covid 19. Jednak ich stosowanie wiąże się z retinopatią siatkówki i arytmią serca, a

także toksycznością. Terapeutyczne podawanie tych farmaceutyków prowadzi do uwolnienia CQ, HCQ i ich metabolitów do ścieków, oczyszczalni ścieków i ostatecznie do wód powierzchniowych.

Roztwory CQ i HCQ o różnych stężeniach napromieniowywano wiązką przyspieszonych elektronów (EB) wykorzystując dawki w zakresie od 0,5 kGy do 7 kGy. Początkowe stężenia CQ i HCQ zmniejszały się wraz ze wzrostem dawki, a skuteczność usuwania zmniejszała się wraz ze wzrostem stężenia CQ i HCQ, zgodnie z kinetyką reakcji pseudo pierwszorzędowych. Degradację radiacyjną CQ i HCQ badano następnie w warunkach, które sprzyjają selektywnemu wytwarzaniu rodników hydroksylowych $\bullet\text{OH}$, solwatowanych elektronów e_{aq}^- i rodników wodorowych $\text{H}\bullet$, oraz dodatkowo w roztworach napowietrzanych i płukanych Ar. Degradacja CQ i HCQ była większa w warunkach faworyzujących powstawanie $\bullet\text{OH}$ w porównaniu z degradacją uzyskaną w roztworach zawierających $\text{H}\bullet$ i e_{aq}^- . Niższą skuteczność usuwania CQ i HCQ w roztworach z e_{aq}^- przypisano ograniczoną ilością reakcji z ich udziałem w porównaniu z ilością reakcji $\bullet\text{OH}$. Jednak reakcje z e_{aq}^- przyczyniły się w większym stopniu do degradacji CQ w porównaniu z HCQ. Przypisano to znacznie wyższym stałym szybkości reakcji e_{aq}^- z CQ. Roztwory napowietrzane (ilość tlenu między 5-10 mg / l) miały wyższą skuteczność usuwania dla CQ i HCQ w porównaniu z roztworem płukanym Ar (ilość tlenu < 1 mg / l). W roztworach napowietrzonych tworzenie się $\text{HO}_2\bullet$ może pozytywnie wpływać na degradację CQ i HCQ. Nie stwierdzono, aby początkowe pH roztworów miało istotny wpływ na skuteczność degradacji. Jednak pH między 2 a 4 sprzyjało usuwaniu CQ i HCQ, a skuteczność usuwania zmniejszała się wraz ze wzrostem pH

Degradację CQ i HCQ badano w obecności wybranych jonów nieorganicznych i kwasu humusowego powszechnie występującego w wodzie naturalnej, a także w obecności H_2O_2 i $\text{S}_2\text{O}_8^{2-}$, które promują wytwarzanie odpowiednio $\bullet\text{OH}$ i $\text{SO}_4\bullet^-$. Obecność CO_3^{2-} , HCO_3^- , NO_3^- , Fe^{2+} , kwasu humusowego i H_2O_2 miała szkodliwy wpływ na degradację CQ i HCQ z użyciem

EB. Składniki te konkurencyjnie wychwytyją $\bullet\text{OH}$ oprócz e_{aq}^- i zmniejszają skuteczność usuwania badanych zanieczyszczeń. Dodatkowo wyższe stężenia Fe^{2+} i kwasu humusowego powodują zmętnienie. Obecność NO_3^- znacznie wpłynęła na degradację CQ w porównaniu z HCQ. Z kolei obecność CO_3^{2-} pozytywnie wpływało na degradację HCQ. NO_3^- zmiata e_{aq}^- , które bardziej przyczyniają się do degradacji CQ niż HCQ. Zmiotane są także rodniki $\bullet\text{OH}$ przez NO_2^- powstające podczas redukcji NO_3^- . Obecność $\text{S}_2\text{O}_8^{2-}$ zwiększała skuteczność usuwania CQ i HCQ wraz ze wzrostem stężenia $\text{S}_2\text{O}_8^{2-}$ i dawki. Pod wpływem EB $\text{S}_2\text{O}_8^{2-}$ zostaje przekształcany w silnie utleniający $\text{SO}_4^{\bullet-}$. Dodatkowo powstają rodniki $\bullet\text{OH}$, które dodatkowo zwiększają wydajność. W roztworach alkoholu tert-butyłowego zwiększenie stopnia degradacji przypisano $\text{SO}_4^{\bullet-}$.

Do oceny degradacji CQ i HCQ w procesie EB wykorzystano kilka właściwości fizykochemicznych. Stężenie jonów chlorkowych zwiększało się wraz ze wzrostem dawek, co wynikało z odrywania atomów chloru z chlorowanych związków organicznych obróbki z wykorzystaniem EB. Dodatkowo wystąpiła nityfikacja, ważny proces w uzdatnianiu związków organicznych zawierających azot, o czym świadczy zmniejszające się stężenie całkowitego azotu Kjeldahla i rosnące stężenia NO_3^- i NH_4^+ wraz ze wzrostem dawki napromieniowania. Zmniejszoną skuteczność usuwania CQ i HCQ przy wyższych dawkach przypisano tworzeniu NO_3^- , który wymiata e_{aq}^- i $\bullet\text{OH}$ przez powstający NO_2^- . Całkowita mineralizacja CQ i HCQ nie została osiągnięta, co stwierdzono po analizie całkowitego węgla organicznego i chemicznego zapotrzebowania na tlen uzyskanymi. Jednak degradacja CQ i HCQ doprowadziła do wytworzenia związków organicznych o niższej masie cząsteczkowej. Zmiany odczynu z lekko kwaśnego przy pH 5,5 na pH 3,5 przypisano tworzeniu się kwasów organicznych. Wyniki wykazały wzrost stężenia kwasów organicznych wraz ze wzrostem dawki podczas napromieniowywania CQ i HCQ. Podobne zmiany pH odnotowano w degradacji CQ i HCQ pod wpływem utleniania w procesie elektro-fentona, co przypisuje się

tworzeniu kwasów szczawiowego i oksamowego. Inne badania również nawiązują do powstawania aldehydów i ketonów w degradacji związków organicznych.

Zbadano wpływ zastosowania wiązki elektronów wspomagany przez roztwór Fentona (EB-F) na skuteczność usuwania CQ i HCQ. Wstępne eksperymenty z wykorzystaniem tego roztworu wykazały zwiększoną skuteczność usuwania CQ i HCQ, gdy stężenie H_2O_2 było pięciokrotnie większe niż Fe^{2+} . Skuteczność ta wzrastała wraz ze wzrostem stężenia H_2O_2 z 0,1 do 2 mM z zachowaniem stosunku H_2O_2 do Fe^{2+} . Jednak po dalszym zwiększeniu zawartości H_2O_2 w stosunku do Fe^{2+} (od 10-krotnego do 20-krotnego) skuteczność usuwania zmniejszyła się z powodu zmiatania rodników $\bullet\text{OH}$. Podobny efekt zaobserwowano dla wyższych stężeń Fe^{2+} (2-krotnie i 5-krotnie wyższych w stosunku do H_2O_2). Zatem stosunek molowy H_2O_2 do Fe^{2+} znacząco wpływa na procesy zachodzące z wykorzystaniem roztworu Fentona. Stosunki molowe dodatkowo wpłynęły na proces z wykorzystaniem EB-F. Jednak w przeciwieństwie do procesu z wykorzystaniem roztworu Fentona, skuteczność usuwania CQ i HCQ była wysoka w nadmiarze H_2O_2 (20-krotnie więcej niż Fe^{2+}). Przypisano to utrzymującym się reakcjom H_2O_2 z odtworzonym Fe^{2+} dającym efekt synergistyczny podczas zastosowania wiązki elektronów (EB-F) wspomaganej przez roztwór Fentona. Zaobserwowano, że skuteczność usuwania przy zastosowaniu EB-F poprawiła się o $\approx 10\%$ dla dawki napromieniowania wynoszącej 7 kGy i z zastosowaniem roztworu H_2O_2 stężeniu 2 mM i stosunku H_2O_2 : Fe^{2+} wynoszącym 20:1 w porównaniu ze skutecznością usuwania przy zastosowaniu jedynie wiązki elektronów i dawki 7 kGy. Jednak lepsza skuteczność usuwania była wyższa przy niższych dawkach od 0,5 kGy do 2 kGy. Odchlorowanie i nitryfikacja z kolei zachodziły bardziej intensywnie w przy zastosowaniu EB-F niż przy wykorzystaniu samej tylko wiązki elektronów. Również całkowity węgiel organiczny oraz chemiczne zapotrzebowanie na tlen uległy zmniejszeniu w większym stopniu po wykorzystaniu EB-F. Dlatego proces EB-F poprawia ogólną wydajność usuwania CQ i HCQ.

Przeprowadzono symulacje matematyczne z wykorzystaniem oprogramowania CHEMSIMUL w celu dalszego zbadania degradacji CQ i HCQ w procesach EB i EB-F. Korzystając z dostępnych informacji z badań radiolizy impulsowej CQ i HCQ, a także badań radiolizy wody, zbadano degradację CQ i HCQ i porównano je z wynikami eksperymentalnymi. Degradacja CQ i HCQ była szybsza w warunkach symulowanych w porównaniu z warunkami eksperymentalnymi. Przypisano to niemożności symulacji wpływu produktów degradacji na skuteczność usuwania. Całkowite usunięcie CQ i HCQ osiągnięto przy mniej niż 2 kGy w symulacjach. Jednakże, podobnie jak w warunkach eksperymentalnych, skuteczność usuwania CQ i HCQ zmniejszała się wraz ze wzrostem ich stężenia, co zaobserwowano przy różnych dawkach promieniowania. Ponadto udział rodników $\bullet\text{OH}$ był wyższy niż e_{aq}^- w degradacji CQ i HCQ. Co więcej, e_{aq}^- w większym stopniu przyczyniło się do degradacji CQ niż HCQ, co przypisuje się wyższym stałym szybkości e_{aq}^- z CQ. Jednakże, chociaż stała szybkości dla e_{aq}^- z CQ była wyższa niż $\bullet\text{OH}$, udział rodników $\bullet\text{OH}$ w degradacji CQ był nadal wyższy. Podobne obserwacje poczyniono w eksperymentach laboratoryjnych. Przypisano to temu, że rodniki $\bullet\text{OH}$ mogły atakować cząsteczki CQ i HCQ częściej w porównaniu z e_{aq}^- . Dodatkowo w warunkach eksperymentalnych e_{aq}^- jest wychwytywany przez produkty degradacji, takie jak NO_3^- . Stałe szybkości wymiatania e_{aq}^- przez NO_3^- są znacznie wyższe, co zmniejszy udział e_{aq}^- w degradacji CQ. Na udział e_{aq}^- i $\bullet\text{OH}$ w degradacji CQ i HCQ miało wpływ początkowe pH. Udział $\bullet\text{OH}$ zmniejszał się wraz ze wzrostem pH, podczas gdy udział e_{aq}^- wzrastał wraz ze wzrostem pH. pH wpływa na wytwarzanie $\bullet\text{OH}$ i e_{aq}^- w warunkach napromieniowywania środowiska wodnego, a tym samym wpływa na skuteczność usuwania omawianych związków organicznych. Te wnioski uzyskane dzięki symulacjom pozwalają wyjaśnić obserwacje poczynione na podstawie wyników eksperymentalnych. Podobnie, zarówno eksperymenty, jak i symulacja wykazują zgodność w zmniejszonej skuteczności usuwania CQ i HCQ w warunkach silnie zasadowych ($\text{pH} > 10$). W tych warunkach reakcje $\bullet\text{OH}$ z OH^- prowadzą do

zmniejszenia stężenia rodników $\bullet\text{OH}$, dodatkowo zwiększone stężenie e_{aq}^- powoduje częste występowanie reakcji rekombinacji e_{aq}^- i prowadzi do zmniejszenia stopnia degradacji.

Produkty degradacji CQ i HCQ zostały następnie określone za pomocą LCMS, a informacje te wykorzystano do zaproponowania mechanizmu degradacji dla CQ i HCQ. Wyniki wskazują, że degradacja CQ i HCQ odbywa się za pośrednictwem reakcji z rodnikami $\bullet\text{OH}$ i e_{aq}^- . Najczęściej zachodzą reakcje przyłączenia rodników $\bullet\text{OH}$ do pierścieni aromatycznych i pirydynowych. Ponadto reakcje N-dealkilacji i odchlorowania przyczyniły się do degradacji CQ i HCQ. Zaproponowano kilka półproduktów degradacji. Ponadto tworzenie NO_3^- , NH_4^+ , Cl^- , kwasów organicznych oraz redukcja TOC i ChZT świadczy o mineralizacji CQ i HCQ. Jednak z pomiarów TOC i ChZT wynika, że nie uzyskano pełnej mineralizacji. Z eksperymentów i wyników symulacji wynika, że obróbka wiązką elektronów inicjuje degradację CQ i HCQ w roztworach wodnych, a na wydajność procesu wpływa dawka promieniowania, początkowe stężenie zanieczyszczeń, początkowe pH roztworów, warunki napromieniania, które selektywnie generują rodniki, obecność jonów nieorganicznych i kwasów organicznych. Obróbka z wykorzystaniem EB-F charakteryzuje się wyższą wydajnością usuwania zarówno dla CQ, jak i HCQ z wyższym uwalnianiem Cl^- , NO_3^- , NH_4^+ oraz redukcją TOC i ChZT. Ogólnie rzecz biorąc, skuteczność usuwania CQ poprawiła się nawet o 37% przy 0,5 kGy i o 10% przy 2 kGy zarówno dla CQ, jak i HCQ. Analiza zależności struktury ekologicznej i aktywności (ECOSAR) CQ, HCQ i produktów ich degradacji wykazała, że degradacja CQ i HCQ skutkuje powstaniem mniej toksycznych produktów.

CONTENTS

1. Introduction	1
1.1. Emerging pollutants and the environment	3
1.2. Radiation processing of wastewater	9
1.3. Scope of the Study	15
1.4. Objectives of the Study	17
2. Literature Review	18
2.1. Removal technologies of emerging pollutants.....	19
2.1.1. Engineered wetlands and natural systems.....	19
2.1.2. Biological treatment Methods	20
2.1.3. Mineral Surface Adsorption and Ion Exchange	20
2.1.4. Membrane technologies	22
2.1.5. Chemical Oxidation	23
2.1.6. Electrochemical Oxidation	23
2.1.7. Catalysis (Photolysis/Photocatalysis, Fenton Processes)	24
2.2. Application of ionizing radiation in water treatment.....	32
2.3. The theory of water radiolysis	34
2.3.1. The Physical Stage	36
2.3.2. The Physicochemical Stage	36
2.3.3. The Chemical Stage	37
2.4. Reaction of Radiolysis products	38
2.4.1. Hydrated/Aqueous electron.....	39
2.4.2. Hydrogen.....	41
2.4.3. Hydrogen Peroxide	43
2.4.4. Molecular Hydrogen.....	43
2.4.5. Hydroxyl Radical	44
2.4.6. Perhydroxyl Radical	46
2.5. Review of radiation process in wastewater management	48
2.5.1. Gamma Radiation.....	49
2.5.2. Electron beam radiation.....	52
2.6. Sterilization activity of electron beam	58
3. Methodology.....	61

3.1.	Chemicals and Materials.....	61
3.2.	Analytical techniques.....	61
3.2.1.	UV spectrophotometry and HPLC Analysis.....	61
3.2.2.	LC-MS methods.....	62
3.2.3.	Colorimetric methods.....	62
3.3.	Preparation of catalysts.....	68
3.4.	Radiation Processing.....	69
3.4.1.	Accelerator Set-up.....	71
3.4.2.	Determination of Dose.....	71
3.4.3.	Radiation chemical yield.....	75
3.7.	Mathematical modeling of radiation-induced degradation of CQ and HCQ.....	75
3.8.	Ecotoxicity Analysis.....	76
4.	Results and Discussion.....	79
4.1.	Radiation dose effects on CQ and HCQ degradation.....	79
4.2.	The degradation of CQ and HCQ under $\bullet\text{OH}$, e_{aq}^- , $\text{H}\bullet$, and aerated conditions.....	82
4.3.	Effect of Initial Pollutant Concentration on the Removal Efficiency.....	83
4.4.	Effect of Initial Solution pH on the Removal Efficiency.....	86
4.5.	Effect of inorganic ions, humic acid, and H_2O_2 on the removal efficiency of CQ and HCQ...	91
4.6.	Electron Beam Coupled with Catalytic Oxidation.....	97
4.6.1.	Electron Beam-Fenton assisted degradation of CQ and HCQ.....	97
4.6.2.	Electron Beam coupled with $g\text{-C}_3\text{N}_4$ catalyst.....	106
4.6.3.	Electron Beam coupled with TiO_2 catalyst.....	108
4.7.	Degradation monitoring.....	110
4.7.1.	Change in solution pH.....	111
4.7.2.	Cl^- generation.....	114
4.7.3.	Nitrogen.....	116
4.7.4.	Changes in Oxygen demand.....	119
4.8.	Mathematical simulation of radiation-induced degradation of CQ and HCQ.....	122
4.8.1.	Changes in pH.....	126
4.8.2.	Effect of different initial pH in the degradation of CQ and HCQ.....	126
4.8.3.	Effect of initial pollutant concentration on the simulated degradation of CQ and HCQ	129
4.8.4.	The effect of inorganic ions, and H_2O_2 on the simulated degradation of CQ and HCQ	130
4.8.5.	Simulation of EB-F process for degradation of CQ and HCQ from aqueous solutions	131

4.9. Degradation products of CQ	133
4.10. Degradation products of HCQ	137
4.11. Toxicity Analysis.....	141
5. Conclusion.....	144
Bibliography	148
APPENDICES	171
Appendix 1	171
Appendix 2	172
Appendix 3	173
Appendix 4	174
Appendix 5	178
Appendix 6	179
Appendix 7	180
Appendix 8	181
Appendix 9	182
Appendix 10	183
Appendix 11	184
Appendix 12	186

LIST OF FIGURES

Fig. 1-1 (a) Quinoline, (b) CQ and (c) HCQ.....	16
Fig. 2-1 Radiolytic yields (G-Values) of water radiolysis products.....	35
Fig. 3-1 Reaction scheme for the analysis of ammonium ions.....	65
Fig. 3-2 Steps in the preparation of g-C ₃ N ₄ catalysts.....	69
Fig. 3-3 Experimental Set-Up for irradiation of aqueous samples at ILU6 accelerator	71
Fig. 4-1 UV-Vis spectrum for the degradation of 125mg/L of (A) CQ and (B) HCQ under EB irradiation at dose between 0.5 kGy and 7 kGy.	81
Fig. 4-2 Removal efficiency of (a) CQ and (b) HCQ under different irradiation conditions .83	83
Fig. 4-3 Effect of the initial concentration of CQ and HCQ on the removal efficiency.....	85
Fig. 4-4 Removal efficiency of 125mg/L under electron beam irradiation at different initial pH (a) CQ and (b)HCQ. (c) Dose constant variation with pH at 3kGy. (d) The fraction of protonated states of CQ at different pH (Schroeder et al., 2015) and (e) HCQ at different pH (Catrinel Ion et al., 2022).....	88
Fig. 4-5 Changes in pH of the solution with dose during the degradation of 125mg/L CQ solution (c) CQ (d)HCQ.....	90
Fig. 4-6 Effect of different ions and additives on the EB-initiated degradation of (a) CQ, and (b) HCQ solution.....	94
Fig. 4-7 Efficiency of Fenton process for (a) CQ and (c) HCQ, (b) Fenton degradation of CQ at 5× molar ratio with 2mM H ₂ O ₂ . (d) Fenton degradation of HCQ at 5× molar ratio with 2mM H ₂ O ₂	100
Fig. 4-8 EB-F degradation of (A) 125mg/L CQ and (B) 125mg/L HCQ solution. Results are presented for the different concentrations of H ₂ O ₂ with different H ₂ O ₂ :Fe ²⁺ molar ratios at 2kGy.....	102
Fig. 4-9 Chromatograms for the degradation of CQ and HCQ under EB irradiation and under EB- Fenton process (a) Degradation of CQ under EB treatment (b) Degradation of CQ under EB-F. (c) Degradation of HCQ under EB (d) Degradation of HCQ under EB-F. H ₂ O ₂ =2mM, Fe ²⁺ =0.1mM.	103
Fig. 4-10 (A) The removal efficiency for 125mg/L CQ and HCQ under EB irradiation and EB- Fenton assisted process (B) Calculated G- values for CQ and HCQ under EB, and EB-F	104
Fig. 4-11 Electron beam coupled with catalytic degradation of (a) CQ and (b) HCQ at catalyst loading of 0.2g/L. Cat II-MCN, Cat III-MIL-Fe(Mn)-NH ₂ , Cat IV-g-C ₃ N ₄ /MIL-Mn(Fe)-NH ₂ , Cat V-MCN/MIL-Mn(Fe)-NH ₂	108
Fig. 4-12 Degradation of (a) CQ and (b) HCQ under electron beam irradiation with varying concentrations of TiO ₂ as a catalyst	110
Fig. 4-13 (a) Changes in pH during EB irradiation of 125mg/L CQ and HCQ. (b) Generation of organic acids during degradation of 125mg/L CQ and HCQ under EB and EB-F (EBF) processes	111
Fig. 4-14 Changes in pH during the electron beam-initiated degradation of CQ and HCQ solution (A) & (C) at different initial H ₂ O ₂ concentrations for CQ and HCQ respectively (B) & (D) at different initial concentrations of Fe ²⁺ for CQ and HCQ respectively	112
Fig. 4-15 (A) Release of Cl ⁻ with increasing dose during radiolysis of 125mg/L of CQ and HCQ solution under the EB and EB-F processes. (B) Release of Cl ⁻ under conditions	

promoting $\bullet\text{OH}$ generation (presence of N_2O) or e_{aq}^- generation (presence of 0.5M tBuOH)	115
Fig. 4-16 (a) Reduction in Total Kjeldahl nitrogen (b) Formation of NO_3^- and (c) Generation of NH_4^+ in the degradation of 125mg/L of CQ and HCQ solutions under electron beam and electron beam Fenton irradiation	118
Fig. 4-17 Changes in dissolved O_2 concentration during EB and EB-F irradiation of 125mg/L (A) CQ and (B) HCQ, 2mM H_2O_2 and different ratios of Fe^{2+}	120
Fig. 4-18 Variation in (a) COD and (b)TOC during EB and EB-F degradation of 125mg/L solutions of CQ and HCQ	121
Fig. 4-19 Simulated and experimental degradation of 125mg/L of CQ and HCQ in aqueous solution under electron beam irradiation	123
Fig. 4-20 Simulated degradation of (a) CQ and (b) HCQ under electron beam irradiation and formation of intermediate products under action of $\bullet\text{OH}$ and e_{aq}^-	124
Fig. 4-21 Formation of Cl^- and reduction in dissolved O_2 concentration with the degradation of CQ and HCQ.	125
Fig. 4-22 Changes in pH during simulated degradation of aqueous solutions of CQ and HCQ	126
Fig. 4-23 Changes in initial pH of solutions with irradiation during simulated degradation of (A) CQ and (B) HCQ	127
Fig. 4-24 Effect of different initial solution pH on the simulated degradation of aqueous solutions. (a) reactions of $\bullet\text{OH}$ radical with CQ (b) reactions of e_{aq}^- with CQ (c) reactions of $\bullet\text{OH}$ radical with HCQ (d) reactions of e_{aq}^- with HCQ	128
Fig. 4-25 Effect of initial pollutant concentration on the degradation of (A) CQ and (B) HCQ and their respective dose constants (C)	130
Fig. 4-26 Effects of selected inorganic ions on the simulated degradation of (a) CQ and (b) HCQ under electron beam irradiation at 0.5 kGy	131
Fig. 4-27 Simulated degradation of (a) CQ and (b) HCQ under EB-F process at 0.5kGy	132
Fig. 4-28 LC-MS mass spectra for CQ showing mass fragmentation of the degradation products of CQ under EB irradiation	134
Fig. 4-29 Proposed degradation scheme of CQ under EB process	135
Fig. 4-30 MS Spectrum for the identified degradation products of HCQ under the EB-F process	138
Fig. 4-31 LC-MS chromatogram of the degradation of HCQ at different doses under (A) EB irradiation and (B) EB-F process.	139
Fig. 4-32 Proposed degradation scheme of HCQ in aqueous solution	140
Fig. 4-33 Toxicity analysis of CQ and degradation products	142
Fig. 4-34 Toxicity analysis of HCQ and degradation products	142

LIST OF TABLES

Table 1.1 Pros and Cons of gamma radiation and electron beam radiation processing methods	13
Table 1.2 Properties of common radiation sources (Trojanowicz et al., 2017)	14
Table 2.1 Wastewater treatment methods used in the treatment of pharmaceutically active compounds	26
Table 4.1 Rate constants for the reaction of quinoline and its derivatives with •OH radical and e_{aq}^-	80
Table 4.2 Rate constant k for different concentrations of CQ and HCQ and corresponding R ² values	84
Table 4.3 Toxicity classification based on ECOSAR (Reuschenbach et al., 2008).....	141

ABBREVIATION

AOP	Advanced Oxidation Process
BOD	Biological Oxygen demand
COD	Chemical Oxygen demand
DBPs	Disinfection byproducts
ECOSAR	Ecological Structure-Activity Relationship
EDCs	Endocrine Disrupting Compounds
LET	Linear energy transfer
PhAC	Pharmaceutically active compounds
EB	Electron Beam
EB-F	Fenton assisted Electron beam
EO	Electrochemical Oxidation
HAA	Haloacetamides
MIL	Materials of Institute Lavoisier
N- DBPs	Nitrogen disinfection byproducts
PPCPs	Pharmaceuticals and Personal Care Products
ROS	Reactive Oxygen Species
THM	Trihalomethanes

TOC	Total organic carbon
TKN	Total Kjeldahl nitrogen
WWF	The World-Wildlife Fund for nature
ARG	Antibiotic-resistant Genes
CEWICs	cyclodextrin-epichlorohydrin water-insoluble copolymers
EO-BDD	Electrochemical oxidation using boron-doped diamond,
CW	Constructed wetland
CW-GBCF	Constructed wetland fragrance cultivation
CW-GS	Constructed wetland with gravel sand
CW-GWH	Constructed wetland with gravel water hyacinth
PPMPs	Polypyrene microspheres
QSAR	Quantitative Structure-Activity Relationship
VF-CW	Vertical flow constructed wetland

CHAPTER ONE

1. Introduction

Water resource scarcity coupled with pollution are global concerns exacerbated by high demand in urban and industrial acceleration (Lin et al., 2020). The World-Wildlife Fund for nature (WWF) estimates that 1.1 billion people lack access to reliable water supply, 2.7 billion people experience inadequate water supply at least one month in the year, and 2.4 billion people are faced with inadequate sanitation and are susceptible to water-borne diseases. Globally, as of 2019, the 13th death risk factor was unsafe drinking water which was responsible for 1.23M deaths. Additionally, although 70% of the earth's surface is covered by water, only 3% is available for human consumption with the remaining portion confined in inaccessible ice caps (Worldwildlifefund, 2023). The stress burden on the available water resources creates the need for recovering ground, surface, and wastewater by incorporating treatment methods that eliminate pollutants and make it suitable for repurposing by attaining the prerequisite guidelines on water quality.

Generally, domestic, municipal, industrial, or agricultural practices are the main sources of chemical and biological pollutants in the aquatic environment. Emerging pollutants (EPs) such as chemicals used in pharmaceuticals and personal care products (PPCPs) are released into the environment through domestic, hospital, pharmaceutical wastewater, landfill leachate, and animal manure. These pollutants are rarely monitored in conventional water quality indices but pose potential detrimental effects to the environment, plants, and human and animal health (Kasonga et al., 2021; Llamas et al., 2020). Their concentrations range between ng/L– μ g/L in water, soil, wastewater, and sludge (Kawabata et al., 2013; Liu et al., 2020). Regulations governing point sources such as manufacturing industries ensure relatively lower pollutant injections compared to nonpoint sources such as households and agricultural runoff (Rahman

et al., 2009). The contamination of water results in changes in nutrient levels, abundance, biomass, diversity of organisms, bioaccumulation of organic and inorganic compounds, and the alteration of trophic interaction among species (Hossain et al., 2018). Pharmaceutical residues affect aquatic biota and microbial populations by exacerbating the development of secondary bacterial resistance or infusing drug-resistant bacteria into the environment (Li et al., 2013).

The natural water cycle performs water purification through filtration, evaporation, oxidation, and photolysis. Similar techniques are utilized in conventional wastewater treatment. However, they are inefficient in eliminating most anthropogenic pollutants due to high concentrations, solubility, and persistence. Dilution, hydrolysis, biodegradation, sorption, and other properties dictate the attrition of these pollutants (Wang et al., 2015). The contaminants in natural systems vary greatly because of natural transport processes and reaction mechanisms dependent on physicochemical properties, environmental factors, and chemical partitioning to water, air, soil, and sediment (Pinasseau et al., 2020b). Analytical techniques seek to identify chemical variants previously below the detection limits of existing equipment. These chemicals if toxic, endanger the life of aquatic organisms and terrestrial life (Delgado et al., 2019). Deficiencies in detection techniques, low concentrations, and the spatial variability between locations add to the challenges in accounting for most EPs (Chiaia-Hernández et al., 2020).

EPs such as pharmaceutically active compounds (PhACs) present in aquatic environments are a concern to human and ecological health due to their large number and insufficient information about them. Moreover, the design, pharmacokinetics, and contraindications of PhACs implicate them in disrupting key processes in sensitive non-target organisms (González-González et al., 2022; Peer Muhamed Noorani et al., 2024). The consumption of therapeutic drugs leads to the excretion of metabolites, and unmetabolized PhACs in urine and feces which are discharged into the sewage and septic systems and finally into the aquatic environment.

Limited or non-existent data concerning the fate, transport, and toxicity of these compounds at the current environmental concentrations coupled with limitations in chemical analysis methods, expense, and time consumption make elucidation of these properties daunting (Dong et al., 2022). Personal care products range from fragrances, UV filters, insect repellents, antibacterial, surfactants, and flame retardants used daily and therefore have high production volume and high contribution to pollutant influx. However, EPs do not need to be highly persistent to negatively affect ecosystems and human health as their degradation is offset by their sustained input into the environment (Bugueño-Carrasco et al., 2021; Kanakaraju et al., 2018; Llamas et al., 2020).

The more persistent a compound is, the greater the potential for transportation of suspended solids to locations far away from the source or to bioaccumulate (Chiaia-Hernández et al., 2020). EPs are transported from the initial point and non-point sources to secondary deposition sites including ground water (Bork et al., 2021; Linke et al., 2023; Pinasseau et al., 2020b). Banned pollutants are detected in aquatic ecosystems at high frequencies and levels attesting to their slow degradation (Kovács et al., 2015; Wojnárovits et al., 2018). Their recalcitrance toward biodegradation and their physical-chemical properties i.e., the relatively high solubility, and low hydrophobicity lead to their tendency to remain in the aqueous phase, rather than partitioning into microbial biomass and resulting biosolids.

1.1. Emerging pollutants and the environment

Many registered chemical substances including pharmaceuticals, and personal care products are potentially dangerous. Antibiotics, estrogen steroids, antidepressants, calcium channel blockers, genotoxic and antiepileptic drugs i.e., phenytoin, valproate, and carbamazepine that initiate apoptosis in brain development, analgesics, beta-blockers, hormones, and hormone-mimics are commonly reported PhACs. Parabens, common antimicrobial preservatives in cosmetics, toiletries, pharmaceuticals, and even foodstuffs have been shown to have residual

estrogenic activity (Delgado et al., 2019). Quinolones, fluoroquinolones, and sulfonamides are effective due to their broad-spectrum activity and exceptional oral absorption but are potentially ecotoxic and genotoxic (Garcia-Molina et al., 2013; Li et al., 2013). DDT an organochlorine pesticide, and its metabolites possess endocrine-disruptive properties, a long half-life, and stable chemical properties that pose difficulty in degradation and removal in routine water treatment processes (Kasonga et al., 2021; Lu et al., 2019). The high consumption of antibiotics in human, animal, and aquaculture applications contributes to the antimicrobial agents, drug-resistant bacteria, and genes present in surface and groundwater (Giebułtowicz et al., 2018).

Natural or synthetic endocrine-disrupting compounds (EDCs) block or mimic natural hormones (e.g., estrogens) and interfere with the hormonal system. The EDCs affect the hormone system firstly by the agonistic effect by mimicking hormones and binding to the receptor sites of target cells and eliciting a response. Secondly, in the antagonistic effect, they block hormones by binding to the receptors and preventing normal hormone receptor interactions. In the third mechanism both agonistic and antagonistic binding to the same receptors results in subtle changes in receptor conformation (Rahman et al., 2009). Estrogenic EDCs mimic or block natural estrogen, whereas androgenic forms mimic or block natural testosterone, and thyroidal variants directly or indirectly impact the functions of the thyroid (Snyder et al., 2003). EDCs can be harmful to the human reproductive system, and cause endocrine and reproductive disorders in fish, birds, and mammals (Inam et al., 2019). Population declines and reproductive disorders including imposex (tributyltins), supernumerary limbs, and missing limbs in amphibians, changes in the levels of sex steroids, gonadal histology, female egg yolk precursor, vitellogenin in male fish are reported effects of exogenous EDCs. Additionally, genotoxicity induction, enzymatic alterations, oxidative stress, decreased swimming embryo activity, physiological changes and behavioral symptoms

of the heart, kidneys, lungs and intestinal epithelium, cell degeneration, renal tubule epithelial cell necrosis, and alveolar emphysema in *Rattus norvegicus* also make up the caucus of harmful effects of pollutants (Andrade et al., 2002; Sweeney et al., 2015; Vandenberg et al., 2012). Furthermore, perchlorate ClO_4^- has been shown to competitively inhibit iodine transport to the thyroid gland (McLanahan et al., 2009). Low sperm quality and quantity in human males, increased incidence of prostate cancers, and breast and testicular cancers result from protracted exposure to EDCs (Rehman et al., 2018). Pharmaceutical, and personal care products (PPCPs) can interfere with individual growth and development, inhibit metabolic pathways, and decrease the gene expression levels of hematopoietic stem cells in vivo (Snyder et al., 2003; Wei et al., 2021). Emerging organic pollutants pose ecological risks even in trace concentrations. Their detection and concentrations in aquatic organisms are reflective of their distribution in water and eventual entrance into the food web with consequences on human health and the ecosystem (Tang et al., 2020).

Bisphenol A (BPA), nonylphenol (NP), and triclosan (TCS) are infamous EDCs due to their toxicity and persistence in the environment and are regarded as some of the representative EDCs (Gao et al., 2020). BPA used for epoxy resin, polycarbonate Plastics (PC) production, food and beverage packaging, baby bottles, and dental sealants has been reported to be carcinogenic despite increased global consumption and has been banned in China, and Canada, and restricted use in Malaysia, the United States, and the European union. Nonylphenol (NP) is used for the synthesis of NP ethoxylates surfactants and conversely, their main degradation product is used in industrial, commercial, and domestic products i.e., detergents, personal care products and insecticides, lubricants, defoamers, emulsifiers, and paints, textile, and metal processing industries. They are accumulative and among the 27 controlled persistent toxic pollutants by the United Nations Environmental Protection Agency (Vargas-Berrones et al., 2020). Triclosan (TCS), is a broad-spectrum antibacterial agent frequently used in soaps,

toothpaste, facial cleansers, and preservatives with potential estrogenic activity and slight teratogenicity (Dhillon et al., 2015; Luo et al., 2019).

Marine organisms are studied to ascertain the internal distribution of persistent organic pollutants compared to their terrestrial counterparts. Dietary uptake is the major route of exposure for plants and animals. The shorter food chain length in terrestrial food webs is believed to lower the accumulation of EPs. However, it is important to understand the internal distribution of these chemicals both in consumed animals and in human beings (Shin et al., 2020). The internal distribution and fate of EPs depend on their biological and physicochemical properties, chain lengths, and functional groups. Hydrophobic compounds such as dioxins are predisposed to the adipose tissues of humans (Lee et al., 2017), and per-fluoroalkyl substances (PFASs) accumulate in the livers of birds, fish, and humans due to their lipophilicity by binding to the liver fatty acid and serum albumin proteins. Furthermore, long-chain PFASs are predisposed to accumulating in the liver and kidney tissues. Organophosphorus flame retardants (PFRs) metabolites and plasticizers have been found in ovoviviparous species in water snakes and small common carp in contaminated ponds (Liu et al., 2020).

Veterinary antibiotics are released into agricultural fields via manure, drug manufacturing process, disposal of drug containers, medical waste, and application of drug-containing waste material. The consumption of antibiotic-exposed crop plants harms human and animal health. Evidence suggests adverse effects of antibiotics on the growth and performance of plants (Chaturvedi et al., 2021; Minden et al., 2017; Youssef and Bashour, 2017). Delayed germination and post-germinative development by direct damage, decreased photosynthetic pigments, reduced number and size of mature leaves, and inhibition of root elongation are some of the reported effects. The plant species and the antibiotic determine the response e.g., phytotoxic, homeotic, or mutational (Tasho and Cho, 2016). Herbs have been reported to be more sensitive to antibiotics compared to grasses. The growth and development of *Phaseolus*

vulgaris L., *Glycine max*, *Medicago sativa*, and *Zea mays*, among other plants have been affected by commonly used therapeutic chemicals (Jjemba, 2002). Phytotoxic effects ranging from inhibition of soil phosphate activity, soil respiration, and soil microbial and enzymatic activities have been reported (Liu et al., 2009). Pharmaceuticals and personal-care products (PPCPs) accumulate in plants (ng to mg Kg⁻¹) with suspected toxicity to the plants. PPCPs are taken up accumulated, and metabolized by plants eventually affecting the plants, their microbiota, and the organisms feeding on them, including humans (Bartrons and Peñuelas, 2017). Plants are excellent natural bio-indicators of global pollution owing to their wide distribution on the planet and potential to accumulate chemical compounds from the atmosphere, water, and soil (Picó et al., 2023).

The inadvertent generation of pollutants from wastewater treatment practices is another concern. Chlorination is a vital water treatment process. However, disinfection byproducts (DBPs) are unintentionally generated by the application of chlorine and chloramine disinfection processes (Al-Abri et al., 2019; Mazur and Lebedev, 2022). Enhanced coagulation and chloramination create DBPs such as brominated/iodinated DBPs and nitrogenous DBPs (Wang et al., 2015). DBPs have high cytotoxicity and mutagenicity and pose a human health hazard risk (Xu et al., 2014). Chloramines deployed as alternative disinfectants to reduce the formation of trihalomethanes (THMs) and haloacetamides (HAAs), promote the formation of nitrogenous disinfection byproducts (N-DBPs). Dissolved organic nitrogen compounds in wastewater and raw water are precursors for N-DBPs that pose a greater health risk compared to chlorine-DBPs (Xu et al., 2014).

PPCPs and most EPs are inefficiently removed by conventional water treatment processes involving coagulation, precipitation, acidification, and biosorption therefore impacting water quality (Snyder et al., 2003; Wei et al., 2021). PPCPs in human and veterinary drugs, hormones, cosmetic formulations, their metabolites, and their transformation products are detected in

wastewater, surface, ground water, drinking water, sludge, and sediments (Martínez-Alcalá et al., 2021). Most water quality standards do not specifically incorporate or regulate pharmaceuticals and EDCs. However, Australia and the United Kingdom have set the pace for the regulation of these compounds in waste water for reuse (Lu et al., 2019). The acute toxicity effects on humans or animals, difficult volatilization, and ease of bio-accumulation of PPCPs threaten the ecological environment and human health (Couto et al., 2019). Approximately 33% of manufactured and 25% of sold drugs are disposed of alongside household waste in Germany and Austria respectively. In the United Kingdom, 63.2% of unwanted medicines comprise household wastes and 11.5% are flushed down the sink or toilet. Beta-blocker nadolol is excreted from the human body unmetabolized while carbamazepine only 3% is excreted unchanged (Rahman et al., 2009). Steroids, plasticizers, detergent metabolites, analgesics, lipid regulators, antibiotics, steroid hormones, anti-epileptics, X-ray media contrasts (iopromide), caffeine, and detergent metabolites are in surface waters and sewage treatment plant (STP) effluents (Llamas et al., 2020).

Most EDCs and PPCPs have higher polarity, acidic or basic functional groups, coupled with the occurrence at trace levels (1mg/L) pose challenges in both removal processes and analytical detection (Snyder et al., 2003). Waste water treatment plants (WWTPs) eliminate the potential risk of known contaminants. However, the efficiency of the systematic removal and degradation of PPCPs depends on their physicochemical properties and the operational parameters of the WWTP; hydraulic retention time, sludge retention time, dissolved oxygen concentration, temperature, and pH (Kawabata et al., 2013). The biodegradation of organic compounds by activated sludge treatment follows the order of saturated aliphatic > unsaturated aliphatic > aromatics > chlorinated compounds. These persistent pharmaceuticals are decomposable by further water treatment methods such as ionizing radiation (Kimura et al., 2012).

Pharmaceuticals have successfully been removed from sewage influents using membrane bioreactors, activated sludge processes, UV-induced degradation, absorption, biodegradation, and sunlight photodegradation. Regulations or guidelines for water reuse conventionally focus on compliance with parameters such as turbidity, chemical oxygen demand (COD), biological oxygen demand (BOD), total suspended solids (TSS), bacteria, residual chlorine, etc. Secondary effluent from WWTPs, and effective tertiary or advanced treatment processes often meet most of the prescribed criteria. Activated sludge treatment in conventional WWTPs involving sorption onto sludge flocs, microbial processes, and volatilization, can degrade PPCPs. Microbial biodegradation is a fundamental removal/degradation mechanism for organic pollutants and removes the PPCPs by utilizing them in metabolic functions i.e., the nitrification process in an aerated tank converts ammonia to nitrate by nitrifying microorganisms (Martínez-Alcalá et al., 2021). However, PPCPs are not efficiently removed but are more likely sorbed into the solids. Delgado et al. (2019) working with a rotating biological contact (RBC) commonly used in waste water treatment observed that PPCPs remained unaffected by photodegradation even after 72hrs (Delgado et al., 2019). Electrochemical oxidation, activated carbon, membrane filtration, advanced oxidation, biosorption, and adsorption are some of the treatment methods developed to mitigate contaminants of emerging concern. Advanced oxidation processes (AOPs) such as photo-Fenton, sonolysis, electrochemical oxidation, radiation, and ozonation utilize the highly reactive $\bullet\text{OH}$ radicals to progressively oxidize organic compounds into innocuous products. These methods however require high energy and capital inputs to run and maintain (Kanakaraju et al., 2018).

1.2. Radiation processing of wastewater

The application of radiation technologies as the method of water and wastewater purification is effective for a wide range of organic and inorganic pollutants (Makarov and Ponomarev,

2018; Sampa et al., 2007). Ionizing radiation efficiently generates oxidizing hydroxyl ($\cdot\text{OH}$) radicals and strongly reducing e_{aq}^- following water radiolysis. Both *advanced oxidation and reduction processes* (AO/RPs) are performed simultaneously or selectively through the application of appropriate scavengers for specific reactive species (Trojanowicz, 2020). The primary radicals that form during water irradiation can react with the target harmful organic molecules, with dissolved organic compounds (DOC), chloride, bicarbonate, carbonate ions, nitrites, and nitrates to form secondary radicals (Csay et al., 2012; Wojnárovits and Takács, 2017, 2016). Ozone, H_2O_2 , or persulfate, are known to increase the oxidation efficiency of organic pollutants by transforming reductive intermediates to oxidizing species during irradiation.

Gamma-rays from radioisotope sources or accelerated electrons are preferred for persistent organic pollutant (POPs) destruction in waters and wastewater. Gamma irradiation sources (such as ^{60}Co or ^{137}Cs) are commonly used but there is a growing preference for the electron accelerator machines owing to their very high dose rate, ease of handling, and adaptability. The generated reactive species are reactive towards a myriad of organic pollutants. Rate coefficients of $\cdot\text{OH}$ radicals with selected antibiotic molecule reactions have been computed. Compounds with aromatic rings or conjugated double bonds have rate coefficients in the range of $(6 - 8) \times 10^9 \text{ M}^{-1} \text{ s}^{-1}$ range where the basic reaction involves radical addition. The presence of strong electron-withdrawing groups and N atoms gives smaller rate coefficients. Molecules without aromatic rings have smaller values in the range of $(3 - 6) \times 10^9 \text{ M}^{-1} \text{ s}^{-1}$ with hydrogen abstraction being the dominant reaction (Wojnárovits et al., 2018). Electron-beam treatment of natural water and wastewater is a proven way of neutralizing various biohazardous pollutants but the high cost of accelerators and their relatively low power limits their application and economic feasibility (Ponomarev, 2020a; Ponomarev and Ershov, 2020). Water treatment requires much lower doses at a very high flow rate. The daily water consumption and

wastewater discharge are huge - from tens and hundreds of thousands of cubic meters in large industrial enterprises to millions of cubic meters in megacities.

Ionizing radiation is economically attractive with a wide range of applications and potential degradation of domestic, agricultural, industrial, and municipal wastewater. Its advantages over conventional wastewater treatment and other AOPs are minimal by-product formation, performance minimally reduced by turbidity, and no additional byproduct treatment required. Radiation technology provides the possibility for simultaneous oxidative and reductive processes for the removal of organic pollutants and heavy metals. The ability to integrate radiation technology alongside other treatment processes such as ozonation, coagulation, or biodegradation is an added advantage for synergistic purposes (Trojanowicz et al., 2018a). However, controversial perception about radiation technology persists. Albeit, no extensive use limits the adoption of these technologies (Jan et al., 2015). High-energy, radiolytic processing using electron beam (EB), γ -rays or non-thermal plasma (NTP) of water matrices have shown promising results in many applications both as a stand-alone process or combined with others in the degradation of emerging organic pollutants, removal, and inactivation of microorganisms and parasites (Capodaglio, 2019). Irradiation has been found simultaneously effective in reducing the pathogenic load of *Coliforms*, *Salmonella*, and viruses at doses up to 1kGy (Maruthi et al., 2013; Sampa et al., 2007). Antibiotic resistance genes and bacteria caused by the presence of antibiotics in water and are a risk to human and animal health are also susceptible to direct damage by radiation and indirect damage by $\bullet\text{OH}$ radicals (Chu et al., 2021; Shen et al., 2019).

The limitation of EB processes use is a limited water penetration (from 1 to 5 cm, depending on beam energy) of the beams that necessitate the design of delivery systems to overcome this drawback (Trojanowicz et al., 2020). Similarly, gamma ray radiation requires longer exposure times for doses comparable to e-beam, regular replacement of radionuclides, and the persistent

potential risk of radiation contamination (Pai and Wang, 2022). Naturally occurring compounds (e.g., O_2 , HCO_3^- , CO_2^- , Cl^- , NO_2^- , NO_3^- , DOC) present in wastewater affect the process efficiency or require a higher energy input due to their radical scavenging action. The presence of NO_3^- inhibits the removal of antibiotics such as norfloxacin, tetracycline, and ciprofloxacin due to the ease with which NO_3^- reacts with $\cdot OH$, e_{aq}^- and $\cdot H$ therefore reducing their availability (Zhuan and Wang, 2019). Notwithstanding, electron beam accelerators have been applied for off-gases, wastewater treatment, and biological sludge from wastewater treatment plants (Chmielewski and Han, 2017, 2016). Additionally, electron accelerators have been used to treat non-biodegradable emulsifier “nekal” (in Russia). and textile-dyeing wastewater (China) (S. Wang et al., 2022).

Electron beam radiation differs from gamma radiation with respect to dose rates and penetration. Additionally, it's considered safer and cheaper, requiring reduced inventory, flexibility in dose changes, lower material degradation therefore reduced product damage, uniformly controlled dose for precise dose delivery with no shielding from other products, non-radioactive source therefore no security, transportation / on-off technology, and re-sourcing of radionuclide is not required from depletion of radioactive cobalt. Energetic electrons produced by the accelerator propagate the treatment process by modifying the physical and chemical properties of the material it traverses. The ratio of energy given to the material per unit length (LET) is higher than that of gamma rays. The absorbed dose rate is very large since the electron beam has directivity to the direction of acceleration. Reaction control, operation, and maintenance can be performed easily as the electron accelerator is an electromechanical system. Electron beams have been used for medical equipment sterilization, water treatment, food preservation, material (polymer) modification, and pollution mitigation. Table 1.1 provides an overview of some of the differences between electron beam and gamma irradiation.

Table 1.1 Pros and Cons of gamma radiation and electron beam radiation processing methods

Parameter	Gamma irradiation	Electron beam
Irradiation doses	Low to medium. Cannot be quickly adjusted because of low dose rates	Medium to high. Quickly adjustable because of higher dose rates
Processing time	Longer time >24hrs	Shorter time <8mins for low doses
Operation	Cannot be turned off. Gamma radiation released isotropically	Can be turned off. The electron beam can be directed
Penetration	High penetration capability for all material types	Low penetration dependent on the density
Eco-Friendliness	Radioactive material requires disposal and regulatory control. Low eco-friendliness	Uses electricity to generate electrons; High eco-friendliness
Operation Cost	Low. Requires replenishment of gamma source and disposal	Low. Greater demand for electricity compared to gamma source
Capital Cost	Medium. Depends on the cost of radioactive sources, and the installation of control systems, infrastructure, and operations	The high initial cost of installation and infrastructure compared to gamma

Energy and current are principal characteristics of electron beam accelerators. Predominantly, 0.15 to 10 MeV energy ranges of electron beams are used for processing. Low energy electrons of 0.15 to 0.5 MeV are used in the treatment of surfaces, irradiation of coatings and polymeric films, and high energy beams (5-10 MeV) are used for sterilization of medical products and processing treatment of food (Ozer, 2017). Table 1.2 shows the properties of available radiation sources.

Table 1.2 Properties of common radiation sources (Trojanowicz et al., 2017)

Radiation Source	Energy (kW)	Dose rate (MGyh⁻¹)
X-ray		
250kV	5×10^{-9}	1.8×10^{-5}
⁶⁰Co γ source		
5×10^5 Ci	1.8×10^{-5}	0.65
1.0×10^6 Ci	0.36	1.30
Electron accelerators		
1mA, 1MeV	2	7.2×10^3
10mA, 10MeV	100	3.6×10^5
50mA, 10MeV	500	1.8×10^5

Variables i.e., absorbed dose, electron beam energy, depth of penetration, and line speed determine the control of the process to predict the production and quality of the product. Different absorbed doses are a prerequisite for the efficacy of different applications. Similarly, electron beam energy determines the penetration depth which is also dependent on the density of material being irradiated. Line speed shows the processing rate of the material under the beam. Electron accelerator types used for industrial applications are high voltage direct current, microwave, and radio frequency systems.

The cocktail of pollutants in wastewater makes it difficult for biological treatment and conventional waste water treatments to efficiently remove them. The cost of any treatment system, resulting in degradation intermediates and efficiency highly impacts the adoption of technologies. Combinational treatment has been proposed and researched by scientists ranging from reverse osmosis (RO) filtration with biodegradation (Hylling et al., 2019), chemical oxidation and biological treatment, UV or chlorine treatment, thin films on oxide substrates (Miao et al., 2019), ultrasound and photocatalysis, sonication and photocatalysis.

1.3. Scope of the Study

Halogenated organic compounds many of which are toxic are used in refrigeration, pesticides, solvents, and pharmaceuticals (Wu et al., 2009). Chlorinated emerging organic pollutants pose a substantial threat to the ecosystem as well as a challenge in their removal from wastewater by conventional wastewater treatment methods (Kimura et al., 2012; Makarov and Ponomarev, 2018). Additionally, nitrogen-containing compounds are of concern in wastewater treatment due to eutrophication, algal blooms, bacteria growth, and increased biological oxygen demand (Klare et al., 1999). N-heteroaromatics are also considered toxic, mutagenic, carcinogenic, and of concern when they contaminate surface and ground water (Nicolaescu et al., 2003). Furthermore, pharmaceutically active compounds, due to their pharmacokinetics and properties are of environmental interest.

Quinoline (Fig.1.1), consists of a benzene ring fused to a pyridine ring and was first isolated from coal tar and therefore occurs naturally. More importantly, quinoline derivatives are used in antiseptics, pharmaceuticals (i.e. chloroquine (CQ) and hydroxychloroquine (HCQ)), dyes, paints, insecticides, fungicides, and herbicides. Quinoline and its derivatives are recalcitrant, bio-accumulative, toxic, and persistent. CQ and HCQ have been detected in surface water, ground water, domestic wastewater, and the recent influx of the drug during Covid 19 period (Morales-Paredes et al., 2022) although their efficacy in SARS-Covid 19 treatment faced challenges (Aljadeed, 2022; Manivannan et al., 2021). The nitrogen atom in the cyclic ring of quinoline increases hydrophilic tendencies therefore the potential for quinoline and its derivatives (i.e., CQ and HCQ) persistence in the aquatic environment. In wastewater streams, quinolines have been removed with >80% efficiency. However, due to their strong sorption properties and poor degradation, they are more persistent in sewage sludge. The application of sewage sludge to soils provides a route for these pharmaceuticals into the terrestrial environment (Dorival-García et al., 2013).

This study investigated the degradation of selected chlorinated quinoline derivatives; CQ and HCQ (Fig 1-1) that have been used as pharmaceuticals under electron beam irradiation. CQ and HCQ are predominantly antimalarial prophylaxis alongside other indications i.e. inflammatory arthritis, systemic lupus erythematosus (quinacrine), rheumatoid arthritis (RA), dermatological, immunological, cancerous, and infectious diseases (Al-Bari, 2014).

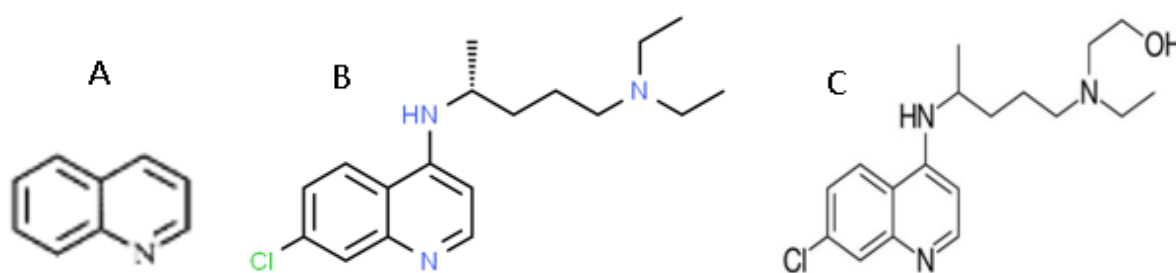


Fig. 1-1 (a) Quinoline, (b) CQ and (c) HCQ

The resistance of the pathogens *Plasmodium falciparum* and *Plasmodium vivax* to CQ prophylaxis led to disuse in affected areas. However, CQ analogs are still widely used in the prophylactic treatment of malaria. CQ analogs are water soluble and almost completely absorbed from the gastrointestinal tract. They have strong affinities for blood constituents and bind to plasma proteins and several body tissues during therapeutic administration. Excretion is therefore slow and it's excreted in small amounts in bile, sweat, and saliva, but majorly via the renal system where urine pH affects its elimination. It can either be excreted as N-desethylchloroquine or altered. HCQ differs from CQ only by a hydroxyl group and is 3-fold less toxic. HCQ is excreted from the body through the renal system where 23-25% of the compound is unmodified. It's potentially persistent and bio-accumulative with a high solubility (86mgmL^{-1}) and production volume. Dabić, Babić & Škorić (2019) observed a minimal degree of hydrolytic degradation (<5%) of HCQ. Conventionally, hydrolytic degradation of 10% at 50°C corresponds to a half-life of approximately 30 days equivalent to the half-life of 1 year at

25°C implying that HCQ is stable and its fate in the environment and removal are worth investigating (Dabić et al., 2019).

The highly stable structures of CQ and HCQ and their low concentrations contribute to the challenge of their removal (Ferreira and Carvalho, 2023). HCQ and CQ were degraded (98.3%) under gamma irradiation in an aqueous solution (Bors et al., 1991; Boujelbane et al., 2022; Zaouak et al., 2022). Additionally, HCQ and CQ were degraded using membrane bioreactors, electrochemical oxidation, and photodegradation. To the best of our knowledge, no extensive work has been reported on their degradation under electron beam radiation. Additionally, these compounds only have a slight difference in structure and would provide insight into how variations in structure would affect degradation.

1.4. Objectives of the Study

The main aim of this research work is the development of radiation-induced pathways for the destruction of halogenated EOPs. This objective will be achieved through the following objectives;

1. To study the degradation of CQ and HCQ under electron beam radiation technology.
2. To investigate the influence of different parameters (dose, dose rate, pH of the solution, anions, etc.) on the degradation efficiency of CQ and HCQ
3. To identify the products of CQ and HCQ degradation following EB irradiation.
4. To investigate suitable methods for improving the efficiency of the treatment of CQ and HCQ under EB treatment
5. To develop a numerical simulation of CQ and HCQ degradation to elaborate the degradation mechanism.

CHAPTER TWO

2. Literature Review

Pure fresh water is necessary for human health and socio-economic activities. Unfortunately, the upsurge in population density makes water intake and sewage discharge points closer to each other resulting in poor-quality water treatment that threatens human health and the environment. Despite existing regulations of water purification and measures to improve treatment systems around the world, the biological and chemical pollution of fresh water bodies is steadily increasing. Society is facing serious environmental problems caused by the critical condition of water sources and the risk of foreseeable water pollution via unplanned wastewater discharges exacerbates water-related emergencies (Ponomarev and Ershov, 2020).

Prescribed water remediation technologies while retaining economic attractiveness, provide desired versatility in eliminating undesired constituents. Non-ionizing radiation (UV) and ionizing radiation i.e., gamma rays from ^{60}Co or ^{137}Cs , and electron beams from an accelerator are researched and utilized in wastewater treatment. Radiation processing offers a cost-effective and exceptionally efficient treatment process capable of achieving the desired water quality by removing chemical and biological contaminants (Jan et al., 2015). The utilization of radiation to change the properties of materials it traverses through is the basis of radiation processing. Heat and chemicals have conventionally been used to modify materials. Alternatively, radiation requires less energy to effect similar chemical changes in materials (Hossain et al., 2018). Ionizing and non-ionizing radiation are extensively researched to understand the removal of impurities, BOD, COD, color, pH, elemental composition, inactivation of microbes such as coliforms and pathogens, and the degradation of natural, and synthetic chemicals while retaining economic feasibility.

2.1. Removal technologies of emerging pollutants

Different methods are developed, researched, improvised, and implemented to meet the need for techniques for water treatment that result in the desirable quality of drinking water or discharged wastewater. These techniques vary from the conventional constructed wetlands to advanced oxidative processes and membrane technology. A brief overview of the applications of these methods in dealing with the problems of EPs is discussed. Additionally, Table 2.1 provides an overview of the applications of various treatment techniques in eliminating pollutants.

2.1.1. Engineered wetlands and natural systems

Conventional surface water treatment plants (SWTPs) use coagulation by alum, ferric chloride, and/or synthetic polymers in combination with flocculation, sedimentation, filtration, and disinfection to process wastewater with exceptionally high removal of biological particles and pathogens with moderate removal efficiency for dissolved organic carbon (DOC) (Snyder et al., 2003). Constructed wetlands (CWs) are common ecological wastewater treatment technologies classified into surface flow, subsurface flow, and vertical flow CWs depending on the flow direction of wastewater. Absorption and degradation are the main physical-chemical processes taking place in the constructed wetlands. Adsorption is facilitated by the substrate, soil, and sediment in the packed beds of the CW. Roots stems, and leaves of plants within the CWs facilitate absorption. Microbial degradation, photolysis, and hydrolysis influence the degradation processes of EPs.

The removal efficiency of CWs is affected by treatment temperature, CW configuration, and plant species. However, optimization and the development of combined processes of CWs and other technologies are under study. Conventional treatments involving coagulation, sedimentation, and filtration remove less than 25% of most EDCs and PPCPs. Clarification

using ferric chloride (FeCl_3) as a coagulant removes 15% of the average concentration of organic contaminants (Rahman et al., 2009). Studies have also shown the removal of chemical oxygen demand, total Kjeldahl nitrogen, and total phosphorous (Vo et al., 2019).

2.1.2. Biological treatment Methods

Aerobic and anaerobic treatment methods are widely used as biological treatment methods for wastewater. Activated sludge, membrane bioreactors, and composting are some of the biotechnologies used in water treatment. Activated sludge utilizes biological coagulation, adsorption, and oxidation of sludge. However, temperature, pollutants present, and other factors may greatly affect its efficiency. The residence time and temperature impact the removal (Gani et al., 2019; Snyder et al., 2003). Higher composting temperature increases the degradation efficiency of the composting process (Yu et al., 2019). Sutherland and Ralph (2019) provided a review on microalgal bioremediation of chemicals of emerging concern (CECs) (Sutherland and Ralph, 2019). Bilal et al., (2019) presented a review on the removal of CECs by enzyme-assisted biodegradation (Bilal et al., 2019).

2.1.3. Mineral Surface Adsorption and Ion Exchange

Adsorption is a mass transfer process involving hydrophobic and electrostatic interactions with the adsorbent. Common adsorbents are activated carbon, silica gel, and activated alumina. Adsorption materials with high adsorption and low prices are in high demand. Carbon adsorption materials (CAMs) such as activated carbon (AC), carbon nanotubes (CNs), graphene, and biochar are also used for removing pollutants. Properties such as specific surface area, pore structure, pH, temperature, the dosage of adsorbent, interfering substances in water, charge, hydrophobicity, and surface functional groups impact their adsorption capacity. Hydrophobic interactions dominate the removal mechanism of most non-polar organic compounds in activated carbon adsorption systems. Alternatively, ion exchange interactions

result in the removal of polar solutes. Low temperatures reduced the adsorption of hydrophobic micropollutants, dissolved organic matter (DOM) in surface water, and micropollutants absorbed by activated carbon would exhibit competitive behavior; and a high dose of adsorbent and long adsorption time could promote the adsorption, but at the same time, it increases costs and energy demand (Nam et al., 2014).

The ability of activated carbon to remove compounds affecting the taste and odor of water is of interest. Powdered activated carbon (PAC) and granulated activated carbon (GAC) have shown 50-90% efficiency in laboratory-scale removal of antibiotics with reduced efficiency of between 10-20% in natural waters. However, GAC has very high removal of micropollutants during the first weeks but progressively, more strongly adsorbable constituents displace previously adsorbed compounds (Snyder et al., 2003). GAC is recommended by USEPA for the removal of endocrine-disrupting compounds such as methoxychlor, endosulfan, DDT, and polychlorinated biphenyls (Rahman et al., 2009). Powdered activated carbon (PAC) even though is less expensive, is more labor-intensive and less efficient than GAC (Najafpoor et al., 2019).

Coagulation potentially removes non-polar and molecular weight EPs either using coagulants or a combination. Mn^{3+} oxidation is a commonly used coagulant. Iron coagulation and sedimentation process combined with Mn^{3+} peroxidation (Mn^{3+} -C/S), hypochlorite peroxidation, and permanganate peroxidation are used in targeting acesulfame, carbamazepine, bisphenol S, and nano-ZnO (Ai et al., 2019; Yan et al., 2019). The removal of chemicals of emerging concern (CECs) using metal-organic framework nano adsorbents (MOF-NAs) under different water quality conditions, their synthesis, regeneration, and efficiency during water and wastewater treatment processes have been reviewed (Joseph et al., 2019).

2.1.4. Membrane technologies

Porous or nonporous membranes operating in pressure-driven, electric-driven, concentration difference-driven, and temperature-driven modes are extensively used to intercept pollutants. They are categorized as microfiltration (MF), ultrafiltration (UF), nanofiltration (NF), and reverse osmosis (RO) based on pore sizes (Liu et al., 2020). They are simple to operate and occupy small floor spaces with a desirably high pollutant removal rate with efficiency dependent on the membrane flux, pore size, hydrophobicity, and pollutant characteristics. Although Reverse osmosis (RO) and nanofiltration are effective for the elimination of EDCs and PPCPs, they are costly and brine disposal is a challenge (Rahman et al., 2009).

Nanofiltration (NF) and reverse osmosis (RO) membranes have a high rejection rate. However, NF membranes have lower operation pressure compared to RO membranes therefore more desirable for energy consumption. The membrane surface can assume certain charge orientations through functionalization. Negatively charged NF membranes have little affinity in separating heavy metals, bio-macromolecules, basic dyestuff, and multivalent cations while positively charged NF membranes such as the $\text{SiO}_2/\text{Y}_2\text{O}_3$ remove bacterial and viral pollutants. Others such as the hyperbranched polyethyleneimine (PEI) have given 90% removal efficiency for Cu^{2+} in wastewater in addition to organic ions and dyes (Wang et al., 2020).

Membrane bioreactors (MBR), combining microbial degradation and membrane separation are highly adaptable, easy to automate, and occupy small ground. However, they are expensive, and fouling restricts its application (Zhen et al., 2019). Electro-membrane bioreactors (EMB) use current on the membrane to reduce the fouling rate and improve the removal efficiency (Borea et al., 2019).

2.1.5. Chemical Oxidation

Chemical oxidation destroys the molecular structure, completely oxidizes, and decomposes some organic pollutants into stable, low-toxicity, or nontoxic substances by a redox reaction. Ozonation, advanced oxidation, and electrochemical oxidation are some of the processes used in chemical oxidation. Additionally, Cl_2 , ClO_2 , H_2O_2 , permanganate (MnO_4^-), and their combinations, such as UV/ O_3 , and UV/ H_2O_2 have been used in chemical oxidation (Gao et al., 2020). In drinking water treatment systems, Cl_2 , ClO_2 , and O_3 are commonly used for chemical oxidation, deodorizing, removing color, iron, manganese, and disinfection (Snyder et al., 2003). O_3 is a selective electrophile while $\cdot\text{OH}$ radical reacts less selectively (Rahman et al., 2009). Low utilization potential of O_3 , limited target pollutants, incomplete oxidation, or mineralizing pollutants are some of the challenges experienced. Catalysts and other oxidation technologies are used to overcome these deficiencies (Liu et al., 2020).

Advanced oxidation processes (AOPs) produce oxidizing free radicals such as $\cdot\text{OH}$ and $\text{SO}_4^{\cdot-}$, that mineralize some EPs into CO_2 , and H_2O or transform them into less toxic and easily biodegradable small molecular organics therefore reducing the COD and BOD in the treated effluents. Oxidation is achieved through exposure to photochemical, ionizing radiations, or chemicals (Abdel Rahman and Hung, 2020). AOPs have high efficiency, wide application range, and low secondary pollution. Fe^{2+} ion-activated persulfate/bisulfite could be a good process for the removal of pollutants with the added benefit of having a low activation energy, low cost, and high efficiency (Liu et al., 2020).

2.1.6. Electrochemical Oxidation

Electrochemical oxidation (EO) has high efficiency and good controllability for the removal of EPs. However, the production of degradation intermediates and electrode deactivation are some of its drawbacks. Both inert electrodes (i.e., IrO_2 , Pt, and RuO_2) and the active electrode (i.e.,

SnO₂, PbO₂, and boron-bearing diamond) are commonly used. Combined processes such as electro-Fenton oxidation, and photo-electro-Fenton oxidation improve the efficiency of EO. In addition, optimizing process parameters, electrolyte, voltage, and electrode are believed to improve efficiency (Liu et al., 2020). Electrochemical methods have high efficiency, relatively smaller equipment sizes, rapid startup, the ability to operate in ambient conditions, and minimal sludge generation (Mook et al., 2012).

2.1.7. Catalysis (Photolysis/Photocatalysis, Fenton Processes)

Photocatalytic degradation presents strong oxidation ability and mild reaction conditions influenced by pH, light source type, and catalyst properties. Graphene-based TiO₂/Ag composite (GTA) photocatalysts reduce the survival of antibiotic-resistant bacteria (ARB) and their antibiotic-resistance genes (ARGs) under simulated sunlight (Guo and Tian 2019). MnWO₄ nanorods anchored on g-C₃N₄ nanosheets (MnWO₄@g-C₃N₄) (S. et al., 2019), modified natural magnetite (Fe₃O₄-R400) and H₂O₂ (Serrano et al., 2020), photosensitizing catalysts incorporated into a chitosan carrier (PCICC) (Foszpańczyk et al., 2019), magnesium substituted Zn nano-ferrite (Zn_{1-x}Mg_xFe₂O₄) (Dhiman, 2021), BiOCl catalyst under UV-B light (al Sarihi et al., 2019), modified carbon nitride (CN) photocatalyst, Fenton and photo-Fenton process, enzyme catalysis, microalgae–bacteria (MB), purple phototrophic bacteria (PPB) consortia, Piezoelectric catalysis, Ag-doped graphitic carbon nitride (g-C₃N₄) material, cobalt (Co) doped TiO₂ have been developed to degrade a sleuth of EPs in aqueous solutions. Research is ongoing to address various drawbacks in photocatalysts ranging from poor conductivity and wide band gap (3.2 eV) experienced with TiO₂ and its predisposal to absorb UV $\lambda < 387\text{nm}$ with no photocatalytic activity in the visible light spectrum (Liu et al., 2020). UV irradiation has been reported to induce photo adduct formation, photo-oxidation, photo rearrangement, photocyclization, decarboxylation, and dehalogenation that cause photodegradation of fluoroquinolones (Kawabata et al., 2013).

Most of the methods mentioned utilize a passive phase transfer of pollutants apart from biological treatment, chemical oxidation, catalysis, and electrochemical methods that produce reactive moieties that react with pollutants present in wastewater and transform them into labile species. However, the toxicity of some chemical pollutants would hinder biological processes whereas most chemical processes would likely cause secondary pollution due to an influx of the chemical reagents utilized. Additional cost implications in acquiring the oxidants along with the huge volumes of reactants impede the practical applications of these methods. Table 2.1 showcases some methods that have been used in the removal of various substances of interest in water.

Table 2.1 Wastewater treatment methods used in the treatment of pharmaceutically active compounds

Method	Conditions	Efficiency	Comments	Reference
Engineered wetlands and Natural systems				
CW	Diclofenac, ibuprofen, benzafibrate, carbamazepine sulfamethoxazole	<10% except for diclofenac (66%)		(Rahman et al., 2009)
VF-CW	Acetaminophen	Removal of COD, TKN, and total phosphorous		(Vo et al., 2019)
VF-CW (sand filter; growth of coracoid conch)	Ibuprofen caffeine	89% 97%	Earthworms in VF-CW had little effect on the removal efficiency	(de Oliveira et al., 2019)
CW	Ethinylestradiol,	9-100%		
CW-GS		Ethinyl estradiol and BPA were removed well by CW-GBCF	CW-GWH was the best for removing levonorgestrel.	(Campos et al., 2019)
CW-GWH	Levonorgestrel			
CW-GBCF	bisphenol A,			
Biological treatment Methods				
Activated sludge		92 to 98%		
	Diethylhexyl phthalate	30 % decrease in temperature (42 to 13°C) reduced the removal rate	Increased residence time improved the removal	(Gani et al., 2019; Snyder et al., 2003)
Sterilized/non-sterilized chicken manure.	Tetracyclines.	Temperature-dependent thermal degradation	Higher temperature increases composting efficiency.	(Yu et al., 2019)
<i>Pseudomonas aeruginosa</i> KS2002	Triclosan	>99% transformation of toxic to 2,4-dichlorophenol		

Method	Conditions	Efficiency	Comments	Reference
Activated sludge and ionizing radiation	Oseltamivir, aspirin, and ibuprofen at 5mM	100% (4 hours)		
	Carbamazepine, ketoprofen, mefenamic acid, clofibric acid, and diclofenac	not biodegraded completely after 8 hours,	Eliminated by γ -ray irradiation at 2kGy.	(Kimura et al., 2012)
Hyperthermophilic composting	Tylosin antibiotic fermentation residues	95.0%	Above 60°C for at least 6 days.	(Liao et al., 2019)
	ARGs, flow genes,	75.8%		(Duan et al., 2019)
	Mobile genetic elements	98.5%		
Microalgae bioremediation	BPA and tetracycline	100%	Photolysis and hydrolysis	(Xie et al., 2020)
<i>Chlamydomonas</i> sp. (Tai-03)	Sulfamethoxazole	20%	Toxic transformation intermediates	

Mineral Surface Adsorption and Ion Exchange

α -, β -, and γ - CEWICs	Atrazine	Efficiency increased in the order α - > β - > γ - in 1 hr		(Morin-Crini et al., 2018; Romita et al., 2019)
Powdered activated carbon	Sulfamethazine, trimethoprim, dimethyl carbonate	Removal efficiency between 81% to 98%		(Gao et al., 2020)
Natural zeolite modified using 13.56 MHz radio frequency-driven plasma discharge in argon	Diclofenac sodium (DS)	64% adsorption rate 52% unmodified zeolite		(Garcia et al., 2019)

Method	Conditions	Efficiency	Comments	Reference
Gemini surfactant-modified montmorillonite (GSMM)	1H-benzotriazole (BTA), 5-methyl-1H-benzotriazole (TTA), and 1-hydroxybenzotriazole (HOBT)) and Cu ²⁺	Simultaneous removal of Cu ²⁺ Adsorption efficiency order TTA > BTA > HOBT.	pH influenced Adsorption and was optimal at pH 5	(Li et al., 2019)
Microporous aluminum pillared clay (MAPC) with montmorillonite as raw materials	Imipramine (59.8mg/L) Amoxicillin (7.7mg/L)	Adsorption efficiencies of 332% and 681% higher than natural clay respectively	Specific surface area of 258 m ² /g and a porosity of 0.16 cm ³ /g	(Chauhan et al., 2020)
A magnetic adsorbent derived from <i>Broussonetia papyrifera</i> leaves (MA-BPL).	Methylene blue	187.97mg/g at 288K for a monolayer.	Adsorption was spontaneous, exothermic, and pseudo-second-order kinetics, and Langmuir isotherm model	(Liu et al., 2020)
Reduced graphene oxide (RGO) and graphene oxide (GO).	Tetracycline, oxytetracycline, and chlortetracycline	GO Adsorption chlortetracycline > tetracycline > oxytetracycline, RGO tetracycline > chlortetracycline > oxytetracycline.	low pH value is beneficial to the adsorption of the three tetracyclines on GO and RGO.	(Ai et al., 2019)

Method	Conditions	Efficiency	Comments	Reference
Fe₃O₄/graphene oxide/citrus peel-derived biochar-based nanocomposite (mGOCP)	Ciprofloxacin Sparfloxacin	Adsorption efficiency of 283.44 and 502.37 mg/g respectively.	High surface area of 1,556 cm ² /g	(Zhou et al., 2019)
Activated Carbon (AC)	Caffeine, chlorofibric acid, diclofenac, gallic acid, ibuprofen, and salicylic acid		Pseudo-second-order linear reaction achieving equilibrium in 40 mins	(Álvarez-Torrellas et al., 2016; Gil et al., 2019; Yao et al., 2014)
Nanomaterials such as graphene oxide (GO)	Antibiotic resistance genes Ciprofloxacin	>50% 29% to 43%	γ -Al ₂ O ₃ dosage from 0.33 to 0.78 g/L	(Najafpoor et al., 2019)
Mn³⁺-C/S	Dissolved organic carbon Total nitrogen EPs	72.9%, 31.74% 21.78–93.49%	Advantageous over hypochlorite peroxidation and permanganate peroxidation,	(Ai et al., 2019; Yan et al., 2019)

Membrane Technologies

Microporous membrane doped with microporous β -cyclodextrin polymer	Bisphenol A	>99.9% at 300 Lm ⁻² hr ⁻¹ water flux and 50mg/L feed conc.	Regenerated membrane by ethanol filtration	(Wang et al., 2019)
Olive pomace (OP) and olive solid wastes/chitosan composite (OSW/CC)	Tetracycline	Adsorption of 16 and 1.6 mg/g, respectively		

Method	Conditions	Efficiency	Comments	Reference
Melanin-covered Escherichia coli in a membrane bioreactor (MBR)	CQ 0.1mM influent	98% removal of CQ (20 hours) 10g/L cell loading	Melanin has an affinity for phenothiazine, aminoquinolines, and fluoroquinolones	(Lindroos et al., 2019)
Chitosan extracted from shellfish waste	Amoxicillin diclofenac carbamazepine		High current density improves removal efficiency	(Borea et al., 2019)
Chitosan extracted from shellfish waste	Ketoprofen Diclofenac	>90% absorption	Pseudo-second-order kinetic model and pH-dependent Depends on concentration.	(Rizzi et al., 2019)
Chemical Oxidation				
Catalytic ozonation	Ciprofloxacin	93% in Synthetic wastewater 14-41.2% in real wastewater	pH 5.25 to 9.5	(Najafpoor et al., 2019; Nemat Sani et al., 2019)
Chlorination	The oxidation of reduced inorganic species such as Fe(II), Mn(II), and S(-II).		Free Cl ₂ was predicted to produce chloramines in the presence of NH ₃ ,	(Snyder et al., 2003)
AOPs	Carbamazepine, ciprofloxacin, and ibuprofen	80%–100% and 89%–100%.	20 min for real urban wastewater, neutral pH, 20°C, and different H ₂ O ₂ concentrations	(Rahman et al., 2009)
Palladium/iron nanoparticles	Hexa-bromo-cyclo-dodecane (15mM)	99% removal efficacy in aqueous solution (1g/L in 9hr)	Humic acids improve debromination	(Le et al., 2019)

Method	Conditions	Efficiency	Comments	Reference
Magnetic porous sulfurized Fe_2O_3 (PS- Fe_2O_3) to activate persulfate monoester (PMS)	Atrazine.	100% at neutral and slightly alkaline conditions	Performance better in neutral conditions by PS- Fe_2O_3 than the unmodified Fe_2O_3 . $\text{SO}_4^{\cdot-}$ play lead. Cl^- , HCO_3^- , NO_3^- , and HA inhibits the removal	(Zheng et al., 2019)
$\text{CeO}_2\text{-Fe}_3\text{O}_4$ (CF) nanocomposites to activate peroxymonosulfate	Synthetic dye Direct Red 16 (DR16).	In neutral pH (7.0), DR16 is removed after 25 minutes at a CF loading rate of 0.3g/L.	Fulvic acid, bicarbonate ion, and sodium dodecyl sulfate inhibit the CF-peroxymonosulfate system.	(Ghanbari et al., 2019)
Electrochemical Oxidation				
Flow reactor with boron-doped diamond (BDD) anodes	Ciprofloxacin 100 ppm	100% removal in 20 minutes BDD anode with the least doping. current density of 30 mA/cm^2 , pH of 10, flow rate of 2.5 L/min	Degradation influenced by pH, flow condition, and current density	(Wachter et al., 2019)
Electrochemical photocatalysis on titanium meshes with TiO_2 coating with an electrical polarization (bias) applied to the catalyst.	Carbamazepine	UV/supported TiO_2 + bias > UV/ TiO_2 Degussa P25 > UV/supported TiO_2 > UV.	TiO_2 + bias + UV treatment had more efficiency than TiO_2 + UV or UV	(Murgolo et al., 2019)
EO-BDD coupled with UV radiation and sonication. EO.	HCQ 36-250mg/L CQ 36-250mg/L	100% Anode current densities influenced Acidic, slightly acidic, and neutral pH	Lower concentrations had faster rates of elimination.	(Bensalah et al., 2020; Midassi et al., 2020)

Method	Conditions	Efficiency	Comments	Reference
Catalysis (Photolysis/Photocatalysis, Fenton Processes)				
Photo-catalytic degradation using TiO ₂ as the catalyst and 125W	Amoxicillin	90%	10 mg/L, pH 7.6, TiO ₂ dosage of 563 mg/L, and treatment time of 150 min	(Chinnaiyan et al., 2019)
	Metformin hydrochloride	98% >60% mineralization		
PPMP	Rhodamine B	63.2%–98.43%		(Liu et al., 2020)
Photodegradation by sunlight.	Acetaminophen (AA), dapsone (DP), raloxifene (RL), phenytoin (PH), dexamethasone (DX), amiodarone (AM), indomethacin (IM), naproxen (np) and sulindac (sl)	AM, DP, and DX attained 100% removal while others 50%. UV-C completely degraded all the pharmaceuticals	Except for AA, IM, and PH, all the pharmaceuticals were susceptible to UV-A photodegradation. AA and PH are not degraded by UV-B.	(Kawabata et al., 2013)
Heterogeneous TiO ₂ /β-Bi ₂ O ₃ synthesized by hydrothermal method	HCQ.	91.89% HCQ degradation after 120 min 6 cycles of catalyst, 70.59% degradation	B-Bi ₂ O ₃ nanoparticles improve visible light absorption of TiO ₂ photocatalyst	(Kargar et al., 2021)
Simulated solar irradiation in Milli-Q water and spring water	HCQ	Photolytic degradation with half-lives of 5.5h and 11.6h	Faster degradation promoted at higher PH values	(Babić et al., 2017)

***ARG**- Antibiotic-resistant Genes, **CEWICs** -cyclodextrin-epichlorohydrin water-insoluble copolymers, **EO-BDD**- Electrochemical oxidation using boron-doped diamond, **CW**-Constructed wetland, **CW-GBCF**- Constructed wetland fragrance cultivation, **CW-GS**- Constructed wetland with gravel sand, **CW-GWH**- Constructed wetland with gravel water hyacinth, **PPMPs**-Polypyrene microspheres, **VF-CW**- Vertical flow constructed wetland

2.2. Application of ionizing radiation in water treatment

Ionizing radiation such as electromagnetic gamma, high energy electrons, charged particles, and neutrons are studied for applications in water treatment technologies. Gamma rays and

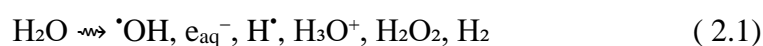
electron beam irradiations are preferred because of their properties, source availability, and economic and safety concerns. Gamma rays are appealing in terms of penetrative capability in aqueous solutions. However, their operation requires more specialized radiation protection for personnel and delivers smaller dose rates compared to electron beams (Trojanowicz, 2020). Electron beam technologies have been used in the modification of polymer products, molecular cross-linking of cable insulation, tire manufacturing, sterilization of medical devices, and curing of coatings (Ponomarev, 2020b). Radiolysis of water using fast electrons with energy in the MeV range ($1 \text{ eV} = 1.602 \times 10^{-19} \text{ J}$) is the most practical and fastest method of water treatment. This creates high concentrations of radicals that can neutralize and disinfect contaminants in the aquatic environment. The mode of action of radiolysis involves the transfer of energy from radiation to the substrate. The absorbed dose (the energy transferred to a unit of mass $1 \text{ Jkg}^{-1} = 1 \text{ Gy}$); absorbed dose rate (increment of the absorbed dose per unit time Gys^{-1}); and radiation chemical yield (G-Value the number of molecules formed or destroyed because of the absorption of radiation energy $1 \mu\text{mol J}^{-1} = 0.1036 \text{ molecules per } 100 \text{ eV}$) are essential parameters.

EB provides extra-large dose rates (10^3 and 10^6 MGyh^{-1}) efficient for treating copious volumes of liquids at large flow rates. Medium energy accelerators capable of producing electron energies ranging between 0.3 to 5 MeV with an average beam power of up to 200 kW are the most used in water treatment. The penetration of the electron is dependent on the energy of electrons; 4 mm for 1 MeV energy, while for 10 MeV about 5 cm in water. These parameters are essential for designing liquid flow in the irradiation chambers to accommodate a fast flow of treated liquid while maintaining efficient penetration by generated electrons (Trojanowicz, 2020). Radiolytic radicals present high reactivity, short lifetime, and ease of generation corresponding to the current trend to reduce the role of chemicals in water treatment and reduce the residual concentration of chemicals in purified water. Electron beam irradiation provides

higher processing rates, low temperature, and lower specific energy expenditure. In addition, it requires no catalysts, activators, or additives. EB can be directly used for processing and electron energy varies with power to match processing requirements to offer desired dose rates (Capodaglio, 2019, 2018; Hossain et al., 2018).

2.3. The theory of water radiolysis

Electron accelerators are relatively easy to use while at the same time delivering high power. Industrial accelerators generate hundreds of billions of accelerated electrons per second each of which subsequently produces tens of thousands of ionizations of water molecules. The radiolysis of water generates reactive oxidizing and reducing radicals regardless of the type of ionizing radiation used. These reactive species drive the neutralization process of dissolved pollutants (Ponomarev & Ershov 2020). Direct radiolysis of water-containing impurities is negligible and the chemical changes in the system take place due to the reaction of the reactive intermediates of water radiolysis. The radiolysis of water can be represented in summary by Eq. (2.1) below.



The yields of water radiolysis products are expressed in either unit of molecules/100eV or $\mu\text{mol}\cdot\text{J}^{-1}$ commonly referred to as the G-values (Buxton, 2001; Buxton et al., 1988; Sampa et al., 2007). The water radiolysis products and their corresponding radiation chemical yields are provided in Fig. 2-1.

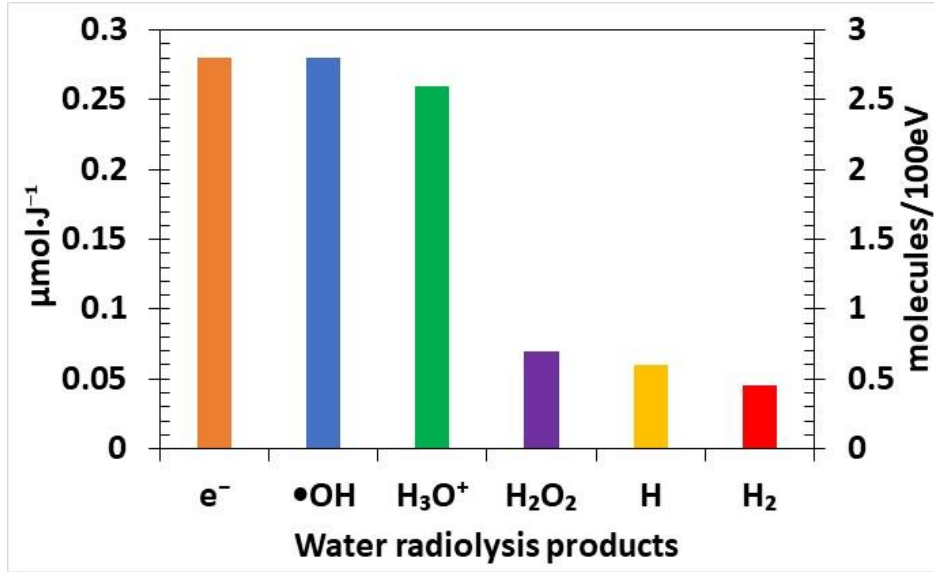


Fig. 2-1 Radiolytic yields (G-Values) of water radiolysis products

The initial radiation-chemical yield G of water decomposition is $1.24 \mu\text{mol J}^{-1}$ (12 molecules per 100 eV). The G -value is calculated according to Eq. (2.2) and Eq. (2.3).

$$G = \frac{\text{No. of molecules formed}}{100\text{eV}} \quad (2.2)$$

Conversely, it can be calculated as

$$G = \frac{C_D N_A}{D \times 1.602 \times 10^{19}} \quad (2.3)$$

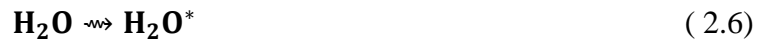
Where C_D is the concentration of a species at dose D and N_A is Avogadro's number. The approximate concentrations of the reactive species can be calculated using Eq. (2.4).

$$C_{RC} = D \times G_{\text{valueRC}} \quad (2.4)$$

Where C_{RC} refers to the reactive compound concentration [$\mu\text{mol/kg}$], D -applied dose [J/kg], and G_{valueRC} is the G -value of the reactive species. The formation of these reactive intermediates is preceded by a series of reactions following irradiation.

2.3.1. The Physical Stage

The initial interaction of radiation with water involves energy transfer to the system leading directly or indirectly to the formation of ionized water molecules ($\text{H}_2\text{O}^{\bullet+}$), pre-solvated electrons e^- (10^{-15}sec) (Eq. (2.5)), and excited water molecules H_2O^* (Eq. (2.6)).



However, excited state water molecules play a less significant role in radiolysis (Wojnárovits and Takács, 2016).

2.3.2. The Physicochemical Stage

The physicochemical stage (10^{-11}sec) establishes thermal equilibrium involving ion-molecule reaction, dissociative relaxation autoionization of excited states, solvation of electrons, and hole diffusion leading to the production of reactive primary species ($\cdot\text{OH}$, e_{aq}^- , H^\bullet), ions (H_3O^+) and molecular products (H_2 and H_2O_2). The radical cation, $\text{H}_2\text{O}^{\bullet+}$ migrates over a distance of a few water molecules by resonance electron transfer. However, $\text{H}_2\text{O}^{\bullet+}$ is a strong acid and gives a proton (proton transfer reaction) to one of the surrounding water molecules to form H_3O^+ and $\cdot\text{OH}$ (Eq. (2.7)).



Electrons ejected in the ionization process become thermalized and hydrated: The dry electron formed in Eq. (2.5) undergoes numerous collisions with the surrounding water molecules and loses its kinetic energy forming the hydrated (solvated/aqueous) electron (Eq. (2.9)).





The excited water molecule dissociates to $\bullet OH$ and H^\bullet (Eq. (2.11)).



Increments in the radiation dose lead to subsequent increases in the concentration of the reactive species but may be overestimated as the direct effect increases (Siwek and Edgecock, 2020; Wojnárovits and Takács, 2016). In highly contaminated environments the reactive species are hindered. The percentage contribution of each species to pollutant removal can be calculated by the relation;

$$C_x = \frac{k_x \times G_x \times 100\%}{k_x \times G_x + k_y \times G_y + k_z \times G_z} \quad (2.12)$$

Where $k_{x,y,z}$ are rate constants [$M^{-1} s^{-1}$] of reactions between the contaminant and the x,y,z reactive species; $G_{x,y,z}$ is the G values of x,y,z radical formation; and C_x is the x radical contribution in contaminant removal.

2.3.3. The Chemical Stage

The chemical stage consists of diffusion away from the point of origin and chemical reaction of primary species (e_{aq}^- , $\bullet OH$, $H_3O_{aq}^+$, and $\bullet H$), to the establishment of chemical equilibrium. It begins in the spur about 10^{-11} sec after the passage of the radiation and about 10^{-10} sec in the bulk of the solution. During the energy deposition following irradiation and in the subsequent fast reactions there is a high probability that two or more reactive species are created close enough to each other that they can mutually influence each other's subsequent reaction possibilities. This isolated space is called a *spur*. There is a competition between the reaction of intermediates in the spur and their diffusing out of the spur (spur expansion). The intermediates that escape the spur in the bulk become homogeneously distributed with respect

to solute molecules. Approximately 40% of the initially produced intermediates are consumed by spur processes. H_2 ($0.047 \mu\text{mol J}^{-1}$) and H_2O_2 ($0.073 \mu\text{mol J}^{-1}$) form and there is also some reformation of water molecules (Eq. (2.13)).



The chemical stage involves the reaction of the evolved reactive species with surrounding molecules simultaneously inducing oxidation and reduction reactions. Ionizing radiations generate high free radical yield per unit energy input (Jan et al., 2015). Natural water contains impurities in mgL^{-1} concentrations whereas concentrations in wastewater are in gL^{-1} . Direct ionization and excitation of water molecules is the predominant reaction. Pollutants are indirectly affected by radiolysis through reactions with the products of water radiolysis. More contaminated water may require a higher absorbed dose of radiation (Ponomarev and Ershov, 2020). It is generally accepted that increasing the temperature increases the primary yields of free radicals $G(e_{aq}^-)$, $G(\text{H}\cdot)$, and $G(\cdot\text{OH})$ while decreasing the molecular yield $g(\text{H}_2\text{O}_2)$. The temperature rise makes diffusion of free radical species out of spurs become more favored than recombination therefore resulting in less molecular recombination products (Meesungnoen et al., 2015).

2.4. Reaction of Radiolysis products

Water radiolysis generates both oxidizing ($\cdot\text{OH}$, $\text{HO}_2\cdot$, O , O^- , $\text{O}_2\cdot^-$, $\text{O}_3\cdot^-$, H_2O_2 , $\text{HO}_3\cdot$, etc.) and reducing (e_{aq}^- , $\text{H}\cdot$) products based on their respective redox potentials. These products contribute to the mineralization of pollutants and decrease toxicity by eliminating functional groups, such as $-\text{Cl}$, $-\text{NO}_2$, $-\text{SH}$, and others. The dissociative capture of an e_{aq}^- , removal of functional groups, the addition of radicals to double bonds, and decomposition of the conjugated bonds system along with oxidation and fragmentation of molecules play a role in the degradation of pollutants. Hydroxyl radicals ($\cdot\text{OH}$) are very reactive towards saturated and

unsaturated hydrocarbons, alcohols, ethers, and amines, which react via the abstraction of a hydrogen atom or the addition to a double bond (Ponomarev and Ershov, 2020). Conversely, e_{aq}^- slowly reacts with these compounds but is active in reactions with nitro and halogen derivatives of organic compounds. Therefore, $\cdot\text{OH}$ radical interacts mainly with hydrocarbon components, and e_{aq}^- predominantly interacts with heteroatom functional groups.

2.4.1. Hydrated/Aqueous electron

The e_{aq}^- is visualized as an excess electron surrounded by oriented water molecules and behaves like a normal univalent ion almost the same size as an iodide ion. It is assumed that it has a fully developed ionic atmosphere before it reacts but, in some instances, the electron may react with the solute before completing the formation of its ionic atmosphere in which case its reactivity with the solute is very high and it has a short half-life calculated by Eq. (2.14) before the reaction (Buxton et al., 1988; Draganic, 2012).

$$t_{\frac{1}{2}} = \frac{0.693}{\sum k_i C_i} \text{ sec} \quad (2.14)$$

k_i is the rate constant for the reaction between the *ith* species and the electron, C_i is the ionic concentration

The e_{aq}^- is a very reactive species with rate constants close to the diffusion-controlled values. The half-life of the electron, even in dilute solutions is very short (a few tens of microseconds) but depends on the presence of impurities in the solution. Molecular oxygen is a very efficient radical scavenger as evidenced by the production of H_2O_2 during radiolysis and H_3O^+ from dissociation of water. The concentration of e_{aq}^- also affects its lifetime: The higher the concentration, the shorter the lifetime, because the reaction of recombination is favored. Its standard reduction potential is -2.9 V and it reacts rapidly with species having positive reduction potentials. Its mode of reaction can be generally represented as the one-electron

transfer process. The rate constants of the e_{aq}^- range from $\sim 10^1 M^{-1}s^{-1}$ up to the diffusion-controlled limit with small activation energies in the range of 6-30 kJmol⁻¹ suggesting that the presence of a vacant orbital in the solute into which the electron can transfer is the dominant kinetic parameter. All e_{aq}^- reactions are electron-transfer reactions resulting in the primary product of the electron-transfer reaction acquiring an additional electron (Eq. (2.15)).



The primary product is thermodynamically unstable and undergoes further reactions such as protonation, dissociation, disproportionation, or charge transfer. A non-dissociative electron capture reaction e_{aq}^- is shown by Eq. (2.16).



another non-dissociative electron capture by an ion



Dissociative capture reaction is also characteristic of e_{aq}^-



The e_{aq}^- are powerful reductants that react with nucleophiles through an electron transfer process over distances greater than the encounter distance. It can react in its dry and presolvation state. In its reactions with organic molecules, it also acts as a nucleophile with reactivity-enhanced by electron-withdrawing substituents adjacent to the alkene double bonds or attached to the aromatic rings. The presence of substituent halogen molecules also increases reactivity by facilitating the elimination of the halide ion from the negative ion formed (Eq. (2.19)).



In reactions with organic molecules, e_{aq}^- reacts as a nucleophile (standard one-electron reduction potential $E^0(aq/ e_{aq}^-) = -2.9$ V). It reacts preferentially with low-lying vacant molecular orbital structures, such as aromatic hydrocarbons, conjugated olefins, carboxyl compounds, and halogenated hydrocarbons. Its reactivity is greatly enhanced by an electron-withdrawing substituent adjacent to the double bonds or attached to the aromatic rings. Increased reactivity is also observed when organic molecules contain substituent halogen atoms, in which case the negative ion forms and rapidly eliminates the halide ion. The e_{aq}^- reacts with many compounds that can release an anion by dissociative electron capture; these reactions can occur only when single bonds are involved in the process. Compounds with high electron affinity (e.g., nitro- and cyano-derivatives) react with e_{aq}^- with diffusion-controlled rate constants of $2.59 \times 10^{10} \text{ M}^{-1} \text{ s}^{-1}$ with the formation of the corresponding radical anions. The rate constants with aldehydes and ketones are $4.9 \times 10^9 \text{ M}^{-1} \text{ s}^{-1}$. The electron is accommodated on the carbonyl carbon. The e_{aq}^- rate constants for the reactions with carboxylic acids, esters, and amides are in the order of $10^7 \text{ M}^{-1} \text{ s}^{-1}$. Simple olefins do not react with e_{aq}^- at appreciable rates, but compounds with extended p-electron delocalization react rapidly with the e_{aq}^- . The k_{e^-} values of maleates and fumarates, which contain conjugated double bonds (e.g., $\text{O}=\text{C}(\text{OH})-\text{HC}=\text{CH}-\text{C}(\text{OH})=\text{O}$), are in the range of diffusion controlled-limit (Wojnárovits and Takács, 2017, 2016).

2.4.2. Hydrogen

The hydrogen atom was initially considered the only reducing species in water radiolysis but two kinds of reducing species were later found present in irradiated water. Hydrogen is a minor reducing radical and less powerful than e_{aq}^- in a neutral solution while in an acidic solution, it can act as an oxidant. The hydrogen atom is the conjugate acid of e_{aq}^- and the major reducing species in an acidic solution. At the beginning of the chemical stage of radiolysis, the amount of H atoms is substantially less than that of e_{aq}^- (very likely by a factor of 5), and their reactivity

is in general considerably weaker. In dilute acidic solutions, the reaction below readily occurs (Eq. (2.20)):



With a reduction potential of -2.3V, the hydrogen atom is a slightly less powerful reducing agent than e_{aq}^- . Generally, the G_{H^\bullet} is ~ 0.6 , independent of pH. The interaction of radiation with water leads to the production of excited water molecules that may undergo dissociation to produce atomic hydrogen (Eq. (2.11)): Increasing the concentration of an efficient scavenger for e_{aq}^- or H_3O^+ reduces the reaction and decreases G_{H^\bullet} . The conversion of hydrogen atoms into e_{aq}^- (Eq. (2.21)) is quite slow compared to the fast conversion of e_{aq}^- into H^\bullet but the reaction is very important in alkaline solutions



In strongly acid media we consider the reaction below (Eq. (2.22)) which is very slow



Whereas the e_{aq}^- reacts with water very slowly ($k = 16M^{-1}s^{-1}$). The H^\bullet atom reduces inorganic ions having more positive reduction potentials than itself, but often at slower rates than e_{aq}^- (Eq. (2.23)).



Additionally, the abstraction of hydrogen from organic molecules in the reaction produces molecular hydrogen (Eq. (2.24))



It also adds to centers of unsaturation (Eq. (2.25)).



2.4.3. Hydrogen Peroxide

In hydrogen-saturated solutions, the $\mathbf{H^{\bullet}}$ atom is produced via the reaction

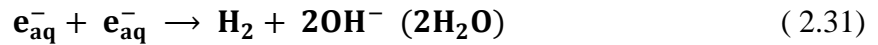


The $\mathbf{H^{\bullet}}$ atom reacts faster with $\mathbf{O_2}$ than with $\mathbf{H_2O_2}$ (Eq. (2.27) to Eq. (2.30)).

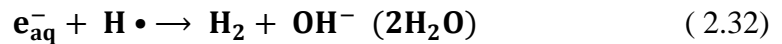


2.4.4. Molecular Hydrogen

The $G_{H_2} \sim 0.45$ irrespective of pH and decrease with increasing concentration of $\mathbf{e_{aq}^-}$ scavengers. The origin of the primary molecular hydrogen may be sought, in the recombination (Eq. (2.31)).



And additionally in the reaction in Eq. (2.32)



but to a lesser extent. The extent of recombination of H atoms is also small (Eq. (2.33)).



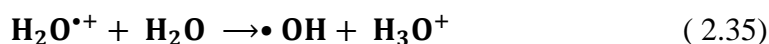
Therefore, from these reactions, a sufficient increase in the concentration of an efficient scavenger (S) for e_{aq}^- must lead to a decrease in G_{H_2} .

2.4.5. Hydroxyl Radical

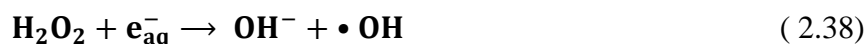
The $\bullet\text{OH}$ radical is a powerful oxidant. The standard reduction potential value $E^\circ = -2.8$ V for the pair $\bullet\text{OH}/\text{OH}^-$ at the acidic solution ($[\text{H}^+] = 1\text{M}$) implies that $\bullet\text{OH}$ can oxidize all inorganic ions existing in higher valence states via a simple electron transfer (Eq. (2.34)).



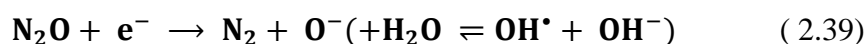
However, oxidation is dependent on the behavior of other primary and secondary radicals present (H^\bullet , e_{aq}^- and HO_2^\bullet) under given conditions. The $\bullet\text{OH}$ radical is produced via Eq. (2.35) and Eq. (2.36).



Additionally, $\bullet\text{OH}$ radicals are produced by the reactions of primary reducing species with H_2O_2 (Eq. (2.37)).



Certain conditions can be introduced in the radiolysis of water such as the addition of N_2O which converts e_{aq}^- into $\bullet\text{OH}$ radicals (Eq. (2.39)).



The $\bullet\text{OH}$ radical oxidizes inorganic ions and reacts with organic molecules. Electron transfer is the most frequent mechanism of OH-induced oxidation of both inorganic anions and cations.

The $\bullet\text{OH}$ radical adds to centers of unsaturation, abstracts the H atom from C-H bonds, and OH addition when reacting with organic molecules (Draganic, 2012). Addition reactions also occur with free radicals. It is more reactive and less selective than the hydrogen atom because of its greater exothermicity. Electron transfer reactions may give rise to a stable product e.g. oxidation of the ferrous ion to the ferric ion (Eq. (2.40)).



In reactions with anions, electron transfer leads to the formation of a free radical (Eq. (2.41))



Where X^- is a halide ion and X^\bullet is the corresponding halide radical Cl, Br, or I. Hydrogen abstraction from an organic molecule can be generally represented by Eq. (2.15).



R represents atomic hydrogen or a functional group. In aqueous solutions of benzene, the addition reaction of the $\bullet\text{OH}$ radical occurs to give the hydroxy-cyclohexadienyl radical in a fast, irreversible reaction at room temperature ($k_{2.43} = 7.8 \times 10^9 \text{ M}^{-1} \text{ s}^{-1}$) (Eq. (2.43)). In the presence of oxygen, the hydroxy-cyclohexadienyl radical is converted into the cis- and trans-isomers of the hydroxycyclohexadienyl peroxy radicals (Pan et al., 1993; von Sonntag and Schuchmann, 2001).



Not only addition reactions to stable molecules but also to free radicals are possible. In aqueous solutions at high electron dose rates, the following reaction in Eq. (2.44) takes place



In acid medium ($0.02 \text{ M H}_3\text{O}^+$) the product obtained has a half-life of 2 sec, which decreases with the change of pH. The disappearance of H_2O_3 can be represented by Eq. (2.45).



There is no evidence that the $\bullet\text{OH}$ radical reacts with oxygen. However, the addition of the $\text{O}^{\bullet-}$ ion radical to O_2 can take place (Eq. (2.46)).



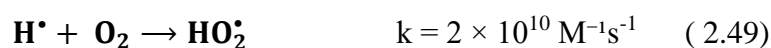
The $\bullet\text{OH}$ radical induces the degradation of organic molecules in water treatment by ionizing radiation and Advanced Oxidation Processes (AOP). The $\bullet\text{OH}$ may react either by direct electron transfer, abstraction of H-atoms from C–H bonds, or by addition to the double bonds. However, direct electron transfer is rarely observed and often involves intermediate complexes. The rate constants of H-atom abstraction reactions are generally in the 1×10^7 – $1 \times 10^9 \text{ M}^{-1} \text{ s}^{-1}$ range. The reactions take place with a considerable selectivity and the rates increase in the order primary < secondary < tertiary H-atom. Due to its electrophilic nature, $\bullet\text{OH}$ reacts readily with C=C and C=N double bonds, but not with C=O double bonds, which are electron-deficient at the carbon atom where the $\bullet\text{OH}$ radical prefers to add. In aromatic compounds, electron-donating substituent directs $\bullet\text{OH}$ into the ortho and para-positions; in the case of the electron-withdrawing substituents, meta-addition is preferred. The dissolved organic carbon (DOC) uses up a large fraction of available $\bullet\text{OH}$ in AOP (Wojnárovits and Takács, 2017).

2.4.6. Perhydroxyl Radical

The origin of the perhydroxyl radical is presumed to be in the intra-spur reaction (Eq. (2.47))



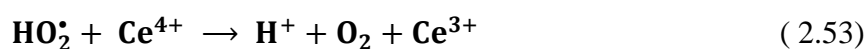
$G_{HO_2\cdot}$ cannot be large for radiations with low Linear energy transfer (LET) values. Increasing the LET leads to an increase in the per hydroxyl radicals' concentration existing at the beginning of the chemical stage of water radiolysis. The value of $G_{HO_2\cdot}$ for LET radiations is small and hence not considered in establishing a quantitative reaction scheme in such cases. Peroxy radical is very important as a secondary radical in the radiolysis of aqueous solutions in the presence of oxygen. Wastewater usually contains oxygen, therefore e_{aq}^- and $H\cdot$ are mostly converted into peroxy radicals (Eq. (2.48) to (2.50)),



The $O_2^{\bullet-}$ is a weak reductant, while $HO_2\cdot$ is a moderate oxidant. Unlike $\cdot OH$, $O_2^{\bullet-}$ and $HO_2\cdot$ may not directly contribute to the degradation of organic pollutants. In the absence of suitable reaction partners, $O_2^{\bullet-}$ and $HO_2\cdot$ disappear from the solution in slow radical-radical reactions giving H_2O_2 (Eq. (2.51) and (2.52)); in neutral solutions, the cross-reaction (Eq. (2.51)) dominates:



Radiation-induced degradation of haloalkanes shows a mechanism based on dehalogenation and uni- and bimolecular reaction of the peroxy radicals formed in oxygen scavenging. Under standard conditions the $HO_2\cdot$ radical is an effective oxidizing agent. The $HO_2\cdot$ radical may also react as a reducing agent (Eq. (2.54)).



The HO_2^\bullet radical is a considerably weaker reducing agent (E° for the couple H^+ , O_2 / HO_2^\bullet is calculated to be 0.3V). In aqueous solutions the reaction in Eq. (2.56) seldom takes place



Like H_2O_2 , the HO_2^\bullet is often inert toward organic substances and its fate lies in dismutation leading to the formation and accumulation of H_2O_2 in solution (Eq. (2.57)).



The form of the HO_2^\bullet radical changes with pH, as shown by kinetic studies of the recombination reaction, $HO_2^\bullet + HO_2^\bullet$ and the reaction $HO_2^\bullet + OH^-$. The neutral (HO_2^\bullet) and basic ($O_2^{\bullet-}$) forms are generally accepted, and pK values of 4.5 have been reported for the equilibrium (Eq. (2.58)).



The amount of H_2O_2 present at the beginning of the chemical stage depends, for a given amount of energy absorbed, only slightly on the pH

2.5. Review of radiation process in wastewater management

Wastewater and effluent discharges cause pollution in water bodies and pose potential risks to living organisms. Electron beam irradiation (EB) is a clean process for the degradation and mineralization of organic pollutants due to the absence of chemical initiators. Concerns regarding the disposal of domestic wastewater without sufficient treatment are increasing, especially in developing countries due to inadequate sewage system development. Pharmaceuticals, personal care products, and their bioactive metabolites are released into wastewater therefore creating a need to understand the mechanisms involved in the removal of pharmaceutical mixtures as well as complex raw wastewater. Membrane technology, bioremediation, photodegradation, and radiation technology are promising processes for water and wastewater treatment. Advanced oxidative processes (AOPs) that utilize reactive oxygen

species (ROS) such as •OH radicals (•OH), H₂O₂, O₃, and superoxide anion radicals (O₂^{•-}) are popular prospects. Ozonation, photo Fenton, photocatalysis, ionizing radiation, and electrochemical oxidation are prominent alternatives to conventional WWTPs. Undoubtedly, radiation-induced processes have desired diversity in applications with reduced drawbacks as experienced in other advanced oxidative processes.

2.5.1. Gamma Radiation

Gamma irradiation between 1 to 4kGy enhanced the biodegradability of lincomycin, sulfamethoxazole, and tetracycline and was proposed for the pretreatment of recalcitrant pollutants to transform them into biodegradable adducts (Kim et al., 2014). The decomposition of solutions increases with increasing absorbed dose (Yu et al., 2008). Using gamma irradiation exponential reductions in carbamazepine concentrations at doses up to 1kGy and concentration of 0.05mgL⁻¹ which is the threshold for chronic pharmaceutical toxicity, have been reported. Similarly, Mefenamic acid and ketoprofen have decomposed at 2 kGy doses. The electrophilic •OH radicals preferentially attack the high electron density places such as the phenyl ring. Thereby, the azepine group in carbamazepine which acts as an electron donor was easily attacked by •OH radicals. Ketoprofen and mefenamic acid, which have electron-accepting groups such as carbonyl and carboxyl, had lower decomposition yields than carbamazepine. Clofibric acid and diclofenac concentrations decreased with dose and were eliminated at 1 kGy dose. The phenyl ring of clofibric acid was substituted by a chlorine group as a weak electron acceptor and an alkoxy group as a strong electron donor, while the phenyl rings of diclofenac have also two chlorine substituents and two electron-donating groups. The electron densities of the phenyl rings of clofibric acid and diclofenac may be similar, and the decomposition curves by gamma-ray irradiation were almost the same (Kimura et al., 2012).

Ibuprofen (28mg/L), a common non-steroidal anti-inflammatory drug has been degraded with 100% efficiency at an absorbed dose of 1.1kGy using gamma radiation. The degradation was enhanced by adding 0.1% H₂O₂ and humic acid but was suppressed by the addition of 0.5% H₂O₂. Acidic pH favored the degradation compared to neutral or alkaline conditions and the degradation was further suppressed by the addition of CO₃²⁻, NO₃⁻, thiourea, and methanol (Zheng et al., 2011). Similar results have been reported in gamma irradiation degradation of diclofenac (30mg/L) where the presence of humic acid(30mg/L) decreased the degradation efficiency from 80% to 62% at doses of 0.8kGy. This is attributed to the competition of humic acids with diclofenac for the available •OH radicals. The decrease was observed with increasing humic acid concentration (Zhuan and Wang, 2020). Diclofenac (50mg/L), has been removed from an aqueous solution with 100% efficiency and 50% from sewage water and sediment when using gamma rays and electron beams at doses of up to 5kGy. These values are comparatively higher than the 50% adsorption reported on sludge (Bojanowska-Czajka, 2021a; Trojanowicz et al., 2018b, 2017).

Sulfamethoxazole (SMX-0.04mM) has been degraded with 99% efficiency at 1kGy under gamma irradiation. However, TOC was not significantly diminished (<13%). High concentrations of Cl⁻ ions inhibited degradation whereas, bicarbonate, carbonate, and phosphate ions were found to be inhibitors at lower concentrations and enhancers at higher concentrations (20-50mM). The carbonate and phosphate radicals generated in the presence of carbonate and phosphate ions respectively, played a key role in sulfamethoxazole degradation at higher concentrations and preferentially attacked the amino group thereby resulting in different intermediate products to •OH radical driven pathway in the absence of these anions. Sulfate ions showed slight inhibition on the degradation of SMX. The increase in the initial concentration of nitrate ions decreased SMX degradation. The scavenging effect of anions for reactive species i.e., •OH radicals, e_{aq}⁻, and hydrogen radicals, plays a key role in these

processes (Wang and Wang, 2018). In other studies, sulfamethoxazole concentrations ranging between 5 to 40 mg/L had removal efficiencies ranging between 100% to 40% respectively at 0.8kGy indicating the effect of initial concentration on the degradation efficiency under gamma irradiation. Additionally, in the presence of 10 mmol/L CO_3^{2-} , HCO_3^- , the degradation efficiency of sulfamethoxazole declined from 91.7% to 62.1%, and 74.5% respectively. TOC removal was <20% even at low initial concentrations of sulfamethoxazole (Zhuan and Wang, 2019). Pharmaceutical wastewater from an erythromycin (ERY) production factory treated by gamma irradiation with the addition of peroxymonosulfate (PMS, 50 mM) had a removal of 99.2% at the absorbed dose of 25 kGy. It is surmised that ionizing radiation can be applied as pretreatment to degrade the toxic antibiotics and recalcitrant humic substances, which are less effective to be removed by biological treatment (Chu et al., 2021).

Ciprofloxacin and norfloxacin fluoroquinolone antibiotics have been degraded under 0.5kGy gamma irradiation with 70% efficiency at concentrations of 33 and 32mg/L respectively. Only 25% and 10% COD and TOC respectively were achieved at 2kGy when the final fluoroquinolones concentrations were below the detection limit indicating low oxidation and mineralization degrees. Higher oxidation and mineralization were possible at 6kGy. Irradiation led to the conversion of non-biodegradable ciprofloxacin to substances degradable by metabolic processes of microorganisms (Tegze et al., 2018). Gamma irradiation has also been deployed in the destruction of aqueous samples with aniline concentrations ranging between 20 to 200 mg/L (Jia-Tong et al., 2017). losartan, a common antihypertensive drug has efficiently been mineralized at doses of 0.5 to 4 kGy in aqueous solutions with decreasing chemical oxygen demand (COD) and total organic carbon (TOC) with irradiation indicating mineralization (Zaouak et al., 2021). Trihalomethanes (THM) at concentrations of 100 µg/L have been removed with an efficiency of 98% at a dose of 1 kGy. Similarly, $CHCl_3$ has been removed with 92.5% efficiency by increasing the dose to 6 kGy. Additionally, chloroform

concentrations between 145 to 780 $\mu\text{g/L}$ showed reduction efficiency near 95% at doses below 6 kGy. Nitrophenols (1 $\mu\text{mol/L}$) have been reduced using gamma irradiation under O_2 , air or He saturated at a dose of 5 Gy. Degradation of polycyclic aromatic hydrocarbon (PAH) in moist and dry sewage was carried out at 2, 4, 6, 8, and 10 kGy of gamma irradiation dose. The combination of irradiation and H_2O_2 promoted a synergistic effect with increased degradation efficiency of chlorophenols and TOC removal (Hu and Wang, 2007). Antibiotic fermentative residues containing antibiotic resistance genes (ARGs) and residual antibiotics have also been treated using ionizing gamma radiation (Shen et al., 2019). Though gamma irradiation has proven effective in the degradation of a variety of chemicals of emerging concern, its drawbacks concerning handling and long irradiation time limit its commercial applications. These limitations create an inclined interest and preference toward electron beam irradiation.

2.5.2. Electron beam radiation

The application of electron beam processing in industrial and medical processes is promoted by the reliability and ease of producing ionizing radiation using electron beam accelerators. Electron beam irradiation is a non-chemical process and therefore offers an environmentally friendly alternative for degrading pollutants. In laboratory experiments, electron beam treatments (EB) effectively removed the anti-inflammatory aspirin even in the presence of another pharmaceutical (fluoxetine). Negligible mineralization indicated the formation of byproducts under experimental conditions. Increased toxicity and H_2O_2 formation were observed with increasing doses (Tominaga et al., 2021). Diclofenac (DCF), a popular anti-inflammatory drug has been degraded by electron beam at doses of up to 5kGy. Negligible TOC removal was observed even at 7.5 kGy, with the formation of recalcitrant, non-biodegradable by-products (Tominaga et al., 2018a). The psychiatric drug carbamazepine (CBZ) was susceptible to degradation and mineralization under electron beam irradiation at 5kGy (Zheng et al., 2020). Ciprofloxacin has been degraded with 95.86% efficiency at 1kGy

with a TOC reduction of 38% at 5kGy under electron beam irradiation. Conversely in a mixture consisting of ciprofloxacin, metformin, and acetylsalicylic acid, a removal efficiency of 96% was achieved for ciprofloxacin and 81% fluoxetine (Kiyoshi Tominaga et al., 2023). Lincomycin has also been degraded at 5kGy under electron beam irradiation as well as under gamma irradiation as already mentioned (Ham et al., 2014).

Reinholds et al. obtained 90-100% removal efficiencies at 0.5 to 5kGy doses for influent wastewater containing 19 multi-class pharmaceuticals at a wastewater treatment plant. Electron beam irradiation requires shorter exposure times therefore more energy efficient compared to gamma irradiation. Pharmaceutical product residues were reduced in eighty percent of the samples exposed to 0.5 to 5kGy of the electron beam (600 and 1200 kGyh⁻¹) or gamma radiation (22.5 and 37.5 kGyh⁻¹) treatment. However, higher doses >5kGy were required for the decomposition of macrolide antibiotics. Furthermore, bacterial decontamination of wastewater was achieved at radiation doses between 7 to 12 kGy. Increments in the dose resulted in faster degradation and rapid degradation was observed between 0.5 to 3 kGy with maximum removal efficiency of 84 to 100% achieved between 5 to 7 kGy absorbed dose (Reinholds et al., 2017). Other than human pharmaceuticals, pesticides, comprising organochlorinated compounds of anthropogenic origin banned by the Stockholm Convention though still used in certain regions of the world undergo radiolytic degradation via interactions with hydrated electrons with the yields of degradation being larger in polar than in non-polar solvents. In general, the degradation efficiency is larger in aqueous solutions than in organic solvents (Trojanowicz, 2020). Diuron (phenylurea herbicide) degrades in aqueous solutions mainly through the reactions of •OH radicals formed following water radiolysis. The •OH radical adds to the ring to form hydroxy-cyclohexadienyl radical and by inducing dechlorination. Dissolved oxygen enhances the rate of degradation and is highly important to achieve efficient ionizing radiation-induced degradation of diuron in dilute aqueous solution

(Kovács et al., 2015). The destruction of 96% of PCBs and water-dissolved herbicide was demonstrated in research conducted by MIT in 1980 (Hu and Wang, 2007).

The applications of electron beam radiation in the treatment of wastewater are not limited to pharmaceutical wastewater. Bromate a disinfection byproduct and perfluorooctanoic acid (PFOA) have also been degraded using an electron beam in simulated wastewaters (Trojanowicz et al., 2020; L. Wang et al., 2016). Perfluorooctanoic acid (PFOA) and perfluorooctane sulfonate (PFOS) have successfully abated by >80% using electron beam technology at doses up to 50kGy (Kowald et al., 2021). Similarly, bio-refractory organic compounds present in printing and dyeing textile wastewaters have been successfully degraded using e-beam. In these applications, electron beam treatment was found to enhance the biodegradability of the wastewater constituents. This would favor its applications in the pretreatment of otherwise non-biodegradable chemical constituents (Deogaonkar et al., 2017; Deogaonkar-Baride et al., 2021; He et al., 2016; Nasir et al., 2010). Domestic laundry surfactants have also been degraded using electron beams (Selambakkannu et al., 2020). When coupled with a membrane bioreactor, the hybrid electron beam membrane bioreactor system was found to reduce the COD of textile wastewater containing polyvinyl alcohol by 31% (Sun et al., 2016). Effluents from the textile industry contain contaminants such as surfactants, dyes, peroxides, salts, acids, metals, suspended solids and organic compounds, and other additives with high solubility, residual color, and low biodegradability. These chemicals affect dissolved oxygen, turbidity, color, temperature, and consequently, aquatic organisms. Combined processing techniques utilizing activated sludge systems and *Advanced Oxidative Processes* (AOPs) may enhance organic degradation efficiency. Textile effluent decoloration after EB treatment of Red 239 dye under an applied dose of 5 kGy yielded 95% color removal, while 0.5 kGy accounted for 80% color removal (Garcia et al., 2020). Electron beam radiation enhanced the biodegradability of simulated textile effluent

(mixed) pre-treated by activated sludge process. The mixed effluent comprised scouring, desizing, dyeing, and printing process effluents (Deogaonkar et al., 2019). However, E-beam irradiation pre-treatment did not improve the biodegradability of textile effluent even at 80 kGy dose. Alternatively, in the post-treatment of biologically treated samples, e-beam irradiation significantly enhanced biodegradability at low doses of 1 kGy with $\bullet\text{OH}$ radical ('OH) playing an active role. Following electron beam exposure up to 2 kGy dose, the COD, BOD, and BOD/COD ratio increased by 7% and 12% respectively above the average values of COD and BOD. However, with doses of 5 kGy to 80 kGy, the COD and BOD decreased slightly with a reducing BOD/COD ratio which confirms that e-beam radiation doses above 5 kGy do not show a significant improvement in biodegradability of simulated mixed effluent. EB irradiated sample after the activated sludge process becomes considerably biodegradable. Similar observations were reported in the experiments involving dyeing wastewater. Therefore, EB post-treatment is effective for biodegradability enhancement of textile wastewater. The discoloration of remazol black B and orange 3R solutions was effective at 1 and 2.5 kGy which is a comparatively low dose and possibly will add to an appropriate expenditure for irradiation technology. Irradiation of real textile BVT effluents resulted in high-quality color elimination but the sharp toxicity reduction varied widely 97% (0.5 kGy), 54% (2.5 kGy), and 19% (1.0 kGy), BTV1—BTV3 (IAEA, 2013).

The electron beam has also been used in the treatment of sludge from drinking water and sewage treatment and has shown exceptional results in reducing heavy metal content, and polyacrylamide content as well as complete inactivation of pathogens at 25kGy (Ranković et al., 2020). The combination of coagulation, electron beam irradiation, and biological treatment on real pharmaceutical wastewater obtained 94% COD removal and 89% organic content reduction (Changotra et al., 2020). The electron beam has shown efficacy toward hepatitis A virus (HAV), astrovirus (ASV), rotavirus (RV), enterovirus (EV) virus, norovirus

(NVLII) virus, and adenovirus (Roque et al., 2022; J. Wang et al., 2022). Yun Kim et al. reported the neutralization of 2,4,6-trinitrotoluene (TNT, trotyl) and hexahydro-1,3,5-trinitro-1,3,5-triazine (RDX, hexogen) wastewater. Dissolved TNT and RDX are highly toxic, carcinogenic, and easily accumulate in soil, plants, and living organisms to cause mutations. Evaporation and combustion methods used in the treatment of TNT and RDX generate hazardous wastes (ash and gases) and require too much heat. On the other hand, their biodegradability through biological treatment is minimal. However, under electron beam treatment, the formation of nitrates and ammonium indicated their volatilization following reactions with the reducing intermediates of water radiolysis (Yuri Kim et al., 2020). Denitration was alluded to the dissociative capture of e_aq^- and hydrogen radical atom. Furthermore, the absence of nitrite accumulation could be explained by the elimination of the nitro group in the form of $\bullet NO_2$ radical that easily converts to nitrate by reacting with $\bullet OH$, HO_2^\bullet , H_2O_2 . Following EBT, the BOD increased and light organic acids; oxalic and glyoxylic acids in the solution of TNT, and formic acid in the solution of RDX were formed. A dose of 20 kGy gave BOD/COD ratio higher by factors of 8 and 15 for TNT and RDX solutions respectively indicative of an increase in the degree of oxidation of the solute. The organic acids presence indicated the breaking of skeletal bonds (C–C in TNT and C–N in RDX). Electron beam irradiation efficiently decomposes nonylphenol and its derivatives with doses of about 1 kGy.

Acetone, a major byproduct of methyl tert-butyl ether (MTBE a classified carcinogen), is difficult to degrade in normal advanced oxidation processes (AOPs) for MTBE degradation where it is formed in high concentrations. Acetone degradation via electron beam treatment has been reported to be mainly by reactions of the e_aq^- . Nitrate was found to decrease the removal of acetone but alkalinity was found to have no significant effect (Yoon et al., 2009). AOP results indicate that acetone is less reactive towards $\bullet OH$ and is also formed from some

of the MTBE byproducts (TBF, TBA, and MA). Electron beam irradiation has been reported to form conspicuously low concentrations of acetone compared to conventional AOPs which also require high ozone and H₂O₂ concentrations with UV for 99% efficacy. Acetone is easily bio-degradable but an industrial-activated sludge treatment system has been found unable to biodegrade acetone and is also reported to inhibit biochemical processes. Its high water solubility gives it a low adsorptive capacity on granulated activated carbon technology (GAC). Removal efficiency has been observed to increase with increasing absorbed doses at fixed initial concentrations. Alternatively, efficiency decreases with increasing concentration at a fixed absorbed dose. Nitrate is present in industrial, municipal wastewater, and groundwater. Nitrate has a high reactivity with e_{aq}^- and H^\bullet but insignificant reaction towards $\bullet OH$. Nitrate scavenges e_{aq}^- thereby decreasing the removal efficiency of acetone.

Radiation-induced destruction of pollutants has been found effective against a wide assortment of pharmaceuticals, and dyes (Garcia et al., 2020; He et al., 2016; Rauf and Ashraf, 2009; Wojnárovits et al., 2005; Zaouak et al., 2018), pesticides (Sayed, 2014; Serrano et al., 2020), PFOAs (Oshima et al., 2020) and a variety of other EPs. Additionally, Electron Beam irradiation in the treatment of wastewater reduces the pathogenic load (Maruthi et al., 2013). Rate coefficients of $\bullet OH$ radical with antibiotic molecule reactions suggest that compounds with aromatic rings (e.g., amoxicillin) or conjugated double bonds (e.g., tylosin) have rate coefficients in the range of $(6 - 8) \times 10^9 \text{ M}^{-1} \text{ s}^{-1}$ range where radical addition is the primary reaction. Additionally, the presence of strong electron-withdrawing groups and N atoms give smaller rate coefficients whereas molecules without aromatic rings have smaller values in the range of $(3 - 6) \times 10^9 \text{ M}^{-1} \text{ s}^{-1}$ with hydrogen abstraction being the dominant reaction (Wojnárovits, Tóth & Takács (2018)). The main advantages of the applications of radiation technologies are in their capability to provide a dual property of sanitization as well as removal of organic pollutants. Compared to other advanced oxidative processes, radiation-propagated

processes do not require inputs into the matrices and therefore forego the possibility of producing any further contaminants such as depleted catalysts or adsorbents. Additionally, radiation processes appear to be more time-conservative to achieve mineralization or removal in a considerably shorter time compared to other treatment processes. The radiation processes can be used to treat copious volumes of water as is common in most wastewater batch reactors.

UV radiation though effective for poor quality and primary wastewater effluents is limited by the presence of particle-associated microbes. Suspended solid concentration can increase microbial survival by shielding the microbes from UV irradiation. On the other hand, Ionizing radiation degrades organic molecules such as halogenated compounds, dyes, and pesticides in relatively less time than non-ionizing radiation. In combination with oxidants such as ozone or H_2O_2 , the removal efficiency is further improved. Further, UV rays used for microbial inactivation have proved detrimental by generating mutations in microbes. Radio resistivity of pathogens is not fully explored but could also be a problem when using radiation technology. Gamma and electron beam irradiation are effective in curbing harmful algal blooms (HABs) occurring due to ecosystem imbalances such as rising temperatures and escalating anthropogenic nutrient pollution causing eutrophication, releasing odor, taste compounds, and harmful toxins into the surrounding water (Folcik and Pillai, 2020). Gamma rays together with electron beams can be suggested as the most efficient method for wastewater remediation (Jan et al., 2015). Additionally, radiation treatment combined with other techniques e.g., ozonation, H_2O_2 , or TiO_2 greatly enhances the effectiveness of pollutant degradation (Duarte et al., 2002; Sampa et al., 2007).

2.6. Sterilization activity of electron beam

The electron beam processing efficiently eliminates pathogenic microbes and organic contaminants. These outcomes are greatly influenced by the dose rate, energy source, and radiation absorbed dose. Electron beam induces radiolysis of water and produces hydrated

electrons (e_{aq}^-), \bullet OH, H atoms, H_3O^+ ions, H_2O_2 and H_2 . The unpaired electron of the oxidative \bullet OH radical, the reductant e_{aq}^- , and the ionized hydrogen atoms make them highly reactive and effective in degrading heavy metals, and organic and inorganic pollutants while simultaneously imparting disinfection properties against microbes. Radiation dose affects living organisms either directly when absorbed by DNA and other critical cellular components thereby affecting survival or reproductive capacity. Indirect effects emanate when the reactive species generated through irradiation react with the micro and macromolecules of the cells. EB irradiation has a degradative effect on cell walls, alteration of cell permeability, variation in physical components of cell protoplasm, and inactivation of some crucial metabolic enzymes. It has been shown that the logarithmic number of microbes in unit volume linearly decreases with dose (Jan et al. 2015). 3 to 5 kGy dose of ionizing radiation is deleterious to pathogenic microbes in sewage sludge, 1 to 6 kGy doses of gamma radiation are sufficient for disinfection of sewage water and sewage sludge, respectively, whereas viruses exhibit higher resistance to inactivation by ionizing radiation (D_{10} value is 2.5 kGy in sewage sludge). Absorbed doses of between 5 to 10 kGy can inactivate pathogens in water EB treatment (Ponomarev and Ershov, 2020).

UV radiation is effective for poor quality and primary wastewater effluents, but the presence of particle-associated microbes has negative effects on the disinfection process. Suspended solid concentration can increase microbial survival by shielding the microbes from UV irradiation. Further, UV rays used for microbial inactivation have proved detrimental by generating mutations in microbes. Radio resistivity of pathogens is not fully explored but presents a problem when using radiation technology. Gamma and electron beam irradiation are effective in curbing harmful algal blooms (HABs) occurring due to ecosystem imbalances such as rising temperatures and escalating anthropogenic nutrient pollution causing eutrophication,

releasing odor, taste compounds, and harmful toxins into the surrounding water (Folcik and Pillai, 2020).

Sewage sludge has been hygienized using radiation technology. The bacterial population has also been observed to decrease with increasing radiation dose under EB irradiation. The total bacterial counts (TBC), total coliform counts (TC), and E. coli counts declined with time after the EB treatment. EB pretreatment was shown to be a faster way of stabilizing wastewater for reuse for non-potable purposes (Rawat and Sarma, 2013). Maruthi et al. (2013) used EB irradiation in the treatment of wastewater to reduce the pathogenic load. EB doses of 1.5 kGy eliminated coliforms. Furthermore, doses of 10 kGy killed *Cryptococcus laurentii*, *Aspergillus fumigatus*, and *Absidia sp.*, and no larvae of helminths (*Ascaris lumbricoides*) were recovered at doses ≥ 1.5 kGy (Hossain et al., 2018; Maruthi et al., 2013).

CHAPTER THREE

3. Methodology

This section provides an overview of the experimental procedures applied in achieving the research objectives. The conditions, parameters, and instrumental methods have been outlined.

3.1. Chemicals and Materials

Analytical grade HCQ sulfate ($\geq 98\%$), CQ phosphate powder ($\geq 98\%$), potassium dichromate (99%), methanol HPLC grade ($>99.9\%$), hydrogen peroxide (30%), ferrous sulfate heptahydrate ($>99\%$), sodium hydroxide, sulfuric acid (95%), silver nitrate (99%), acetonitrile HPLC grade ($>99.9\%$), dibasic sodium phosphate (98%), sodium nitrate (99%), humic acid sodium salt, sodium persulfate (98%), orthophosphoric acid (98%), triethylamine (99.5%), sodium hydrogen carbonate (99.5%), sodium carbonate (99.5%), and perchloric acid (95%) was procured from Sigma Aldrich (Germany). Low-density polythene sample bags (100mL) with zip locks were purchased locally. Tube tests for chloride ions, total nitrogen, chemical oxygen demand, total organic carbon, and ammonium ion concentration produced by Macherey Nagel (Germany) were purchased from Aqua Labs (Poland).

3.2. Analytical techniques

3.2.1. UV spectrophotometry and HPLC Analysis

A Jasco V670 from Jasco (Poland) and a Nanocolor Vis II from Mercherey Nagel (Germany) spectrophotometers together with a Shimadzu HPLC class VP with a DAD detector were used for the detection of CQ and HCQ with maximum absorption at 343nm wavelength. For the HPLC chromatography, the mobile phase consisted of 70% acetonitrile and 30% 1.4g/L sodium phosphate dibasic with 0.4% triethylamine at pH 3.0. A Gemini NX 5u C19 110A 250X4.6mm column at oven temperature of 40°C and flow rate of 1mL/min was used for HPLC analysis.

3.2.2. LC-MS methods

The identification of CQ and HCQ degradation products was performed on an Agilent LC-MS. In the CQ degradation products, the eluent consisted of 0.1% formic acid (A) in ethanol (B) at a flow rate of 0.3mL/min with the MS in electrospray ionization positive mode. The LC-MS analysis for HCQ degradation products was also performed on the Agilent model with MS in positive mode electron spray ionization. The mobile phase of the chromatography consisted of; phase A deionized water with 0.05% trifluoroacetic acid; Phase B acetonitrile and 0.05% trifluoroacetic acid, flow rate 0.5ml/min, gradient washing: 20% solvent B (0–0.2 min), 20 to 50% B (0.2–1.5 min), 50–90% B (1.5–1.6 min), 90 to 100% B (1.6–2.0 min), 100% B (2.0–2.5 min), 100 to 20 % B (2.5–2.6 min), and 20% B (2.6–3.5 min), wavelength 220nm.

3.2.3. Colorimetric methods

Further identification of degradation products was performed using Nanocolor photometric test tube kits using the Nanocolor VIS II spectrophotometer. Nanocolor test kits produced by Macherey Nagel (Germany) were purchased from Aqua Labs (Poland) for photometric determination of total Kjeldahl nitrogen (1.0-16mg/L), total nitrogen (0.5-50mg/L), nitrate NO_3^- , NH_4^+ (0.2 – 8mg/L), Cl^- (0.5-50mg/L), total organic carbon (20-300mg/L), and chemical oxygen demand (50-300mg/L). The pH measurements were conducted using an Elemetron-CX-461 multi-meter (Poland) while dissolved oxygen was measured using a dissolved oxygen meter from Mettler Toledo (Poland).

3.2.3.1. Tests for Chlorides

Chloride ions quantitatively displace thiocyanate from mercuric thiocyanate leading to the subsequent formation of a red ferric thiocyanate complex that can be measured calorimetrically. The chloride ion concentration in the sample is proportional to the intensity of the color formed.



Chloride 50 test tubes from Macherey Nagel (Germany) contain nitric acid 5–20 % (test tube A), and reagent R2 contains mercury (II) thiocyanate 0.32–0.64 % in methanol 50–100 %. 4.0 mL sample solution (the pH value of the sample must be between pH 4 and 13) was added into test tube A containing nitric acid and thereafter 1.0 mL of reagent R2 was added. Test tube A was then closed and mixed. The test tube was then wiped externally and measured after 3 minutes (Yoshinaga and Ohta, 1990).

3.2.3.2. Determination of total nitrogen, total Kjeldahl nitrogen, and nitrates

The NANOCOLOR® total Kjeldahl nitrogen TKN 16 is suitable for the photometric determination of Kjeldahl nitrogen in surface, groundwater, and wastewater.

3.2.3.2.1. Total Nitrogen

Total nitrogen cumulatively represents the total bound nitrogen; organic nitrogen (urea, peptides, proteins), and inorganic/mineral nitrogen (ammonium/ammonia, nitrate, nitrite) except for elemental nitrogen (N_2). The presence of nitrogen compounds in water bodies is a result of the degradation or decomposition products of nitrogen-containing organic substances. Organic and inorganic nitrogen were oxidized to nitrate using potassium persulfate in an alkaline environment while heated using digestion tubes containing sulfuric acid and sodium hydroxide on a heating block at 100°C for 1 hour. Thereafter, the digestion tubes were left to cool, and chromotropic acid was added to the solution. The solution absorption was read at 345nm.

3.2.3.2.2. Nitrates

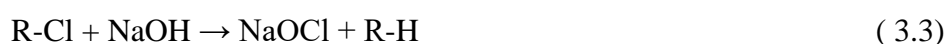
According to ISO 7890-1, all organic and inorganic nitrogen-containing substances are oxidized to nitrate in an acidic medium. Nitrate reacts with 2,6-dimethylphenol in an acidic solution (sulfuric/phosphoric) to form 4-nitro-2,6-dimethylphenol which can be determined photometrically at 345nm and is directly proportional to the nitrate-nitrogen concentration. The Merck test kit allows the concentration to be determined without the use of a calibration curve by multiplying the measured absorbance at 340 nm by a known factor. This method is suitable for the concentration range 0.5 – 25.0 mg/L nitrate-nitrogen (equivalent to 2.2 – 110.7 mg/L nitrate) in a variety of water types including surface, ground, and drinking waters. This test kit is not suitable for chloride concentrations exceeding 1000 mg/L, and thus cannot be used to determine the nitrate-nitrogen concentration in seawater. Any turbid samples must be filtered before analysis and samples with a chemical oxygen demand (COD) above 500 mg/L cannot be analyzed.

3.2.3.2.3. Total Kjeldahl Nitrogen (TKN)

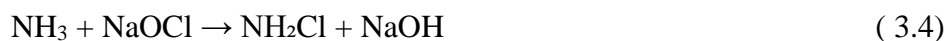
The Total Kjeldahl Nitrogen (TKN) is the total organically bound nitrogen and ammonia nitrogen. In the presence of detectable amounts of nitrate/nitrite, TKN was calculated by subtracting the nitrate/nitrite nitrogen from total nitrogen.

3.2.3.3. Test for Ammonium ion

Colorimetric and photometric determinations based on the Berthelot reaction were performed. Ammonium or ammonia reacts with hypochlorite and salicylate in a strongly alkaline solution (pH ≈ 12.6), in the presence of sodium nitroprusside (sodium (nitrosopentacyanoferrate(III))) as a catalyst to form a blue indophenol. In the first reaction step, hypochlorite is generated in situ from dichloroisocyanuric acid in an alkaline medium.



The hypochlorite reacts with ammonia to form chloramine.



With a catalytic amount of sodium nitroprusside, chloramines react with phenols (here: sodium salicylate) to form quinonimines. The quinonimine reacts with a further equivalent of sodium salicylate, resulting in a blue indophenol (Fig. 3-1).

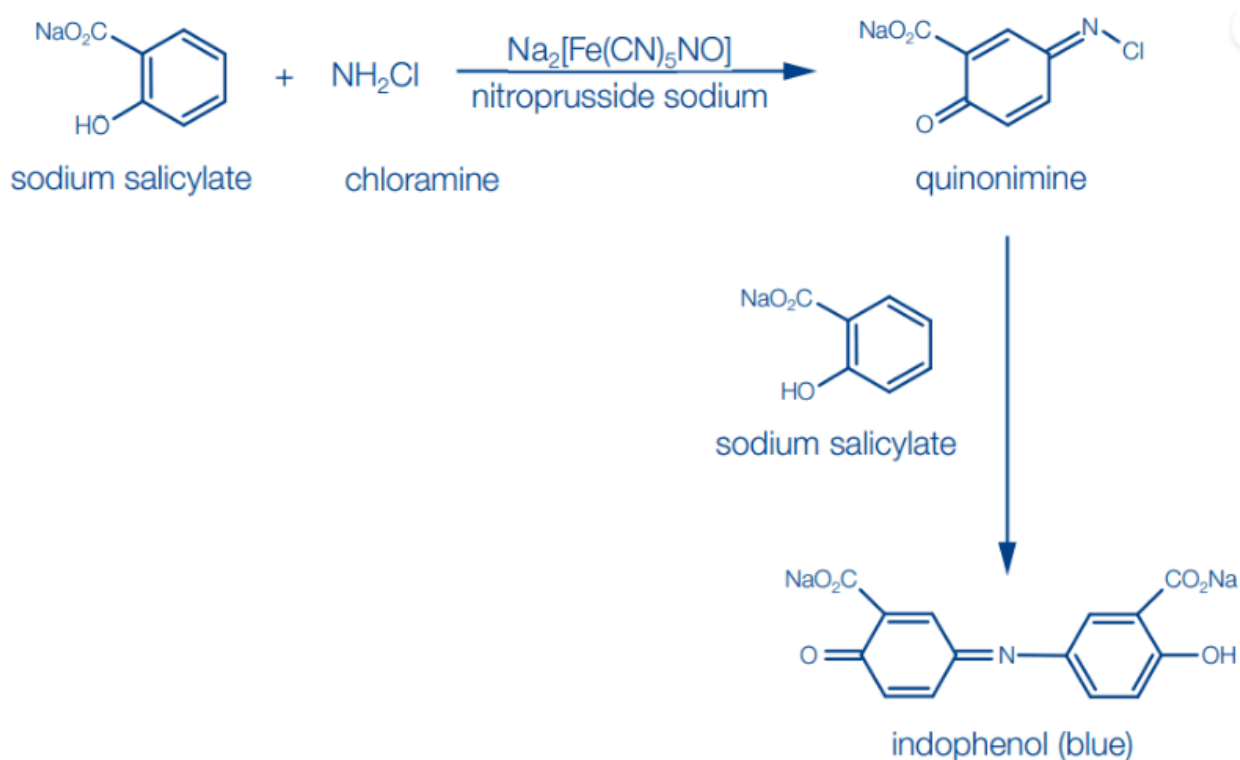


Fig. 3-1 Reaction scheme for the analysis of ammonium ions

3.2.3.4. Test for Total Organic Carbon

Total organic carbon represents the quantity of organic compounds contained in a sample of water either dissolved or undissolved. Biological oxygen demand was the method for wastewater analysis but owing to repeatability and long waiting period (5-day incubation) issues, chemical oxygen demand was preferred because of its stability to toxic substances, precision, and reliability even though high chloride concentration interfered with the test. However, COD produces hazardous mercury, hexavalent chromium, sulfuric acid, silver, and

other wastes depending on the methods used. Total Organic carbon is a method that substitutes both COD and BOD and is faster and more precise, especially for wastewaters (Celine et al., 2017; Dubber and Gray, 2010).

The TOC is the sum of dissolved and undissolved organic carbon compounds. The TC (total carbon) of a sample consists of the TIC (total inorganic carbon) and the TOC. The TOC content of wastewater can reliably be determined with the new tube tests through the removal of inorganic carbon by bubbling a purge gas in an acidic solution according to the non-purgeable organic Carbon (NPOC) method. The inorganic carbon compounds are known to be unstable at low pH and react to CO₂ (Eq. 3.5). The purge gas relieves the CO₂ from the sample and only the non-purgeable organic compounds remain.



Sample decomposition was performed in a heating block at 100°C for 1 hour over an indicator solution. Thereafter, the cuvettes were left to cool and the change in indicator absorption was measured with a NANOCOLOR Vis spectrophotometer.

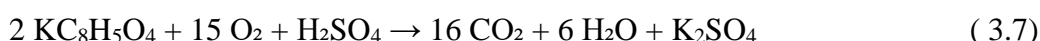
3.3.3.5. Test for Chemical Oxygen Demand

The chemical oxygen demand of water is determined by silver-catalyzed oxidation (increase in the oxidation ability of aliphatic substances) with potassium dichromate / sulfuric acid for 2 hours at 148 °C. The COD covers all oxidizable contents of the sample. In COD testing with a low measurement range, the decrease in the potassium dichromate concentration is determined. In COD tests with a higher measurement range, by contrast, the increase in Cr(III) ion concentration is determined. Possibly present chloride is precipitated by mercury sulfate. Thus, it is removed from the unwanted oxidation to elemental chlorine. Silver sulfate catalyzes to increase the oxidizability of aliphatic substances. Therefore, lower apparent

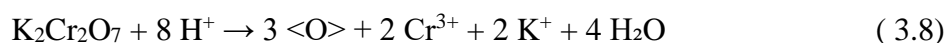
findings are avoided. For example, using potassium hydrogen phthalate (KHP) as a reference substance:



Since each molecule of potassium dichromate $\text{K}_2\text{Cr}_2\text{O}_7$ has the same oxidizing power as 1.5 O_2 molecules, the equivalent reaction is:



As described above, two molecules of KHP consume 15 oxygen molecules. Therefore, the theoretical COD for one milligram KHP is 1.175 milligrams of oxygen O_2 . Tube tests for the determination of COD are precise, time-saving, reliable, and rapid tests for all kinds of water and wastewater samples. COD is not a quantity-based size but an effect parameter (a requirement). In an acid medium, potassium dichromate forms reactive oxygen species, by the reaction with hydrogen ions



These oxygen compounds can oxidize organic compounds to carbon dioxide. The consumption of an oxidizing agent is independent of the size of the molecule. The COD content was photometrically determined from the consumption of potassium dichromate. Depending on the measurement range, the decrease in concentration of the yellow potassium dichromate or the increase in concentration of the green chromium (III) ion is determined. For all tests with a low measurement range, up to the test NANOCOLOR COD 300 (REF 985033), the former applies. From the test, NANOCOLOR COD 600 (REF 985030), the increase of the green chromium (III) is determined. An important process in COD determination was the decomposition carried out for two hours at 148 °C. A faster decomposition at 160 °C for 30 minutes is also possible but not suitable for all tests.

3.3. Preparation of catalysts

Melamine was calcined into pure bulk g-C₃N₄ (Catalyst I) using the calcination method, melamine powder 20 g was added into a crucible with tin foil, and put into a muffle furnace to be heated up to 550 °C at a rate of 5 °C/min and held for 4 h and then cooled down in the furnace, to obtain a yellow bulk sample, and the bulk sample was ground into powder using an onyx mortar and pestle. Then the mesoporous g-C₃N₄ nanosheets were prepared by chemical etching method, 3 g of yellow powdered g-C₃N₄ was added into 20 mL of sulfuric acid and stirred for 12 h to obtain a yellow solution, then 200 mL of deionized water was added into the reacted solution and ultrasonically dispersed to homogeneity, and then centrifuged at 6000 r/min for 4 min, and the precipitates were washed repeatedly with ultrapure water to weakly acidic, and then the samples were placed in an oven at 60°C for 8 h to obtain the white mesoporous nanosheets, labeled as MCN (Catalyst II).

MIL-Mn(Fe)-NH₂ catalyst was prepared by a solvothermal method by weighing 0.521 g of FeCl₃·6H₂O, 0.1662 g of MnO₂ and 0.118 g of 2-amino terephthalic acid and dissolving in 10 mL of N, N-dimethylformamide. The solution was then ultrasonicated for 30 min until sufficiently mixed. The resulting mixed solution was heated at 125 °C for 5 h in a 25 mL high-pressure reactor. The high-pressure reactor was left to cool naturally to room temperature and the powdered sample was separated by filtration and then purified by washing three times with N, N-dimethylformamide, and methanol. the sample was then dried at 100 °C for 24 h under vacuum conditions to obtain the MIL-Fe(Mn)-NH₂ sample (Catalyst III).

The g-C₃N₄/MIL-Mn(Fe)-NH₂ (Catalyst IV) and MCN/MIL-Mn(Fe)-NH₂ (Catalyst V) composites were prepared by the in situ introduction of the solvothermal method, and the preparation process was as shown in Fig. 3-2. Firstly, a certain amount of g-C₃N₄ and MCN prepared according to the above method was accurately weighed and dispersed in 10 mL of N, N-dimethylformamide, and the homogeneous suspension was obtained by ultrasonication for

30 min. 0.1662 g of MnO_2 , 0.521 g of $\text{FeCl}_3 \cdot 6\text{H}_2\text{O}$, and 0.118 g of 2-amino terephthalic acid was continuously added while ultrasonicating the suspension for 30 min to dissolve completely. The resulting suspension was heated at 125°C for 5 h in a high-pressure 25 ml reactor vessel. The reactor vessel and its contents were left to cool to room temperature then the powdered samples were filtered and separated. The sample was washed and purified three times using N, N-dimethylformamide, and methanol before being dried at 100°C for 24 h under vacuum resulting in the final composite material.

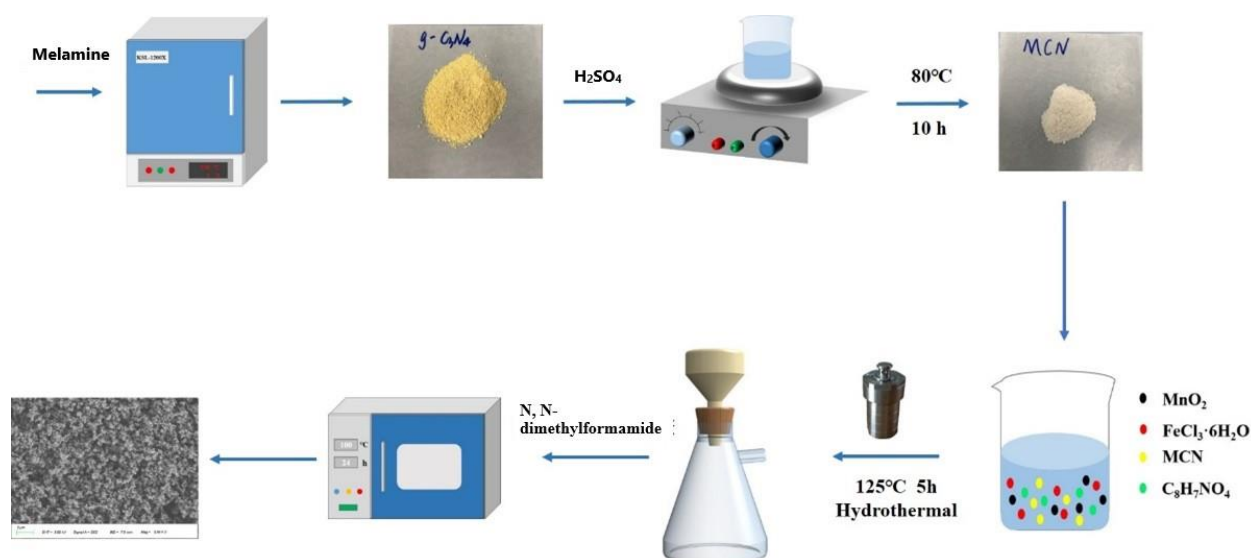


Fig. 3-2 Steps in the preparation of $g\text{-C}_3\text{N}_4$ catalysts

3.4. Radiation Processing

Particle accelerators are designed to propel charged particles through an electric field. The electron beam accelerator produces negatively charged electrons and is comprised of the electron source, accelerating structure, and delivery system. Thermionic emission is the principle by which the electrons are released from the cathode. The beam density is dependent on the temperature and cathode material properties. The cathode is usually the most crucial part of the electron source and its lifespan is defined by the cathode quality. After emission from

the cathode, the electrons are accelerated toward the anode, which is positively charged, under the influence of a force (F_e) created by the electric field (Zbigniew Zimek, 2018).

$$F_e = q \times E_d \quad (3.9)$$

Where q is the charge of the particle charge (electron 1.602×10^{-19} Cuolombs) and E_d is the density of the electrical field ($V/m = N/C$). In electron beam accelerators, three types of electric field generators are commonly used; high voltage direct current (DC), radio frequency (RF), and microwave linear accelerators (LINACs). The electron beam power(kW), electron beam current (mA), applied dose (kGy), and exposure time (s) are important technical features for the operation of the accelerator and affect the overall electron beam irradiation process. The energy (in MeV) of accelerated electrons is proportional to the applied voltage ($1 \text{ MeV} = 1.602 \times 10^{-13} \text{ J}$). The power, beam current, and electron energy are described by the equation:

$$P = U \times I \quad (3.10)$$

Where P is power (kW), U is the energy of the electrons (MeV) and I is the beam current (mA). The beam power and exposure time determine the electron beam dose. Low accelerating voltage translates to an extended exposure time and/or increasing the beam current to maintain the efficiency of removal. Increasing the accelerating voltage and the beam current increases the overall accelerator capital cost which is dependent on power, as this determines the electricity requirement. The efficiency for converting electrical power into beam power depends on the accelerator technology but is in the range of 60–80% (IAEA - International Atomic Energy Agency and IAEA, 2013). The energy of the applied electrons is the foremost consideration in an e-beam irradiation installation for both wastewater and sludge treatment as it affects operations costs, and determines the penetration depth of the electrons. In practice, the maximum energy that can be used is 10 MeV, as above this, the electron beam can start to activate the material (Kim et al., 2020; Siwek and Edgecock, 2020).

3.4.1. Accelerator Set-up

The HF resonance accelerator ILU 6 (1988) at The Institute of Nuclear Chemistry and Technology, Warsaw Poland was used for the irradiation of the aqueous samples. The technical parameters of the accelerator were 1.6 MeV, 2Hz, and 50mA. The samples in plastic sleeves were placed 30cm under the accelerator window (Figure 3.2). The 100mL sleeve bags were filled with a sample volume of 35mL. The sample thickness is estimated to be 1.5mm. The accelerator is set to 1.65MeV Energy and a current of 50mA. The dimensions of the setup are shown in Fig. 3.2. The targeted doses for this experiment are 0.5, 1, 1.5, 2, 3.5, and 7kGy.

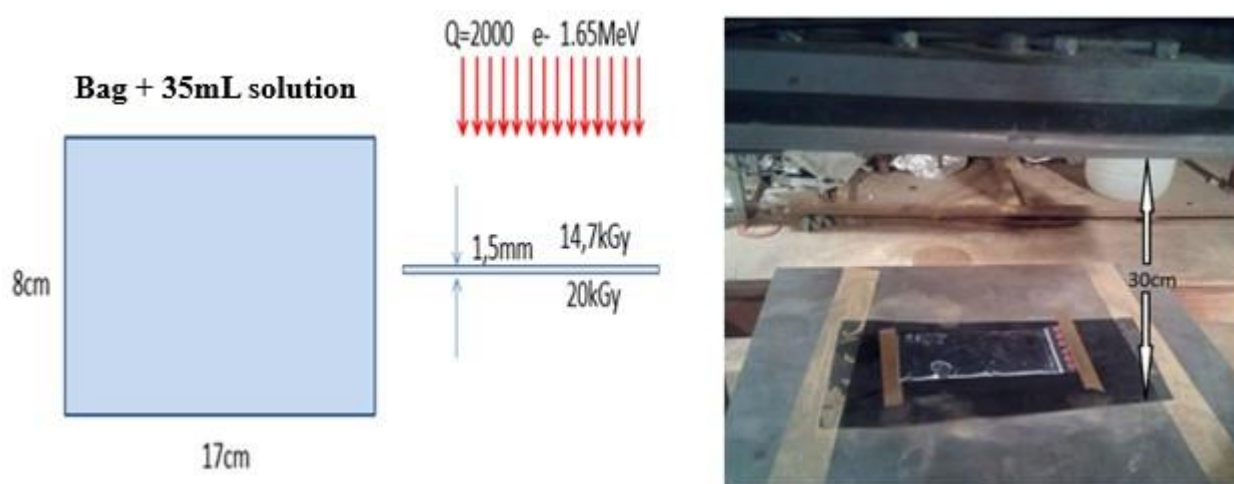


Fig. 3-3 Experimental Set-Up for irradiation of aqueous samples at ILU6 accelerator

3.4.2. Determination of Dose

Radiation processing requires the determination of applied doses and dose rates in different media of varying chemical composition and properties (Generalova et al., 1988, 1985). Absorbed dose rate, absorbed dose, the energy of electrons, type of radiation (β -particles, and photons), flux density, and fluence are important quantities for radiation characterization. Radiation-induced reduction of dichromate ions in dilute acid has previously been applied for high-dose radiation dosimetry (Hoang Hoa Mai and Nguyen Dinh Duong, 1994; INTERNATIONAL ATOMIC ENERGY AGENCY, 2002). The methods used for the

preparation, measurement, and calculation of results are essentially as described in ISO/ASTM 51401:2013(E). Commercial low-range dichromate dosimeters are composed of 0.35mM $\text{Ag}_2\text{Cr}_2\text{O}_7$ in 0.1M aqueous perchloric acid calibrated over the range 0.5-5 kGy. High-range dosimeters contain 2 mM potassium dichromate and 0.5 mM silver dichromate in 0.1 M aqueous perchloric acid. The 0.0005M potassium dichromate solutions were prepared in dilute perchloric acid (0.1M). Silver nitrate was added to the dosimeter solution to improve the dose-response and net absorbance, precision, stability, and independence of response upon dose rate. Potassium dichromate (0.5mM), silver nitrate (0.25mM), in perchloric acid (0.1M) were used to perform dosimetry evaluation. The potassium dichromate dosimeter is based on the reduction of Cr^{6+} (in $[\text{Cr}_2\text{O}_7]^{-2}$) to Cr^{3+} in acidified solution. The absorbed dose (Gy) is calculated using the expression;

$$D = \frac{\Delta\text{Absorbance(OD)}}{\rho\epsilon l} \quad (3.11)$$

Where;

ϵ is the extinction coefficient

l is the length of the cuvette (1cm for Jasco UV-Vis/1.4cm for Nanocolor VIS II)

ρ is the density of the solution ($\approx 1.004 \text{ g/cm}^3$ at 25°C)

G is the G value of production of Cr^{3+} $0.382\mu\text{M}$

The optical maximum absorption peak for dichromate solutions is 350nm with a lower peak at 440nm dependent on the concentrations of dichromate ions in the solution. The radiation yield, G-value denotes the number of species of one type changed by the absorption of 100eV radiation energy. The G-value for the reduction of dichromate ions to chromic ions can be evaluated as;

$$G(-Cr_2O_7) = \frac{\text{No. of Dichromate ion reduced}}{\text{Radiation E absorbed (eV)}} \times 100 \quad (3.12)$$

Radiation energy absorbed in the dosimeter solution is given in D (kGy), and reduced dichromate concentration is presented in C (mol L⁻¹). The number of dichromate ions reduced per cubic centimeter of the dosimeter solution is

$$\frac{\Delta C \times N}{1000} \quad (3.13)$$

Where; N - Avogadro's number = 6.023x10²³

A radiation dose of D kGy in the dosimeter solution equal to D×6.242x10¹⁸ eV per gram of dosimeter solution. If the density of the dosimeter solution is ρ gram per cubic meter, then we can write the following statement:

D×6.242x10¹⁸ eV per cm³ of dosimeter solution

$$G(-Cr_2O_7) = \frac{\Delta C \times N \times 100}{D \times \rho \times 6.242 \times 10^{18} \times 1000} = \frac{\Delta C \times 9649}{D \times d} \quad (3.14)$$

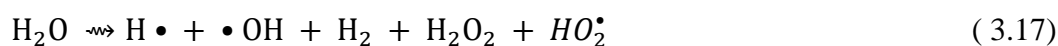
If the reduction in dichromate concentration, ΔC , is determined by spectrophotometry measurement, then ΔC can be evaluated from the absorbance

$$\Delta A = \Delta C \epsilon l \quad (3.15)$$

ΔA is the decrease in absorbance of the irradiated solution compared with the unirradiated

$$D = \frac{\Delta A \times 9649}{G \epsilon l \rho} \text{ kGy} \quad (3.16)$$

The irradiation of the dosimeter solution results in a flurry of reaction processes that generate radiolysis products



Hydrogen atoms (H•) and hydrogen peroxide (H₂O₂) reduce Cr(VI) to Cr(III) whereas •OH radicals (•OH) re-oxidize Cr(III) back to Cr(VI).



When radiolytic hydrogen (H₂) is allowed to build up in the solution (in case of high dose rate for example), the reaction converts the oxidizing •OH radical into a reducing hydrogen atom therefore reducing the radiation yield of Cr(VI), G(-Cr₂O₇).



Silver ion (Ag⁺) is an efficient scavenger of •OH radicals by reaction



This reaction stabilizes the G(-Cr₂O₇). The presence of Ag⁺ in the solution keeps the dosimeter solution from severe dose rate effects due to Eq. (2.23).



Solutions not containing Ag⁺ are not recommended as dosimeters. Silver dichromate can be obtained from the chemical process



The G-value of dichromate reduction caused by gamma radiation is around 0.38- 0.397. 0.5mM Ag₂Cr₂O₇ in 0.1 M HClO was applied to a dose range of 0.5 to 7 kGy and solutions were

saturated with air by bubbling. 35mL of these solutions were filled into an LDPE sleeve bag corresponding to the desired dimensions of the experiment.

3.4.3. Radiation chemical yield

The radiation chemical yield (G-value), G-value defined as the number of reactive molecules per 100 eV absorbed energy was calculated using the following equation

$$G(\text{CQ or HCQ}) = \frac{\Delta C \times N_A}{D \times 6.241 \times 10^{16}} \quad (3.25)$$

G is G-value ($\mu\text{mol J}^{-1}$),

D is the absorbed dose (Gy),

ΔC is the pollutant concentration (mol L^{-1}) at D,

$N_A = 6.023 \times 10^{23}$ is the Avogadro's number

6.24×10^{16} the conversion factor from Gy to 100 eV L^{-1} .

3.7. Mathematical modeling of radiation-induced degradation of CQ and HCQ

CHEMSIMUL is a computer program adapted for the simulation of chemical kinetics by incorporating complex reactions such as those in radiolytic processes with pulse trains, or radiolysis from nuclear waste. The reaction system is translated into a series of ordinary differential equations to be solved by the program. Additionally, it incorporates the principles of mass and stoichiometric balance to ensure adherence to scientific principles.

The chemistry of water radiolysis and H_2O_2 in aqueous systems is extensively researched and the rate constants for the reactions are derived. In chapter 2, water radiolysis resulting in the generation of reactive species was discussed. Reactions of Fe^{2+} with H_2O_2 generate $\bullet\text{OH}$ radicals in Fenton's oxidation, Reactions of Fe^{2+} and Fe^{3+} in aqueous solutions are also

considered in this kinetic model (Appendix 4). In this kinetic model, •OH radicals produced bring about the degradation of organics. Additionally, reactions of hydrated electrons and their influence on the Fenton reaction and the degradation of organic pollutants are also considered. The degradation of target compounds was simulated in a constant volume batch reactor observing mass balance. The concentration of species i (C_i) in the solution at any time (t) is described by the following ordinary differential equation:

$$\frac{dC_i}{dt} = r_i \quad (3.26)$$

where r_i is the rate of formation of species i per unit volume. Equations derived for each species are presented as ordinary differential equations and numerically solved in CHEMSIMUL to describe the change in concentrations of each species with respect to time.

The batch system simulation conditions were performed in a 35 mL volume of water. The oxygen concentration was 8mg/L as is in natural water and at an initial pH of 7. The concentration of CQ was adjusted between 25 to 125mg/L during the simulation. Additionally, pH was varied between 2 and 12 to show the effect of pH on the degradation process. Fenton-assisted degradation was also simulated under different concentrations of Fe^{2+} and H_2O_2 at different molar ratios. The results were compared to experimental results.

3.8. Ecotoxicity Analysis

Vertebrate testing is discouraged for the Registration, Evaluation, Authorisation, and Restriction of Chemical substances (REACH) under the European Union's regulation. Alternative non-testing approaches are more preferred and encouraged such as the quantitative structure-activity relationships (QSARs) (Melnikov et al., 2016). The ECOlogical Structure-Activity Relationship Model (ECOSAR) is used to analyze ecotoxicity where there is a lack of data for risk assessment. Quantitative structure-activity relationships (QSARs) predict the aquatic toxicity of new industrial chemicals in the absence of test data and ECOSAR offers a

pragmatic approach to QSARs. The similarity of structure and similarity in measured effect levels from aquatic toxicity data of chemicals are used to develop QSARs. QSAR models adhere to the Organisation for Economic Co-operation and Development (OECD) validation principles i.e. defined end points, unambiguous algorithm, a defined domain of applicability, appropriate measures of goodness-of-fit, robustness, and predictivity, and a mechanistic interpretation. QSARs estimate ecotoxicity by relating the potency of chemicals to the central nervous system and their lipophilicity.

Ecological Structure Activity Relationships (ECOSAR) estimates acute aquatic toxicity via the Mayer–Overton relationship for chemicals in which the aquatic toxicity has been previously measured within a structurally similar class and is trained on a large data set of Ecotoxicity studies from the ECOTOX database that follow OCSPP guideline. ECOSAR is used by the US EPA to predict aquatic toxicity of chemicals to fish, aquatic invertebrates (daphnids), and green algae (Reuschenbach et al., 2008). The database is divided into 111 structural classes and linear regression models between LC_{50} toxicity estimates and $\log P$ were developed for substances in each class. The algorithms used in the SARS reflect a linear regression relating aquatic toxicity of chemicals and their octanol-to-water ratio (K_{ow}). When chemicals belong to multiple chemical classes the most conservative (most toxic) estimate is provided based on the principle of excess toxicity. The SMILES notation, CAS numbers, and $\log K_{ow}$ value are primary inputs and in the absence of K_{ow} , K_{ow} is calculated with the EPISUITE KOWWIN. The KOWWIN module evaluates the partitioning of neutral compounds only; thus, the toxicity of organic acids and bases is estimated based on QSARs for non-ionized molecules of the same class. The program requires SMILES strings or CAS numbers as inputs to estimate LC_{50} thresholds and can process multiple substances in batch mode. ECOSAR is designed to perform best on compounds with $\log P < 5$ and molecular weight < 1000 amu. Chemicals that do not meet the latter two criteria, or are structurally dissimilar from the domain of every QSAR model within

ECOSAR, are considered outside the applicability domain (Melnikov et al., 2016). ECOSAR predictions indicate an 87–90% agreement between predictions and measured data for more than 2000 different chemicals and with <3% false negatives (Sanderson et al., 2003). ECOSAR is a free computer program used by

ECOSAR can only evaluate organic chemical substances with discrete structures and is not recommended for inorganic or organometallic chemicals, polymers, and chemicals with MW >1,000, mixtures, and nanomaterials. Additionally, the estimated aquatic toxicity is for screening purposes determining the need for further aquatic toxicity testing, and determining species sensitivity. However, the estimated values do not replace quantitative environmental risk assessment. Furthermore, for ECOSAR to work, there is a log K_{ow} cut-off; when the log K_{ow} is ≤ 5.0 for fish and daphnid, or ≤ 6.4 for green algae, ECOSAR provides reliable estimates for acute effects. However, if the log K_{ow} exceeds those limits, empirical data suggests that the decreased solubility of these lipophilic chemicals results in “no effects at saturation” during a 48-hour to 96-hour test. Similarly, for chronic exposures, the log K_{ow} cut-off is 8.0 or greater (indicating a poorly soluble chemical), and “no effects at saturation” are expected in saturated solutions even with long-term exposures. In addition, for solid chemical substances, it is important to compare the toxicity estimates with the water solubility (US EPA, 2012).

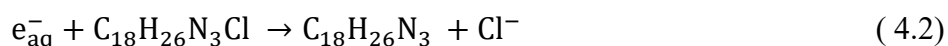
CHAPTER FOUR

4. Results and Discussion

The results of the degradation of CQ and HCQ are presented in this section, Different parameters including the effect of the absorbed dose, selective radical generation, initial pollutant concentration, initial pH of aqueous solutions, and dissolved oxygen were investigated. Additionally, the influence of different inorganic ions and additives on radiation-induced degradation of CQ and HCQ is described. Other parameters significant in the evaluation of wastewater treatment processes have also been applied to describe the degradation efficiency of CQ and HCQ under electron beam treatment.

4.1. Radiation dose effects on CQ and HCQ degradation

The reactions of water radiolysis products with a wide variety of compounds are described using pulse radiolysis. Similar studies suggest that CQ and HCQ are susceptible to attacks by the $\bullet\text{OH}$ radicals and the e_{aq}^- generated during the radiolysis water by ionizing radiation. The rate constants for the reactions of $\bullet\text{OH}$ and e_{aq}^- with quinoline, CQ, HCQ, and amodiaquine are presented in Table 4.1. The $\bullet\text{OH}$ and the e_{aq}^- play important roles in the degradation of CQ molecules via addition reactions and dissociative electron attachment according to Eq. (4.1) and Eq. (4.2) respectively. Reaction rate constants of CQ with $\bullet\text{OH}$ and e_{aq}^- at a pH of 8.5 have been previously evaluated and are shown in Table 4.1 (Bors et al., 1991).



Similarly, the corresponding reactions for these reductive and oxidative reactions with HCQ are provided in Eqs. (4.3) and Eq. (4.4) respectively with corresponding reaction rates in Table 4.1 (Rath et al., 2023).

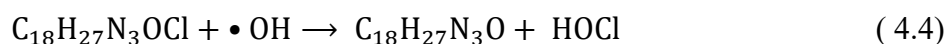
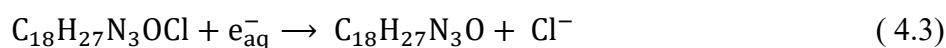
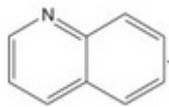
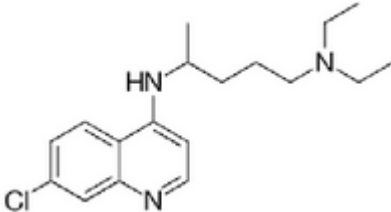
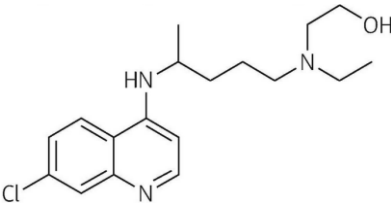
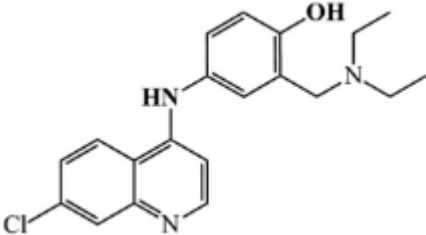


Table 4.1 Rate constants for the reaction of quinoline and its derivatives with $\bullet OH$ radical and e_{aq}^-

Compound	$\bullet OH$ $k(M^{-1}s^{-1})$	e_{aq}^- $k(M^{-1}s^{-1})$	Structure
Quinoline	1.0×10^{10}		
Chloroquine	7.3×10^9	4.8×10^{10}	
Hydroxychloroquine	9.5×10^9	2.0×10^9	
Amodiaquine	9.0×10^9	1.6×10^{10}	

Under electron beam (EB) irradiation, both CQ and HCQ concentrations reduced with increasing absorbed dose according to Fig. 4-1a & Fig. 4-1b, respectively. The degradation of HCQ was proposed to be preceded by the formation of both $[HCQ^+]$ cation and $[HCQ: OH]$ adduct as transient intermediates in the reaction between HCQ and $\bullet OH$ radicals with two absorptions at 330–340 nm (Rath et al., 2023). The cation was further suggested to decay at a

slower rate compared to the OH adduct. Similar radical adduct formation have been reported in the degradation of amodiaquine and acetaminophen (Kovács et al., 2020).

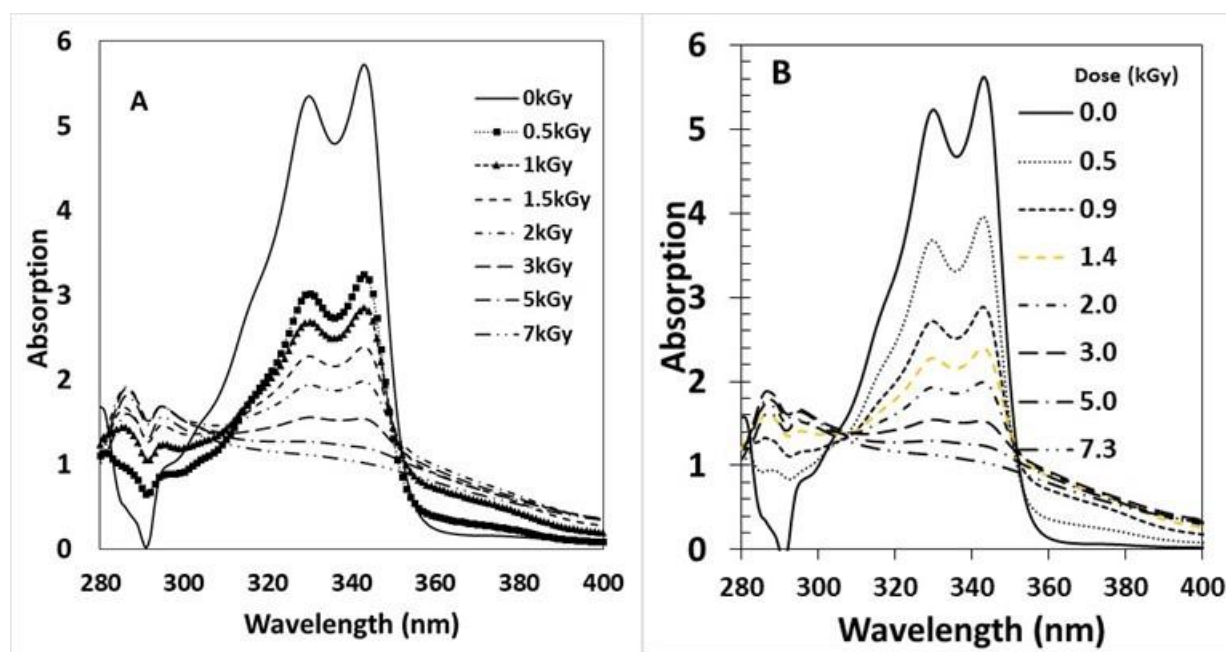


Fig. 4-1 UV-Vis spectrum for the degradation of 125mg/L of (A) CQ and (B) HCQ under EB irradiation at dose between 0.5 kGy and 7 kGy.

Mechanistic studies report that $\bullet\text{OH}$ is reactive towards aromatic and heterocyclic compounds and preferentially adds to the aromatic ring leading to the formation of hydroxycyclohexadienyl radicals (Nicolaescu et al., 2003). However, there is no specificity on where $\bullet\text{OH}$ addition occurs in the aromatic ring but computation studies show that the addition of $\bullet\text{OH}$ to both benzene and pyridine rings of the quinoline molecule is energetically favorable (see Appendix 3). Similar mathematical abstractions support $\bullet\text{OH}$ addition to the quinoline rings (Sanches-Neto et al., 2023). Additionally, the alkyl chain of CQ and HCQ is susceptible to $\bullet\text{OH}$ attacks leading to the dealkylation of the aromatic ring.

Gamma radiolytic degradation studies propose $\bullet\text{OH}$ radical attacks lead to the dealkylation of the aromatic part of HCQ by breaking the C-N bond in the aliphatic tertiary amine. The studies proposed the formation of 7-chloro-4-quinolinamine and 1-(N-ethylN-hydroxy-

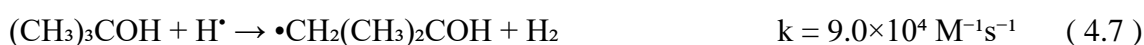
methylenamino)-4-amino pentane as main byproducts (Zaouak et al., 2022). Subsequently, 4-Amino-7-hydroxy-benzo pyridine is formed after •OH radical attack onto 7-chloro-4-quinolinamine that breaks the C–Cl bond and releases chloride ions. Similar mechanisms were proposed in the gamma radiolytic and ferrate degradation of HCQ (Boujelbane et al., 2022; Dong et al., 2022) These reactions involving OH addition and dissociative electron attachment lead to the dealkylation, dechlorination, and subsequent degradation of CQ and HCQ. At $\alpha = 0.05$, the removal of CQ under EB treatment is significantly higher than for HCQ (See Appendix 5).

4.2. The degradation of CQ and HCQ under •OH, e_{aq}^- , H•, and aerated conditions

The radiolysis of water under certain conditions promotes the selective generation of reactive species. The contribution of •OH radicals on the degradation of CQ and HCQ was studied by irradiation of solutions containing CQ and HCQ saturated with N₂O gas at a pH >3. In these conditions, the e_{aq}^- reacts with N₂O to form •OH radical (Eq. (4.5)) therefore increasing the concentration of •OH radicals in the solutions.



The reactions of H• radicals were studied in N₂O purged solutions spiked with 0.5M tert-butanol at pH <2. In these conditions, the •OH and e_{aq}^- species are scavenged by tert-butanol and N₂O respectively. Additionally, in acidic pH <2, most of the e_{aq}^- react with H⁺ to form H• radicals (Eq. (4.8)). Radicals formed from the reactions of tert-butanol with •OH and H• are considered inert (Eq. (4.6) & (4.7)).



The removal efficiency for CQ (Fig. 4-2a) and HCQ (Fig. 4-3b) was higher in the $\bullet\text{OH}$ conditions than under the e_{aq}^- . Reactions with $\text{H}\bullet$ atoms had higher removal efficiencies than for e_{aq}^- but lower than reactions involving $\bullet\text{OH}$. The removal of CQ and HCQ under aerated conditions was studied in solutions bubbled with air (N_2 -80%, O_2 -20%). Conversely, oxygen-free solutions ($\text{O}_2 < 1 \text{ mg/L}$) were obtained by bubbling Ar gas into the solutions.

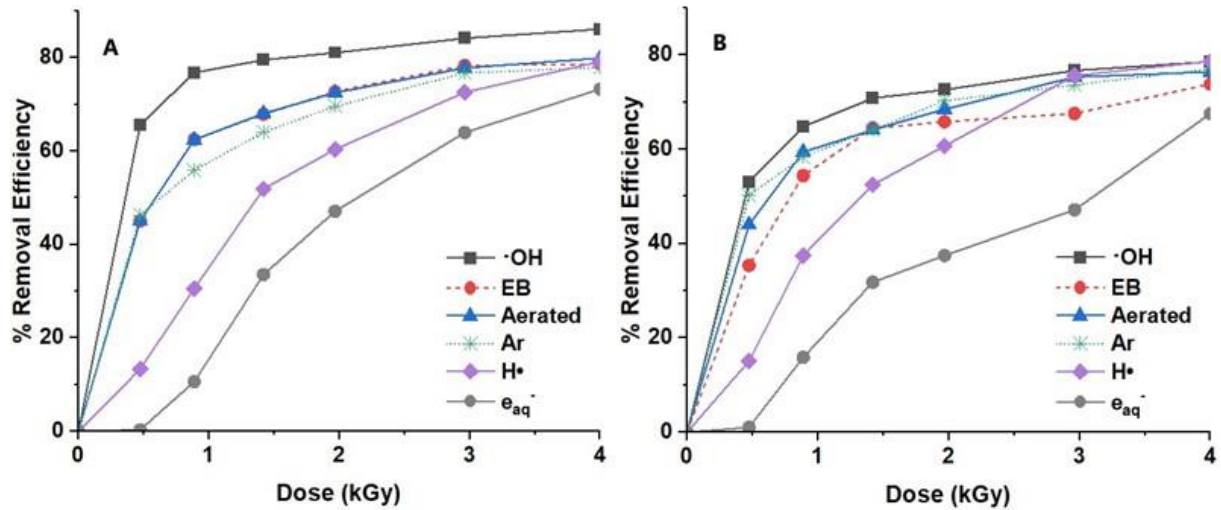
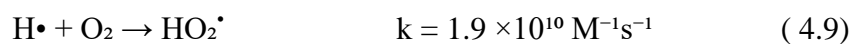


Fig. 4-2 Removal efficiency of (a) CQ and (b) HCQ under different irradiation conditions

The dissolved oxygen in the water reacts with $\text{H}\bullet$ (Eq. (4.9)), e_{aq}^- (Eq. (4.10)), and H^+ . These reactions lead to the formation of perhydroxyl radical ($\text{HO}_2\bullet$) which is a slightly weaker oxidizing species compared to $\bullet\text{OH}$ (Kovács et al., 2020). The $\text{HO}_2\bullet$ will react with organic pollutants and potentially increase the pollutant degradation. The removal of CQ and HCQ was almost similar in aerated and oxygen-free solutions (Fig. 4-2).



4.3. Effect of Initial Pollutant Concentration on the Removal Efficiency

The initial concentrations of CQ and HCQ were varied to study the effect of the initial concentration on the degradation efficiency. The removal efficiency decreased with increasing

concentrations of CQ and HCQ at the same absorbed dose as illustrated in Fig. 4-3a & 4-3d, respectively. Generally, all CQ and HCQ concentrations had degradation efficiencies between 70 and 80% for radiation doses greater than 2kGy. However, for lower concentrations (25mg/L) $\geq 99\%$ removal efficiency was achieved for CQ and $\geq 90\%$ for HCQ at an applied dose of ≈ 7 kGy (Fig. 4-3a & Fig. 4-3d). A similar effect was observed at lower doses. The degradation of CQ and HCQ was further represented using a pseudo-first-order relationship (Eq. (4.11))(Chen and Wang, 2021; Rehman et al., 2017).

$$-\ln \frac{[C]}{[C_0]} = kD \quad (4.11)$$

Where C and C_0 are the final and initial concentrations of the target compound at a dose D (kGy) with a rate constant of k. The results of the k values at different pollutant concentrations at 0.5 kGy for CQ and HCQ are shown in Fig. 4-3b & Fig. 4-3e respectively. The reaction rate k decreased with increasing concentration of CQ and HCQ in the solutions. Furthermore, the rate constants k for the degradation of CQ were higher than those for HCQ (Table 4.2). At $\alpha = 0.05$, the removal efficiency at lower concentrations was significantly higher for both CQ and HCQ (**Appendix 7 & Appendix 8**). However, for the concentration of 75 to 100 mg/L of HCQ, the difference was insignificant (**Appendix 8**).

Table 4.2 Rate constant k for different concentrations of CQ and HCQ and corresponding R^2 values

Conc.	CQ		HCQ	
	k(kGy ⁻¹)	R ²	k (kGy ⁻¹)	R ²
75	1.6567	0.9935	1.1287	0.9974
100	1.3603	0.9982	1.0706	0.9887
125	1.1224	0.9891	0.898	0.9443

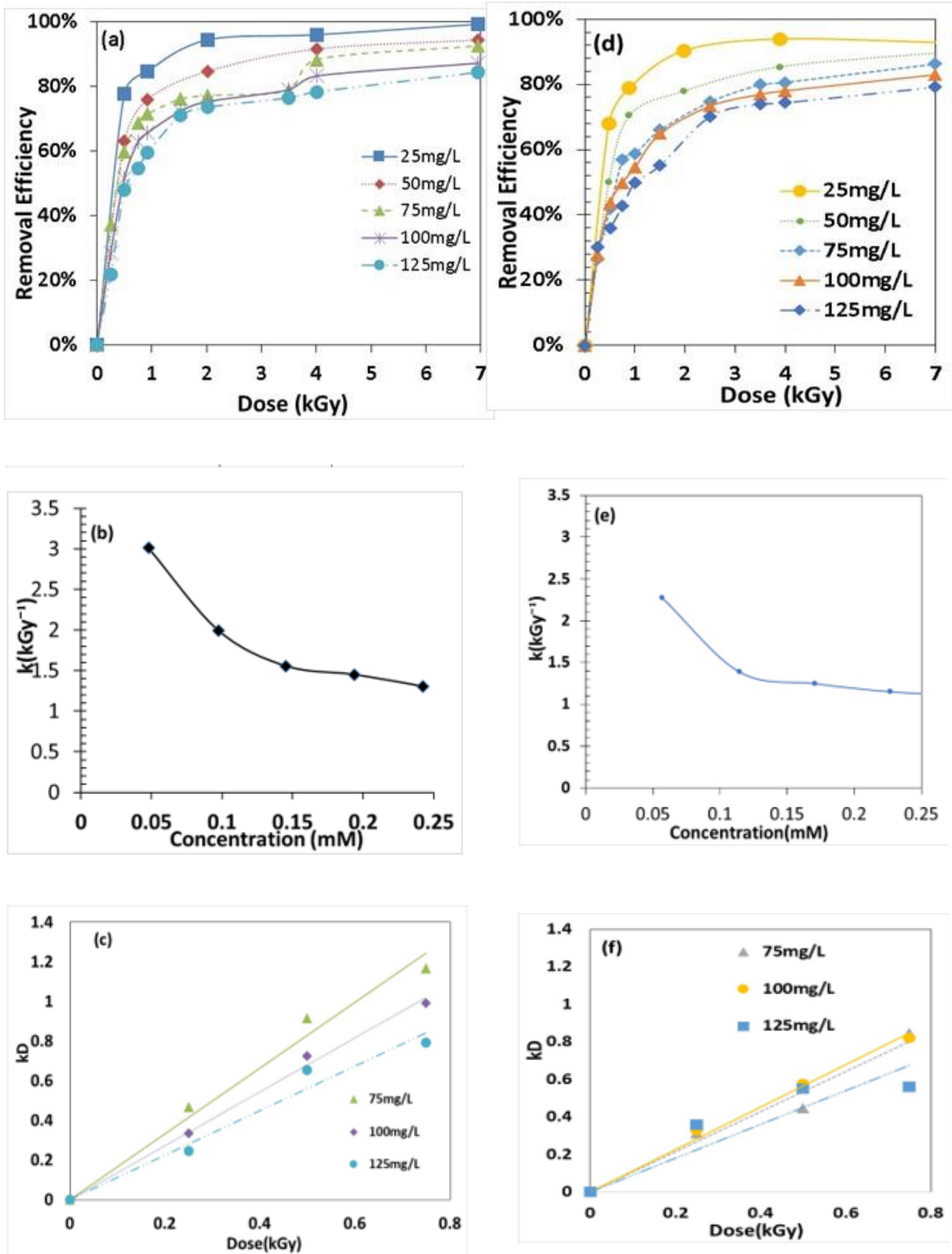


Fig. 4-3 Effect of the initial concentration of CQ and HCQ on the removal efficiency

4.4. Effect of Initial Solution pH on the Removal Efficiency

The solvent pH influences the different radicals generated during the radiolysis of the water. Under alkaline conditions, $\cdot\text{OH}$ readily reacts with OH^- to generate $\text{O}^{\cdot-}$ (Eq. (4.12)) thereby reducing the concentration of $\cdot\text{OH}$ hence the degradation efficiency. Additionally, the $\text{O}^{\cdot-}$ is a less powerful oxidant and its formation reduces the concentration of $\cdot\text{OH}$. $\text{O}^{\cdot-}$ also reacts at a much slower rate thereby affecting the degradation efficiency (Chu and Wang, 2022; Wang and Chu, 2016; N. Wang et al., 2016).



Conversely, in acidic media, the e_{aq}^- reacts with H^+ to produce H^\cdot according to Eq. (4.13). The H^\cdot radicals are less powerful reductants compared to e_{aq}^- towards most pollutants. However, according to the reactions in Fig. 4-3 in N_2O saturated solutions containing 0.5M tert-butanol in $\text{pH} < 2$, H^\cdot had higher removal efficiency compared to e_{aq}^- for both CQ and HCQ removal.



Under EB irradiation, pH enhances or inhibits the production of reactive oxidizing or reducing species and affects the degradation process. In this study, the degradation of CQ was observed to increase with increasing pH. At absorbed doses between 0.5 to 2kGy, the acidic pH of 2 to neutral pH of 7 had relatively lower removal efficiencies for CQ. This could be attributed to reactions involving the $\cdot\text{OH}$ radical and H^\cdot radicals formed in acidic conditions (Eq (4.14)) that reduce the concentration of $\cdot\text{OH}$ radicals.



In alkaline pH, a corresponding increase in CQ removal efficiency was observed (Fig. 4-4a). According to Eq. (4.1) to Eq. (4.4), reactions with the e_{aq}^- have a higher reaction rate compared to $\cdot\text{OH}$ radical reactions with CQ. More e_{aq}^- are produced in alkaline conditions according to

Eq. (4.15) which leads to a higher degradation of CQ. However, at higher production of e_{aq}^- (pH>10), recombination reactions occur which reduce degradation as observed in Fig. 4-4a and 4-4b at pH 12. Even though e_{aq}^- had lower removal efficiency for HCQ compared to $\bullet OH$, its removal under different pH was comparatively like CQ.



At low pH, e_{aq}^- is consumed which would result in lower removal efficiency for CQ and HCQ. Additionally, $\bullet OH$ radicals are known to have a higher reduction potential (2.72V) at acidic pH compared to alkaline conditions (1.89V) therefore their role in CQ and HCQ degradation would be affected at different pH (Dey, 2011). Neutral or acidic media are preferable for the degradation of HCQ under gamma irradiation (Boujelbane et al., 2022; Zaouak et al., 2022). From Fig. 4-4b, more than 80% of the initial HCQ concentration was removed at a maximum dose of 7kGy. However, electrochemical oxidation with boron-doped diamond anodes achieved about 60% removal efficiencies for HCQ at similar pH ranges (Bensalah et al., 2020). An acidic pH of 2 favored the decomposition of HCQ but decomposition reduced in alkaline conditions.

The pH value also affects the reaction pathways by changing the structure and characteristics of contaminants such as their solubility. Certain compounds retain their molecular form when the pH is less than their pK_a . However, when the $pH > pK_a$ the compound loses a proton and becomes negatively charged. Compounds such as diclofenac are insoluble at low pH values (around 3), which is a favorable condition for electron beam irradiation (Cuccarese et al., 2021). Therefore, the optimization of pH may influence the solubility and degradation of some pollutants (Mirzaei et al., 2017). Acidic pH has been reported to favor electron Fenton oxidation, sulfate radical AOPs, and Fe (VI) oxidation (K_2FeO_4) of CQ. The pH of wastewater is a vital component before and after treatment for the eventual discharge of wastewater.

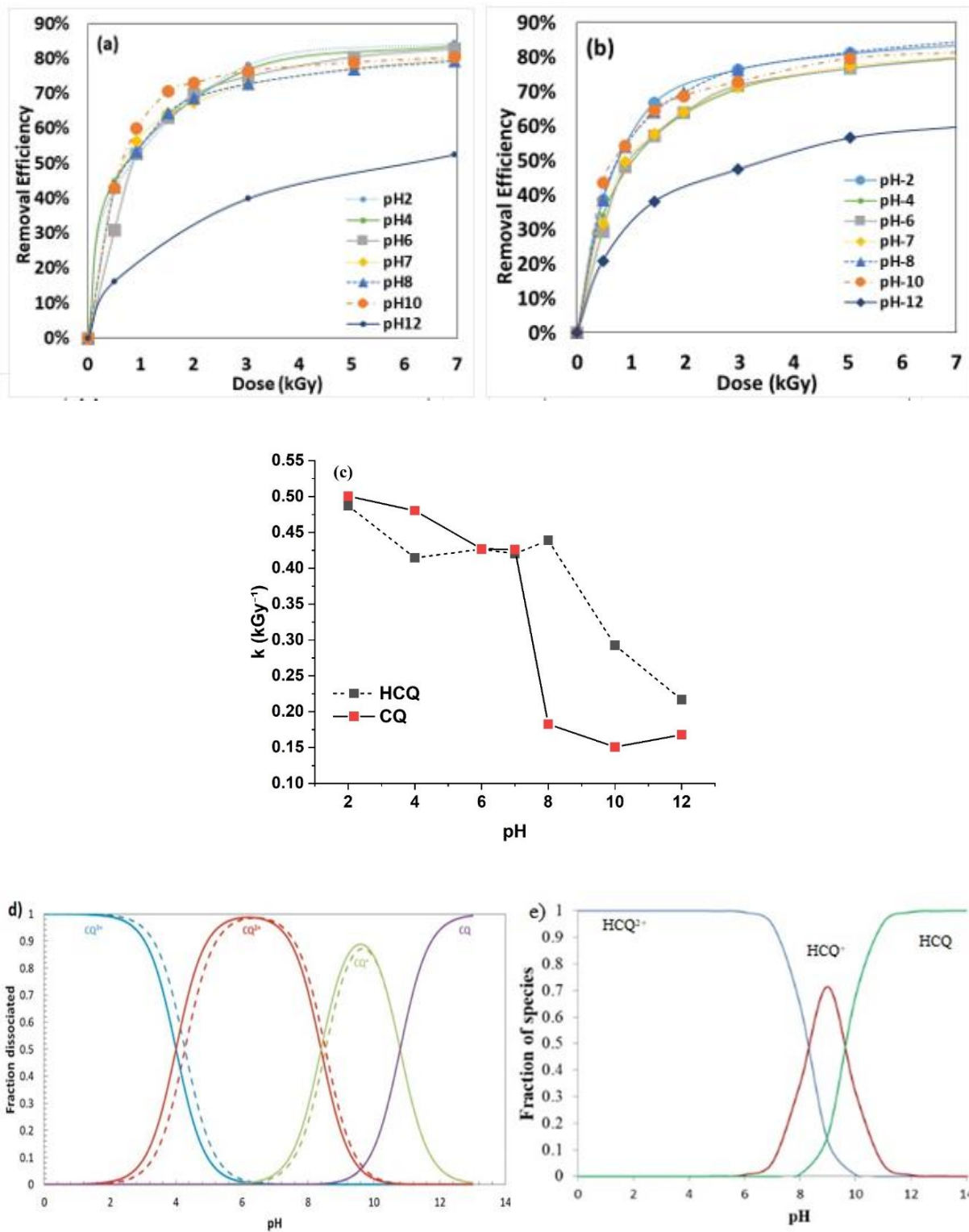


Fig. 4-4 Removal efficiency of 125mg/L under electron beam irradiation at different initial pH (a) CQ and (b)HCQ. (c) Dose constant variation with pH at 3kGy. (d) The fraction of protonated states of CQ at different pH (Schroeder et al., 2015) and (e) HCQ at different pH (Catrinel Ion et al., 2022)

The pKa of CQ is 8.76 and it is a weak acid with a tendency to donate electrons. Therefore, at $\text{pH} < \text{pKa}$ (between pH 2 and 7), CQ is in its non-ionic form (protonated). CQ is triply charged at pH 4.7 (Fig. 4-4d) but at $\text{pH} > 7$ the divalent form of CQ (CQH_2^{2+}) is dominant alongside lesser concentrations of the monovalent and neutral CQ (Schroeder et al., 2015). HCQ is similarly deprotonated at higher pH because of the hydroxyl group (-OH) which has pKa values in the range of 8.2 to 9.5 (Kamble Arun .D et al., 2011). HCQ is a basic substance, completely protonated at acidic pH values, as $\text{H}_2\text{HCQ}^{2+}$. At neutral values of pH, two protonated forms of HCQ are formed: $\text{H}_2\text{HCQ}^{2+}$ and HHCQ^+ (Klouda and Stone, 2020). In alkaline media, the ratio between the protonated form HHCQ^+ : HCQ is 1 to 6, meaning that the HCQ is mostly deprotonated. Similar to CQ at different pH, pH influences the molecular properties of HCQ which has three functional groups with pKa values of <4.0, 8.3, and 9.7. In acidic and neutral conditions, two of the functional groups exist in protonated forms (Rath et al., 2023; Warhurst et al., 2003) which facilitate the rupture of C-N bonds by $\bullet\text{OH}$ radicals attack and lead to the release of the branched group (Bensalah et al., 2020).

Other studies have observed faster HCQ degradation at higher pH values. Higher degradation in alkaline solution (pH 8 to 10) would indicate that deprotonation increases the electron density on HCQ and favors the electrophilic attack by reactive oxygen species, such as $\bullet\text{OH}$ radicals. This implies that the quinoline ring is more susceptible to the attack of $\bullet\text{OH}$ radicals at pH 9 than at pH 4 (Dabić et al., 2019). Regarding the half-life times ($t_{1/2}$), the values increase from a slightly acidic pH to a neutral one and then decrease once again. During gamma irradiation, the favorable range for pH values was from slightly acidic to neutral (Catrinel Ion et al., 2022). However, the HCQ elimination percentage as a function of the irradiation dose was found higher at pH 6.2 and pH 10 than at acidic pH for Experimental conditions: $[\text{HCQ}] = 100 \text{ ppm}$, dose rate = $26.31 \text{ Gy min}^{-1}$ gamma irradiation (Zaouak et al., 2022). Kovacs et al., while studying the degradation of amodiaquine under gamma irradiation observed that

the rate constants for the triethylamine part of amodiaquine were higher in its deprotonated state (pH=6.8) compared to the protonated form. Therefore, the latter form had a lower contribution to the overall degradation (Kovács et al., 2020).

The increasing concentration of solvated electrons at high pH leads to a decrease in the concentration of $\bullet\text{OH}$ radicals so the redox reaction is extremely rapid. At pH = 6.2, the best efficiency is obtained since all reactive species are free and are not involved in other reactions. Gamma radiolysis of 20ppm HCQ at pH of 4, 6.8, and 9 showed an overlap in removal efficiency in acidic to neutral conditions (Boujelbane et al., 2022). A similar observation is made for pH between 4 and 7 under EB treatment (Fig. 4-4a & Fig. 4-4b). However, in basic conditions, the removal efficiency increased with dose. The dose constant k (kGy^{-1}) is observed to decrease with increasing pH for both CQ and HCQ (Fig. 4-4c). However, at pH between 4 and 8 for HCQ there is little difference in the calculated k (kGy^{-1}) therefore showing an overlap in the removal efficiency. A similar overlap between pH 6 and 7 is observed for CQ. Under electrochemical oxidation, >60% of initial HCQ concentration was eliminated for pH between 2 and 12 like what is reported in this work. However, the efficiency decreased with increasing pH (Bensalah et al., 2020).

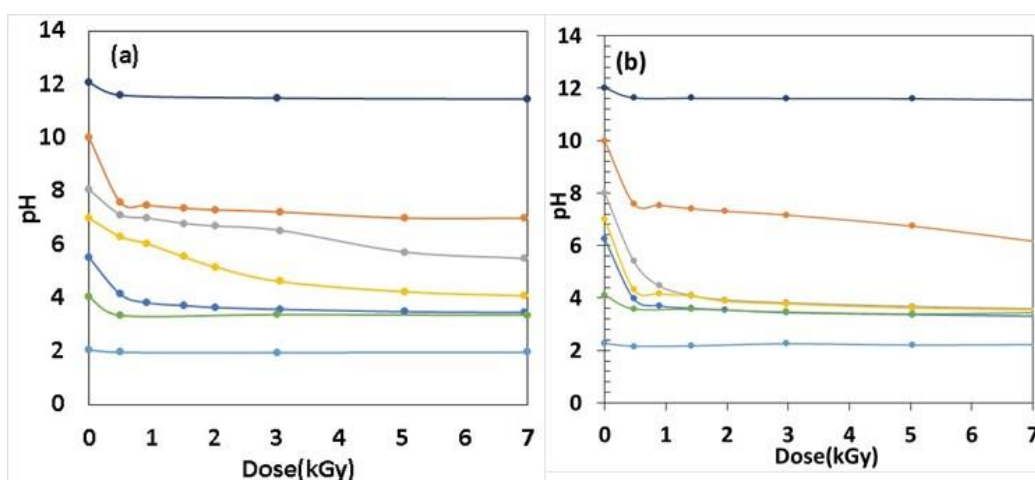


Fig. 4-5 Changes in pH of the solution with dose during the degradation of 125mg/L CQ solution (c) CQ (d)HCQ

Photolysis of HCQ is influenced by the pH and its degradation was faster at higher pH with complete degradation achieved at pH 9 after 40 min and after 22 h at pH 7. At a lower pH 4 complete degradation of HCQ was not obtained even after 52 h of radiation (Dabić et al., 2019). The pH between 4 to 10 is significant for producing the priority reactive species e_{aq}^- , H^\bullet , and $\bullet OH$ and influences the production of reactive species after electron beam radiolysis. Therefore, pH can be a tool for increasing the efficiency of electron beam treatment (Siwek and Edgecock, 2020). The changes in pH during the irradiation process are presented in Fig. 4-5.

During the radiolysis of the aqueous solution of CQ and HCQ, the pH was observed to decrease with increasing dose. For pH between 4 and 8, the pH decreased with increasing applied radiation dose and stabilized at a pH of about 3.5 (Fig. 4-5a & Fig.4-5b). Similar observations were made under gamma irradiation of HCQ at pH between 4 and 8 (Boujelbane et al., 2022). The solution at an initial pH of 2 remained constant throughout the irradiation process. However, the solutions at initial pH of 10 and 12 dropped to values of 6.5 and 11.5 respectively. It has been proposed that the decrease in the pH alludes to the formation of acidic or less basic intermediates during the degradation of CQ and HCQ.

4.5.Effect of inorganic ions, humic acid, and H₂O₂ on the removal efficiency of CQ and HCQ

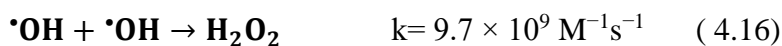
Raw water contains dissolved O₂, chloride ions, carbonate, bicarbonate ions, and different organic molecules (Wojnárovits and Takács, 2016). Most of the natural constituents of water are scavengers or enhancers that influence the overall efficiency of EB processing of water (Capodaglio, 2017). Both organic and inorganic species influence the radiolysis of water and therefore the application of radiation-induced processes in the removal of wastewater contaminants (Duarte et al., 2002; Wojnárovits and Takács, 2016). These constituents include O₂, HCO_3^- , CO_3^{2-} , Cl^- , NO_2^- , NO_3^- , dissolved organic carbon (DOC), and heavy metal (HM) ions (Capodaglio, 2019; Dabić et al., 2019; Wang and Chu, 2016). The rate constants of the

inorganic anions commonly present in the environmental samples with $\cdot\text{OH}$ or e_{aq}^- are in the same range as those of some persistent organic pollutants (POPs) and pesticides (Trojanowicz, 2020). Humic acids (dissolved organic matter) and nitrate ions act as photosensitizers, scavengers of radicals, or irradiation filters. Halides, bicarbonate, and iron (III) can generate or consume the reactive species. Similarly, these constituents in sewage sludge, wastewater, or natural water scavenge the reactive chemical species during EB irradiation thereby decreasing or increasing the overall process efficiency. Siwek and Edgecok (2020) described the actions of various natural constituents of water in scavenging water radiolysis reactive species (Siwek and Edgecock, 2020).

Atrazine degradation under gamma-ray irradiation decreased in the presence of 1 mM of NO_3^- , NO_2^- , Br^- , $\text{S}_2\text{O}_8^{2-}$, HCO_3^- and CO_3^{2-} due to their competition for reactive radicals (Khan et al., 2015). Similar moieties in addition to fulvic acid have been shown to influence the degradation of capecitabine under electron beam irradiation (Huo et al., 2020) and indomethacin (IDM) in aqueous solution where additionally HCO_3^- , SO_4^{2-} , and humic acid had a deleterious effect on efficiency (Duan et al., 2022). The presence of antioxidants like ascorbic acid and gallic acid slows down the degradation of HCQ under gamma radiolysis (Rath et al., 2023). Bicarbonate (HCO_3^-) scavenges $\cdot\text{OH}$ radicals' and affects the photodegradation rates of HCQ by the formation of carbonate radicals $\text{CO}_2^{\cdot-}$ while also creating alkaline conditions (Dabić et al., 2019). The effects of some common naturally occurring ions such as CO_3^{2-} , HCO_3^- , NO_3^- , and Fe^{2+} , dissolved organic matter in the form of humic acid, and molecules of interest i.e., $\text{S}_2\text{O}_8^{2-}$, and H_2O_2 on the degradation of CQ and HCQ under electron beam irradiation was investigated.

During the radiolysis of water, H_2O_2 is produced from reactions of the $\cdot\text{OH}$ radicals within the non-homogeneous track (Eq. (4.16)). The H_2O_2 reacts with the e_{aq}^- (Eq. (4.17)), $\cdot\text{OH}$ radicals (Eq. (4.18)), and H^{\cdot} atoms (Eq. (4.19)). It suggested that, at higher initial concentrations of

H₂O₂, the reaction of H₂O₂ with •OH influences degradation efficiency than that with e_{aq}⁻ (Iwamatsu et al., 2018).



In wastewater, H₂O₂ is consumed in Fenton-like processes with metal ions present in the wastewater. Additional •OH radicals generated in the Fenton-like processes propagate the degradation of organic pollutants present in the water. H₂O₂ and Fe²⁺ salts are the primary Fenton reagents. The effect of the respective Fenton reagents on the removal efficiency of CQ under electron beam irradiation was evaluated. The removal efficiency for CQ (Fig. 4-7a) and HCQ (Fig. 4-7b) was observed to slightly decrease with increasing concentrations of both H₂O₂ and Fe²⁺. In the presence of excess H₂O₂, HO₂[•] radical is generated which is a less powerful oxidant than •OH radical (Eq. (4.18)). Additionally, ferrous salts participating in Fenton-like processes may compete with the organic pollutants for the reactive water radiolysis products. Higher Fe²⁺ concentrations also increase the turbidity of water. However, unlike UV processes, the electron beam can penetrate turbid water. These factors collectively or exclusively affect the removal efficiency. Similar inhibition by H₂O₂ is reported for atrazine degradation (Khan et al., 2015).

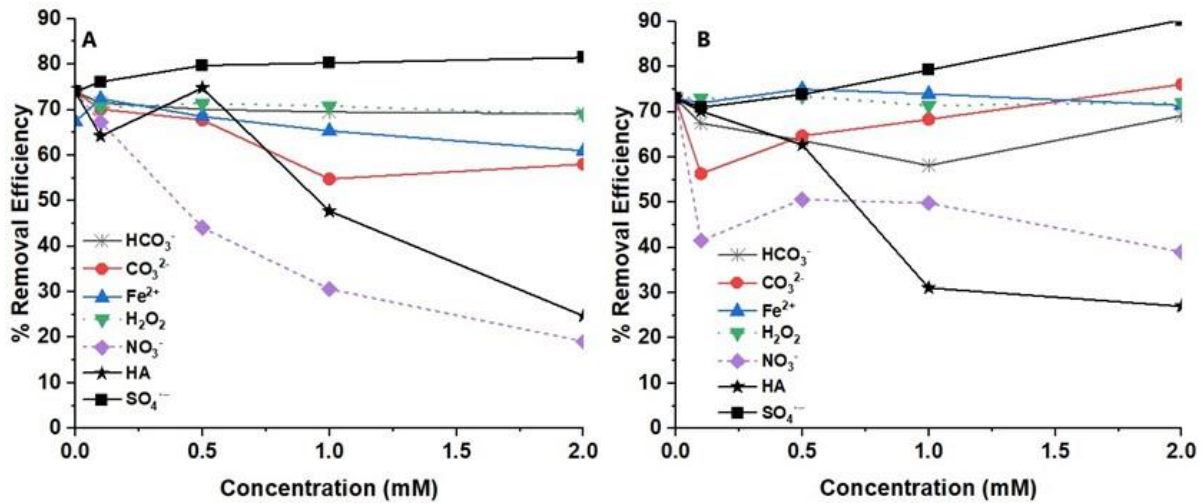


Fig. 4-6 Effect of different ions and additives on the EB-initiated degradation of (a) CQ, and (b) HCQ solution.

Persulfate ($S_2O_8^{2-}$) is applied for in situ chemical oxidation of organic contaminants in water. Persulfate is converted into reactive sulfate radicals ($SO_4^{\bullet-}$) and $\bullet OH$ catalytically by ferrous, zero-valent iron, manganate, cobalt salts, UV irradiation, electrochemically, base activation, sonication, or thermal degradation. However, ultraviolet light in subsurface remediation is impractical, cobalt is a toxic metal, Fe (II) salts are rapidly oxidized to insoluble Fe(III)-oxides in the presence of persulfate, and thermal activation is energy intensive (H. Liu et al., 2014). The activation of the persulfate is an integral part of the process (Sonawane et al., 2022). Electron beam irradiation was used to achieve this conversion. The reaction of the e_{aq}^- with $S_2O_8^{2-}$ in aqueous solutions produces the $SO_4^{\bullet-}$ radicals (Eq. (4.20)). Enhanced degradation was observed in EB persulfate activation for the treatment of benzotriazole (Roshani and Karpel Vel Leitner, 2011), and perfluorooctane sulfonate (PFOS) (Kim et al., 2019) as observed in the present study (Fig. 4-6a & Fig. 4-6b). Other reaction involving $SO_4^{\bullet-}$ produce $\bullet OH$ radicals that would further enhance degradation (Eq. (4.21) & (4.22)).





Dissolved organic carbon (DOC) is the fraction of organic substances that pass through a 0.45 μm filter and in high concentrations indicates anthropogenic influences. However, DOC is mostly of natural origin from the decomposition processes of plants or organisms living in water. Humic substances (fulvic and humic acids) are the dominant DOC fractions in freshwater and coastal seawater. In photo-irradiation of surface lake water and nitrate-rich groundwater samples by sunlight, dissolved organic matter (DOM) was observed to be a possible source and sink of $\bullet\text{OH}$ radicals through photoexcitation in the presence of NO_3^- and dissolved iron (Vione et al., 2006). Humic acid (HA) has been found to have synergistic effects on atrazine degradation (Khan et al., 2015). Similar enhancement is observed for humic acid (HA) at 0.5mM concentrations in this study for CQ (see Appendix 1 Fig. 5.1d) but not for HCQ (Fig. 4-6a & Fig. 4-6b). However, with increasing concentrations of HA, degradation of CQ was inhibited. Similar suppression of the degradation of diclofenac after gamma irradiation at 1 kGy in the presence of 0.1mM of humic acid has been observed (Zhuan and Wang, 2020a). The decline can be attributed to the increasing turbidity and the energy of the electron beam being expended in interactions with the HA solutes and reducing the production of $\bullet\text{OH}$ radicals.

Wastewater contains nitrogen-containing compounds that contribute to the presence of nitrate and nitrite ions. Nitrate ions scavenge e_{aq}^- and are reduced to nitrite ions (NO_2^-) that react with the $\bullet\text{OH}$ and promote the addition of NO_2 to aromatic solutes (Marussi and Vione, 2021; Wu et al., 2020). The nitrate anion reacts very rapidly with the e_{aq}^- (Eq. (4.23)) but much more slowly with the $\text{H}\bullet$ atom (Eq. (4.24)) but is sufficient to compete with H_2O_2 at reasonable

concentrations of solute (Hiroki et al., 2002). Therefore, nitrate concentrations above a few millimolar are sufficient to shield H₂O₂ from reactions with e_{aq}^- (Eq. (4.11)).



At higher concentrations, the nitrate scavenges the precursor to the e_{aq}^- thereby influencing H₂O₂ formation and the generation of $\bullet\text{OH}$ diminishes. Experimentally, sodium nitrate or sodium selenate minimizes the attack of H₂O₂ by the e_{aq}^- and H \bullet atom. Furthermore, NO_2^- generated from the reduction of NO_3^- scavenges both the $\bullet\text{OH}$ ($k = 4.1 \times 10^9 \text{ M}^{-1}\text{s}^{-1}$) and the e_{aq}^- ($k = 1.4 \times 10^9 \text{ M}^{-1}\text{s}^{-1}$) though it's a less efficient scavenger of the latter compared to NO_3^- (Chappuis et al., 2023; Yamamoto and Suzuki, 2020). The degradation of CQ and HCQ declined with increasing nitrate concentration at 2kGy dose (Fig. 4-6a & Fig. 4-6b). Nitrate in addition to bicarbonate influenced the radiolytic degradation of 2,4-dichlorophenol. Furthermore, dehalogenation and degradation products were found dependent on the pH, applied dose, and scavengers present (Drzewicz et al., 1999).

Other reactions of $\bullet\text{OH}$ radicals with inorganic salts can generate different inorganic radicals of lower reactivity and different reduction potentials (Buxton et al., 1988). Bicarbonate scavenges both the e_{aq}^- ($k = 1.0 \times 10^6 \text{ M}^{-1}\text{s}^{-1}$) and $\bullet\text{OH}$ (Eq. (4.26)). Divalent carbonate is a much stronger scavenger for $\bullet\text{OH}$ radical radicals than for e_{aq}^- (Eq. (4.25)). The $\text{CO}_3^{\bullet-}$ radicals resulting from these reactions are generally unreactive towards halogenated organic compounds and therefore don't promote degradation (Bettoli et al., 1998). The removal efficiency of CQ and HCQ decreased with increasing $\text{CO}_3^{2-}/\text{HCO}_3^-$ concentration (Fig. 4-6a & Fig. 4-6b). However, the inhibitory effect of the CO_3^{2-} was more pronounced than for HCO_3^- due to its higher affinity for $\bullet\text{OH}$ radicals. In contrast, the removal of HCQ decreased at 0.1mM

CO_3^{2-} then increased with increasing concentration of CO_3^{2-} (Fig. 4-6b see also Appendix 2 Fig. 5.2b). In studies on the photodegradation of HCQ, similar enhanced removal was attributed to the pH effects rather than reactions of $CO_3^{\bullet-}$ (Dabić et al., 2019).



4.6. Electron Beam Coupled with Catalytic Oxidation

Electron beam treatment (EB) is versatile, adaptive, and capable of incorporating other treatment processes to complement it. Pretreatment and posttreatment using EB have been shown to enhance the biological treatment of refractory organic pollutants (Bojanowska-Czajka, 2021b, 2021a). Different catalytic methods were used to promote the degradation of CQ and HCQ under EB treatment of the aqueous solutions.

4.6.1. Electron Beam-Fenton assisted degradation of CQ and HCQ

Fenton (Fe^{2+}/H_2O_2), photo-Fenton ($Fe^{2+}/H_2O_2/UV/sunlight$), and ozonation (O_3/UV) processes are the most widely used AOPs in the treatment of industrial wastewater. However, the harsh operational conditions (e.g. pH of about 3) of the Fenton process limits its practical application. Moreover, large amounts of H_2O_2 and Fe (II) (>50-80ppm) are required in the Fenton process, resulting in the generation of iron-containing sludge, which necessitates further treatment, removal, and disposal. Similarly, in the ozonation process, the low solubility and low mass transfer of ozone, and high operation cost, limit its practical application (S. Wang et al., 2022). However, synergistic effects in the simultaneous applications of two or more AOPs show improved efficiency in the removal of pollutants. Fenton-like processes were chosen in the context of this study utilizing the generation of highly reactive $\bullet OH$ radicals from the decomposition of H_2O_2 in the presence of Fe^{2+} (Eq.(4.27)) in addition to the $\bullet OH$ radicals

generated during water radiolysis. The back reaction (Eq (4.28)) is slower and limits the number of ferrous ions in the solution.



As already described under section 4.4.1, the removal efficiency of CQ and HCQ was lower in solutions containing either H_2O_2 or Fe^{2+} compared to the solutions without any additives. The reduced efficiency was pronounced with increasing concentrations of Fe^{2+} . Radiolysis in the presence of excess H_2O_2 generates the perhydroxyl radical ($\text{HO}_2\cdot$) which is a weaker oxidant compared to the $\cdot\text{OH}$ radical. Additionally, higher concentrations of Fe^{2+} cause turbidity while also increasing the scavenging of reactive species and reducing efficiency. Competition between these additives and the target pollutant for the reactive species impacts the overall efficiency. The H_2O_2 produced during radiolysis of water reacts with e_{aq}^- to form $\cdot\text{OH}$ (Eq. (4.17)). It also participates in Fenton/Fenton-like processes with Fe^{2+} present in the solution. Other studies using Fe^{2+} concentrations of between 0.1 and 0.6 mM indicate enhanced degradation of 20mg/L solution of sulfamethazine by gamma irradiation at a dose of 1kGy (Y. Liu et al., 2014).

4.6.1.1. Degradation of CQ and HCQ under Fenton Oxidation

Fenton and Fenton-like processes generate $\cdot\text{OH}$ radicals that are non-specific and highly reactive oxidants. The molar ratios of $\text{H}_2\text{O}_2:\text{Fe}^{2+}$ influence the Fenton reaction and degradation of organic contaminants. Furthermore, Fenton oxidation provides high performance, non-toxicity, and simplicity with the convenience of operating at room temperature and atmospheric pressure to achieve the desired oxidation of organics (N. Wang et al., 2016). The Fenton-type reactions generate reactive $\cdot\text{OH}$ radicals ($E^0=2.80$ V) that react with organic pollutants present in wastewater. The slow back reaction (Eq. (4.28)) gives the $\cdot\text{OH}$ time to interact with

pollutants in wastewater (Mirzaei et al., 2017). Additionally, perhydroxyl radicals (HO_2^\bullet) are produced in excess H_2O_2 but are weaker oxidants ($E^0=1.65V$). The efficiency of Fenton oxidation in the removal of CQ (Fig. 4-7a) and HCQ (Fig. 4-7c) from aqueous solution was determined. The concentrations of H_2O_2 ranged from 0.1 to 2 mM. For each of these H_2O_2 concentrations, ferrous salt (Fe^{2+}) was added such that the concentration of H_2O_2 was between 20 and 0.2 times the concentration of Fe^{2+} .

The removal efficiency of CQ and HCQ solution during the Fenton process after 3 hours of reaction time improved with increasing H_2O_2 concentration for all the molar ratios. The H_2O_2 concentration 2mM achieved the highest overall removal efficiency for all molar ratios of $H_2O_2:Fe^{2+}$. When H_2O_2 concentration was five times that of Fe^{2+} ($5\times$), the highest removal efficiency for CQ (57%) was observed after 3 hours. However, for HCQ at 2mM H_2O_2 concentration, the removal efficiency was high even at H_2O_2 concentrations that were double the Fe^{2+} (Fig. 4-7c). Fig. 4-7b and 4.7d show the reduction in absorption spectrum for CQ and HCQ respectively at 343nm. Similar increments in the removal of Rhodamine B dye with increasing peroxide concentration under Fenton oxidation have been reported (Wang and Wang, 2022). During the Fenton process, Fe^{2+} is the catalyst, and H_2O_2 (H_2O_2) is the oxidant and dominant source of $\bullet OH$. Therefore, insufficient H_2O_2 decreases the efficiency due to a deficiency of $\bullet OH$ generated by H_2O_2 decomposition.

HCQ had a higher removal efficiency ($>70\%$) under the Fenton oxidation at the same H_2O_2 concentrations and molar ratios compared with CQ. When the concentration of Fe^{2+} was higher than H_2O_2 ($0.5\times$ and $0.2\times$), a deleterious effect on the removal efficiency was recorded for both HCQ and CQ. Similarly, when the peroxide proportion was much higher ($10\times$ and $20\times$), the removal efficiency for CQ and HCQ was suppressed.

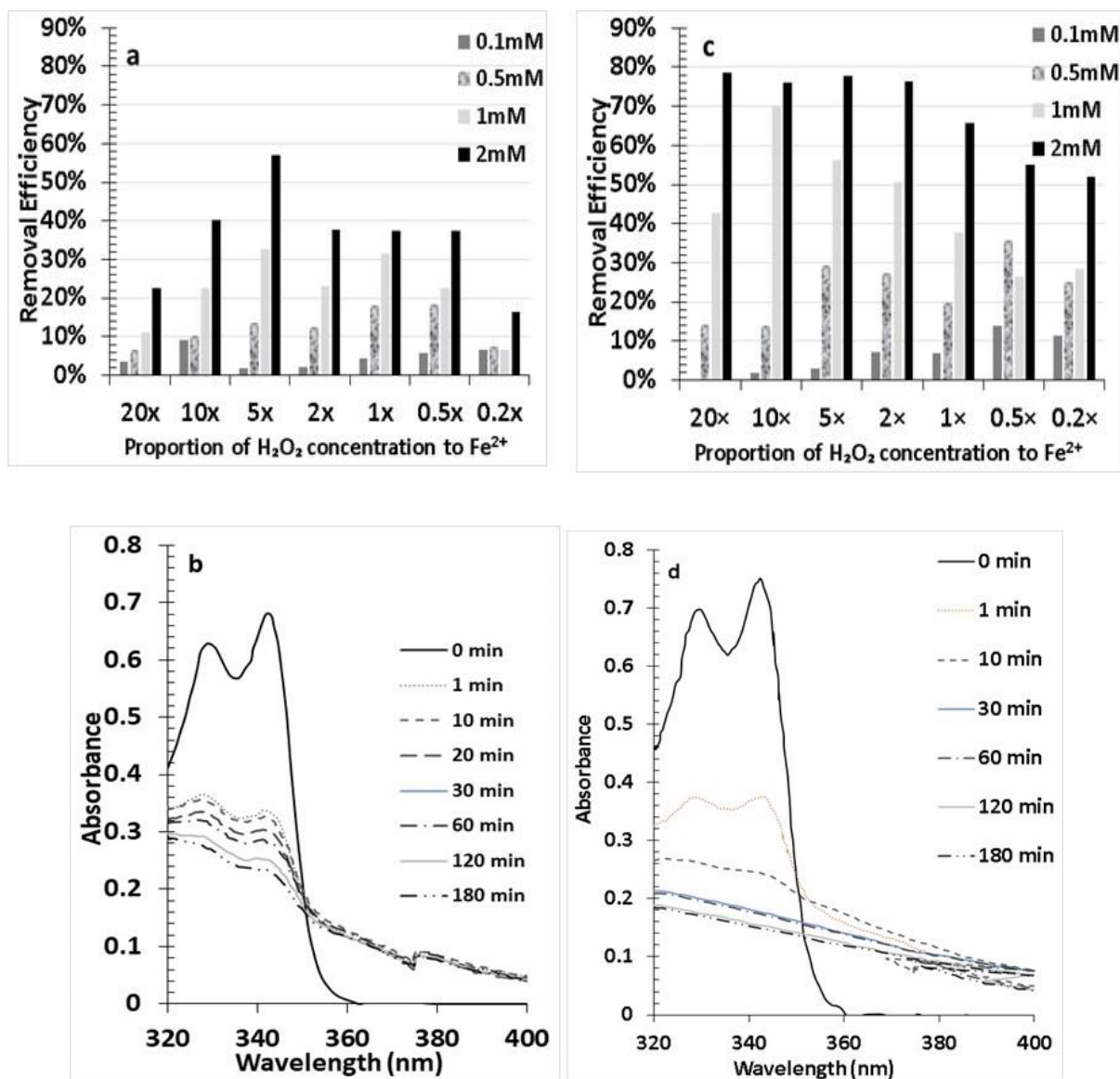


Fig. 4-7 Efficiency of Fenton process for (a) CQ and (c) HCQ, (b) Fenton degradation of CQ at 5× molar ratio with 2mM H_2O_2 . (d) Fenton degradation of HCQ at 5× molar ratio with 2mM H_2O_2 .

High H_2O_2 concentration leads to the scavenging of the $\bullet OH$ radical by the H_2O_2 (Eq. (4.12)). The resulting perhydroxyl radical is a less powerful oxidant compared to $\bullet OH$ radicals. Additionally, excess H_2O_2 has negative implications on COD, BOD, and microorganisms present in biological treatment while inadvertently increasing cost. Similarly, when Fe^{2+} are in higher proportions they scavenge the $\bullet OH$ radicals. The control experiments for H_2O_2 and Fe^{2+} showed no removal of CQ and HCQ even after 3 hours. Having established the efficiency of

the Fenton process in the removal of CQ and HCQ, the effect of Fenton-assisted electron beam irradiation on the process was evaluated.

4.6.1.2. Degradation of CQ and HCQ under Fenton-assisted Electron Beam process

The generation of $\bullet\text{OH}$ radicals is accelerated by utilizing UV radiation in photo Fenton processes. Alternatively, the generation of $\bullet\text{OH}$ radicals is achieved simultaneously by the radiolysis of water (Eq. (2.1)) and the H_2O_2 decomposition in the Fenton process (Eq. (4.27)) using Fenton-assisted EB (EB-F) treatment. Additionally, the e_{aq}^- generated in the radiolysis of water provides a synergistic route for increasing the rate of conversion of Fe^{3+} to Fe^{2+} (Eq. (4.28)) which is the main catalyst in the Fenton process. Results of the Fenton process showed that 2mM H_2O_2 at five times the Fe^{2+} concentration ($5\times$), gave the highest degradation efficiency of 56% and 75% for CQ and HCQ respectively, after 3 hours. Similar concentrations and molar ratios of Fenton reagents were applied in evaluating the Fenton-assisted electron beam treatment of CQ and HCQ (Fig. 4-8).

Contrary to the Fenton oxidation (Fig. 4-7), the highest removal efficiency; 90% for 94% for CQ and HCQ respectively, was attained when the hydrogen peroxide concentration was 20 times that of Fe^{2+} ($20\times$) in the EB-F process at 1mM and 2mM H_2O_2 concentrations, respectively (Fig. 4-8). Additionally, 0.5mM and 2mM H_2O_2 concentrations gave 85 % removal efficiency for CQ while 0.5mM and 1mM H_2O_2 concentration attained 80% and 85% HCQ removal, respectively.

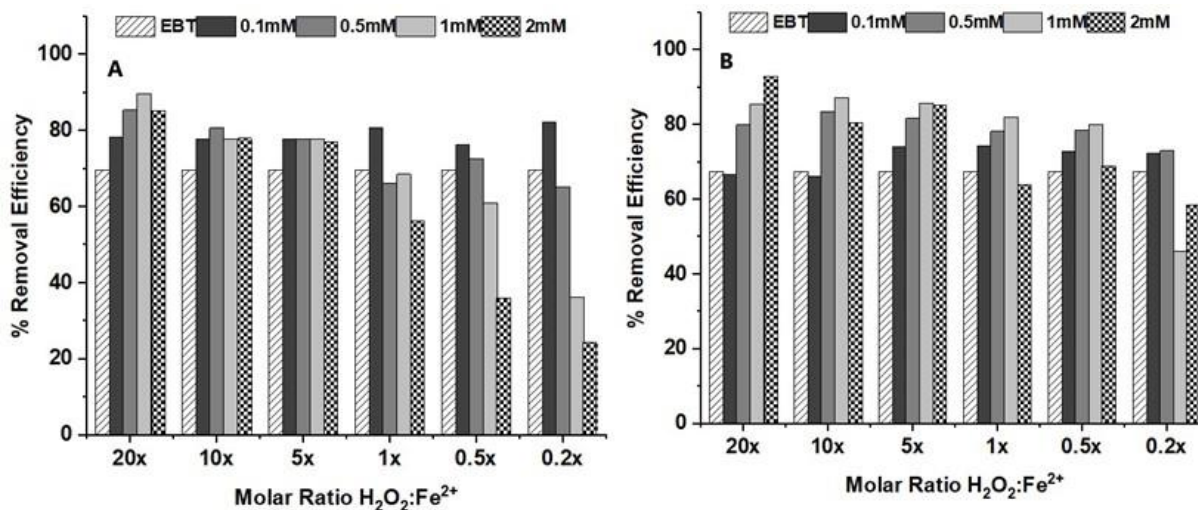


Fig. 4-8 EB-F degradation of (A) 125mg/L CQ and (B) 125mg/L HCQ solution. Results are presented for the different concentrations of H_2O_2 with different $H_2O_2:Fe^{2+}$ molar ratios at 2kGy.

Higher CQ removal was achieved at a lower H_2O_2 concentration at 20× molar ratio compared to HCQ. Furthermore, for all concentrations of excess H_2O_2 , there was an increased improvement in removal efficiency at all molar ratios compared to the EB process. The suppression of removal efficiency observed at excess H_2O_2 molar ratios in Fenton oxidation was not observed. However, this suppression was still observed at high concentrations of Fe^{2+} . The CQ removal efficiencies under EB-F were higher compared to HCQ at corresponding molar ratios and concentrations of Fenton reagents (Fig. 4-9). At $\alpha = 0.05$, the removal efficiencies for CQ and HCQ under EB-F were significantly higher compared to EB (**Appendix 5**).

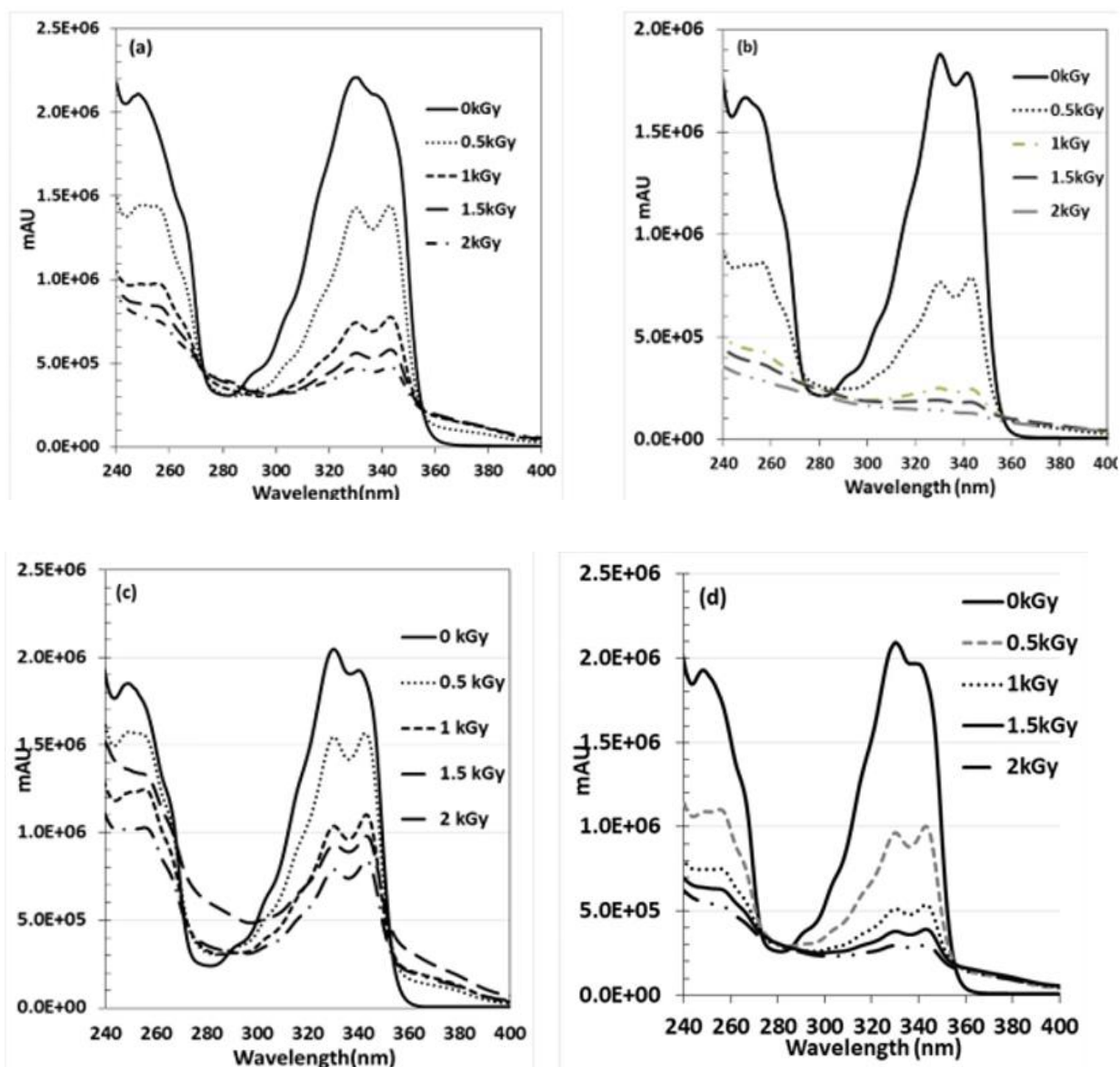


Fig. 4-9 Chromatograms for the degradation of CQ and HCQ under EB irradiation and under EB- Fenton process (a) Degradation of CQ under EB treatment (b) Degradation of CQ under EB-F. (c) Degradation of HCQ under EB (d) Degradation of HCQ under EB-F. $H_2O_2=2mM$, $Fe^{2+}=0.1mM$.

The initial concentration of CQ was reduced by $82\pm 1\%$ and $71\pm 1\%$ under EB-F and EB irradiation respectively at an applied dose of $\approx 2kGy$. This shows a $\approx 10\%$ improvement in the removal of CQ under the EB-F process compared to EB treatment. Similarly, under EB and EB-F processes, HCQ had $68\pm 2\%$ and $78\pm 4\%$ removal efficiency respectively with $\approx 10\%$

improvement at 2 kGy absorbed dose (Fig. 4-10a). Fig. 4-10b shows the decreasing G-Value with increasing dose for 125mg/L of CQ and HCQ under EB and EB-F. Therefore, the EB-F process improves the removal efficiency of CQ and HCQ. It is observed that CQ has a higher removal efficiency under EB irradiation and EB-F processes compared to HCQ. This could be attributed to the variation in structural properties. Furthermore, CQ has comparatively higher reaction rate constants with $\bullet\text{OH}$ and e_{aq}^- compared to HCQ. Additionally, the contribution of the e_{aq}^- to HCQ degradation is lower due to its lower reaction rate with e_{aq}^- compared to CQ (Table 4.1).

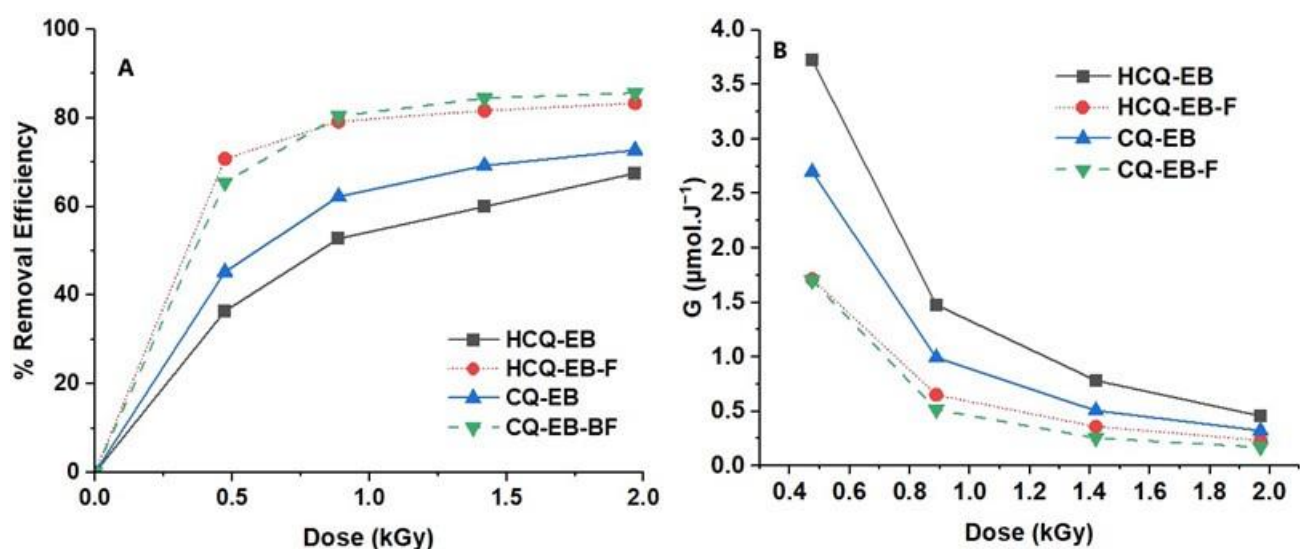


Fig. 4-10 (A) The removal efficiency for 125mg/L CQ and HCQ under EB irradiation and EB-Fenton assisted process (B) Calculated G- values for CQ and HCQ under EB, and EB-F

Homogeneous Fenton reactions are limited by the high $\text{Fe}^{\text{n}+}$ concentration (50-80 ppm) needed for the effective removal of contaminants. The limit for Fe^{2+} for water treatment effluent is 2ppm. Considering that higher concentrations of both Fe^{2+} and H_2O_2 were used in these experiments, it's probable that similarly high concentrations would be in the final solutions after treatment (Mirzaei et al., 2017; N. Wang et al., 2016). The unconverted H_2O_2 must be eliminated before discharging the final effluent due to potential toxicity in biotreatment in

addition to reducing COD removal efficiency. From the results of the Fenton oxidation and EB-F process, the $H_2O_2:Fe^{2+}$ molar ratio is an important factor and in practical wastewater treatment, depends upon the water matrix to be oxidized. Experimentally, it was observed that removal efficiency was lowered at $H_2O_2:Fe^{2+}$ molar ratios higher than $10\times$ in Fenton oxidation due to the scavenging of $\bullet OH$ radicals (Eq. (4.30)). The excess H_2O_2 concentration leads to the production of a less powerful oxidant $HO_2\bullet$. However, this scavenging is minimal in the EB-F process probably due to the reaction of the continuously reconstituted Fe^{2+} (Eq. (4.29)) with the excess peroxide.



Higher than optimal concentrations of Fe^{2+} limit degradation by acting as a scavenger (Eq. (4.31)) and additionally causing turbidity. The removal of HCQ under the EB-F process was higher compared to EB at doses between 0.5 and 2kGy. The self-quenching of reactive species, such as $\bullet OH$ radicals and e_{aq}^- , decreased due to the reaction between e_{aq}^- and H_2O_2 (Eq. (4.31)). The e_{aq}^- reacts with H_2O_2 ($\sim 10^{10} M^{-1}s^{-1}$) to produce $\bullet OH$ radicals which increase the concentration of $\bullet OH$ radicals.



An advantage of EB processes is the capability to penetrate turbid solutions which is not possible in UV-based processes. However, turbidity also increases competition for the reactive species. Higher concentrations of solid catalysts provide higher surface area and active sites but inadvertently increase the concentration of dissolved iron in the solution. The Heterogenous Fenton process is believed to circumvent issues related to ferric sludge generated in Fenton

processes as well as broaden the limited operational pH range of the Fenton process (Mirzaei et al., 2017).

4.6.2. Electron Beam coupled with g-C₃N₄ catalyst

Photocatalysts operational in the visible-light spectrum are deemed environmentally friendly and effective in the degradation of persistent organic pollutants. By utilizing the abundant solar energy, they convert organic pollutants into biodegradable compounds, CO₂, H₂O, and inorganic ions. However, the applications of photocatalysis are fraught with challenges such as their low solar energy conversion efficiency, instability in an aqueous environment, agglomeration, and photo corrosion. 1D/2D MnWO₄ nanorods anchored on g-C₃N₄ nanosheets (MnWO₄@g-C₃N₄) are better than MnWO₄ or g-C₃N₄ nanosheets in photocatalytic degradation of ofloxacin under visible light irradiation with first-order kinetics 4.8 and 3.5 times higher than that of pure MnWO₄ or g-C₃N₄, respectively (S. et al., 2019). Metal-organic frameworks (MOFs) can serve as light-sensitive semiconductors under solar illumination, are porous with infinite three-dimensional networks, stable crystalline structures, high pore volume, and large specific surface area, which are promising in overcoming the shortfalls of conventional photocatalysts including poor adsorption performance (Cao et al., 2020). Materials of Institute Lavoisier (MILs) are some of the most popular MOFs due to their high stability, permanent porosity, and extremely large specific surface area ideal for water treatment adsorbents (Zhang et al., 2022). These properties make them ideal in photocatalytic applications. MIL-68(In)-NH₂ possesses excellent visible-light response with high photocatalytic activity. However, its visible-light absorption edges and separation efficiency of photogenerated electrons and holes limit its application in the photocatalytic degradation of persistent organic pollutants. Heterojunction systems seek to circumvent these challenges by incorporating semiconductors with well-matched band structures within the MOFs.

Graphitic carbon nitride ($g\text{-C}_3\text{N}_4$) is an n-type semiconductor photocatalyst with a band gap of about 2.7 eV, non-toxic, thermally stable, chemically stable due to the strong C-N covalent bonds, low cost, with a relatively simple preparation process. Graphite carbon nitride ($g\text{-C}_3\text{N}_4$) has applications in photocatalytic reactions though it is limited by poor photoexcited charge separation, limited range of visible light absorption, and low surface areas (Luo et al., 2023). The $g\text{-C}_3\text{N}_4$ provides a convenient route for the synthesis of metal-free semiconductor-based catalysts (Biswas and Pal, 2023). Several methods including the construction of heterojunctions enhance its photocatalytic activity by reducing electron-hole pair recombination, small surface area, and low reusability that limits its applications. MOFs with $g\text{-C}_3\text{N}_4$ are promising in the development of efficient heterojunction photocatalysts for wastewater treatment. Doping $g\text{-C}_3\text{N}_4$ is considered an excellent way to improve photocatalytic activity. Magnetic $\text{CuFe}_2\text{O}_4/g\text{-C}_3\text{N}_4$ (CFO/g) photocatalyst demonstrated excellent photo-Fenton performance in the degradation of tetracycline with minimal loss in efficiency (8%) after ten cycles showing excellent stability. The CFO/g heterojunction enhanced the separation of photogenerated electron-hole pairs and visible light absorption range while its magnetic properties made it more easily recycled than traditional catalysts (Sun et al., 2022). Magnetic $g\text{-C}_3\text{N}_4/\text{Fe-MCM-48}$ prepared by uniformly doping the MCM-48 framework with Fe atoms, and then wrapping it with $g\text{-C}_3\text{N}_4$ nanosheet showed a synergistic effect, activity (100% in 11 min), and stability in photocatalytic ozonation of azithromycin (AZY) (Ling et al., 2023). In the present study, 4 catalysts were prepared based on the methods outlined in chapter 3.3. The CQ and HCQ solutions containing the catalysts were then irradiated under the electron beam at different doses between 0.5 and 4kGy. The results for EB combined with catalyst I-IV are presented in Fig. 4-11. Four types of catalysts were investigated namely, MCN (II), MIL-Mn(Fe)- NH_2 (III), $g\text{-C}_3\text{N}_4/\text{MIL-Mn(Fe)-NH}_2$ (IV), and MCN/MIL-Mn(Fe)- NH_2 (V). Catalyst II and IV gave results that were comparable to EB without catalyst

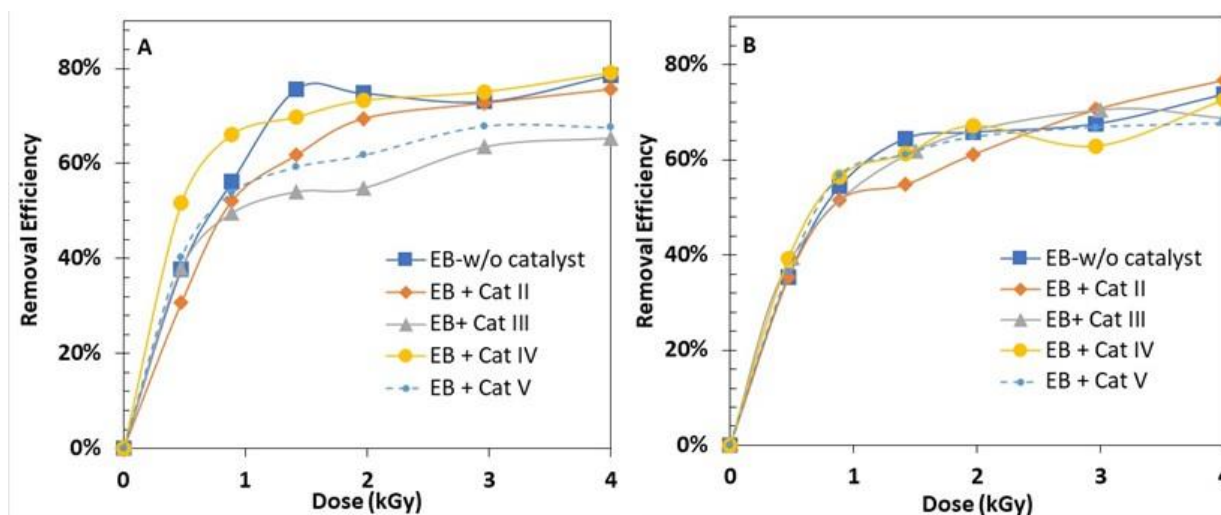


Fig. 4-11 Electron beam coupled with catalytic degradation of (a) CQ and (b) HCQ at catalyst loading of 0.2g/L. Cat II-MCN, Cat III-MIL-Fe(Mn)-NH₂, Cat IV-g-C₃N₄/MIL-Mn(Fe)-NH₂, Cat V-MCN/MIL-Mn(Fe)-NH₂

4.6.3. Electron Beam coupled with TiO₂ catalyst

Semiconductors such as TiO₂ utilize light energy by absorbing photon energy. When the photon energy exceeds its bandgap, an excited electron (e⁻) is transferred from the valence band to the conduction band thereby creating a hole (h⁺). The electron-hole pair has a high activity state acting as a reductant and oxidant. The holes can either react directly with organic molecules or form •OH radicals that subsequently oxidize organic molecules. TiO₂ is an inexpensive, safe, strong oxidant, and chemically stable catalyst popular in the photocatalytic degradation of organic pollutants. TiO₂ has an amphoteric property, and its surface charge is directly dependent on its pH. Its point of zero charge is about pH 6.7. Therefore, its surface charge in alkaline conditions (pH >6.7) is negative and has a positive charge for acidic situations (pH < 6.7). The ionic nature of the antibiotic causes an electrostatic interaction between the catalyst and pollutant. The degradation of the pollutants decreased by increasing the TiO₂ concentration. The accumulation of catalysts in the solutions and prevention of light penetration leads to a decrease in the degradation of pollutants (Hajiani et al., 2022). titanium dioxide (TiO₂) containing

materials have been favored because of their anticipated combination of unique electronic structure, impressive light absorption properties, prolonged excited-state lifetimes, and enhanced charge transport features (Paumo et al., 2021).

Photocatalytic degradation mainly occurs on the surface of TiO₂ therefore prevalent limitations in the transfer of electron and hole pairs inhibit TiO₂ photocatalytic efficiency. Additionally, the recombination of electrons and hole charge carriers leads to the suppression of photocatalytic activity. Furthermore, TiO₂ photocatalysts may have a poor affinity towards organic pollutants (i.e. Hydrophobic organic pollutants) causing low adsorption and slow degradation. The instability of the nanosized particle has also been linked to the aggregation of TiO₂ nanoparticles which may prevent the active centers from receiving the light radiation and consequently hamper photocatalytic activities of TiO₂. Higher scattering conditions of particles, inefficient recovery of the nanosized TiO₂ particles from the treated water, and High band energy of initial TiO₂ photocatalysts also affect applications (Cao et al., 2020). Electron beams have conventionally been used to modify the surfaces of TiO₂ to improve their optical properties (Li et al., 2023; Seo et al., 2012). In this study, electron beam irradiation was performed in the presence of TiO₂.

Under EB/TiO₂, the degradation of CQ was observed to have no substantial change compared to samples that were only degraded under EB at TiO₂ concentration of 0.1mg/L (Fig. 4-12a). However, with increasing the concentration of TiO₂ the removal efficiency was observed to decrease. A similar observation was made for HCQ with increasing concentration of TiO₂. However, for HCQ removal, TiO₂ of 0.15mg/L gave the highest removal efficiency. The order of removal was 0.15mg/L > 0.1 mg/L > 0.2 mg/L > 0.25 mg/L > EB (Fig. 4-12b).

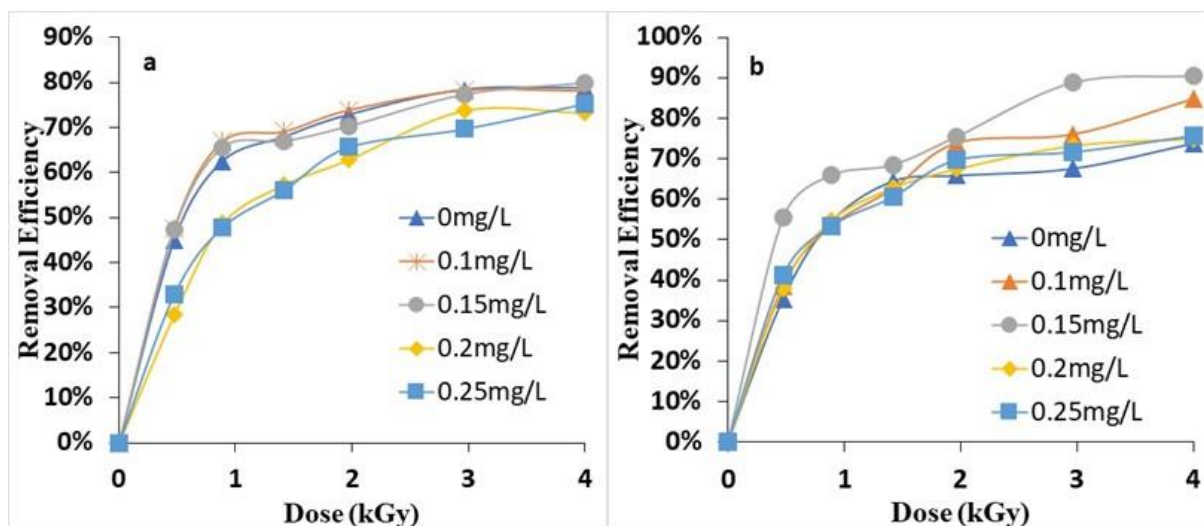


Fig. 4-12 Degradation of (a) CQ and (b) HCQ under electron beam irradiation with varying concentrations of TiO₂ as a catalyst

Increasing concentrations of TiO₂ caused visible turbidity. 1 mmol L⁻¹ 4-chlorophenol solutions showed a decrease in absorption peak at 198nm with increasing TiO₂ contents from 0 to 0.5 g L⁻¹. At a dose of 12kGy, a marked decrease was observed in the concentration of 4 Chlorophenol in solutions containing TiO₂ catalysts. Increasing the concentrations of TiO₂ from 0.5 to 5 g L⁻¹ led to further reduction in the absorption peak at 198nm showing that TiO₂ had a positive effect on degradation (Yang et al., 2007).

4.7. Degradation monitoring

The results for the degradation byproducts are based on the degradation of 125mg/L of CQ and HCQ solutions under EB and EB-F processes. The aqueous solutions were irradiated at absorbed doses between 0.5 and 7kGy. Additionally, parameters used in wastewater treatment such as TOC, COD, and nitrogen content were used to evaluate the effectiveness of CQ and HCQ treatment under EB and EB-F processes. The degradation byproducts discussed in this section are based on the degradation of 125mg/L of CQ & HCQ under EB and EB-F irradiation at neutral pH.

4.7.1. Change in solution pH

During the radiolysis of the CQ and HCQ solutions, the pH was observed to reduce from 6.5 before irradiation to 3.2 at 7kGy as shown in Fig. 4-13a. A similar decrease in pH has been observed in the degradation of ciprofloxacin where pH decreased from 7. to 4 at 5.0 kGy, consistent with the formation of lower molecular weight organic acids and dissolved ions resulting from EB treatment (Kiyoshi Tominaga et al., 2023; Mirzaei et al., 2017). Similar changes in pH during the degradation of diuron by gamma radiolysis, CQ, and HCQ by gamma and electro-Fenton oxidation have been attributed to the formation of lower molecular-weight carboxylic acids, ions, ketones, and aldehydes (Bensalah et al., 2020; Kovács et al., 2015; Midassi et al., 2020; Tominaga et al., 2018a).

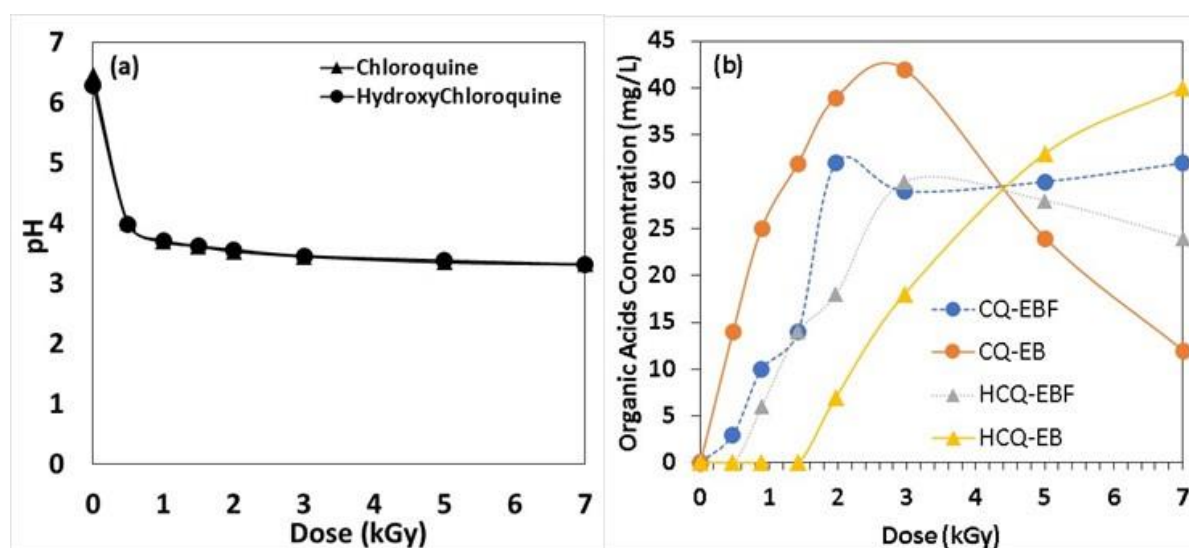


Fig. 4-13 (a) Changes in pH during EB irradiation of 125mg/L CQ and HCQ. (b) Generation of organic acids during degradation of 125mg/L CQ and HCQ under EB and EB-F (EBF) processes

At the lower pH degradation of CQ and HCQ was diminished according to Fig. 4-1 and Fig. 4-2. Additionally, degradation byproducts may compete for the reactive radiolysis species and therefore cause a reduction in the removal efficiency of CQ and HCQ. The reduction in pH in

the degradation of CQ and HCQ was attributed to the formation of organic acids whose concentration increased with increasing irradiation dose (Fig. 4-13b). The initial pH for solutions containing Fenton reagents was also recorded with increasing irradiation dose. The pH of solutions containing H₂O₂ or ferrous salt dropped with increasing concentrations of either additive before irradiation (Fig. 4-14A, B, C, D).

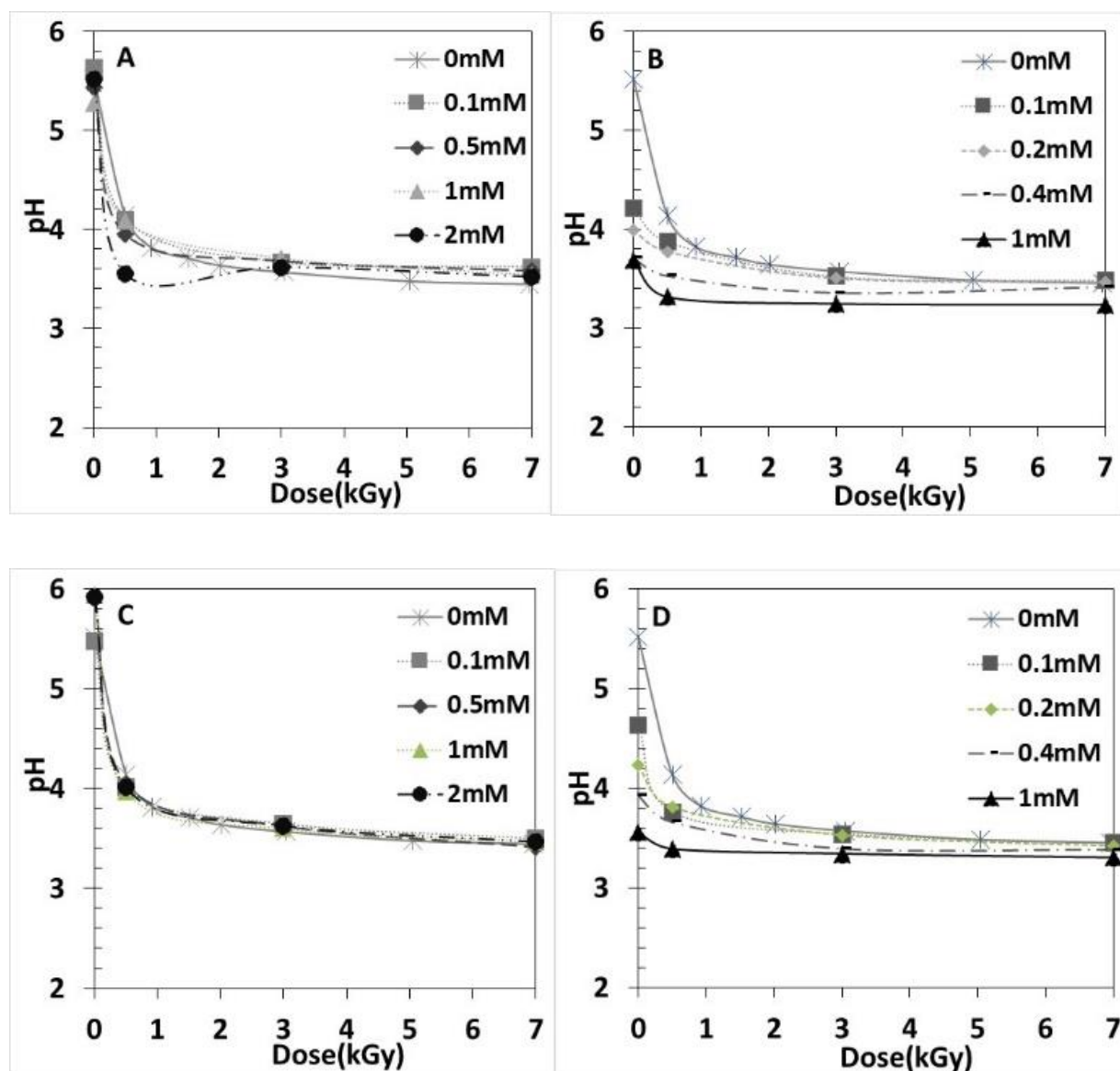


Fig. 4-14 Changes in pH during the electron beam-initiated degradation of CQ and HCQ solution (A) & (C) at different initial H₂O₂ concentrations for CQ and HCQ respectively (B) & (D) at different initial concentrations of Fe²⁺ for CQ and HCQ respectively

For the H₂O₂ concentrations, the pH was slightly acidic between 5 to 6 (Fig. 4-14A) and progressively decreased with dose to pH 3.5 at 7kGy with about 80% removal efficiency for 125mg/L of CQ solution. Similar observations were made for HCQ solutions with different H₂O₂ concentrations (Fig. 4-14C). Alternatively, irradiation with the addition of Fe²⁺ was performed under acidic conditions between a pH of 3.5 to 4.5. The pH was observed to decrease with increasing concentration of Fe²⁺ (FeSO₄) in the degradation of CQ (Fig. 4-14B) as well as in the degradation of HCQ (Fig. 4-14D). It is characteristic for the Fenton process to occur under acidic conditions owing to the Fenton reagents (Jung et al., 2009).

The important parameters pH, H₂O₂ dosage, catalyst dosage, and temperature affect Fenton and Fenton-like processes. The heterogeneous Fenton-like processes are found more effective at a pH of 3. However, neutral conditions (even alkaline conditions) could still achieve better treatment efficiency. These observations are mainly due to the different solubilities of a metal ion (such as the Fe ion) on the surface of a catalyst and the different activities of active sites on the catalyst surface. Conversely, there exists an optimum pH from 2.5 to 3.0 for the degradation of most organic compounds under homogeneous Fenton-like processes. At pH <2.5, the scavenging effect of the •OH radicals by H⁺ (Eq (4.32)) becomes stronger (N. Wang et al., 2016; Wang and Wang, 2022) whereas at pH > 3.0 the hydrolysis and precipitation of Fe³⁺ in the solution can reduce the catalytic capacity (Mirzaei et al., 2017).



Generally, the pH influences the performance of the homogeneous Fenton reactions. A pH of around 2 to 3 is considered optimal for Fenton reactions while at values over 5, poorly soluble ferrous hydroxide is formed (Eq. (4.33)) and its precipitation consumes ferrous ions, inhibits the Fenton reaction, and reduces the penetration of radiation by increasing turbidity (Wang and Wang, 2022).



Additionally, the oxidation potential of $\cdot\text{OH}$ changes at different pH values ($E^0 = 2.8 \text{ V}$ at pH 0 and $E^0 = 1.59 \text{ V}$ at pH 14). At $\text{pH} > 4$, the low rate of H_2O_2 decomposition leads to a decrease in the production of $\cdot\text{OH}$, and H_2O_2 is preferentially decomposed into H_2O and O_2 . In basic media (Eq. (4.34) & (4.35)), H_2O_2 is decomposed to oxygen without generating $\cdot\text{OH}$ radicals (Jung et al., 2009).



Similarly, strongly acidic media reduce the formation of $\cdot\text{OH}$ radicals by forming complexes that react slowly with H_2O_2 thus generating lower amounts of $\cdot\text{OH}$ radicals. Additionally, the abundant H^+ can scavenge the $\cdot\text{OH}$ radical (Eq. (4.36)).



At strongly acidic media (pH about 1), H_2O_2 molecules cannot be decomposed to produce $\cdot\text{OH}$ radicals because, under these conditions, H_2O_2 will solvate an H^+ to form an oxonium ion which is electrophilic and has reduced reactivity with ferrous ions.

4.7.2. Cl^- generation

Elevated chloride levels in water are associated with oil and gas drilling, saltwater intrusion, landfill leachate, fertilizers, septic system effluent, road salt storage, salt mining, deicing agents, and saline/brine water deposits. High chloride levels attack and weaken metallic piping and fixtures and promote corrosion. It also inhibits the growth of vegetation, alters the aesthetic taste of water, and corrodes household appliances and boilers. Fresh water contains $< 500 \text{ mg/L}$ of dissolved salts and saline water 3-5% of dissolved salts. Generally, chloride is not considered a health risk at low concentrations but at high levels, it can cause hyperchloremia in the human

bloodstream and an off-taste in water at concentrations between 200-300mg/L. Chloride is regulated in drinking water because of the aesthetic, cosmetic, and technical effects it has on the body, plumbing, and appliances. Drinking water standard is at 250mg/L and water is considered undrinkable at >1000mg/L.

During the radiolysis of organic compounds with good leaving groups such as halogenated compounds, dissociative electron attachment as shown in Eq. (4.2) & Eq. (4.3) is the most preferred reaction process of the hydrated electron (McAllister et al., 2019; Wang et al., 2017). This is due to the high electron affinity of halogens (Wu et al., 2009). The Cl^- ions present in CQ and HCQ were released with increasing applied radiation doses (Fig. 4-15A). Dechlorination was higher in $\bullet\text{OH}$ conditions compared to e_{aq}^- for both CQ and HCQ (Fig. 4-15B). The chlorine group is presumed to be responsible for the toxicity of organic compounds. Therefore, de-chlorination implies a decrease in the toxicity of the aqueous solution (Makarov and Ponomarev, 2018). At $\alpha = 0.05$, the Cl^- release was faster under EB-F compared to the EB process (Appendix 9).

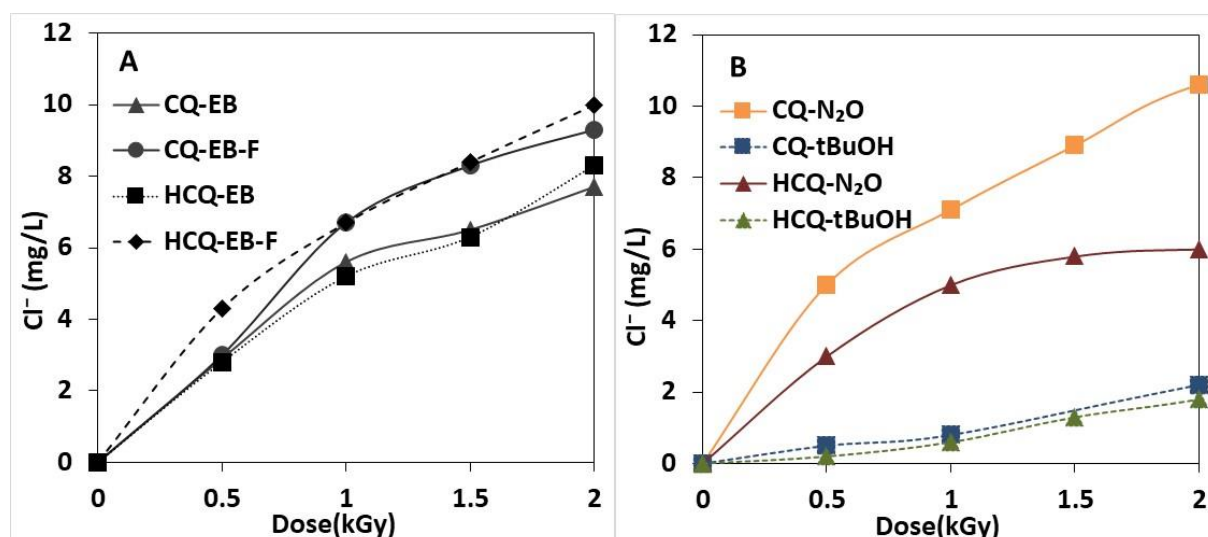


Fig. 4-15 (A) Release of Cl^- with increasing dose during radiolysis of 125mg/L of CQ and HCQ solution under the EB and EB-F processes. (B) Release of Cl^- under conditions promoting $\bullet\text{OH}$ generation (presence of N_2O) or e_{aq}^- generation (presence of 0.5M tBuOH)

Similar dechlorination has been reported while using gamma radiation (Zaouak et al., 2022). The evaluated rate constants for this reaction have been provided in Table 4.1. In the degradation of diuron, chloride release occurred both under $\cdot\text{OH}$ radical reactions and e_{aq}^- reactions. In agreement with reactions of the $\cdot\text{OH}$ radicals, addition to the aromatic ring is expected. Studies of diuron and diclofenac proposed that the addition of OH to the carbon atom bearing the Cl atom would lead to the release of HCl (Kovács et al., 2015).

Chloride release is an important indicator for the degradation of chlorinated molecules and facilitates the understanding of the attack of reactive radicals on special sites of the molecule studied (Kovács et al., 2015). A similar release is observed in the degradation of CQ and its variant HCQ under electron Fenton oxidation (Bensalah et al., 2020; Midassi et al., 2020), as well as in diuron degradation, p-chlorophenol p-CP, and tetrachloroethylene (TCE) under irradiation with increasing dose (Bettoli et al., 1998). Most polychlorinated cyclic compounds are stable, lipophilic, and tend to bioaccumulate in the environment with slow degradation. Chlorinated compounds i.e., pesticides, biphenyls, dibenzodioxins, and dibenzofurans are genotoxic (mutagenic and carcinogenic) and therefore pose a risk to living organisms (Henschler, 1994; Jayaraj et al., 2016).

4.7.3. Nitrogen

Nitrogen is the highest-supplied nutrient in plants found in fertilizers and naturally in decaying plants and animal residues. Bacteria in soil convert various forms of nitrogen into nitrate that is absorbed by plants. Nitrate is highly leachable and can move through the soil profile during rainfall or irrigation and reach groundwater. Nitrogen-containing organic wastewater poses a challenge in wastewater treatment. The nitrogen atom incorporated in the cyclic ring of quinoline increases hydrophilicity, good solubility, and low biodegradation (Babić et al., 2017; Dabić et al., 2019). Nitrate is essential to maintain agricultural productivity. However, leaching

of excess nitrate from agricultural land into freshwater can cause significant issues such as eutrophication. Eutrophication causes an increase in plant and algal growth, which decreases the dissolved oxygen in the water, often leaving the water uninhabitable to organisms. Organic nitrogen decomposes into ammonia, and then it is oxidized to nitrite and finally into nitrate. Nitrate and nitrite water could be from sewage disposal, fertilizer, livestock facilities, or naturally occurring nitrogen sources (Mook et al., 2012). The primary health risk in humans occurs when nitrate is converted into nitrite in the digestive system. Nitrite oxidizes hemoglobin in the red blood cells and forms methemoglobin that lacks the oxygen-carrying ability of hemoglobin thereby creating a condition known as methemoglobinemia (blue baby syndrome) prevalent in infants who don't have sufficient enzyme systems to convert the methemoglobin back to oxyhemoglobin.

The generation of NO_3^- and NO_2^- in the aqueous phase in the presence of ionizing radiation is normal when dealing with nitrogen-containing compounds (Dey, 2011). The oxidative degradation of nitrogen-containing compounds releases nitrate, nitrite, and ammonium ions (Maletzky and Bauer, 1998; Rayaroth et al., 2022). The ammonium, organic nitrogen, nitrate, and nitrite concentrations are the most relevant for the determination of nitrogen in water and wastewater. The total Kjeldahl nitrogen (TKN) was reduced with increasing irradiation dose both under EB and EB-F processing of CQ and HCQ (Fig. 4-16a). The formation of inorganic NO_3^- (Fig. 4-16b) and NH_4^+ (Fig. 4-16c) increased with increasing applied irradiation doses alluding to the nitrification process. About 75% nitrification was achieved during the EB and EB-processing of 125 mg/L solution of CQ and HCQ. The formation of NO_3^- was higher under EB-F processing compared to EB for both CQ and HCQ. Additionally, the decrease in TKN and the formation of NO_3^- was higher in HCQ solutions compared to CQ solutions under both treatment processes. There was a very marked difference in the formation of NH_4^+ under the

EB and EB-F processes. At $\alpha = 0.05$ (**Appendix 9**), EB-F processes had a significantly higher formation of NH_4^+ (Fig. 4-16c).

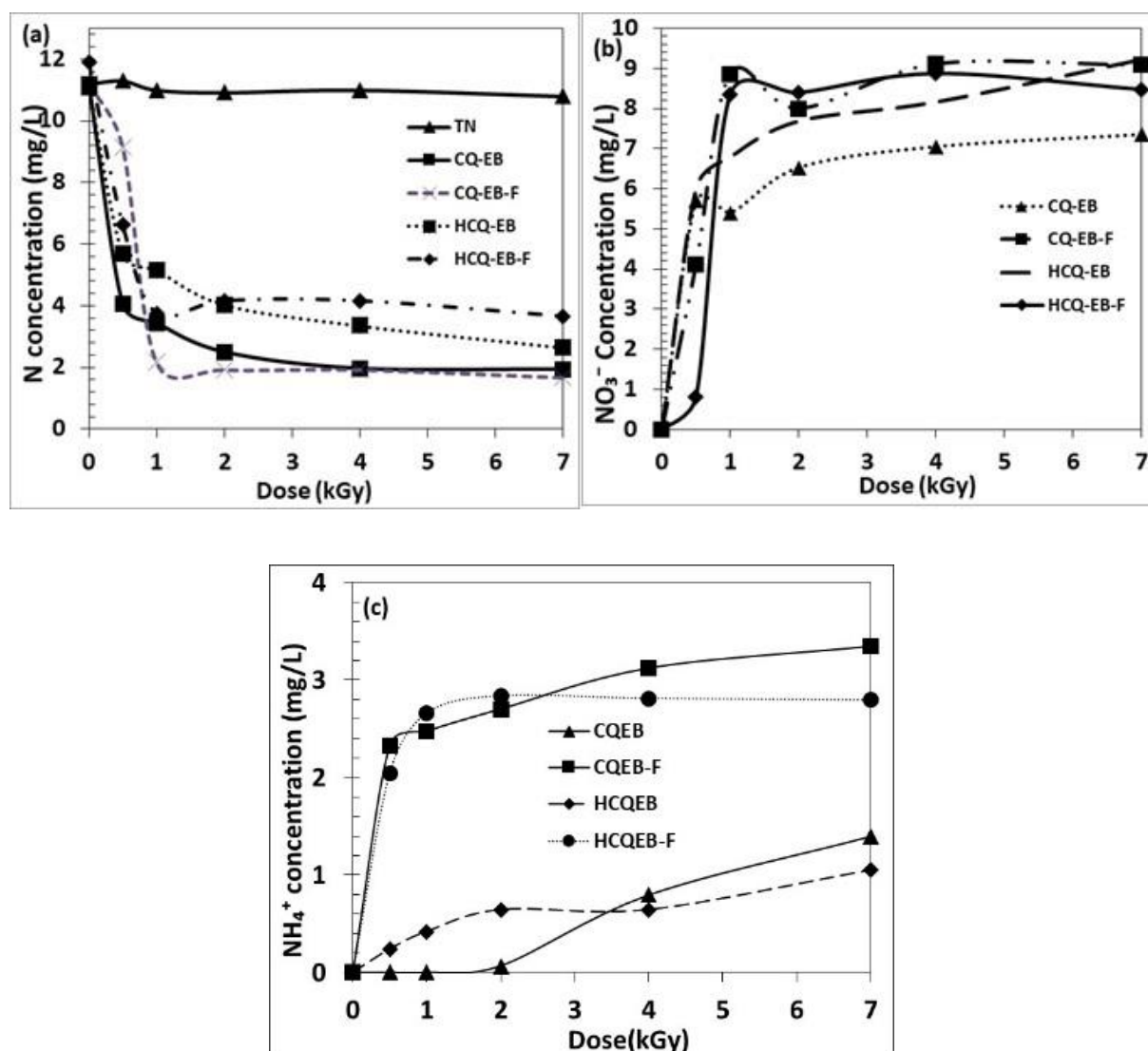


Fig. 4-16 (a) Reduction in Total Kjeldahl nitrogen (b) Formation of NO_3^- and (c) Generation of NH_4^+ in the degradation of 125mg/L of CQ and HCQ solutions under electron beam and electron beam Fenton irradiation

Inorganic nitrogen is predominantly present at the end of the water treatment process compared to freshly polluted water where nitrogen exists as organic nitrogen and ammonia ($\text{TKN} + \text{NH}_3$). Therefore, completely nitrified water has little or no organic nitrogen. However, secondary reactions of mineralized nitrogen species (nitrate and nitrite ions) with the parent or

intermediate compound generate nitrogenous disinfection by-products that are also a concern (Rayaroth et al., 2022).

The formation of NO_3^- and NO_2^- leads to competition for the e_{aq}^- and $\bullet\text{OH}$ radicals leading to the reduced removal efficiency, and nitrification of CQ and HCQ with increasing applied irradiation dose. At higher NO_3^- concentrations, more e_{aq}^- are scavenged which impinges the production of H_2O_2 hence $\bullet\text{OH}$ production. In addition, NO_2^- is also produced by the reduction of NO_3^- and scavenges available $\bullet\text{OH}$ radicals. As was shown in Figures 4-6a & Figures 4-6b, the presence of NO_3^- substantially affects the removal efficiency of CQ and HCQ respectively. This can account for the reduction in removal efficiency of CQ and HCQ with increasing applied irradiation dose.

4.7.4. Changes in Oxygen demand

Dissolved oxygen (DO) reflects the amount of oxygen dissolved in water and is available to living aquatic organisms. The decay of organic matter consumes the dissolved oxygen and the presence of excess organic material, BOD, or COD in lakes and rivers causes eutrophication (oxygen deficiency). A large amount of DO is consumed by aerobic microorganisms to decompose the organic matter. The DO is affected by the water temperature, salt concentration, and atmospheric pressure, and the saturation level decreases with increases in water temperature. During the radiolysis processing of wastewater, the dissolved oxygen reacts with $\bullet\text{OH}$ and $\text{H}\bullet$ radicals formed as previously explained in irradiation of aerated solutions. This may significantly reduce O_2 concentrations while also increasing the removal of organic pollutants via reactions of the resulting $\text{HO}_2\bullet$. From the EB processing of CQ and HCQ solutions, the dissolved O_2 varied from 5.5mg/L before irradiation to 4.7mg/L at 7kGy as shown in Fig. 4-17. Similar slight reductions in the dissolved oxygen were made during the EB-F

assisted radiolysis of 125mg/L solutions of CQ and HCQ at 2mM H₂O₂ concentrations and molar ratios of 20×, 5×, 1×, and 0.2× times the Fe²⁺ concentration.

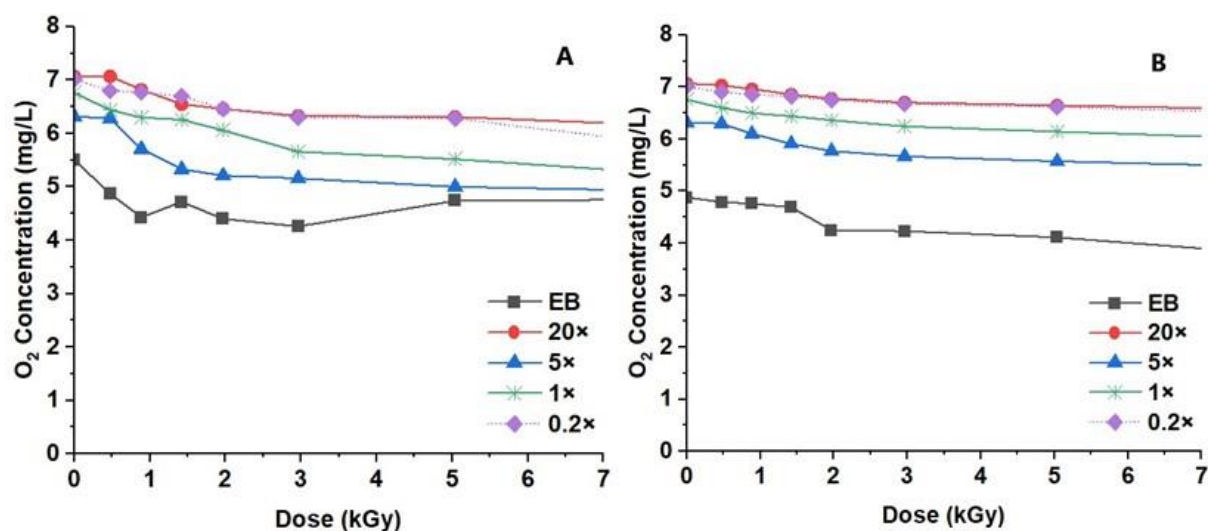
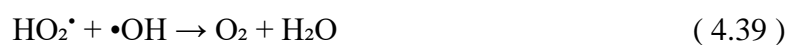


Fig. 4-17 Changes in dissolved O₂ concentration during EB and EB-F irradiation of 125mg/L (A) CQ and (B) HCQ. 2mM H₂O₂ and different ratios of Fe²⁺

Several reactions (Eq. (4.37)-(4.40)) have been proposed for this increase in the concentration of molecular oxygen in Fenton reactions (Santos-Juanes et al., 2011; Zhao et al., 2018).



High dissolved O₂ influences the mineralization of azo dyes under an electron beam by improving the cleavage of the aromatic rings and promoting the reduction of TOC (Hosono et al., 1993). The dissolved O₂ needed to be maintained at optimal concentrations during EB radiolysis for the destruction of substituted aromatic rings in the dye (Suzuki et al., 1978). However, dissolved oxygen scavenges e_{aq}^- and H[•] therefore reducing the equilibrium

concentration of these species and their reactions with target pollutants (Lee et al., 2023). However, in the results of aerated solutions, the removal efficiency was higher than in solutions with dissolved O₂ (Fig. 4-3a & Fig. 4-3b).

The Oxygen demand can also be determined using the biochemical oxygen demand (BOD), chemical oxygen demand (COD), and total organic carbon (TOC). There was a slight decrease in the COD (Fig. 4-18a) and TOC (Fig. 4-18b) with increasing radiation doses and the decreasing concentration of CQ and HCQ.

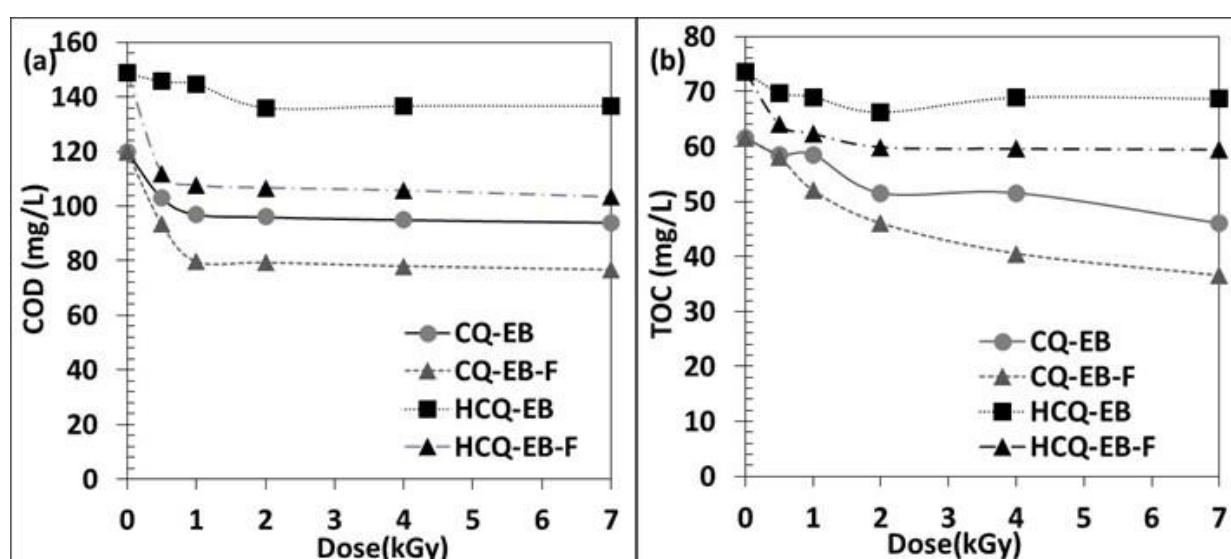


Fig. 4-18 Variation in (a) COD and (b) TOC during EB and EB-F degradation of 125mg/L solutions of CQ and HCQ

The observations in TOC and COD reduction indicate the formation of other organic byproducts that are slowly degraded in the present conditions (Paul et al., 2011). In other studies, with an apparent insignificant reduction in COD and TOC, the resulting degradation products exhibited a higher biological oxygen demand and, therefore, were more susceptible to biological degradation. HCQ is observed to have higher COD and TOC compared to CQ. Similar TOC elimination has been reported under electrochemical oxidation and the slower removal efficiency is attributed to the production of more refractory carboxylic acids and

aliphatic chains (Bensalah et al., 2020). Radiolytic decomposition of HCQ under gamma irradiation showed an increase in COD and TOC elimination with increasing applied irradiation dose with the removal efficiency >90% at doses up to 8kGy (Zaouak et al., 2022). Complete mineralization of 20ppm HCQ was similarly achieved under gamma irradiation at 3kGy with no intermediates being detected (Boujelbane et al., 2022). The level of mineralization is dependent on the initial pollutant concentration possibly due to the generation of higher degradation intermediate concentrations that scavenge the reactive radicals. Zaouak et al. (2022) also demonstrated that higher dose rates gave higher removal efficiency under gamma irradiation. However, residence time in most treatment methods for mineralization is between 3 to 8hrs whereas in the current EB and EB-F process, the treatment time was <5 minutes.

4.8. Mathematical simulation of radiation-induced degradation of CQ and HCQ

The radiation chemistry of water and aqueous solutions attracts attention as a convenient way to investigate the interaction of ionizing radiation with condensed matter. Mathematical models provide ideal ways to study interactions of interest as most constants that lead to the formation of radiolysis products have been determined. Additionally, the development of time-resolved analytical techniques contributed to the development of machine-based models to passively study chemical processes. Models describing the data on the formation of stable products of water radiolysis, H₂O₂, O₂, and H₂, were reported in several publications (Jenks, 1965; Jenks and Griess, 1967; Boyd et al., 1980; Burns et al., 1983).

For simulation, 110 reactions (Appendix 4) based on radiolysis of aqueous systems were used to simulate the degradation of CQ and HCQ solutions under EB irradiation (Buxton et al., 1988). Aminoquinoline compounds are theoretically susceptible to oxidation by •OH radical, the azide (N₃[•]), and reduction by the e_{aq}⁻. Studies on quinoline derivatives i.e., amodiaquine, and primaquine have yielded results to support this premise (Kovács et al., 2020). However, quinoline (the parent compound) is not reactive with the azide radical (Nicolaescu et al., 2003).

CQ and HCQ have been shown to decompose in aqueous and organic solvents under irradiation and generate degradation products (Tønnesen et al., 2007).

The degradation of CQ and HCQ in aqueous solutions under EB was investigated using simulations based on water radiolysis. The reactions of the highly oxidizing $\bullet\text{OH}$ radicals and the reductive e_{aq}^- generated during the radiolysis of water aided the removal of CQ and HCQ (Bors et al., 1991; Rath et al., 2023). The corresponding rate constants for the reactions were provided in Table 4.1 and Eq. (4.1) to Eq. (4.4). The rate constants ($\text{M}^{-1}\text{s}^{-1}$) suggest that the reactions of CQ with the e_{aq}^- are faster compared to the $\bullet\text{OH}$ radicals while the $\bullet\text{OH}$ has a higher reaction rate for HCQ compared to the e_{aq}^- . The simulated removal of CQ and HCQ were 70% and 50% at 0.5kGy respectively (Fig. 4-19). However, in the experimental set-up, at 0.5kGy, only 40% and 36% degradation were attained for CQ and HCQ, respectively.

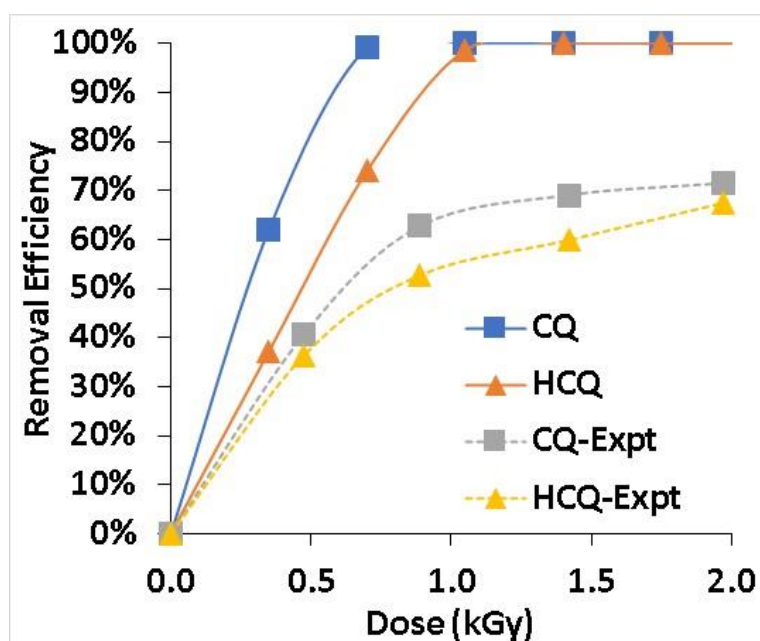


Fig. 4-19 Simulated and experimental degradation of 125mg/L of CQ and HCQ in aqueous solution under electron beam irradiation

Oxidative transformation of quinoline and HCQ using pulse radiolysis suggests the addition of the $\bullet\text{OH}$ molecule to both the pyridine and benzene rings of quinoline to form OH-adducts as

shown in Fig. 4-20b for HCQ (Nicolaescu et al., 2003; Rath et al., 2023). By convention, similar addition is expected on the CQ molecule due to similarity in structure (Fig. 4-20a).

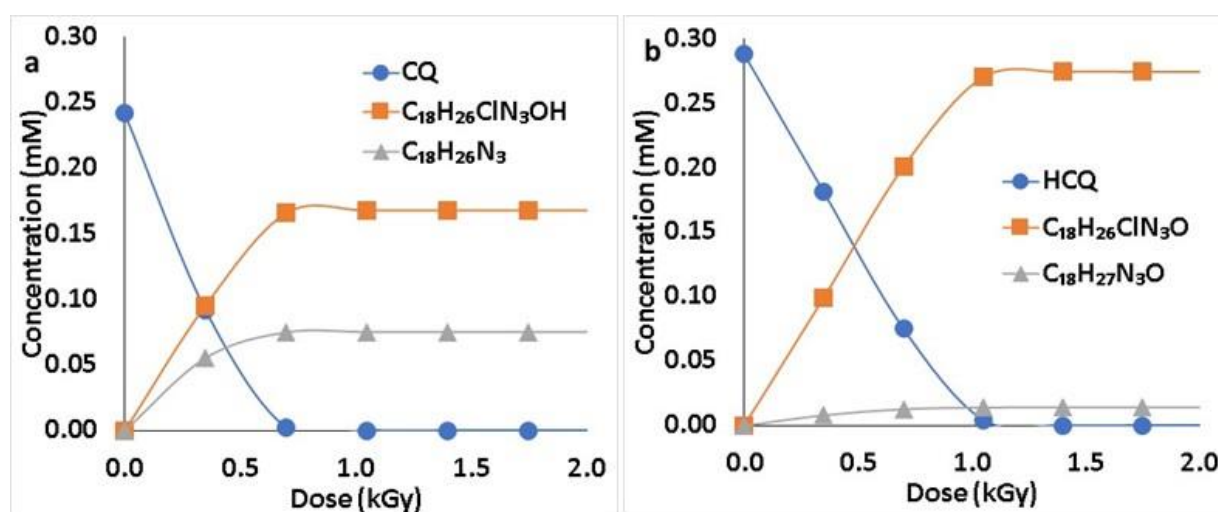


Fig. 4-20 Simulated degradation of (a) CQ and (b) HCQ under electron beam irradiation and formation of intermediate products under action of $\bullet\text{OH}$ and e_{aq}^- .

The formation of the hydroxycyclohexadienyl radicals is a common observation. Phenoxy radicals and aminyl radicals may form after the release of HCl from the $\bullet\text{OH}$ adducts or H-abstraction from the N-H group respectively (Kovács et al., 2015). The addition of OH to the CQ and HCQ molecule leads to the formation of OH adducts ($\text{C}_{18}\text{H}_{26}\text{ClN}_3\text{OH}$ and $\text{C}_{18}\text{H}_{26}\text{ClN}_3\text{O}$ respectively). Reactions with $\bullet\text{OH}$ radicals had the highest contribution to the degradation of CQ and HCQ (Fig. 4-20). Compared to HCQ, CQ (Fig. 4-20a) had a higher rate of degradation with e_{aq}^- ($\approx 50\%$) against $\leq 10\%$ for HCQ (Fig. 4-20b). The higher contribution of e_{aq}^- to CQ degradation is due to the higher reaction rate it has compared to HCQ. Additionally, these reactions impact the rate of formation of Cl^- primarily from dissociative electron attachment with e_{aq}^- (Eq. (4.2) & Eq. (4.3)). The rate of formation of Cl^- was higher for CQ than HCQ (Fig. 4-21). However, the Cl^- concentrations are much lower than those obtained in the experimental conditions (Fig. 4-15a). Kovacs et. al. proposed the direct substitution of the Cl atom on diuron by $\bullet\text{OH}$ resulting in the release of the Cl^- . However, in the simulation, only the

reaction for the dissociative electron attachment is accounted for therefore can contribute to the lower Cl^- concentration. In the experimental results (Fig. 4-15b), the Cl^- release occurred both under $\bullet\text{OH}$ and e_{aq}^- conditions and the $\bullet\text{OH}$ conditions had a much higher Cl^- release compared to the e_{aq}^- conditions.

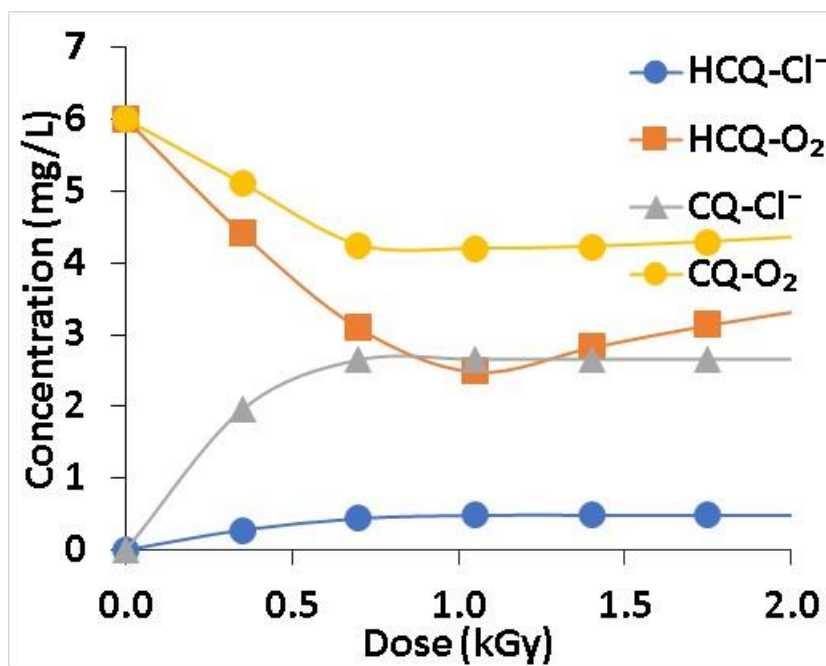


Fig. 4-21 Formation of Cl^- and reduction in dissolved O_2 concentration with the degradation of CQ and HCQ.

Additionally, the dissolved O_2 decreased with increasing irradiation. As explained in Chapter 4.2., in aerated conditions, dissolved O_2 reacts with $\text{H}\bullet$ and e_{aq}^- to form perhydroxyl radical ($\text{HO}_2\bullet$) that is a less powerful oxidant than $\bullet\text{OH}$, and this accounts for the reduction in O_2 . The perhydroxyl radicals could promote the degradation of organic pollutants. However, the current simulation does not account for perhydroxyl reactions. Similar to experimental results, the dissolved oxygen was only partially consumed (Fig. 4-21).

4.8.1. Changes in pH

The pH under irradiation influences the generation of reactive species in water radiolysis and therefore the reactions of these species with pollutants. Additionally, changes in the pH of aqueous solutions containing organic pollutants during degradation are associated with the formation of carboxylic acids, aldehydes, and ketones as has been discussed in Chapter 4.6.1. The pH of the aqueous solutions dropped from 6 to 3.8 with increasing irradiation and reducing CQ and HCQ concentration. A similar reduction in pH was observed in the experimental conditions which was attributed to the formation of organic acids (Fig. 4-13).

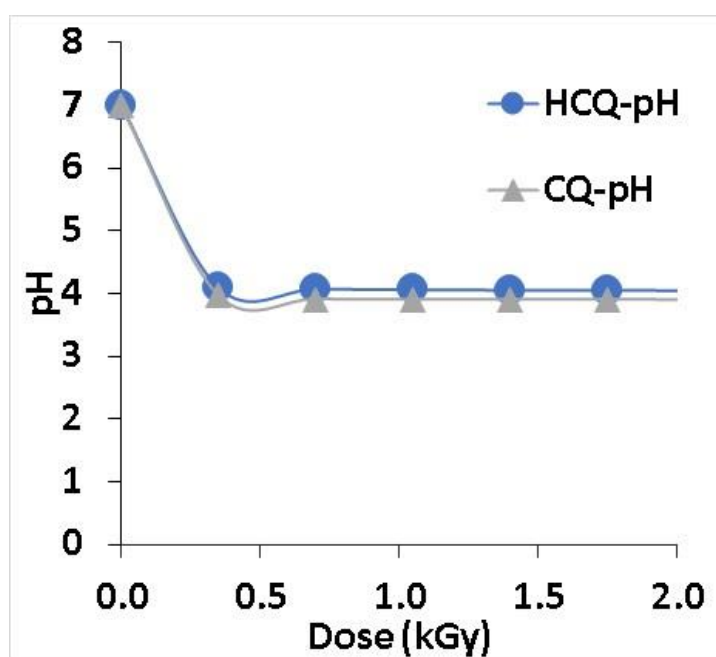


Fig. 4-22 Changes in pH during simulated degradation of aqueous solutions of CQ and HCQ

4.8.2. Effect of different initial pH in the degradation of CQ and HCQ

The effect of different initial pH on the radiolytic degradation of CQ and HCQ was experimentally evaluated (Fig. 4-5). The pH of the aqueous solutions changes with increasing dose and simultaneous reduction in CQ and HCQ concentrations both experimentally (Fig. 4-13) and during the simulated degradation (Fig. 4-23).

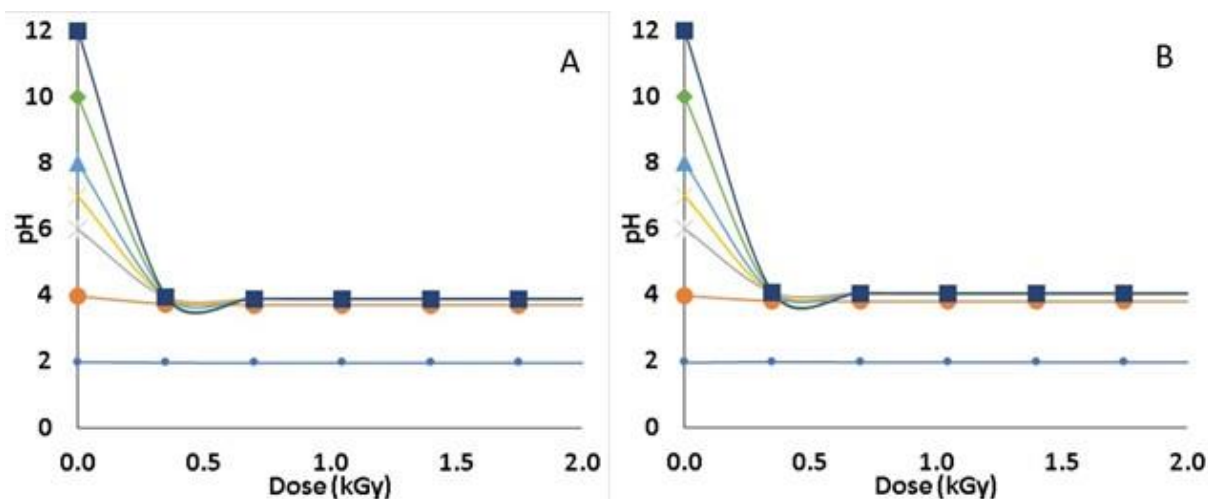


Fig. 4-23 Changes in initial pH of solutions with irradiation during simulated degradation of (A) CQ and (B) HCQ

The simulation's initial pH was varied between 2 to 12 to see the effects (Fig. 4-23). For pH >4, the pH reduced with increasing dose when starting irradiation at different initial pH. These changes in pH are attributed to the formation of organic acids. The effect of pH on the generation of water radiolysis products and the subsequent effect on the reactions of these species with target chemical pollutants is of interest. The reactions of the $\bullet\text{OH}$ radical with CQ and HCQ based on Eq. (4.1) and Eq. (4.4) respectively were simulated at different initial pH in Fig. 4-24a and Fig. 4-24c. Additionally, reactions of the e_{aq}^- were also evaluated for both CQ and HCQ in Fig. 4-24b and Fig. 4-24d respectively.

From Fig. 4-20, the reactions of $\bullet\text{OH}$ and e_{aq}^- with CQ and HCQ led to the formation of OH adducts and the release of Cl^- respectively. Based on the formation of these products, the reactions of $\bullet\text{OH}$ and e_{aq}^- under different pH were evaluated during the simulation. The concentration of the OH adducts was observed to decrease with increasing pH (Fig. 4-24a and Fig. 4-24c). As explained in chapter 4.3, $\bullet\text{OH}$ readily reacts with OH^- in alkaline conditions to generate the less powerful and slow reacting $\text{O}^{\bullet-}$ (Eq. (4.12)). This reduces the $\bullet\text{OH}$ radicals in

the system and the degradation efficiency (Chu and Wang, 2022; Wang and Chu, 2016; N. Wang et al., 2016).

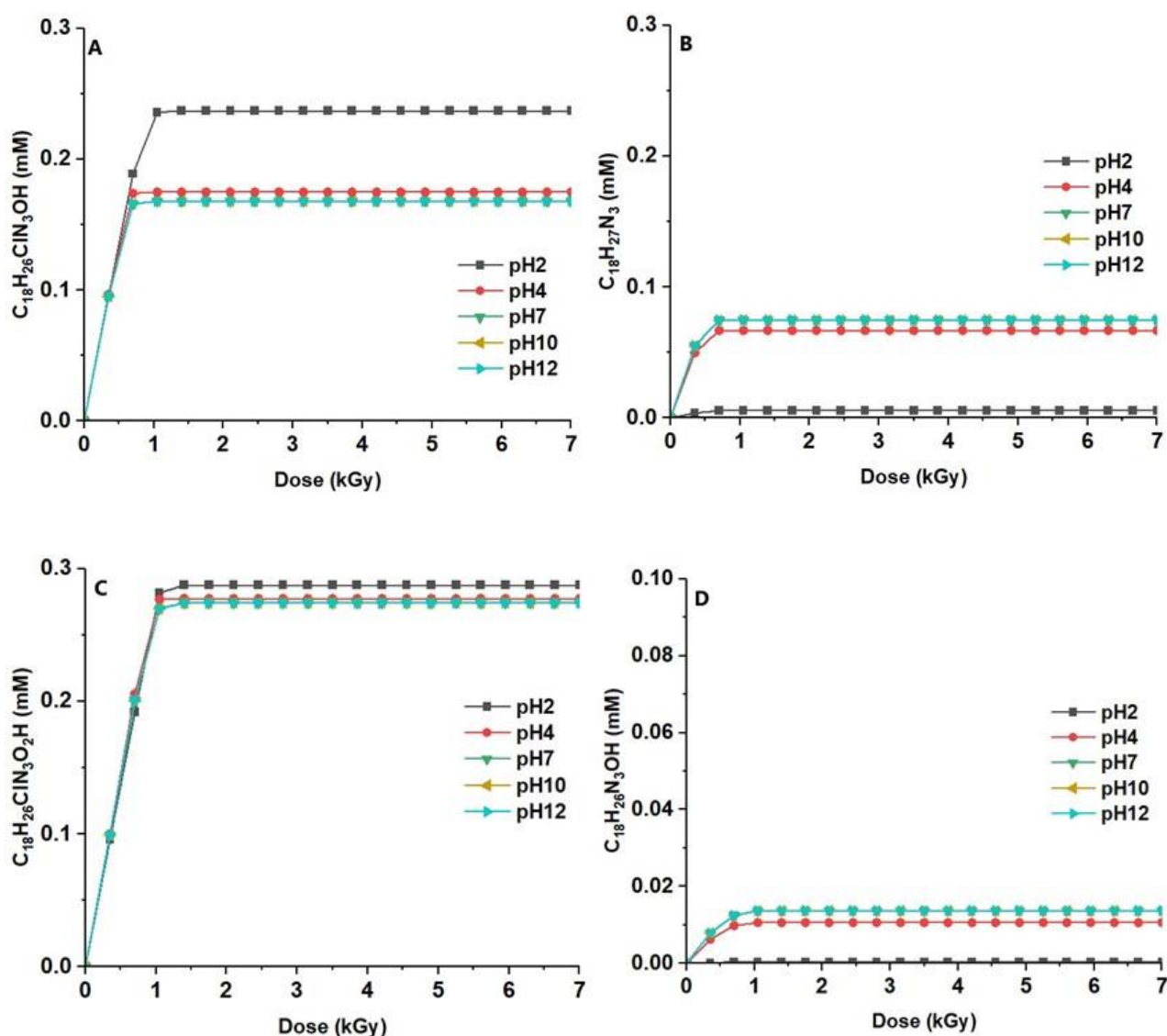


Fig. 4-24 Effect of different initial solution pH on the simulated degradation of aqueous solutions. (a) reactions of $\bullet\text{OH}$ radical with CQ (b) reactions of e_{aq}^- with CQ (c) reactions of $\bullet\text{OH}$ radical with HCQ (d) reactions of e_{aq}^- with HCQ

At pH 2 the formation of the OH adducts was favored (Fig. 4-24a & c). In acidic media, the e_{aq}^- reacts with H^+ to produce $\text{H}\bullet$ radicals that are less powerful reductants compared to e_{aq}^- (Eq. (4.13)). $\text{H}\bullet$ reacts with H_2O_2 to form $\bullet\text{OH}$ radicals therefore enhancing the efficiency. In

the experimental phase, in acidic conditions $\text{pH} < 2$, in the presence of 0.5M tert butanol, and N_2O purged solutions where $\text{H}\cdot$ reactions dominate, the removal of CQ and HCQ was higher compared to conditions involving e_{aq}^- (Fig. 4-3). The reactions of the e_{aq}^- are favored in alkaline conditions compared to acidic conditions (Fig. 4-24b and Fig. 4-24d). In alkaline conditions, more e_{aq}^- are generated via the reactions of $\text{H}\cdot$ with OH^- (Eq. (4.15)). However, in strongly alkaline conditions recombination of e_{aq}^- dominates and may lead to decreased removal as was observed in the experiment (Fig. 4-5).

4.8.3. Effect of initial pollutant concentration on the simulated degradation of CQ and HCQ

In Chapter 4.2, the initial pollutant concentration was observed to influence the degradation of CQ and HCQ under EB irradiation. With increasing pollutant concentration, the removal efficiency and rate constant also decreased (Fig. 4-4). The degradation of CQ and HCQ was reported to follow pseudo-first-order kinetics according to Eq. (4.11). In the simulated degradation of CQ and HCQ in Fig. 4-25a and 4.25b, respectively, similar results were obtained with the removal efficiency as well as the rate constant (Fig. 4-25c) reducing with increasing concentration of the target pollutants.

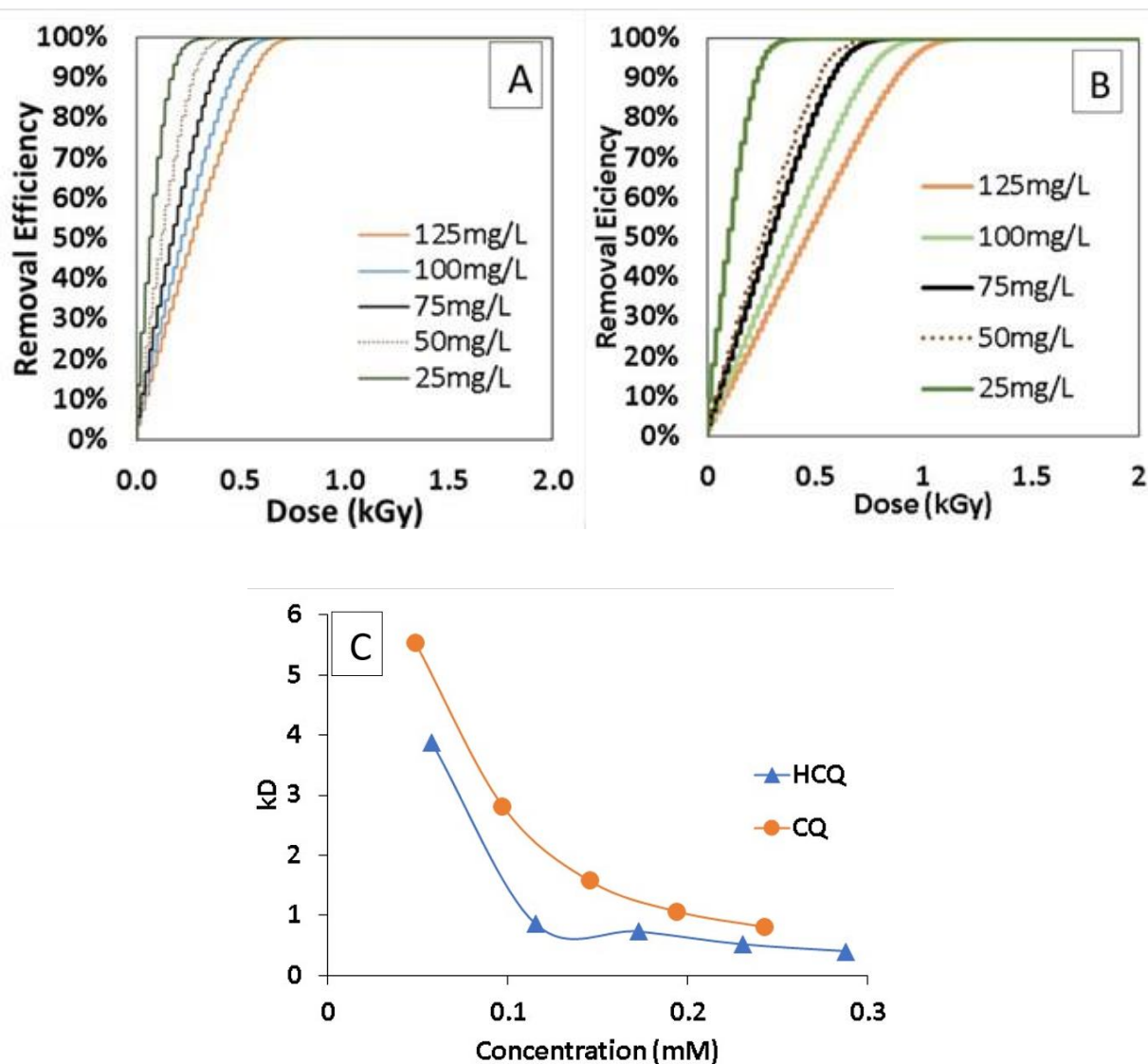


Fig. 4-25 Effect of initial pollutant concentration on the degradation of (A) CQ and (B) HCQ and their respective dose constants (C)

4.8.4. The effect of inorganic ions, and H₂O₂ on the simulated degradation of CQ and HCQ

As demonstrated in Chapter 4.4, some naturally occurring inorganic ions are scavengers for the reactive water radiolysis products. Scavenging may lead to the generation of other reactive species while also depleting the available reactive species. These actions will affect the degradation process. In the experimental setup, the presence of CO₃²⁻, HCO₃⁻, NO₃⁻, and Fe²⁺ with increasing concentration caused a reduction in the removal efficiency of CQ and HCQ

(Fig. 4-7). Similar effects were obtained in the simulated degradation of CQ (Fig. 4-26a) and HCQ (Fig. 4-26b). These inorganic ions are in direct competition for the $\bullet\text{OH}$ and e_{aq}^- generated in water radiolysis.

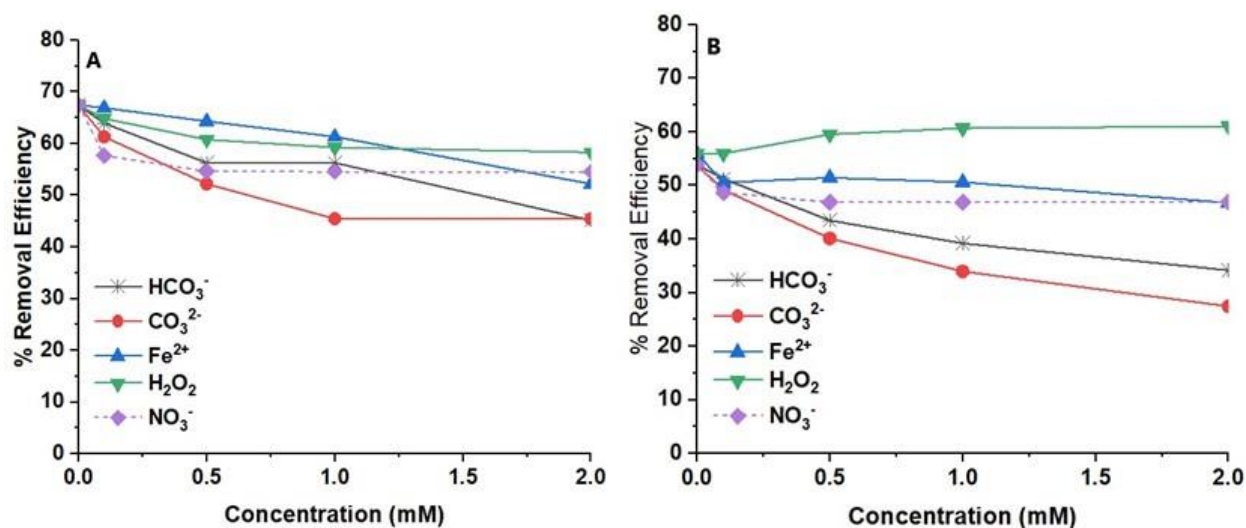


Fig. 4-26 Effects of selected inorganic ions on the simulated degradation of (a) CQ and (b) HCQ under electron beam irradiation at 0.5 kGy

4.8.5. Simulation of EB-F process for degradation of CQ and HCQ from aqueous solutions

The effect of H_2O_2 and Fe^{2+} on the experimental degradation of aqueous solution of CQ and HCQ was previously presented (Fig. 4-6). The presence of H_2O_2 and Fe^{2+} did not significantly change the degradation of CQ and HCQ. However, slight reductions in the removal efficiency were observed with increasing concentrations of H_2O_2 and Fe^{2+} from 0.1 to 2mM. In the current simulation (Fig.4.27), the removal of CQ and HCQ increased with increasing the concentration of H_2O_2 likely from the formation of more $\bullet\text{OH}$ radicals (Fig. 4-26b). In the simulation, there was an improved removal efficiency for CQ and HCQ in the presence of Fenton reagents with H_2O_2 concentration $>0.1\text{M}$ under irradiation compared to irradiation only (EB). The removal efficiency also increased with increased concentration of H_2O_2 at all the molar ratios

investigated. A similar observation was made in the experimental condition under Chapter 4.5.1.2. However, unlike in the experiment where high concentrations of Fe^{2+} led to a decrease in efficiency, this effect was lower in the simulation (Fig. 4-27). Therefore EB-F shows a marked improvement in the removal of CQ and HCQ compared to EB.

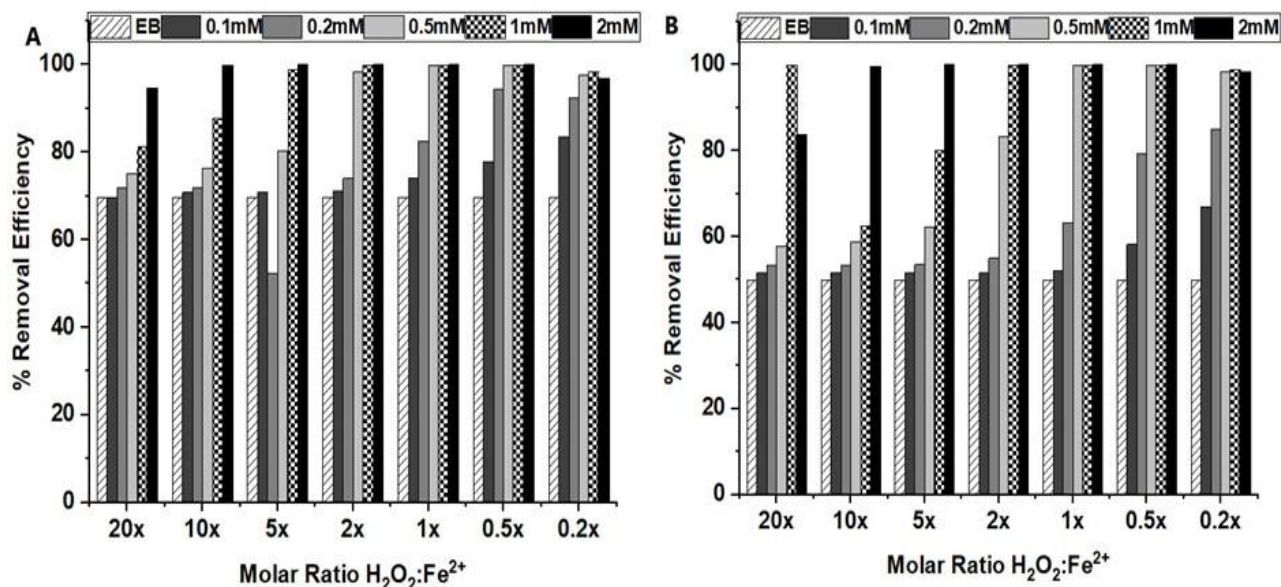


Fig. 4-27 Simulated degradation of (a) CQ and (b) HCQ under EB-F process at 0.5kGy

Mathematical abstractions were able to predict the degradation of CQ and HCQ under EB irradiation. Even though the simulations showed a greater removal efficiency compared to the experimental results, this could be attributed to the matrix effects of actual aqueous solutions that were not accounted for in the simulation. However, it has been shown that the presence of certain inorganic ions affects the removal efficiency of CQ and HCQ under EB processing. The formation of NO_3^- in the degradation of CQ and HCQ would be a major contributor to the observed decline in removal efficiency in experimental conditions. Additionally, the effects of different inorganic ions H_2O_2 showed almost similar results to those obtained in the experiment. The effect of pH from the simulation provided insight into how the $\cdot\text{OH}$ and e_{aq}^- contribute to the degradation of CQ and HCQ.

4.9. Degradation products of CQ

LC-MS analysis of the CQ samples at different irradiation doses was performed to determine the degradation products and the mechanism of CQ degradation following the EB-F process. The molecular ion peak for CQ was recorded at $m/z = 320$ ($[M + H]^+$), with other fragments at $m/z = 247$ and 74 as illustrated in the MS spectrograph in Fig 12B (Boonprasert et al., 2012; Singhal et al., 2007). The $m/z 74$ fragment represents the $N-C_4H_{12}$ removed during the β -elimination of the aliphatic chain of the parent ion. The intermediates following CQ degradation were identified at $m/z = 370, 158, 159, 279,$ and 292 (Fig. 4-27 A, C, D, E, & F). These intermediates are similar to those observed for CQ degradation by other methods and their formation suggests almost similar degradation kinetics (Doddaga and Peddakonda, 2013; Dong et al., 2022).

The degradation of CQ involves primarily OH additions to the aromatic ring that leads to the formation of $m/z = 370$ (Fig. 4-27A). Alternatively, Doddaga and Peddakonda proposed the formation of the chloroquine N-oxide via the attack of $\bullet OH$ at the tertiary amine nitrogen instead of the pyridine nitrogen in the oxidation of CQ (Doddaga and Peddakonda, 2013). In the work of Dong et al. (2022), this oxide was determined to be an intermediate to the formation of desethylchloroquinolone ($m/z = 292$ Figs. 4.28F & 4.29). The m/z of 292 is consistent with the loss of neutral ethylene ($-C_2H_4$) molecules from CQ. The β -elimination of the aliphatic chain of the parent CQ leads to $m/z 247$ and further addition of OH to the aromatic ring leads to the formation of $m/z 279$. The direct addition of OH to the carbon bearing the Cl atom leads to the elimination of the Cl atom as described in chapter 4.6.2. The $\bullet OH$ radicals are highly reactive towards aromatic and heterocyclic rings and preferentially add to the aromatic ring. No specificity in OH addition is reported and it can add to both the aromatic and pyridine rings of the quinoline (Nicolaescu et al., 2003; Sanches-Neto et al., 2023).

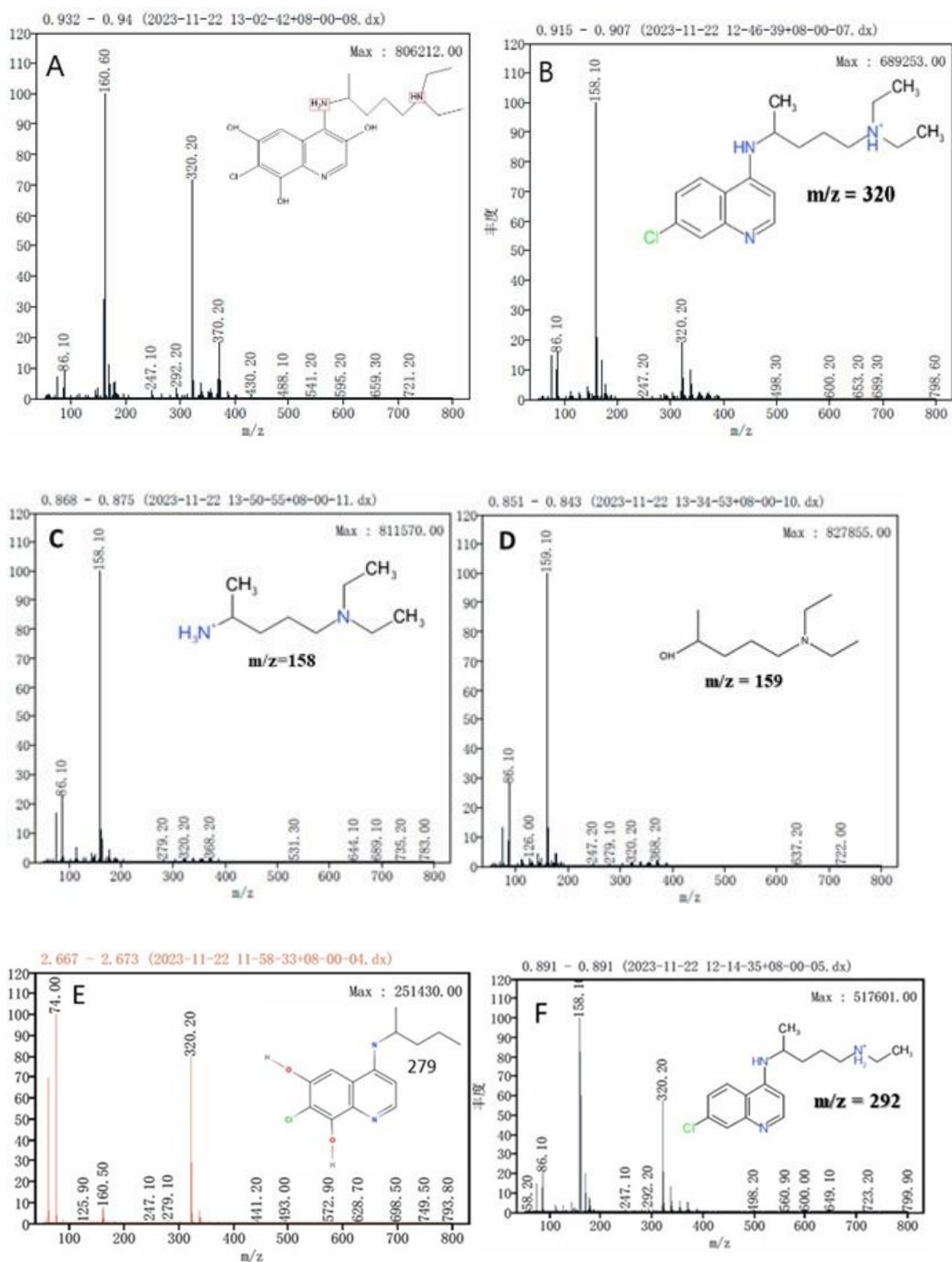


Fig. 4-28 LC-MS mass spectra for CQ showing mass fragmentation of the degradation products of CQ under EB irradiation

The degradation of CQ under electron beam irradiation can be attributed to a series of OH additions to the aromatic ring, dealkylation, and chloride ion substitution by OH molecule or dissociative electron attachment as previously discussed. Similar dealkylation with oxidation has been reported in the presence of H₂O₂ (Dong et al., 2022). Additionally, under photochemical degradation (240–600nm light) in aqueous solutions (pH 7.4), N-dealkylation of CQ is proposed to be the major reaction leading to several products (Ahmad et al., 2016). Under electro-Fenton oxidation, the degradation of CQ is proposed to begin with the N-dealkylation of the aromatic ring leading to the formation of 7-chloro-4-quinolinamine followed by the release of chloride ions by attack of •OH radical on the C bearing the Cl atom (Midassi et al., 2020). Similar dealkylation with subsequent substitution of Cl atom by OH leading to the formation $m/z = 158$ is proposed.

The aromatic intermediates formed in the degradation of CQ undergo subsequent oxidative ring opening to form aliphatic carboxylic acids, with the nitrification of organic nitrogen in the form of nitrates and ammonium ions. Such a mechanism would be supported by the formation of $m/z = 159$ which has been proposed as the CQ degradation products formed in the presence of H₂O₂ (Coelho et al., 2017). Similar products have also been observed and confirmed by MS and NMR in other works (Ahmad et al., 2016; Nord et al., 1991). In the photodegradation process, the Cl attached to the benzene ring is substituted by OH and additional OH substitutes the ortho-carbon hydrogen (Xiang et al., 2023). This mechanism can also be proposed with the formation of $m/z = 247$. The dehydration of OH on two ortho-carbons would lead to the formation of the –COOH followed by decarboxylation and •OH substitution. Further proof of degradation of the products of CQ degradation is observed through the formation of inorganic ions that represent the mineralization of CQ. Similarly, in this experiment chlorides, nitrates, carboxylic acids, and ammonium ions are released similar to those reported in electro-Fenton oxidation (Midassi et al., 2020).

4.10. Degradation products of HCQ

LC-MS analysis was performed to determine the degradation products following the electron beam irradiation of HCQ. The $[M+H]^+$ peak for HCQ was observed at $m/z = 336$ with mass fragments at $m/z = 292$, $m/z = 247$, and $m/z = 74$ (Fig. 4-30A). Other additional mass fragments were identified and recorded in similar analyses (Boujelbane et al., 2022; Saim and Behira, 2021; Zaouak et al., 2022). The formation of new peaks with increasing irradiation from 0.5kGy to 2kGy is shown from the chromatograms in Fig. 4-31. Photodegradation products of HCQ have previously been reported as N-dehydroxyethyl-7-dechloro-7-hydroxy HCQ (m/z 274), dechlorinated HCQ (m/z 302), N-dealkylated HCQ (m/z 179), HCQ N-oxide (m/z 352), and desethylhydroxychloroquine (m/z 308) (Saini and Bansal, 2013). Under gamma irradiation, degradation products such as HCQ N-oxide (m/z 352), m/z 174, and m/z 262 were reported (Boujelbane et al., 2022). Furthermore, products with m/z 179, and m/z 161 have been reported also under gamma radiolysis of aqueous solutions of HCQ (Zaouak et al., 2022). Similarly, Bensalah et al. obtained $m/z = 179$, and 175 following α dealkylation of HCQ under electrochemical oxidation.

Mathematical abstractions propose multiple sites of attack of $\bullet OH$ on HCQ molecule. However, $\bullet OH$ addition to the aromatic ring is the most thermodynamically favored degradation channel by $\bullet OH$ attack on the neutral form of HCQ based on Gibbs free energy (Sanches-Neto et al., 2023). Similar computations have suggested that the addition reactions of $\bullet OH$ to both the benzene and pyridine rings of quinoline are energetically favorable with reaction energies ranging from 18.6 to 23.9 kcal/mol to form $\bullet OH$ adducts in water (Nicolaescu et al., 2003). The formation of similar OH adducts has been reported in gamma radiolysis of HCQ (Zaouak et al., 2022).

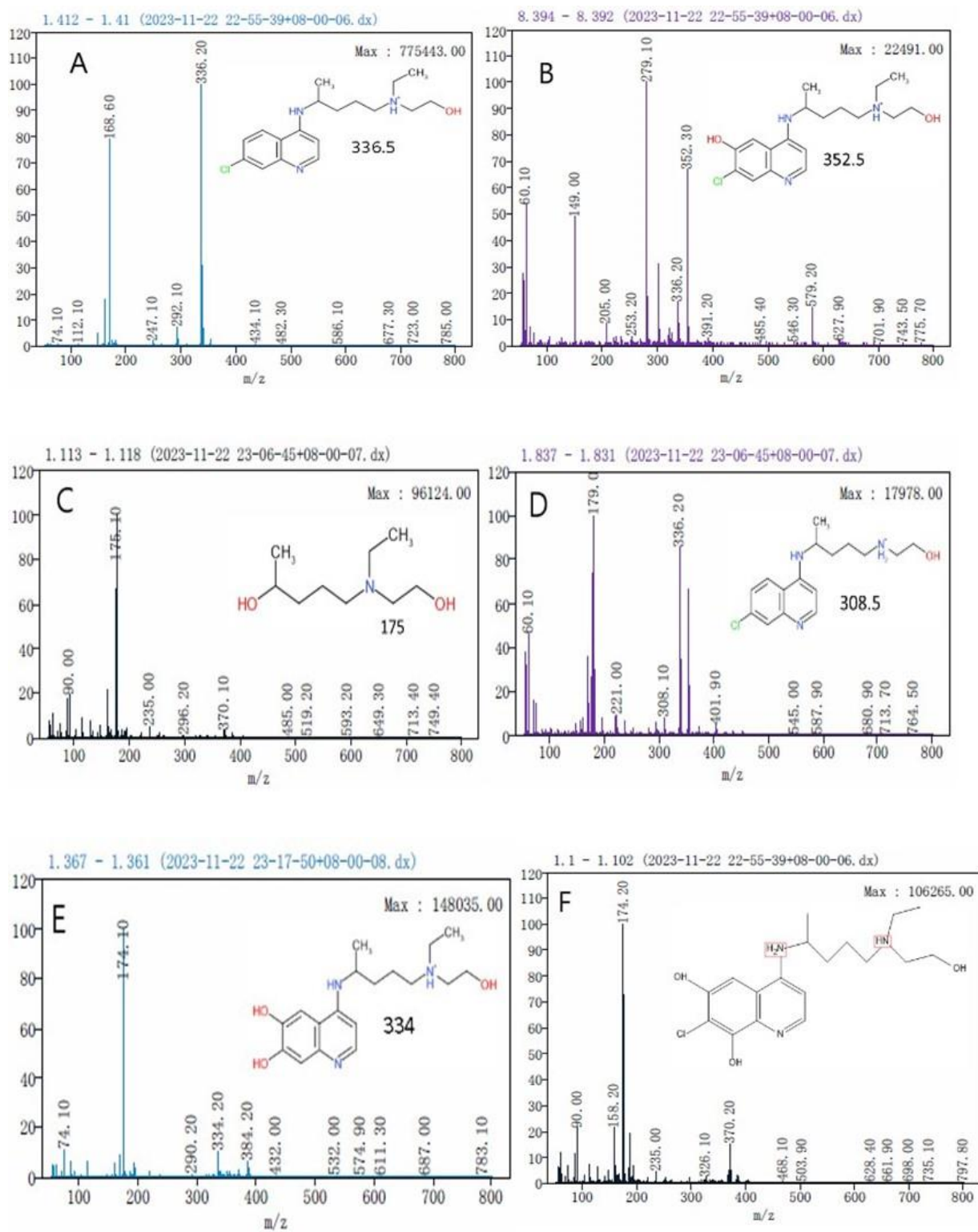


Fig. 4-30 MS Spectrum for the identified degradation products of HCQ under the EB-F process

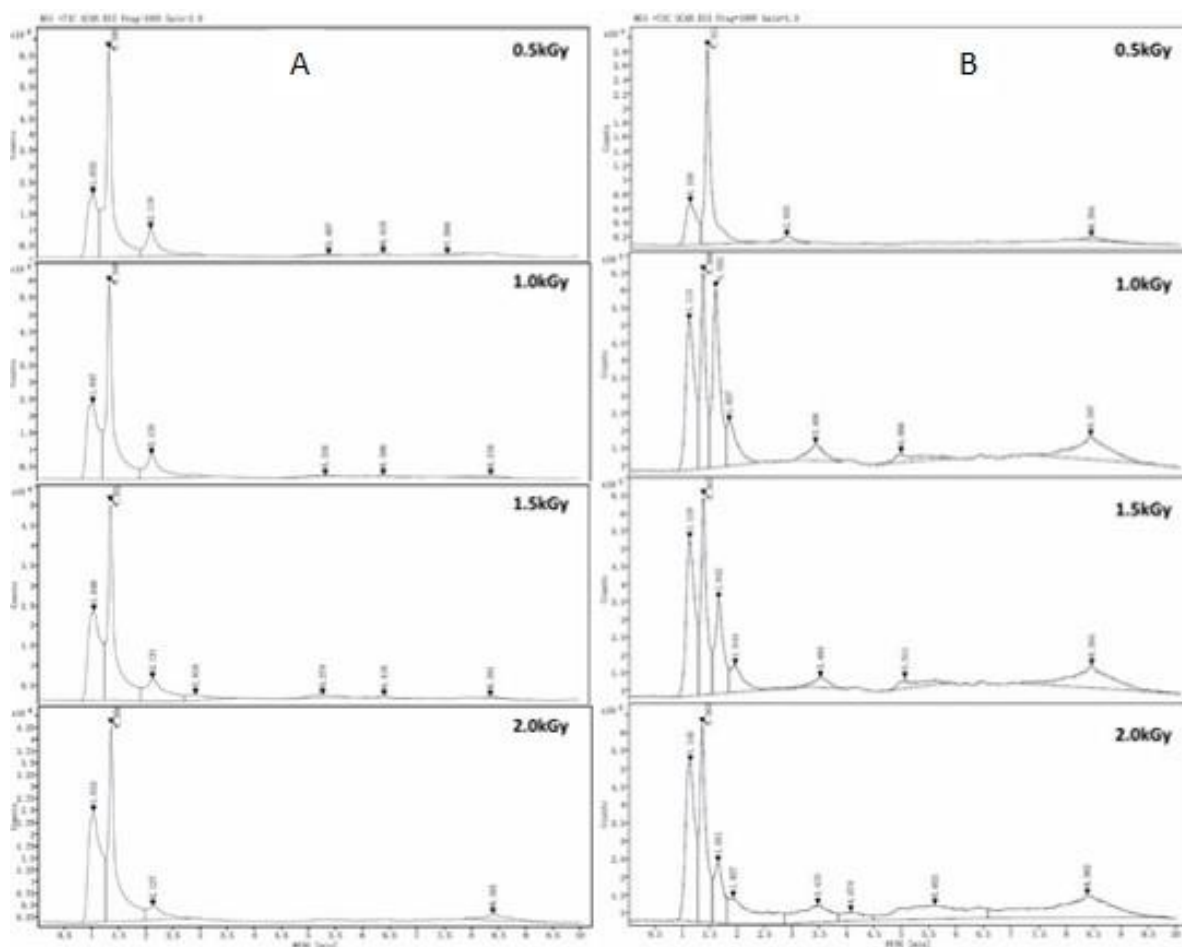


Fig. 4-31 LC-MS chromatogram of the degradation of HCQ at different doses under (A) EB irradiation and (B) EB-F process.

Therefore, the degradation of HCQ is proposed to proceed via OH addition to the aromatic ring that leads to the formation of m/z 370, 352, 279, and 334 as shown in the degradation scheme in Fig. 4-32. Additionally, α dealkylation of the aromatic ring leads to the formation of m/z 179 and 175. Dealkylation at the tertiary nitrogen is likely to lead to the formation of several products with m/z 308, 292, and 279. Dehalogenation is additionally one of the prominent features of most halogenated organic species as has been previously discussed (Makarov and Ponomarev, 2018). Dechlorination occurs either through dissociative electron attachment reactions involving the e_{aq}^- or direct substitution of the Cl atom by the OH atom in addition to reactions to the aromatic ring (Kovács et al., 2015). Eventually, the aromatic intermediates

undergo an oxidative ring opening to form aliphatic carboxylic acids (i.e., oxalic and oxamic acids), and inorganic nitrogen such as nitrates and ammonium ions (Bensalah et al., 2020).

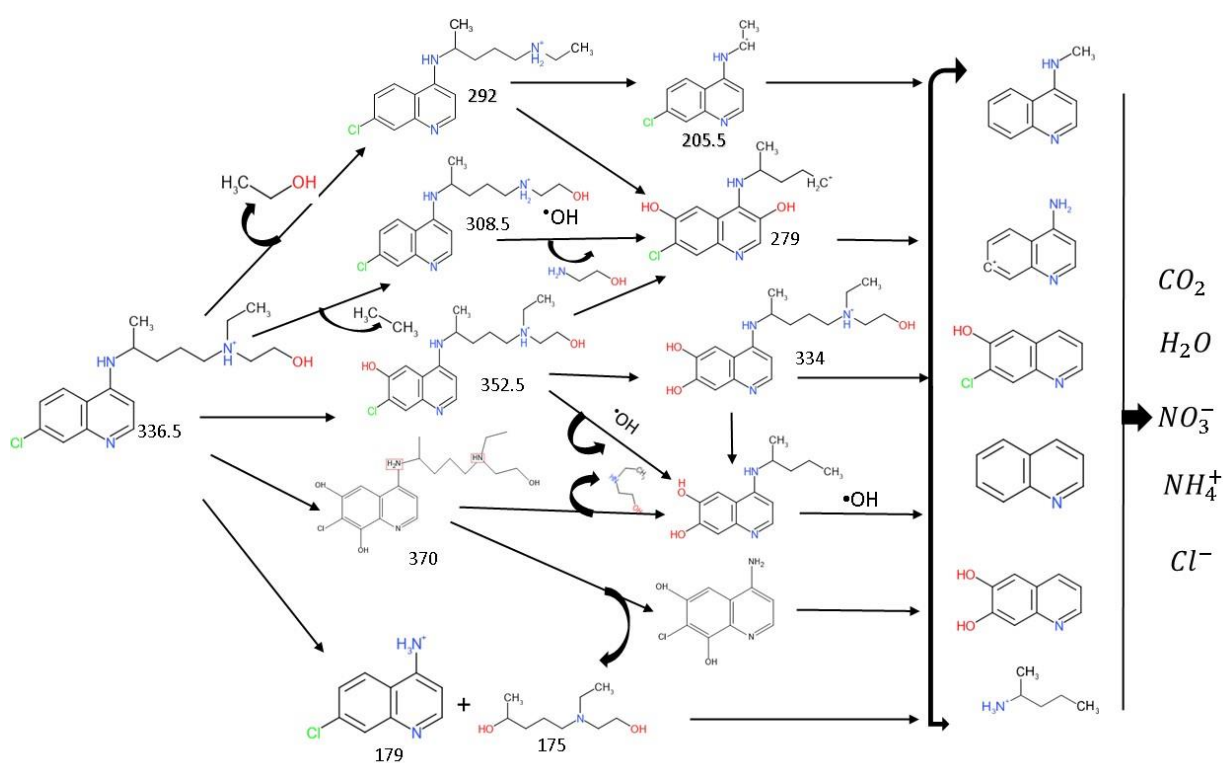


Fig. 4-32 Proposed degradation scheme of HCQ in aqueous solution

Irradiation of HCQ in water or isopropanol identified desethyl-chloroquine (m/z 292), desethanolhydroxychloroquine (m/z 308), and a third product which is HCQ without the $N-C_4H_{10}O$ at the tertiary amine (Tønnesen et al., 1988). Chonker et al., also identified compounds m/z 292, m/z 308, m/z = 263, and 339 as metabolites of HCQ. Three degradation products m/z 292, m/z 324, and m/z = 364 with lower retention times than HCQ have also been reported in photodegradation studies of HCQ. The formation of compounds m/z 292, and m/z 324 detected during irradiation experiments result from the shortening of the side chain on the nitrogen atom, by the loss of ethene from HCQ to yield desethylhydroxychloroquine, or by primary double shortening of the side chain on the nitrogen (Xu et al., 2022). The main products that were detected in the current study are m/z 370, 292, 308, 352, 175, and 334 alongside the inorganic nitrates, ammonium, and chloride species. All organic by-products can undergo further

oxidative decomposition through •OH radical attack opening aromatic rings to carboxylic acids (among them oxamic and oxalic acids) and releasing inorganic nitrogen species predominantly in the form of NO₃⁻ and NH₄⁺ (Zaouak et al., 2022). The carboxylic acids are slowly mineralized to CO₂ (Bensalah et al., 2020).

4.11. Toxicity Analysis

In this study, Ecological Structure Activity Relationships (ECOSAR) available from the US Environmental Protection Agency were used to predict the biotoxicity of CQ, HCQ, and their predicted degradation products based on the Quantitative Structure-Activity Relationship (QSAR) model. The acute and chronic toxicity in fish, daphnia, and green algae were evaluated. The Acute toxicity was assessed using LC₅₀ values (the concentration causing 50% mortality in fish after 96 hours of exposure and in daphnia after 48 hours), EC₅₀ values (the concentration causing 50% inhibition of green algae growth after 96 hours of exposure), along with chronic toxicity value (ChV). Acute toxicity was based on the EU-Directive 93/67/EEC. Additionally, the "Guidelines for Evaluation of Hazardous Chemicals in China" (HJ/TI 154-2004), offers comparable standards for assessing toxicity (Table 4.3.).

Table 4.3 Toxicity classification based on ECOSAR (Reuschenbach et al., 2008)

Classification	Concentration (mg/L) EU EU-Directive 93/67/EEC	Concentration (mg/L) Ch HJ/TI 154-2004
highly toxic	LC ₅₀ /EC ₅₀ ≤ 1	LC ₅₀ /EC ₅₀ ≤ 0.1
Toxic	1 < LC ₅₀ /EC ₅₀ ≤ 10	0.1 < LC ₅₀ /EC ₅₀ ≤ 1
Harmful	10 < LC ₅₀ /EC ₅₀ ≤ 100	1 < LC ₅₀ /EC ₅₀ ≤ 10
Harmless	LC ₅₀ /EC ₅₀ > 100	LC ₅₀ /EC ₅₀ > 10

Generally, according to ECOSAR, HCQ is less toxic compared to CQ on the three organisms (Fig. 4-33 and Fig. 4.34). HCQ is predicted with reference to acute toxicity to be harmful to fish (13.5mg/L), toxic to daphnia (1.82mg/L) and green algae (1.18mg/L). However, CQ was predicted to be toxic to fish (1.14mg/L) and highly toxic to daphnia (0.224mg/L) and green algae (0.104mg/L) according to the less conservative EU-Directive 93/67/EEC. The chronic

toxicity of HCQ was predicted to be much lower than for CQ. However, both CQ and HCQ are predicted to be highly toxic (<1mg/L ChV).

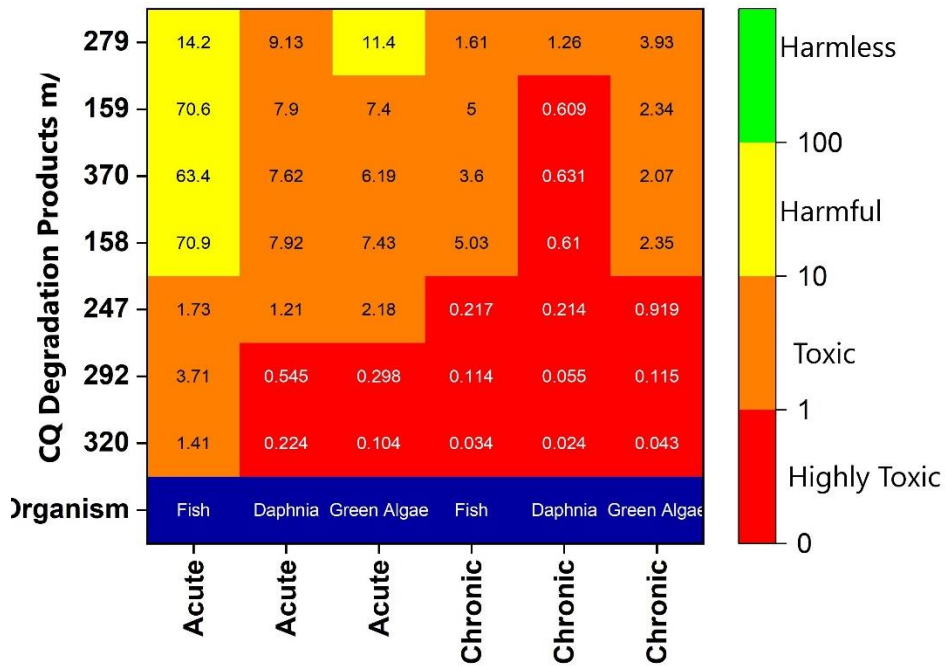


Fig. 4-33 Toxicity analysis of CQ and degradation products

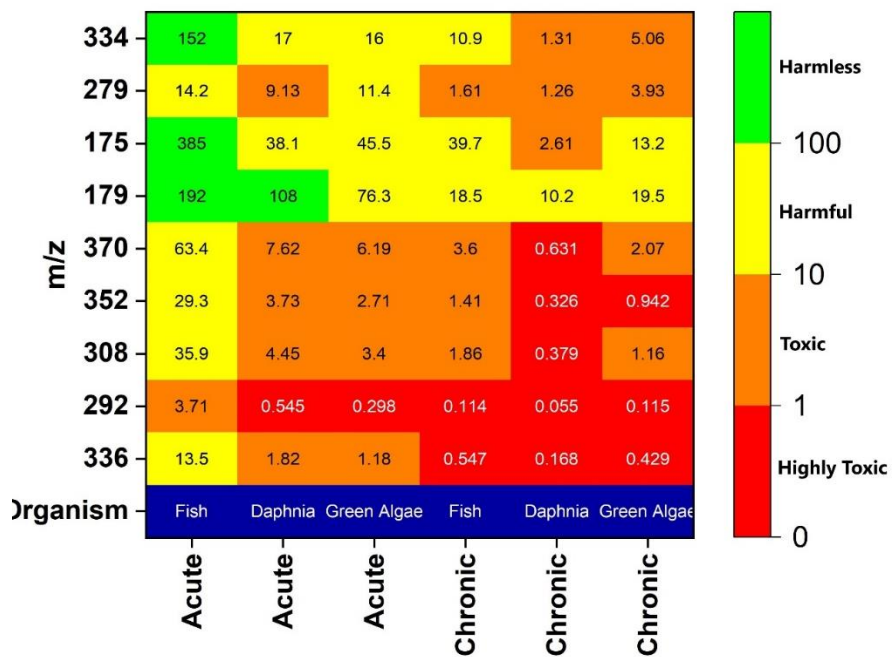


Fig. 4-34 Toxicity analysis of HCQ and degradation products

All the degradation products were predicted to be generally less toxic compared to the parent chemical compound. However, HCQ degradation byproducts were generally less toxic compared to the CQ degradation products. Other than m/z 292 and 247 in CQ degradation, other degradation products were predicted to be harmful (10-100mg/L) based on the EU-Directive 93/67/EEC on acute toxicity to fish and toxic to daphnia, and green algae. Although m/z m/z 292 was toxic to fish, it was predicted to be highly toxic to daphnia and green algae (<1mg/L). Chronic toxicity of m/z 158, 370, and 159 was categorized to be highly toxic (<1mg/L) to daphnia. The m/z 247 and 292 were categorized as highly toxic to fish, daphnia, and green algae with regard to chronic toxicity. The byproducts of HCQ degradation were predicted to have generally lower toxicity with m/z 179, 175, and 334 categorized as harmless (>100mg/L) to fish with regards to acute toxicity but harmful to daphnia and green algae (10-100mg/L). However, m/z 175 and 334 were categorized as being toxic to daphnia when concerning chronic toxicity. ECOSAR, generally predicts the baseline or the minimum toxicity and often underestimates the ecotoxicity of pharmaceuticals because of their modes of action (Bu et al., 2021; US EPA, 2012).

CHAPTER FIVE

5. Conclusion

CQ and HCQ solutions of 125mg/L concentration were degraded with an efficiency of $\geq 75\%$ under an electron beam process at a dose of 2 to 7kGy in ambient conditions. The initial concentration of CQ and HCQ solutions affected the degradation efficiencies under EB treatment. Lower concentrations of CQ and HCQ had higher removal efficiencies and efficiency decreased with increasing the initial concentration of CQ and HCQ. The degradation of CQ and HCQ followed pseudo-first-order degradation kinetics and the dose constant decreased with increased concentration of CQ and HCQ in the solutions at selected absorbed doses. Both the $\bullet\text{OH}$ radical and the e_{aq}^- played roles in the decomposition of CQ and HCQ from the solutions. However, the role of the e_{aq}^- was more prominent in the degradation of CQ compared to HCQ. This was attributed to previously reported rate constants where the rate of e_{aq}^- reaction with CQ is much higher compared to reaction with HCQ molecules. These observations were further elaborated based on mathematical simulations the contribution of e_{aq}^- to HCQ degradations was lower. Furthermore, irradiation in N_2O saturated solutions or 0.5M tert butanol showed that $\bullet\text{OH}$ radicals had a higher contribution to CQ and HCQ degradation compared to e_{aq}^- .

The pH of the CQ and HCQ solutions progressively dropped from the initial pH of 6 to a pH of 3.5 with increasing absorbed dose. This was attributed to the formation of carboxylic acids as has been reported in other studies. Increased concentrations of organic acids in the solutions with increasing absorbed doses were observed. In addition to the change in pH, the effect of the initial pH on the degradation of CQ and HCQ was reported. At lower pH, the removal efficiency was higher but progressively decreased with increasing pH from 2 to 8. However, further increments in pH to 10 and 12 decreased the removal efficiency. The effects of pH were

attributed to the state of the CQ and HCQ molecules at different pH. Additionally, the affects the radiolysis products ($\bullet\text{OH}$ and e_{aq}^-) therefore affecting the degradation processes.

The presence of CO_3^{2-} , HCO_3^- , NO_3^- , Fe^{2+} , humic acid, $\text{S}_2\text{O}_8^{2-}$, and H_2O_2 affected the degradation of CQ and HCQ under EB irradiation. The presence of CO_3^{2-} , HCO_3^- , NO_3^- , Fe^{2+} , H_2O_2 , and humic acid suppressed the degradation of CQ and HCQ with increasing concentration by scavenging the available reactive radicals. Increasing the concentration of Fe^{2+} and humic acid also caused turbidity and affected the overall removal efficiency. However, the presence of $\text{S}_2\text{O}_8^{2-}$ with increasing concentration caused the enhancement in the removal efficiency by generating the strongly oxidizing $\text{SO}_4^{\bullet-}$ by reactions with e_{aq}^- . Additionally, $\bullet\text{OH}$ radicals formed further promote degradation. Experiments in 0.5M tert butanol showed $\text{SO}_4^{\bullet-}$ that $\text{SO}_4^{\bullet-}$ contributed to the degradation of CQ and HCQ even in the absence of $\bullet\text{OH}$ radicals. However, the removal efficiency was lower than for EB treatment and selective $\bullet\text{OH}$ generation. Therefore, $\text{SO}_4^{\bullet-}$ driven processes can enhance the EB process.

Fenton-assisted EB (EB-F), EB/g- C_3N_4 based catalysts, and EB/ TiO_2 catalysts were further investigated to improve the removal efficiency for CQ and HCQ. The Fenton-assisted EB process gave an improvement in the removal efficiency of CQ compared to EB/g- C_3N_4 -MIL and EB/ TiO_2 catalysts. However, the EB/ TiO_2 process positively affected HCQ degradation at 0.15g/L catalyst loading but increasing catalyst concentration resulted in degradation decline. In Fenton-assisted EB (EB-F), the molar ratios of the Fenton reagents were a key determinant in the removal efficiency of CQ and HCQ. In excess H_2O_2 , the removal of CQ and HCQ was higher in the EB-F compared to the EB process. However, when the Fe^{2+} concentrations were higher, the removal efficiency was reduced. The H_2O_2 is the main source of $\bullet\text{OH}$ radicals in the Fenton process. Therefore, higher concentrations generate more $\bullet\text{OH}$ radicals. However, higher Fe^{2+} concentrations lead to the scavenging of $\bullet\text{OH}$ radicals as well as causing turbidity. Excess H_2O_2 in the Fenton processes was shown to have lower removal efficiency attributed to the

scavenging of $\bullet\text{OH}$ radicals. However, this was not observed in the Fenton-assisted EB (EB-F) process. Additionally, in the Fenton-assisted EB (EB-F) process, the rate of conversion of Fe^{3+} to Fe^{2+} is accelerated through the reactions with e_{aq}^- . This ensures the Fenton reactions are sustained during the irradiation causing further improvement to the degradation of CQ and HCQ. The degradation of CQ and HCQ under EB and Fenton-assisted EB (EB-F) processes did not lead to complete mineralization which was evident from the insignificant COD and TOC reduction. The formation of organic compounds with slower degradation is proposed to contribute to the lower mineralization. However, the TOC and COD removal was higher in the Fenton-assisted EB (EB-F) process compared to the EB process. Additionally, the degradation efficiency, dechlorination, and nitrification of CQ and HCQ were higher in Fenton-assisted EB (EB-F) compared to EB treatment. Therefore, the Fenton-assisted EB (EB-F) treatment improved the overall EB process.

The radiation-induced degradation of CQ and HCQ led to the formation of several by-products that were identified using the liquid chromatography-mass spectrometry method. Similar oxidative decomposition byproducts have been observed in gamma radiolysis, photodegradation, and electrochemical oxidation. From these products, a degradation mechanism was proposed for the degradation of CQ and HCQ under the EB and EB-F processes. The $\bullet\text{OH}$ radicals and e_{aq}^- attacks on the target molecules were the primary reactions leading to the degradation of CQ and HCQ. It's proposed that further $\bullet\text{OH}$ attacks lead to aromatic rings opening and the production of carboxylic acids (among them oxamic and oxalic acids) in addition to the release of inorganic species in the form of Cl^- , NO_3^- , and NH_4^+ . The carboxylic acids are slowly oxidized and require the consumption of a high irradiation dose to be slowly mineralized into carbon dioxide and water (Bensalah et al., 2020). Therefore, Electron beam treatment effectively degraded CQ and HCQ in aqueous solutions. However, based on the TOC and COD results, complete mineralization was not achieved. Additionally,

the degradation of CQ was faster compared to HCQ. Furthermore, it has been shown that the Fenton-assisted EB (EB-F) process is a suitable way to improve the process efficiency. Based on ECOSAR analysis of the degradation byproducts, the degradation byproducts of CQ and HCQ were predicted to be less toxic than the parent compounds.

Bibliography

- Abdel Rahman, R.O., Hung, Y.T., 2020. Application of ionizing radiation in wastewater treatment: An overview. *Water (Switzerland)* 12. <https://doi.org/10.3390/w12010019>
- Ahmad, I., Ahmed, S., Anwar, Z., Sheraz, M.A., Sikorski, M., 2016. Photostability and Photostabilization of Drugs and Drug Products. *International Journal of Photoenergy*. <https://doi.org/10.1155/2016/8135608>
- Ai, Y., Liu, Y., Huo, Y., Zhao, C., Sun, L., Han, B., Cao, X., Wang, X., 2019. Insights into the adsorption mechanism and dynamic behavior of tetracycline antibiotics on reduced graphene oxide (RGO) and graphene oxide (GO) materials. *Environ Sci Nano* 6. <https://doi.org/10.1039/c9en00866g>
- al Sarihi, F.T.H., Marzouqi, F. al, Kuvarega, A.T., Karthikeyan, S., Selvaraj, R., 2019. Easy conversion of BiOCl plates to flowers like structure to enhance the photocatalytic degradation of endocrine disrupting compounds. *Mater Res Express* 6. <https://doi.org/10.1088/2053-1591/ab4de0>
- Al-Abri, M., Al-Ghafri, B., Bora, T., Dobretsov, S., Dutta, J., Castelletto, S., Rosa, L., Boretti, A., 2019. Chlorination disadvantages and alternative routes for biofouling control in reverse osmosis desalination. *NPJ Clean Water*. <https://doi.org/10.1038/s41545-018-0024-8>
- Al-Bari, A.A., 2014. Chloroquine analogues in drug discovery: New directions of uses, mechanisms of actions and toxic manifestations from malaria to multifarious diseases. *Journal of Antimicrobial Chemotherapy* 70, 1608–1621. <https://doi.org/10.1093/jac/dkv018>
- Aljadeed, R., 2022. The Rise and Fall of Hydroxychloroquine and Chloroquine in COVID-19. *J Pharm Pract*. <https://doi.org/10.1177/0897190021997399>
- Álvarez-Torrellas, S., Rodríguez, A., Ovejero, G., García, J., 2016. Comparative adsorption performance of ibuprofen and tetracycline from aqueous solution by carbonaceous materials. *Chemical Engineering Journal* 283. <https://doi.org/10.1016/j.cej.2015.08.023>
- Andrade, A.J.M., Araújo, S., Santana, G.M., Ohi, M., Dalsenter, P.R., 2002. Reproductive Effects of Deltamethrin on Male Offspring of Rats Exposed during Pregnancy and Lactation. *Regulatory Toxicology and Pharmacology* 36, 310–317. <https://doi.org/10.1006/RTPH.2002.1586>
- Babić, S., Dabić, D., Ćurković, L., 2017. Fate of hydroxychloroquine in the aquatic environment. 15th International Conference on Environmental Science and Technology 1–5.
- Bartrons, M., Peñuelas, J., 2017. Pharmaceuticals and Personal-Care Products in Plants. *Trends Plant Sci* 22, 194–203. <https://doi.org/10.1016/j.tplants.2016.12.010>
- Bensalah, N., Midassi, S., Ahmad, M.I., Bedoui, A., 2020. Degradation of hydroxychloroquine by electrochemical advanced oxidation processes. *Chemical Engineering Journal* 402, 126279. <https://doi.org/10.1016/j.cej.2020.126279>
- Bettoli, M.G., Ravanelli, M., Tositti, L., Tubertini, O., Guzzi, L., Martinotti, W., Queirazza, G., Tamba, M., 1998. Radiation induced decomposition of halogenated organic compounds in water. *Radiation Physics and Chemistry* 52, 327–331. [https://doi.org/10.1016/S0969-806X\(98\)00027-9](https://doi.org/10.1016/S0969-806X(98)00027-9)
- Bilal, M., Adeel, M., Rasheed, T., Zhao, Y., Iqbal, H.M.N., 2019. Emerging contaminants of high concern and their enzyme-assisted biodegradation – A review. *Environ Int* 124, 336–353. <https://doi.org/10.1016/J.ENVINT.2019.01.011>

- Biswas, S., Pal, A., 2023. A Brief Review on the Latest Developments on Pharmaceutical Compound Degradation Using g-C₃N₄-Based Composite Catalysts. *Catalysts*. <https://doi.org/10.3390/catal13060925>
- Bojanowska-Czajka, A., 2021a. Decomposition of diclofenac in sewage from municipal wastewater treatment plant using ionizing radiation. *Nukleonika* 66. <https://doi.org/10.2478/nuka-2021-0029>
- Bojanowska-Czajka, A., 2021b. Application of radiation technology in removing endocrine micropollutants from waters and wastewaters—a review. *Applied Sciences (Switzerland)*. <https://doi.org/10.3390/app112412032>
- Boonprasert, R., Sri-in, J., Pongnarin, P., Chatsiricharoenkul, S., Chandranipapongse, W., 2012. Development of the Liquid Chromatography Tandem Mass Spectrometry Method for Determination of Chloroquine and Desethyl- chloroquine in Human Plasma. *Siriraj Med J* 64.
- Borea, L., Ensano, B.M.B., Hasan, S.W., Balakrishnan, M., Belgiorno, V., de Luna, M.D.G., Ballesteros, F.C., Naddeo, V., 2019. Are pharmaceuticals removal and membrane fouling in electromembrane bioreactor affected by current density? *Science of The Total Environment* 692, 732–740. <https://doi.org/10.1016/J.SCITOTENV.2019.07.149>
- Bork, M., Lange, J., Graf-Rosenfellner, M., Hensen, B., Olsson, O., Hartung, T., Fernández-Pascual, E., Lang, F., 2021. Urban storm water infiltration systems are not reliable sinks for biocides: evidence from column experiments. *Sci Rep* 11. <https://doi.org/10.1038/s41598-021-86387-9>
- Bors, W., Golenser, J., Chevion, M., Saran, M., 1991. REDUCTIVE AND OXIDATIVE RADICAL REACTIONS OF SELECTED ANTIMALARIAL DRUGS. *Oxidative Damage & Repair* 234–240. <https://doi.org/10.1016/B978-0-08-041749-3.50046-2>
- Boujelbane, F., Nasr, K., Sadaoui, H., Bui, H.M., Gantri, F., Mzoughi, N., 2022. Decomposition mechanism of hydroxychloroquine in aqueous solution by gamma irradiation. *Chemical Papers* 76, 1777–1787.
- Bu, Q., Li, Q., Liu, Y., Cai, C., 2021. Performance Comparison between the Specific and Baseline Prediction Models of Ecotoxicity for Pharmaceuticals: Is a Specific QSAR Model Inevitable? *J Chem* 2021. <https://doi.org/10.1155/2021/5563066>
- Bugueño-Carrasco, S., Monteil, H., Toledo-Neira, C., Sandoval, M.Á., Thiam, A., Salazar, R., 2021. Elimination of pharmaceutical pollutants by solar photoelectro-Fenton process in a pilot plant. *Environmental Science and Pollution Research* 28, 23753–23766. <https://doi.org/10.1007/s11356-020-11223-y>
- Buxton, G. v., 2001. Radiation Chemistry - Present Status and Future Trends. *Studies in Physical and Theoretical Chemistry* 87, 145–162.
- Buxton, G. V., Greenstock, C.L., Helman, W.P., Ross, A.B., 1988. Critical Review of rate constants for reactions of hydrated electrons, hydrogen atoms and hydroxyl radicals ($\cdot\text{OH}/\cdot\text{O}$ in Aqueous Solution. *J Phys Chem Ref Data* 17, 513–886. <https://doi.org/10.1063/1.555805>
- Campos, J.M., Queiroz, S.C.N., Roston, D.M., 2019. Removal of the endocrine disruptors ethinyl estradiol, bisphenol A, and levonorgestrel by subsurface constructed wetlands. *Science of The Total Environment* 693, 133514. <https://doi.org/10.1016/J.SCITOTENV.2019.07.320>

- Cao, W., Yuan, Y., Yang, C., Wu, S., Cheng, J., 2020. In-situ fabrication of g-C₃N₄/MIL-68(In)-NH₂ heterojunction composites with enhanced visible-light photocatalytic activity for degradation of ibuprofen. *Chemical Engineering Journal* 391. <https://doi.org/10.1016/j.cej.2019.123608>
- Capodaglio, A.G., 2019. Contaminants of emerging concern removal by high-energy oxidation-reduction processes: State of the art. *Applied Sciences (Switzerland)* 9. <https://doi.org/10.3390/app9214562>
- Capodaglio, A.G., 2018. Could eb irradiation be the simplest solution for removing emerging contaminants from water and wastewater? *Water Pract Technol* 13, 172–183. <https://doi.org/10.2166/wpt.2018.027>
- Capodaglio, A.G., 2017. High-energy oxidation process: an efficient alternative for wastewater organic contaminants removal. *Clean Technol Environ Policy* 19, 1995–2006. <https://doi.org/10.1007/s10098-017-1410-5>
- Catrinel Ion, A., Mlak-Marginean, M., Savin, M., Dăescu, M., 2022. THE INFLUENCE OF THE AQUEOUS COMPOSITION OVER DEGRADATION OF HYDROXYCHLOROQUINE. *Bull., Series B* 84, 2022.
- Celine, A., Scott, A., Biller, D., 2017. Online total organic carbon (TOC) monitoring for water and wastewater treatment plants processes and operations optimization, in: *Drinking Water Engineering and Science*. <https://doi.org/10.5194/dwes-10-61-2017>
- Changotra, R., Rajput, H., Guin, J.P., Khader, S.A., Dhir, A., 2020. Techno-economical evaluation of coupling ionizing radiation and biological treatment process for the remediation of real pharmaceutical wastewater. *J Clean Prod* 242. <https://doi.org/10.1016/j.jclepro.2019.118544>
- Chappuis, F., Grilj, V., Tran, H.N., Zein, S.A., Bochud, F., Bailat, C., Incerti, S., Desorgher, L., 2023. Modeling of scavenging systems in water radiolysis with Geant4-DNA. *Physica Medica* 108. <https://doi.org/10.1016/j.ejmp.2023.102549>
- Chaturvedi, P., Shukla, P., Giri, B.S., Chowdhary, P., Chandra, R., Gupta, P., Pandey, A., 2021. Prevalence and hazardous impact of pharmaceutical and personal care products and antibiotics in environment: A review on emerging contaminants. *Environ Res* 194, 110664. <https://doi.org/10.1016/j.envres.2020.110664>
- Chauhan, M., Saini, V.K., Suthar, S., 2020. Removal of pharmaceuticals and personal care products (PPCPs) from water by adsorption on aluminum pillared clay. *Journal of Porous Materials* 27. <https://doi.org/10.1007/s10934-019-00817-8>
- Chen, X., Wang, J., 2021. Degradation of antibiotic Cephalosporin C in different water matrices by ionizing radiation: Degradation kinetics, pathways, and toxicity. *Science of The Total Environment* 791, 148253. <https://doi.org/10.1016/J.SCITOTENV.2021.148253>
- Chiaia-Hernández, A.C., Scheringer, M., Müller, A., Stieger, G., Wächter, D., Keller, A., Pintado-Herrera, M.G., Lara-Martin, P.A., Bucheli, T.D., Hollender, J., 2020. Target and suspect screening analysis reveals persistent emerging organic contaminants in soils and sediments. *Science of the Total Environment* 740, 140181. <https://doi.org/10.1016/j.scitotenv.2020.140181>
- Chinnaiyan, P., Thampi, S.G., Kumar, M., Balachandran, M., 2019. Photocatalytic degradation of metformin and amoxicillin in synthetic hospital wastewater: effect of classical parameters. *International Journal of Environmental Science and Technology* 16. <https://doi.org/10.1007/s13762-018-1935-0>

- Chmielewski, A.G., Han, B., 2017. Electron Beam Technology for Environmental Pollution Control 37–66. https://doi.org/10.1007/978-3-319-54145-7_2
- Chmielewski, A.G., Han, B., 2016. Electron Beam Technology for Environmental Pollution Control. *Top Curr Chem* 374, 1–30. <https://doi.org/10.1007/s41061-016-0069-4>
- Chu, L., Wang, J., 2022. Treatment of oil-field produced wastewater by electron beam technology: Demulsification, disinfection and oil removal. *J Clean Prod* 378, 134532. <https://doi.org/10.1016/J.JCLEPRO.2022.134532>
- Chu, L., Wang, J., He, S., Chen, C., Wojnárovits, L., Takács, E., 2021. Treatment of pharmaceutical wastewater by ionizing radiation: Removal of antibiotics, antimicrobial resistance genes and antimicrobial activity. *J Hazard Mater* 415, 125724. <https://doi.org/10.1016/J.JHAZMAT.2021.125724>
- Coelho, A.S., Chagas, C.E.P., de Pádua, R.M., Pianetti, G.A., Fernandes, C., 2017. A comprehensive stability-indicating HPLC method for determination of chloroquine in active pharmaceutical ingredient and tablets: Identification of oxidation impurities. *J Pharm Biomed Anal* 145, 248–254. <https://doi.org/10.1016/J.JPBA.2017.06.023>
- Couto, C.F., Lange, L.C., Amaral, M.C.S., 2019. Occurrence, fate and removal of pharmaceutically active compounds (PhACs) in water and wastewater treatment plants—A review. *Journal of Water Process Engineering* 32, 100927. <https://doi.org/10.1016/J.JWPE.2019.100927>
- Csaj, T., Rácz, G., Takács, E., Wojnárovits, L., 2012. Radiation induced degradation of pharmaceutical residues in water: Chloramphenicol. *Radiation Physics and Chemistry* 81, 1489–1494. <https://doi.org/10.1016/j.radphyschem.2012.01.021>
- Cuccarese, M., Brutti, S., De Bonis, A., Teghil, R., Mancini, I.M., Masi, S., Caniani, D., 2021. Removal of diclofenac from aqueous solutions by adsorption on thermo-plasma expanded graphite. *Sci Rep* 11. <https://doi.org/10.1038/s41598-021-83117-z>
- Dabić, D., Babić, S., Škorić, I., 2019. The role of photodegradation in the environmental fate of hydroxychloroquine. *Chemosphere* 230. <https://doi.org/10.1016/j.chemosphere.2019.05.032>
- de Oliveira, M., Atalla, A.A., Frihling, B.E.F., Cavalheri, P.S., Migliolo, L., Filho, F.J.C.M., 2019. Ibuprofen and caffeine removal in vertical flow and free-floating macrophyte constructed wetlands with *Heliconia rostrata* and *Eichornia crassipes*. *Chemical Engineering Journal* 373, 458–467. <https://doi.org/10.1016/J.CEJ.2019.05.064>
- Delgado, N., Navarro, A., Marino, D., Peñuela, G.A., Ronco, A., 2019. Removal of pharmaceuticals and personal care products from domestic wastewater using rotating biological contactors. *International Journal of Environmental Science and Technology* 16, 1–10. <https://doi.org/10.1007/s13762-018-1658-2>
- Deogaonkar, S., Pate, M., Rawat, K.P., Sarma, K.S.S., 2017. Use of electron beam irradiation for solution of biodegradation enhancement in textile industry. *BTRA Scan* 47.
- Deogaonkar, S.C., Wakode, P., Rawat, K.P., 2019. Electron beam irradiation post treatment for degradation of non biodegradable contaminants in textile wastewater. *Radiation Physics and Chemistry* 165. <https://doi.org/10.1016/j.radphyschem.2019.108377>

- Deogaonkar-Baride, S., Wakode, P., Rawat, K.P., 2021. Treatment of Biorefractory Organic Compounds in Dyeing and Printing Process Textile Wastewater with Electron Beam Radiation. *J Hazard Toxic Radioact Waste* 25. [https://doi.org/10.1061/\(asce\)hz.2153-5515.0000603](https://doi.org/10.1061/(asce)hz.2153-5515.0000603)
- Dey, G.R., 2011. Nitrogen compounds' formation in aqueous solutions under high ionizing radiation: An overview. *Radiation Physics and Chemistry* 80, 394–402. <https://doi.org/10.1016/J.RADPHYSICHEM.2010.10.010>
- Dhillon, G.S., Kaur, S., Pulicharla, R., Brar, S.K., Cledón, M., Verma, M., Surampalli, R.Y., 2015. Triclosan: Current status, occurrence, environmental risks and bioaccumulation potential. *Int J Environ Res Public Health*. <https://doi.org/10.3390/ijerph120505657>
- Dhiman, M., 2021. Application of Magnetic Nano Particles and their Composites as Adsorbents for Waste Water Treatment: A Brief Review. <https://doi.org/10.21741/9781644901595-7>
- Doddaga, S., Peddakonda, R., 2013. Chloroquine-N-oxide, a major oxidative degradation product of chloroquine: Identification, synthesis and characterization. *J Pharm Biomed Anal* 81–82, 118–125. <https://doi.org/10.1016/J.JPBA.2013.04.004>
- Dong, F., Li, J., Lin, Q., Wang, D., Li, C., Shen, Y., Zeng, T., Song, S., 2022. Oxidation of chloroquine drug by ferrate: Kinetics, reaction mechanism and antibacterial activity. *Chemical Engineering Journal* 428. <https://doi.org/10.1016/j.cej.2021.131408>
- Dorival-García, N., Zafra-Gómez, A., Navalón, A., González-López, J., Hontoria, E., Vílchez, J.L., 2013. Removal and degradation characteristics of quinolone antibiotics in laboratory-scale activated sludge reactors under aerobic, nitrifying and anoxic conditions. *J Environ Manage* 120, 75–83. <https://doi.org/10.1016/j.jenvman.2013.02.007>
- Draganic, 2012. This is Volume 26 of PHYSICAL CHEMISTRY 26.
- Drzewicz, P., Pańta, P., Gluszewski, W., Trojanowicz, M., 1999. Effect of selected scavengers on radiolytic degradation of 2,4-dichlorophenol for environmental purposes. *J Radioanal Nucl Chem* 242. <https://doi.org/10.1007/BF02347368>
- Duan, M., Zhang, Y., Zhou, B., Wang, Q., Gu, J., Liu, G., Qin, Z., Li, Z., 2019. Changes in antibiotic resistance genes and mobile genetic elements during cattle manure composting after inoculation with *Bacillus subtilis*. *Bioresour Technol* 292, 122011. <https://doi.org/10.1016/J.BIORTECH.2019.122011>
- Duan, Y., Zhou, W., Shao, H., Zhang, Z., Shi, W., Xu, G., 2022. Electron beam induced degradation of indomethacin in aqueous solution: kinetics, degradation mechanism, and toxicity assessment. *Environmental Science and Pollution Research* 29, 19283–19294. <https://doi.org/10.1007/S11356-021-16348-2/TABLES/2>
- Duarte, C.L., Sampa, M.H.O., Rela, P.R., Oikawa, H., Silveira, C.G., Azevedo, A.L., 2002. Advanced oxidation process by electron-beam-irradiation-induced decomposition of pollutants in industrial effluents. *Radiation Physics and Chemistry* 63, 647–651. [https://doi.org/10.1016/S0969-806X\(01\)00560-6](https://doi.org/10.1016/S0969-806X(01)00560-6)
- Dubber, D., Gray, N.F., 2010. Replacement of chemical oxygen demand (COD) with total organic carbon (TOC) for monitoring wastewater treatment performance to minimize disposal of toxic analytical waste. *J Environ Sci Health A Tox Hazard Subst Environ Eng* 45, 1595–1600. <https://doi.org/10.1080/10934529.2010.506116>

- Ferreira, M.T., Carvalho, C.D.S., 2023. Chloroquine and hydroxychloroquine in the environment and aquatic organisms: a review. *Revista Ambiente e Agua*. <https://doi.org/10.4136/ambiente-agua.2880>
- Folcik, A.M., Pillai, S.D., 2020. A critical review of ionizing radiation technologies for the remediation of waters containing Microcystin-LR and *M. aeruginosa*. *Radiation Physics and Chemistry* 177, 109128. <https://doi.org/10.1016/j.radphyschem.2020.109128>
- Foszpańczyk, M., Bilińska, L., Gmurek, M., Ledakowicz, S., 2019. Heterogeneous oxidation of phenolic compounds with photosensitizing catalysts incorporated into chitosan. *Catalysts* 9. <https://doi.org/10.3390/catal9110891>
- Gani, K.M., Bux, F., Kazmi, A.A., 2019. Diethylhexyl phthalate removal in full scale activated sludge plants: Effect of operational parameters. *Chemosphere* 234, 885–892. <https://doi.org/10.1016/J.CHEMOSPHERE.2019.06.130>
- Gao, X., Kang, S., Xiong, R., Chen, M., 2020. Environment-friendly removal methods for endocrine disrupting chemicals. *Sustainability (Switzerland)* 12, 1–16. <https://doi.org/10.3390/su12187615>
- Garcia, J.J.M., Nuñez, J.A.P., Salapare, H.S., Vasquez, M.R., 2019. Adsorption of diclofenac sodium in aqueous solution using plasma-activated natural zeolites. *Results Phys* 15, 102629. <https://doi.org/10.1016/J.RINP.2019.102629>
- Garcia, V.S.G., Rosa, J.M., Borrelly, S.I., 2020. Toxicity and color reduction of a textile effluent containing reactive red 239 dye by electron beam irradiation. *Radiation Physics and Chemistry* 172, 108765. <https://doi.org/10.1016/j.radphyschem.2020.108765>
- Garcia-Molina, R., Abril, I., de Vera, P., Paul, H., 2013. Comments on recent measurements of the stopping power of liquid water. *Nucl Instrum Methods Phys Res B* 299, 51–53. <https://doi.org/10.1016/j.nimb.2013.01.038>
- Generalova, V. V., Gurskii, M.N., Pikaev, A.K., 1988. Dosimetry in radiation processing in the U.S.S.R. *International Journal of Radiation Applications and Instrumentation. Part C. Radiation Physics and Chemistry* 31, 449–466. [https://doi.org/10.1016/1359-0197\(88\)90212-3](https://doi.org/10.1016/1359-0197(88)90212-3)
- Generalova, V. V., Gurskii, M.N., Pikaev, A.K., 1985. Dosimetry in radiation processing. *Radiation Physics and Chemistry* 25, 719–728. [https://doi.org/10.1016/0146-5724\(85\)90152-9](https://doi.org/10.1016/0146-5724(85)90152-9)
- Ghanbari, F., Ahmadi, M., Gohari, F., 2019. Heterogeneous activation of peroxymonosulfate via nanocomposite CeO₂-Fe₃O₄ for organic pollutants removal: The effect of UV and US irradiation and application for real wastewater. *Sep Purif Technol* 228, 115732. <https://doi.org/10.1016/J.SEPPUR.2019.115732>
- Giebułtowicz, J., Tyski, S., Wolinowska, R., Grzybowska, W., Zaręba, T., Drobniewska, A., Wroczyński, P., Nałęcz-Jawecki, G., 2018. Occurrence of antimicrobial agents, drug-resistant bacteria, and genes in the sewage-impacted Vistula River (Poland). *Environmental Science and Pollution Research*. <https://doi.org/10.1007/s11356-017-0861-x>
- Gil, A., Taoufik, N., García, A.M., Korili, S.A., 2019. Comparative removal of emerging contaminants from aqueous solution by adsorption on an activated carbon. *Environmental Technology (United Kingdom)* 40. <https://doi.org/10.1080/09593330.2018.1464066>

- González-González, R.B., Sharma, P., Singh, S.P., Américo-Pinheiro, J.H.P., Parra-Saldívar, R., Bilal, M., Iqbal, H.M.N., 2022. Persistence, environmental hazards, and mitigation of pharmaceutically active residual contaminants from water matrices. *Science of The Total Environment* 821, 153329. <https://doi.org/10.1016/J.SCITOTENV.2022.153329>
- Hajjani, M., Gholami, A., Sayadi, M.H., 2022. Removal of pharmaceutical pollutants from aquatic environments using heterogeneous photocatalysis. *Advances in Environmental Technology* 8. <https://doi.org/10.22104/aet.2022.5595.1523>
- Ham, H.S., Cho, H.W., Myung, S.W., 2014. Degradation efficiency and characterization of lincomycin by electron beam irradiation. *Mass Spectrometry Letters* 5. <https://doi.org/10.5478/MSL.2014.5.3.89>
- He, S., Sun, W., Wang, J., Chen, L., Zhang, Y., Yu, J., 2016. Enhancement of biodegradability of real textile and dyeing wastewater by electron beam irradiation. *Radiation Physics and Chemistry* 124, 203–207. <https://doi.org/10.1016/j.radphyschem.2015.11.033>
- Henschler, D., 1994. Toxicity of Chlorinated Organic Compounds: Effects of the Introduction of Chlorine in Organic Molecules. *Angewandte Chemie International Edition in English* 33, 1920–1935. <https://doi.org/10.1002/ANIE.199419201>
- Hiroki, A., Pimblott, S.M., Laverne, J.A., 2002. Hydrogen peroxide production in the radiolysis of water with high radical scavenger concentrations. *Journal of Physical Chemistry A* 106. <https://doi.org/10.1021/jp0207578>
- Hoang Hoa Mai, Nguyen Dinh Duong, 1994. SILVER DICHROMATE - A SUITABLE DOSIMETER FOR RADIATION PROCESSING. Hanoi.
- Hosono, M., Arai, H., Aizawa, M., Yamamoto, I., Shimizu, K., Sugiyama, M., 1993. Decoloration and degradation of azo dye in aqueous solution supersaturated with oxygen by irradiation of high-energy electron beams. *Applied Radiation and Isotopes* 44, 1199–1203. [https://doi.org/10.1016/0969-8043\(93\)90064-H](https://doi.org/10.1016/0969-8043(93)90064-H)
- Hossain, K., Maruthi, Y.A., Das, N.L., Rawat, K.P., Sarma, K.S.S., 2018. Irradiation of wastewater with electron beam is a key to sustainable smart/green cities: a review. *Appl Water Sci* 8, 1–11. <https://doi.org/10.1007/s13201-018-0645-6>
- Hu, J., Wang, J., 2007. Degradation of chlorophenols in aqueous solution by γ -radiation. *Radiation Physics and Chemistry* 76, 1489–1492. <https://doi.org/10.1016/J.RADPHYSICHEM.2007.02.058>
- Huo, Z., Wang, S., Shao, H., Wang, H., Xu, G., 2020. Radiolytic degradation of anticancer drug capecitabine in aqueous solution: kinetics, reaction mechanism, and toxicity evaluation. *Environmental Science and Pollution Research* 27. <https://doi.org/10.1007/s11356-020-08500-1>
- Hylling, O., Nikbakht Fini, M., Ellegaard-Jensen, L., Muff, J., Madsen, H.T., Aamand, J., Hansen, L.H., 2019. A novel hybrid concept for implementation in drinking water treatment targets micropollutant removal by combining membrane filtration with biodegradation. *Science of The Total Environment* 694, 133710. <https://doi.org/10.1016/J.SCITOTENV.2019.133710>
- IAEA - International Atomic Energy Agency, IAEA, 2013. Guidelines for the Development, Validation and Routine Control of Industrial Radiation Processes. IAEA Radiation Technology Series 148.

- Inam, E.J., Nwoke, I.B., Udosen, E.D., Offiong, N.A.O., 2019. Ecological risks of phenolic endocrine disrupting compounds in an urban tropical river. *Environmental Science and Pollution Research* 26. <https://doi.org/10.1007/s11356-019-05458-7>
- INTERNATIONAL ATOMIC ENERGY AGENCY, 2002. *Dosimetry for Food Irradiation*. VIENNA.
- Iwamatsu, K., Sundin, S., LaVerne, J.A., 2018. Hydrogen peroxide kinetics in water radiolysis. *Radiation Physics and Chemistry* 145, 207–212. <https://doi.org/10.1016/J.RADPHYSICHEM.2017.11.002>
- Jan, S., Kamili, A.N., Parween, T., Hamid, R., Parray, J.A., Siddiqi, T.O., Mahmooduzzafar, Ahmad, P., 2015. Feasibility of radiation technology for wastewater treatment. *Desalination Water Treat* 55, 2053–2068. <https://doi.org/10.1080/19443994.2014.937749>
- Jayaraj, R., Megha, P., Sreedev, P., 2016. Organochlorine pesticides, their toxic effects on living organisms and their fate in the environment. *Interdiscip Toxicol* 9, 90. <https://doi.org/10.1515/INTOX-2016-0012>
- Jia-Tong, L., Yong-Sheng, L., Qing, S., Da-Qian, H., Dan, Z., Wen-Bao, J., 2017. The treatment of aniline in aqueous solutions by gamma irradiation. *Journal of Advanced Oxidation Technologies* 20. <https://doi.org/10.1515/jaots-2016-0173>
- Jjemba, P.K., 2002. The potential impact of veterinary and human therapeutic agents in manure and biosolids on plants grown on arable land: A review. *Agric Ecosyst Environ* 93, 267–278. [https://doi.org/10.1016/S0167-8809\(01\)00350-4](https://doi.org/10.1016/S0167-8809(01)00350-4)
- Joseph, L., Jun, B.M., Jang, M., Park, C.M., Muñoz-Senmache, J.C., Hernández-Maldonado, A.J., Heyden, A., Yu, M., Yoon, Y., 2019. Removal of contaminants of emerging concern by metal-organic framework nano-adsorbents: A review. *Chemical Engineering Journal* 369, 928–946. <https://doi.org/10.1016/J.CEJ.2019.03.173>
- Jung, Y.S., Lim, W.T., Park, J.Y., Kim, Y.H., 2009. Effect of pH on Fenton and Fenton-like oxidation. <http://dx.doi.org/10.1080/09593330802468848> 30, 183–190. <https://doi.org/10.1080/09593330802468848>
- Kamble Arun .D, Vasant D. Barhate, Madhukar.H.Salunke, Lakshmi Narasimham, 2011. Automated Potentiometric Titration Method for Determination of pKa Values: An Application to Hydroxychloroquine Sulphate. *Journal of Pharmacy Research* 4, 3794–3797.
- Kanakaraju, D., Glass, B.D., Oelgemöller, M., 2018. Advanced oxidation process-mediated removal of pharmaceuticals from water: A review. *J Environ Manage* 219, 189–207. <https://doi.org/10.1016/J.JENVMAN.2018.04.103>
- Kargar, F., Bemani, A., Sayadi, M.H., Ahmadpour, N., 2021. Synthesis of modified beta bismuth oxide by titanium oxide and highly efficient solar photocatalytic properties on hydroxychloroquine degradation and pathways. *J Photochem Photobiol A Chem* 419. <https://doi.org/10.1016/j.jphotochem.2021.113453>
- Kasonga, T.K., Coetzee, M.A.A., Kamika, I., Ngole-Jeme, V.M., Benteke Momba, M.N., 2021. Endocrine-disruptive chemicals as contaminants of emerging concern in wastewater and surface water: A review. *J Environ Manage* 277, 111485. <https://doi.org/10.1016/j.jenvman.2020.111485>

- Kawabata, K., Sugihara, K., Sanoh, S., Kitamura, S., Ohta, S., 2013. Photodegradation of pharmaceuticals in the aquatic environment by sunlight and UV-A,-B and-C irradiation. *Journal of Toxicological Sciences* 38, 215–223. <https://doi.org/10.2131/jts.38.215>
- Khan, J.A., Shah, N.S., Khan, H.M., 2015. Decomposition of atrazine by ionizing radiation: Kinetics, degradation pathways and influence of radical scavengers. *Sep Purif Technol* 156, 140–147. <https://doi.org/10.1016/j.seppur.2015.09.064>
- Kim, H.Y., Lee, O.-M., Kim, T.-H., Yu, S., 2014. Enhanced Biodegradability of Pharmaceuticals and Personal Care Products by Ionizing Radiation. *Water Environment Research* 87. <https://doi.org/10.2175/106143014x14062131178033>
- Kim, T.H., Lee, S.H., Kim, H.Y., Doudrick, K., Yu, S., Kim, S.D., 2019. Decomposition of perfluorooctane sulfonate (PFOS) using a hybrid process with electron beam and chemical oxidants. *Chemical Engineering Journal* 361, 1363–1370. <https://doi.org/10.1016/J.CEJ.2018.10.195>
- Kim, Y., Ershov, B.G., Ponomarev, A. V., 2020. Features and Ways to Upgrade Electron-Beam Wastewater Treatment. *High Energy Chemistry* 54, 462–468. <https://doi.org/10.1134/S0018143920060089/FIGURES/5>
- Kimura, A., Osawa, M., Taguchi, M., 2012. Decomposition of persistent pharmaceuticals in wastewater by ionizing radiation. *Radiation Physics and Chemistry* 81, 1508–1512. <https://doi.org/10.1016/j.radphyschem.2011.11.032>
- Kiyoshi Tominaga, F., Fonseca Boiani, N., Tiekko Silva, T., Gomes dos Santos, J., Temponi Lebre, D., Leo, P., Ivone Borrelly, S., 2023. Electron beam irradiation applied for the detoxification and degradation of single ciprofloxacin aqueous solution and multiclass pharmaceutical quaternary mixture. *Sep Purif Technol* 307, 122818. <https://doi.org/10.1016/J.SEPPUR.2022.122818>
- Klare, M., Waldner, G., Bauer, R., Jacobs, H., Broekaert, J.A.C., 1999. Degradation of nitrogen containing organic compounds by combined photocatalysis and ozonation. *Chemosphere* 38, 2013–2027. [https://doi.org/10.1016/S0045-6535\(98\)00414-7](https://doi.org/10.1016/S0045-6535(98)00414-7)
- Klouda, C.B., Stone, W.L., 2020. Oxidative stress, proton fluxes, and chloroquine/hydroxychloroquine treatment for covid-19. *Antioxidants*. <https://doi.org/10.3390/antiox9090894>
- Kovács, K., He, S., Mile, V., Csay, T., Takács, E., Wojnárovits, L., 2015. Ionizing radiation induced degradation of diuron in dilute aqueous solution. *Chem Cent J* 9, 1–10. <https://doi.org/10.1186/s13065-015-0097-0>
- Kovács, K., Simon, Á., Balogh, G.T., Tóth, T., Wojnárovits, L., 2020. High-energy ionizing radiation-induced degradation of amodiaquine in dilute aqueous solution: radical reactions and kinetics. *Free Radic Res* 54, 185–194. <https://doi.org/10.1080/10715762.2020.1736579>
- Kowald, C., Brorman, E., Shankar, S., Klemashevich, C., Staack, D., Pillai, S.D., 2021. PFOA and PFOS breakdown in experimental sand, laboratory-grade water, investigation-derived groundwater and wastewater effluent samples at 50 kGy electron beam dose. *Radiation Physics and Chemistry* 180. <https://doi.org/10.1016/j.radphyschem.2020.109323>
- Le, T.T., Yoon, H., Son, M.H., Kang, Y.G., Chang, Y.S., 2019. Treatability of hexabromocyclododecane using Pd/Fe nanoparticles in the soil-plant system: Effects of humic acids. *Science of The Total Environment* 689, 444–450. <https://doi.org/10.1016/J.SCITOTENV.2019.06.290>

- Lee, C.S., Londhe, K., Grdanovska, S., Cooper, C.A., Venkatesan, A.K., 2023. Emerging investigator series: low doses of electron beam irradiation effectively degrade 1,4-dioxane in water within a few seconds. *Environ Sci (Camb)* 9, 2226–2237. <https://doi.org/10.1039/D3EW00111C>
- Lee, D.H., Jacobs, D.R., Park, H.Y., Carpenter, D.O., 2017. A role of low dose chemical mixtures in adipose tissue in carcinogenesis. *Environ Int* 108, 170–175. <https://doi.org/10.1016/J.ENVINT.2017.08.015>
- Li, P., Khan, M.A., Xia, M., Lei, W., Zhu, S., Wang, F., 2019. Efficient preparation and molecular dynamic (MD) simulations of Gemini surfactant modified layered montmorillonite to potentially remove emerging organic contaminants from wastewater. *Ceram Int* 45, 10782–10791. <https://doi.org/10.1016/J.CERAMINT.2019.02.152>
- Li, W., Shi, Y., Gao, L., Liu, J., Cai, Y., 2013. Occurrence and removal of antibiotics in a municipal wastewater reclamation plant in Beijing, China. *Chemosphere* 92, 435–444. <https://doi.org/10.1016/j.chemosphere.2013.01.040>
- Li, X., Wei, H., Song, T., Lu, H., Wang, X., 2023. A review of the photocatalytic degradation of organic pollutants in water by modified TiO₂. *Water Science and Technology* 88. <https://doi.org/10.2166/wst.2023.288>
- Liao, H., Zhao, Q., Cui, P., Chen, Z., Yu, Z., Geisen, S., Friman, V.P., Zhou, S., 2019. Efficient reduction of antibiotic residues and associated resistance genes in tylosin antibiotic fermentation waste using hyperthermophilic composting. *Environ Int* 133, 105203. <https://doi.org/10.1016/J.ENVINT.2019.105203>
- Lin, X., Xu, J., Keller, A.A., He, L., Gu, Y., Zheng, W., Sun, D., Lu, Z., Huang, J., Huang, X., Li, G., 2020. Occurrence and risk assessment of emerging contaminants in a water reclamation and ecological reuse project. *Science of the Total Environment* 744. <https://doi.org/10.1016/j.scitotenv.2020.140977>
- Lindroos, M., Hörnström, D., Larsson, G., Gustavsson, M., van Maris, A.J.A., 2019. Continuous removal of the model pharmaceutical chloroquine from water using melanin-covered *Escherichia coli* in a membrane bioreactor. *J Hazard Mater* 365, 74–80. <https://doi.org/10.1016/j.jhazmat.2018.10.081>
- Ling, Y., Liu, H., Li, B., Zhang, B., Wu, Y., Hu, H., Yu, D., Huang, S., 2023. Efficient photocatalytic ozonation of azithromycin by three-dimensional g-C₃N₄ nanosheet loaded magnetic Fe-MCM-48 under simulated solar light. *Appl Catal B* 324, 122208. <https://doi.org/10.1016/J.APCATB.2022.122208>
- Linke, F., Edun, O., Junginger, T., Payraudeau, S., Preusser, F., Imfeld, G., Lange, J., 2023. Biocides in Soils of Urban Stormwater Infiltration Systems—Indications of Inputs from Point and Non-point Sources. *Water Air Soil Pollut* 234. <https://doi.org/10.1007/s11270-023-06613-0>
- Liu, B., Zhang, S. gen, Chang, C.C., 2020. Emerging pollutants—Part II: Treatment. *Water Environment Research* 92, 1603–1617. <https://doi.org/10.1002/wer.1407>
- Liu, F., Ying, G.G., Tao, R., Zhao, J.L., Yang, J.F., Zhao, L.F., 2009. Effects of six selected antibiotics on plant growth and soil microbial and enzymatic activities. *Environmental Pollution* 157, 1636–1642. <https://doi.org/10.1016/j.envpol.2008.12.021>

- Liu, H., Bruton, T.A., Doyle, F.M., Sedlak, D.L., 2014. In Situ Chemical Oxidation of Contaminated Groundwater by Persulfate: Decomposition by Fe(III)-and Mn(IV)-Containing Oxides and Aquifer Materials. <https://doi.org/10.1021/es502056d>
- Liu, Y., Hu, J., Wang, J., 2014. Fe²⁺ enhancing sulfamethazine degradation in aqueous solution by gamma irradiation. *Radiation Physics and Chemistry* 96, 81–87. <https://doi.org/10.1016/J.RADPHYSICHEM.2013.08.018>
- Llamas, M., Vadillo-Pérez, I., Candela, L., Jiménez-Gavilán, P., Corada-Fernández, C., Castro-Gámez, A.F., 2020. Screening and distribution of contaminants of emerging concern and regulated organic pollutants in the heavily modified Guadalquivir river basin, southern Spain. *Water (Switzerland)* 12, 1–19. <https://doi.org/10.3390/w12113012>
- Lu, G.H., Piao, H.T., Gai, N., Shao, P.W., Zheng, Y., Jiao, X.C., Rao, Z., Yang, Y.L., 2019. Pharmaceutical and Personal Care Products in Surface Waters from the Inner City of Beijing, China: Influence of Hospitals and Reclaimed Water Irrigation. *Arch Environ Contam Toxicol* 76, 255–264. <https://doi.org/10.1007/s00244-018-0578-y>
- Luo, Y., Zhu, Y., Han, Y., Ye, H., Liu, R., Lan, Y., Xue, M., Xie, X., Yu, S., Zhang, L., Yin, Z., Gao, B., 2023. REVIEW Open Access g-C₃N₄-based photocatalysts for organic pollutant removal: a critical review. <https://doi.org/10.1007/s44246-023-00045-5>
- Luo, Z., He, Y., Zhi, D., Luo, L., Sun, Y., Khan, E., Wang, L., Peng, Y., Zhou, Y., Tsang, D.C.W., 2019. Current progress in treatment techniques of triclosan from wastewater: A review. *Science of The Total Environment* 696, 133990. <https://doi.org/10.1016/J.SCITOTENV.2019.133990>
- Makarov, I.E., Ponomarev, A. V., 2018. Radiation-Induced Degradation of Organic Compounds and Radiation Technologies for Purification of Aqueous Systems, in: *Ionizing Radiation Effects and Applications*. <https://doi.org/10.5772/intechopen.72074>
- Maletzky, P., Bauer, R., 1998. The Photo-Fenton method — Degradation of nitrogen containing organic compounds. *Chemosphere* 37, 899–909. [https://doi.org/10.1016/S0045-6535\(98\)00093-9](https://doi.org/10.1016/S0045-6535(98)00093-9)
- Manivannan, E., Karthikeyan, C., Moorthy, N.S.H.N., Chaturvedi, S.C., 2021. The Rise and Fall of Chloroquine/Hydroxychloroquine as Compassionate Therapy of COVID-19. *Front Pharmacol*. <https://doi.org/10.3389/fphar.2021.584940>
- Martínez-Alcalá, I., Guillén-Navarro, J.M., Lahora, A., 2021. Occurrence and fate of pharmaceuticals in a wastewater treatment plant from southeast of Spain and risk assessment. *J Environ Manage* 279. <https://doi.org/10.1016/j.jenvman.2020.111565>
- Marussi, G., Vione, D., 2021. Secondary formation of aromatic nitroderivatives of environmental concern: Photolysis processes triggered by the photolysis of nitrate and nitrite ions in aqueous solution. *Molecules*. <https://doi.org/10.3390/molecules26092550>
- Maruthi, Y.A., Das, N.L., Hossain, K., Rawat, K.P., Sarma, K.S., Sabharwal, S., 2013. Application of Electron Beam Technology for Disinfection of Sewage Water to Minimize Public Health Risks. *European Journal of Sustainable Development* 2, 31–42. <https://doi.org/10.14207/ejsd.2013.v2n2p31>

- Mazur, D.M., Lebedev, A.T., 2022. Transformation of Organic Compounds during Water Chlorination/Bromination: Formation Pathways for Disinfection By-Products (A Review). *Journal of Analytical Chemistry* 77. <https://doi.org/10.1134/S1061934822140052>
- McAllister, M., Kazemigazestane, N., Henry, L.T., Gu, B., Fabrikant, I., Tribello, G.A., Kohanoff, J., 2019. Solvation effects on dissociative electron attachment to thymine. *Journal of Physical Chemistry B* 123. <https://doi.org/10.1021/acs.jpccb.8b11621>
- McLanahan, E.D., Andersen, M.E., Campbell, J.L., Fisher, J.W., 2009. Competitive inhibition of thyroidal uptake of dietary iodide by perchlorate does not describe perturbations in rat serum total T4 and TSH. *Environ Health Perspect* 117. <https://doi.org/10.1289/ehp.0800111>
- Meesungnoen, J., Sanguanmith, S., Jay-Gerin, J.P., 2015. Yields of H₂ and hydrated electrons in low-LET radiolysis of water determined by Monte Carlo track chemistry simulations using phenol/N₂O aqueous solutions up to 350 °C. *RSC Adv* 5, 76813–76824. <https://doi.org/10.1039/c5ra15801j>
- Melnikov, F., Kostal, J., Voutchkova-Kostal, A., Zimmerman, J.B., Anastas, P.T., 2016. Assessment of predictive models for estimating the acute aquatic toxicity of organic chemicals. *Green Chemistry* 18. <https://doi.org/10.1039/c6gc00720a>
- Miao, H., Yang, J., Peng, G., Li, H., Zhu, Y., 2019. Enhancement of the degradation ability for organic pollutants via the synergistic effect of photoelectrocatalysis on a self-assembled perylene diimide (SA-PDI) thin film. *Sci Bull (Beijing)* 64, 896–903. <https://doi.org/10.1016/J.SCIB.2019.05.006>
- Midassi, S., Bedoui, A., Bensalah, N., 2020. Efficient degradation of chloroquine drug by electro-Fenton oxidation: Effects of operating conditions and degradation mechanism. *Chemosphere* 260, 127558. <https://doi.org/10.1016/j.chemosphere.2020.127558>
- Minden, V., Deloy, A., Volkert, A.M., Leonhardt, S.D., Pufal, G., 2017. Antibiotics impact plant traits, even at small concentrations. *AoB Plants* 9. <https://doi.org/10.1093/aobpla/plx010>
- Mirzaei, A., Chen, Z., Haghghat, F., Yerushalmi, L., 2017a. Removal of pharmaceuticals from water by homo/heterogeneous Fenton-type processes – A review. *Chemosphere* 174, 665–688. <https://doi.org/10.1016/J.CHEMOSPHERE.2017.02.019>
- Mirzaei, A., Chen, Z., Haghghat, F., Yerushalmi, L., 2017b. Removal of pharmaceuticals from water by homo/heterogeneous Fenton-type processes – A review. *Chemosphere* 174, 665–688. <https://doi.org/10.1016/J.CHEMOSPHERE.2017.02.019>
- Mook, W.T., Chakrabarti, M.H., Aroua, M.K., Khan, G.M.A., Ali, B.S., Islam, M.S., Abu Hassan, M.A., 2012. Removal of total ammonia nitrogen (TAN), nitrate and total organic carbon (TOC) from aquaculture wastewater using electrochemical technology: A review. *Desalination*. <https://doi.org/10.1016/j.desal.2011.09.029>
- Morales-Paredes, C.A., Rodríguez-Díaz, J.M., Boluda-Botella, N., 2022. Pharmaceutical compounds used in the COVID-19 pandemic: A review of their presence in water and treatment techniques for their elimination. *Science of The Total Environment* 814, 152691. <https://doi.org/10.1016/J.SCITOTENV.2021.152691>
- Morin-Crini, N., Winterton, P., Fourmentin, S., Wilson, L.D., Fenyvesi, É., Crini, G., 2018. Water-insoluble β -cyclodextrin–epichlorohydrin polymers for removal of pollutants from aqueous

- solutions by sorption processes using batch studies: A review of inclusion mechanisms. *Prog Polym Sci* 78, 1–23. <https://doi.org/10.1016/J.PROGPOLYMSCI.2017.07.004>
- Murgolo, S., Franz, S., Arab, H., Bestetti, M., Falletta, E., Mascolo, G., 2019. Degradation of emerging organic pollutants in wastewater effluents by electrochemical photocatalysis on nanostructured TiO₂ meshes. *Water Res* 164, 114920. <https://doi.org/10.1016/J.WATRES.2019.114920>
- Najafpoor, A.A., Nemati Sani, O., Alidadi, H., Yazdani, M., Navaei Fezabady, A.A., Taghavi, M., 2019. Optimization of ciprofloxacin adsorption from synthetic wastewaters using γ -Al₂O₃ nanoparticles: An experimental design based on response surface methodology. *Colloid Interface Sci Commun* 33, 100212. <https://doi.org/10.1016/J.COLCOM.2019.100212>
- Nam, S.W., Choi, D.J., Kim, S.K., Her, N., Zoh, K.D., 2014. Adsorption characteristics of selected hydrophilic and hydrophobic micropollutants in water using activated carbon. *J Hazard Mater* 270, 144–152. <https://doi.org/10.1016/J.JHAZMAT.2014.01.037>
- Nasir, N.M., Ming, T.T., Ahmadun, F.R., Sobri, S., 2010. Decomposition and biodegradability enhancement of textile wastewater using a combination of electron beam irradiation and activated sludge process. *Water Science and Technology* 62. <https://doi.org/10.2166/wst.2010.239>
- Nemati Sani, O., Navaei fezabady, A.A., Yazdani, M., Taghavi, M., 2019. Catalytic ozonation of ciprofloxacin using γ -Al₂O₃ nanoparticles in synthetic and real wastewaters. *Journal of Water Process Engineering* 32, 100894. <https://doi.org/10.1016/J.JWPE.2019.100894>
- Nicolaescu, A.R., Wiest, O., Kamat, P. V., 2003. Radical-induced oxidative transformation of quinoline. *Journal of Physical Chemistry A* 107. <https://doi.org/10.1021/jp027112s>
- Nord, K., Karlsen, J., Tønnesen, H.H., 1991. Photochemical stability of biologically active compounds. IV. Photochemical degradation of chloroquine. *Int J Pharm* 72, 11–18. [https://doi.org/10.1016/0378-5173\(91\)90375-X](https://doi.org/10.1016/0378-5173(91)90375-X)
- Oshima, A., Tanaka, T., Nakaya, H., Senba, R., Satoh, K., 2020. Pentadecafluorooctanoic-acid-free polytetrafluoroethylene and mechanism of PFOA formation by γ -irradiation. *Sci Rep* 10, 1–7. <https://doi.org/10.1038/s41598-020-70918-x>
- Ozer, Z.N., 2017. Electron beam irradiation processing for industrial and medical applications, in: *EPJ Web of Conferences*. <https://doi.org/10.1051/epjconf/201715401019>
- Pai, C.W., Wang, G.S., 2022. Treatment of PPCPs and disinfection by-product formation in drinking water through advanced oxidation processes: Comparison of UV, UV/Chlorine, and UV/H₂O₂. *Chemosphere* 287. <https://doi.org/10.1016/j.chemosphere.2021.132171>
- Pan, X.M., Schuchmann, M.N., Von Sonntag, C., 1993. Oxidation of benzene by the OH radical. A product and pulse radiolysis study in oxygenated aqueous solution. *Journal of the Chemical Society, Perkin Transactions 2*. <https://doi.org/10.1039/p29930000289>
- Paul, J., Rawat, K.P., Sarma, K.S.S., Sabharwal, S., 2011. Decoloration and degradation of Reactive Red-120 dye by electron beam irradiation in aqueous solution. *Applied Radiation and Isotopes* 69, 982–987. <https://doi.org/10.1016/J.APRADISO.2011.03.009>
- Paumo, H.K., Dalhatou, S., Katata-Seru, L.M., Kamdem, B.P., Tijani, J.O., Vishwanathan, V., Kane, A., Bahadur, I., 2021. TiO₂ assisted photocatalysts for degradation of emerging organic pollutants in water and wastewater. *J Mol Liq*. <https://doi.org/10.1016/j.molliq.2021.115458>

- Peer Muhamed Noorani, K.R., Flora, G., Surendarnath, S., Mary Stephy, G., Amesho, K.T.T., Chinglenthoba, C., Thajuddin, N., 2024. Recent advances in remediation strategies for mitigating the impacts of emerging pollutants in water and ensuring environmental sustainability. *J Environ Manage* 351, 119674. <https://doi.org/10.1016/J.JENVMAN.2023.119674>
- Picó, Y., Campo, J., Alfarhan, A.H., El-Sheikh, M.A., Barceló, D., 2023. Wild and ruderal plants as bioindicators of global urban pollution by air, water and soil in Riyadh and Abha, Saudi Arabia. *Science of The Total Environment* 888, 164166. <https://doi.org/10.1016/J.SCITOTENV.2023.164166>
- Pinasseau, L., Wiest, L., Volatier, L., Mermillod-Blondin, F., Vulliet, E., 2020a. Emerging polar pollutants in groundwater: Potential impact of urban stormwater infiltration practices. *Environmental Pollution* 266, 115387. <https://doi.org/10.1016/j.envpol.2020.115387>
- Pinasseau, L., Wiest, L., Volatier, L., Mermillod-Blondin, F., Vulliet, E., 2020b. Emerging polar pollutants in groundwater: Potential impact of urban stormwater infiltration practices. *Environmental Pollution* 266, 115387. <https://doi.org/10.1016/J.ENVPOL.2020.115387>
- Ponomarev, A. v., 2020a. High-speed electron-beam water treatment: A technological consideration. *Radiation Physics and Chemistry* 172. <https://doi.org/10.1016/j.radphyschem.2020.108812>
- Ponomarev, A. v., 2020b. High-speed electron-beam water treatment: A technological consideration. *Radiation Physics and Chemistry* 172, 108812. <https://doi.org/10.1016/j.radphyschem.2020.108812>
- Ponomarev, A. v., Ershov, B.G., 2020. The Green Method in Water Management: Electron Beam Treatment. *Environ Sci Technol* 54, 5331–5344. <https://doi.org/10.1021/acs.est.0c00545>
- Rahman, M.F., Yanful, E.K., Jasim, S.Y., 2009. Endocrine disrupting compounds (EDCs) and pharmaceuticals and personal care products (PPCPs) in the aquatic environment: Implications for the drinking water industry and global environmental health. *J Water Health* 7, 224–243. <https://doi.org/10.2166/wh.2009.021>
- Ranković, B., Sagatova, A., Vujčić, I., Mašić, S., Veljović, Đ., Pavićević, V., Kamberović, Ž., 2020. Utilization of gamma and e-beam irradiation in the treatment of waste sludge from a drinking water treatment plant. *Radiation Physics and Chemistry* 177. <https://doi.org/10.1016/j.radphyschem.2020.109174>
- Rath, M.C., Keny, S.J., Upadhyaya, H.P., Adhikari, S., 2023. Free radical induced degradation and computational studies of hydroxychloroquine in aqueous solution. *Radiation Physics and Chemistry* 206, 110785. <https://doi.org/10.1016/j.radphyschem.2023.110785>
- Rauf, M.A., Ashraf, S.S., 2009. Radiation induced degradation of dyes-An overview. *J Hazard Mater* 166, 6–16. <https://doi.org/10.1016/j.jhazmat.2008.11.043>
- Rawat, K.P., Sarma, K.S.S., 2013. Enhanced biodegradation of wastewater with electron beam pretreatment. *Applied Radiation and Isotopes* 74, 6–8. <https://doi.org/10.1016/j.apradiso.2012.12.013>
- Rayaroth, M.P., Aravindakumar, C.T., Shah, N.S., Boczkaj, G., 2022. Advanced oxidation processes (AOPs) based wastewater treatment - unexpected nitration side reactions - a serious

- environmental issue: A review. *Chemical Engineering Journal* 430, 133002.
<https://doi.org/10.1016/J.CEJ.2021.133002>
- Rehman, F., Sayed, M., Khan, J.A., Khan, H.M., 2017. Removal of crystal violet dye from aqueous solution by gamma irradiation. *Journal of the Chilean Chemical Society* 62.
<https://doi.org/10.4067/S0717-97072017000100011>
- Rehman, Saba, Usman, Z., Rehman, Sabeen, Aldraihem, M., Rehman, N., Rehman, I., Ahmad, G., 2018. Endocrine disrupting chemicals and impact on male reproductive health. *Transl Androl Urol*. <https://doi.org/10.21037/tau.2018.05.17>
- Reinholds, I., Pugajeva, I., Perkons, I., Lundanes, E., Rusko, J., Kizane, G., Nikolajeva, V., Mutere, O., Petrina, Z., Baumane, L., Bartkevics, V., 2017. Decomposition of multi-class pharmaceutical residues in wastewater by exposure to ionising radiation. *International Journal of Environmental Science and Technology* 14, 1969–1980. <https://doi.org/10.1007/s13762-017-1290-6>
- Reuschenbach, P., Silvani, M., Dammann, M., Warnecke, D., Knacker, T., 2008. ECOSAR model performance with a large test set of industrial chemicals. *Chemosphere* 71.
<https://doi.org/10.1016/j.chemosphere.2007.12.006>
- Rizzi, V., Lacalamita, D., Gubitosa, J., Fini, P., Petrella, A., Romita, R., Agostiano, A., Gabaldón, J.A., Fortea Gorbe, M.I., Gómez-Morte, T., Cosma, P., 2019. Removal of tetracycline from polluted water by chitosan-olive pomace adsorbing films. *Science of The Total Environment* 693, 133620.
<https://doi.org/10.1016/J.SCITOTENV.2019.133620>
- Romita, R., Rizzi, V., Semeraro, P., Gubitosa, J., Gabaldón, J.A., Gorbe, M.I.F., López, V.M.G., Cosma, P., Fini, P., 2019. Operational parameters affecting the atrazine removal from water by using cyclodextrin based polymers as efficient adsorbents for cleaner technologies. *Environ Technol Innov* 16, 100454. <https://doi.org/10.1016/J.ETI.2019.100454>
- Roque, J., Santos, P., Margaça, F.M.A., Caeiro, M.F., Cabo Verde, S., 2022. Inactivation mechanisms of human adenovirus by e-beam irradiation in water environments. *Appl Microbiol Biotechnol* 106, 3799–3809. <https://doi.org/10.1007/S00253-022-11958-3>
- Roshani, B., Karpel Vel Leitner, N., 2011. Effect of persulfate on the oxidation of benzotriazole and humic acid by e-beam irradiation. *J Hazard Mater* 190, 403–408.
<https://doi.org/10.1016/J.JHAZMAT.2011.03.059>
- S., L.P., Saravanakumar, K., Mamba, G., Muthuraj, V., 2019. 1D/2D MnWO₄ nanorods anchored on g-C₃N₄ nanosheets for enhanced photocatalytic degradation ofloxacin under visible light irradiation. *Colloids Surf A Physicochem Eng Asp* 581, 123845.
<https://doi.org/10.1016/J.COLSURFA.2019.123845>
- Saim, S., Behira, B., 2021. Impact of Chloroquine as treatment of pandemic COVID-19 on environment, *Journal of Materials and Environmental Science*.
- Saini, B., Bansal, G., 2013. Characterization of four new photodegradation products of hydroxychloroquine through LC-PDA, ESI-MSⁿ and LC-MS-TOF studies. *J Pharm Biomed Anal* 84, 224–231. <https://doi.org/10.1016/J.JPBA.2013.06.014>

- Sampa, M.H.O., Takács, E., Gehringer, P., Rela, P.R., Ramirez, T., Amro, H., Trojanowicz, M., Botelho, M.L., Han, B., Solpan, D., Cooper, W.J., Emmi, S.S., Wojnárovits, L., 2007. Remediation of polluted waters and wastewater by radiation processing. *Nukleonika* 52, 137–144.
- Sanches-Neto, F.O., Coutinho, N.D., Aquilanti, V., Silva, W.A., Carvalho-Silva, V.H., 2023. Mechanism and Kinetics of the Degradation of Nitazoxanide and Hydroxychloroquine Drugs by Hydroxyl Radicals: Theoretical Approach to Ecotoxicity. *J Braz Chem Soc* 34. <https://doi.org/10.21577/0103-5053.20230025>
- Sanderson, H., Johnson, D.J., Wilson, C.J., Brain, R.A., Solomon, K.R., 2003. Probabilistic hazard assessment of environmentally occurring pharmaceuticals toxicity to fish, daphnids and algae by ECOSAR screening. *Toxicol Lett* 144, 383–395. [https://doi.org/10.1016/S0378-4274\(03\)00257-1](https://doi.org/10.1016/S0378-4274(03)00257-1)
- Santos-Juanes, L., Sánchez, J.L.G., López, J.L.C., Oller, I., Malato, S., Sánchez Pérez, J.A., 2011. Dissolved oxygen concentration: A key parameter in monitoring the photo-Fenton process. *Appl Catal B* 104, 316–323. <https://doi.org/10.1016/J.APCATB.2011.03.013>
- Sayed, M., 2014. Analysis of Pesticides in Water Samples and Removal of Monocrotophos by γ -Irradiation. *J Anal Bioanal Tech* 05, 1–10. <https://doi.org/10.4172/2155-9872.1000181>
- Schroeder, R.L., Pendleton, P., Gerber, J.P., 2015. Physical factors affecting chloroquine binding to melanin. *Colloids Surf B Biointerfaces* 134, 8–16. <https://doi.org/10.1016/J.COLSURFB.2015.06.040>
- Selambakkannu, S., Othman, N.A.F., Bakar, K.A., Thailan, K.M., Karim, Z., 2020. Degradation of surfactants from domestic laundry effluent by electron beam irradiation. *Mater Today Proc* 46, 1807–1812. <https://doi.org/10.1016/j.matpr.2020.10.061>
- Seo, H.O., Sim, C.W., Kim, K.D., Kim, Y.D., Park, J.H., Lee, B.C., Lee, K.H., Lim, D.C., 2012. Influence of High-energy electron-beam on photocatalytic activity of TiO₂ films on carbon-fiber deposited by atomic layer deposition. *Radiation Physics and Chemistry* 81, 290–294. <https://doi.org/10.1016/J.RADPHYSICHEM.2011.11.026>
- Serrano, E., Munoz, M., de Pedro, Z.M., Casas, J.A., 2020. Fast oxidation of the neonicotinoid pesticides listed in the EU Decision 2018/840 from aqueous solutions. *Sep Purif Technol* 235, 116168. <https://doi.org/10.1016/J.SEPPUR.2019.116168>
- Shen, Y., Chu, L., Zhuan, R., Xiang, X., Sun, H., Wang, J., 2019. Degradation of antibiotics and antibiotic resistance genes in fermentation residues by ionizing radiation: A new insight into a sustainable management of antibiotic fermentative residuals. *J Environ Manage* 232, 171–178. <https://doi.org/10.1016/J.JENVMAN.2018.11.050>
- Shin, E. su, Jeong, Y., Barghi, M., Seo, S.H., Kwon, S.Y., Chang, Y.S., 2020. Internal distribution and fate of persistent organic contaminants (PCDD/Fs, DL-PCBs, HBCDs, TBBPA, and PFASs) in a *Bos Taurus*. *Environmental Pollution* 267, 115306. <https://doi.org/10.1016/j.envpol.2020.115306>
- Singhal, P., Gaur, A., Behl, V., Gautam, A., Varshney, B., Paliwal, J., Batra, V., 2007. Sensitive and rapid liquid chromatography/tandem mass spectrometric assay for the quantification of chloroquine in dog plasma. *J Chromatogr B Analyt Technol Biomed Life Sci* 852. <https://doi.org/10.1016/j.jchromb.2007.01.032>

- Siwek, M., Edgecock, T., 2020. Application of electron beam water radiolysis for sewage sludge treatment—a review. *Environmental Science and Pollution Research* 27, 42424–42448. <https://doi.org/10.1007/s11356-020-10643-0>
- Snyder, S.A., Westerhoff, P., Yoon, Y., Sedlak, D.L., 2003. Pharmaceuticals, personal care products, and endocrine disruptors in water: Implications for the water industry. *Environ Eng Sci* 20, 449–469. <https://doi.org/10.1089/109287503768335931>
- Sonawane, S., Rayaroth, M.P., Landge, V.K., Fedorov, K., Boczkaj, G., 2022. Thermally activated persulfate-based Advanced Oxidation Processes — recent progress and challenges in mineralization of persistent organic chemicals: a review. *Curr Opin Chem Eng* 37, 100839. <https://doi.org/10.1016/J.COACHE.2022.100839>
- Sun, W., Chen, J., Chen, L., Wang, J., Zhang, Y., 2016. Coupled electron beam radiation and MBR treatment of textile wastewater containing polyvinyl alcohol. *Chemosphere* 155. <https://doi.org/10.1016/j.chemosphere.2016.04.030>
- Sun, X., Huang, L., Wang, G., Feng, H., Zhou, S., Zhao, R., Wang, D., Li, Z., 2022. Efficient degradation of tetracycline under the conditions of high-salt and coexisting substances by magnetic CuFe₂O₄/g-C₃N₄ photo-Fenton process. *Chemosphere* 308. <https://doi.org/10.1016/j.chemosphere.2022.136204>
- Sutherland, D.L., Ralph, P.J., 2019. Microalgal bioremediation of emerging contaminants - Opportunities and challenges. *Water Res* 164, 114921. <https://doi.org/10.1016/J.WATRES.2019.114921>
- Suzuki, N., Miyata, T., Sakumoto, A., Hashimoto, S., Kawakami, W., 1978. The degradation of an azo dye in aqueous solutions by high-intensity electron-beam irradiation. *Int J Appl Radiat Isot* 29, 103–108. [https://doi.org/10.1016/0020-708X\(78\)90031-5](https://doi.org/10.1016/0020-708X(78)90031-5)
- Sweeney, M.F., Hasan, N., Soto, A.M., Sonnenschein, C., 2015. Environmental Endocrine Disruptors: Effects on the human male reproductive system. *Rev Endocr Metab Disord*. <https://doi.org/10.1007/s11154-016-9337-4>
- Tang, Y., Zhong, Y., Li, H., Huang, Y., Guo, X., Yang, F., Wu, Y., 2020. Contaminants of emerging concern in aquatic environment: Occurrence, monitoring, fate, and risk assessment. *Water Environment Research* 92, 1811–1817. <https://doi.org/10.1002/wer.1438>
- Tasho, R.P., Cho, J.Y., 2016. Veterinary antibiotics in animal waste, its distribution in soil and uptake by plants: A review. *Science of the Total Environment* 563–564, 366–376. <https://doi.org/10.1016/j.scitotenv.2016.04.140>
- Tegze, A., Sági, G., Kovács, K., Homlok, R., Tóth, T., Mohácsi-Farkas, C., Wojnárovits, L., Takács, E., 2018. Degradation of fluoroquinolone antibiotics during ionizing radiation treatment and assessment of antibacterial activity, toxicity and biodegradability of the products. *Radiation Physics and Chemistry* 147, 101–105. <https://doi.org/10.1016/J.RADPHYSICHEM.2018.02.015>
- Tominaga, F.K., dos Santos Batista, A.P., Silva Costa Teixeira, A.C., Borrely, S.I., 2018a. Degradation of diclofenac by electron beam irradiation: Toxicity removal, by-products identification and effect of another pharmaceutical compound. *J Environ Chem Eng* 6, 4605–4611. <https://doi.org/10.1016/j.jece.2018.06.065>

- Tominaga, F.K., Dos Santos Batista, A.P., Silva Costa Teixeira, A.C., Borrelly, S.I., 2018b. Degradation of diclofenac by electron beam irradiation: Toxicity removal, by-products identification and effect of another pharmaceutical compound. *J Environ Chem Eng* 6, 4605–4611. <https://doi.org/10.1016/j.jece.2018.06.065>
- Tominaga, F.K., Silva, T.T., Boiani, N.F., de Jesus, J.M.S., Teixeira, A.C.S.C., Borrelly, S.I., 2021. Is ionizing radiation effective in removing pharmaceuticals from wastewater? *Environmental Science and Pollution Research* 28. <https://doi.org/10.1007/s11356-020-11718-8>
- Tønnesen, H.H., Grislingaas, A.L., Woo, S.O., Karlsen, J., 1988. Photochemical stability of antimalarial. I. Hydroxychloroquine. *Int J Pharm* 43. [https://doi.org/10.1016/0378-5173\(88\)90276-1](https://doi.org/10.1016/0378-5173(88)90276-1)
- Tønnesen, H.H., Kristensen, S., Nord, K., 2007. Photoreactivity of selected antimalarial compounds in solution and in the solid state. <https://doi.org/10.1039/9781847550712-00087>
- Trojanowicz, M., 2020. Removal of persistent organic pollutants (POPs) from waters and wastewaters by the use of ionizing radiation. *Science of the Total Environment* 718, 134425. <https://doi.org/10.1016/j.scitotenv.2019.134425>
- Trojanowicz, M., Bartosiewicz, I., Bojanowska-Czajka, A., Szreder, T., Bobrowski, K., Nałęcz-Jawecki, G., Męczyńska-Wielgosz, S., Nichipor, H., 2020. Application of ionizing radiation in decomposition of perfluorooctane sulfonate (PFOS) in aqueous solutions. *Chemical Engineering Journal* 379, 122303. <https://doi.org/10.1016/j.cej.2019.122303>
- Trojanowicz, M., Bobrowski, K., Szreder, T., Bojanowska-Czajka, A., 2018a. Gamma-ray, X-ray and Electron Beam Based Processes. *Advanced Oxidation Processes for Wastewater Treatment: Emerging Green Chemical Technology* 257–331. <https://doi.org/10.1016/B978-0-12-810499-6.00009-7>
- Trojanowicz, M., Bojanowska-Czajka, A., Bartosiewicz, I., Kulisa, K., 2018b. Advanced Oxidation/Reduction Processes treatment for aqueous perfluorooctanoate (PFOA) and perfluorooctanesulfonate (PFOS) – A review of recent advances. *Chemical Engineering Journal* 336, 170–199. <https://doi.org/10.1016/j.cej.2017.10.153>
- Trojanowicz, M., Bojanowska-Czajka, A., Capodaglio, A.G., 2017. Can radiation chemistry supply a highly efficient AO(R)P process for organics removal from drinking and waste water? A review. *Environmental Science and Pollution Research* 24, 20187–20208. <https://doi.org/10.1007/s11356-017-9836-1>
- US EPA, 2012. Methodology Document for the ECOlogical Structure-Activity Relationship Model (ECOSAR) Class Program [WWW Document]. <http://www.epa.gov/sites/production/files/2015-09/documents/ecosartechfinal.pdf> (accessed March, 2015).
- Vandenberg, L.N., Colborn, T., Hayes, T.B., Heindel, J.J., Jacobs, D.R., Lee, D.-H., Shioda, T., Soto, A.M., vom Saal, F.S., Welshons, W. v, Zoeller, R.T., Myers, J.P., 2012. Hormones and Endocrine-Disrupting Chemicals: Low-Dose Effects and Nonmonotonic Dose Responses. <https://doi.org/10.1210/er.2011-1050>
- Vargas-Berrones, K., Bernal-Jácome, L., Díaz de León-Martínez, L., Flores-Ramírez, R., 2020. Emerging pollutants (EPs) in Latin América: A critical review of under-studied EPs, case of study - Nonylphenol-. *Science of The Total Environment* 726, 138493. <https://doi.org/10.1016/J.SCITOTENV.2020.138493>

- Vione, D., Falletti, G., Maurino, V., Minero, C., Pelizzetti, E., Malandrino, M., Ajassa, R., Olariu, R.I., Arsene, C., 2006. Sources and sinks of hydroxyl radicals upon irradiation of natural water samples. *Environ Sci Technol* 40. <https://doi.org/10.1021/es052206b>
- Vo, H.N.P., Koottatep, T., Chapagain, S.K., Panuvatvanich, A., Polprasert, C., Nguyen, T.M.H., Chaiwong, C., Nguyen, N.L., 2019. Removal and monitoring acetaminophen-contaminated hospital wastewater by vertical flow constructed wetland and peroxidase enzymes. *J Environ Manage* 250. <https://doi.org/10.1016/j.jenvman.2019.109526>
- von Sonntag, C., Schuchmann, H.P., 2001. The chemistry behind the application of ionizing radiation in water-pollution abatement. *Studies in Physical and Theoretical Chemistry* 87, 657–670. [https://doi.org/10.1016/S0167-6881\(01\)80025-2](https://doi.org/10.1016/S0167-6881(01)80025-2)
- Wachter, N., Aquino, J.M., Denadai, M., Barreiro, J.C., Silva, A.J., Cass, Q.B., Bocchi, N., Rocha-Filho, R.C., 2019. Electrochemical degradation of the antibiotic ciprofloxacin in a flow reactor using distinct BDD anodes: Reaction kinetics, identification and toxicity of the degradation products. *Chemosphere* 234, 461–470. <https://doi.org/10.1016/J.CHEMOSPHERE.2019.06.053>
- Wang, F., Archirel, P., Muroya, Y., Yamashita, S., Pernot, P., Yin, C., El Omar, A.K., Schmidhammer, U., Teuler, J.M., Mostafavi, M., 2017. Effect of the solvation state of electron in dissociative electron attachment reaction in aqueous solutions. *Physical Chemistry Chemical Physics* 19, 23068–23077. <https://doi.org/10.1039/C7CP03997B>
- Wang, J., Chu, L., 2016. Irradiation treatment of pharmaceutical and personal care products (PPCPs) in water and wastewater: An overview. *Radiation Physics and Chemistry* 125, 56–64. <https://doi.org/10.1016/J.RADPHYSICHEM.2016.03.012>
- Wang, J., Wang, S., Chen, C., Hu, J., He, S., Zhou, Y., Zhu, H., Wang, X., Hu, D., Lin, J., 2022. Treatment of hospital wastewater by electron beam technology: Removal of COD, pathogenic bacteria and viruses. *Chemosphere* 308, 136265. <https://doi.org/10.1016/J.CHEMOSPHERE.2022.136265>
- Wang, L., Batchelor, B., Pillai, S.D., Botlaguduru, V.S.V., 2016. Electron beam treatment for potable water reuse: Removal of bromate and perfluorooctanoic acid. *Chemical Engineering Journal* 302, 58–68. <https://doi.org/10.1016/J.CEJ.2016.05.034>
- Wang, N., Zheng, T., Zhang, G., Wang, P., 2016. A review on Fenton-like processes for organic wastewater treatment. *J Environ Chem Eng* 4, 762–787. <https://doi.org/10.1016/J.JECE.2015.12.016>
- Wang, R., Jones, K.C., Zhang, H., 2020. Monitoring Organic Pollutants in Waters Using the Diffusive Gradients in the Thin Films Technique: Investigations on the Effects of Biofouling and Degradation. *Environ Sci Technol* 54, 7961–7969. <https://doi.org/10.1021/acs.est.0c00224>
- Wang, S., Wang, J., 2022. Electron Beam Technology Coupled to Fenton Oxidation for Advanced Treatment of Dyeing Wastewater: From Laboratory to Full Application. *ACS Environmental Science and Technology Water*. <https://doi.org/10.1021/acsestwater.2c00040>
- Wang, S., Wang, J., 2018. Radiation-induced degradation of sulfamethoxazole in the presence of various inorganic anions. *Chemical Engineering Journal* 351, 688–696. <https://doi.org/10.1016/J.CEJ.2018.06.137>

- Wang, S., Wang, J., Chen, C., He, S., Hu, J., Zhang, Y., 2022. First full-scale application of electron beam technology for treating dyeing wastewater (30,000 m³/d) in China. *Radiation Physics and Chemistry* 196, 110136. <https://doi.org/10.1016/J.RADPHYSICHEM.2022.110136>
- Wang, X., Mao, Y., Tang, S., Yang, H., Xie, Y.F., 2015. Disinfection byproducts in drinking water and regulatory compliance: A critical review. *Front Environ Sci Eng* 9, 3–15. <https://doi.org/10.1007/s11783-014-0734-1>
- Wang, Z., Zhang, B., Fang, C., Liu, Z., Fang, J., Zhu, L., 2019. Macroporous membranes doped with micro-mesoporous β -cyclodextrin polymers for ultrafast removal of organic micropollutants from water. *Carbohydr Polym* 222, 114970. <https://doi.org/10.1016/J.CARBPOL.2019.114970>
- Warhurst, D.C., Steele, J.C.P., Adagu, I.S., Craig, J.C., Cullander, C., 2003. Hydroxychloroquine is much less active than chloroquine against chloroquine-resistant *Plasmodium falciparum*, in agreement with its physicochemical properties. *Journal of Antimicrobial Chemotherapy* 52, 188–193. <https://doi.org/10.1093/JAC/DKG319>
- Wei, X., Zhang, Q., Cao, S., Xu, X., Chen, Y., Liu, L., Yang, R., Chen, J., Lv, B., 2021. Removal of pharmaceuticals and personal care products (PPCPs) and environmental estrogens (EEs) from water using positively charged hollow fiber nanofiltration membrane. *Environmental Science and Pollution Research* 28, 8486–8497. <https://doi.org/10.1007/s11356-020-11103-5>
- Wojnárovits, L., Pálfi, T., Takács, E., Emmi, S.S., 2005. Reactivity differences of hydroxyl radicals and hydrated electrons in destructing azo dyes. *Radiation Physics and Chemistry* 74, 239–246. <https://doi.org/10.1016/j.radphyschem.2005.04.019>
- Wojnárovits, L., Takács, E., 2017. Wastewater treatment with ionizing radiation. *J Radioanal Nucl Chem* 311, 973–981. <https://doi.org/10.1007/s10967-016-4869-3>
- Wojnárovits, L., Takács, E., 2016. Radiation Induced Degradation of Organic Pollutants in Waters and Wastewaters. *Top Curr Chem* 374. <https://doi.org/10.1007/s41061-016-0050-2>
- Wojnárovits, L., Tóth, T., Takács, E., 2018. Critical evaluation of rate coefficients for hydroxyl radical reactions with antibiotics: A review. *Crit Rev Environ Sci Technol* 48, 575–613. <https://doi.org/10.1080/10643389.2018.1463066>
- Worldwildlifefund, 2023. Water Scarcity-Threats [WWW Document]. <https://www.worldwildlife.org/threats/water-scarcity>.
- Wu, M., Shi, W., Wang, Y., Jiao, Z., Wang, J., Ding, G., Fu, J., 2009. Degradation of halogenated benzenes in solution by electron beam irradiation method. *Environ Technol* 30. <https://doi.org/10.1080/09593330802468954>
- Wu, Y., Bu, L., Duan, X., Zhu, S., Kong, M., Zhu, N., Zhou, S., 2020. Mini review on the roles of nitrate/nitrite in advanced oxidation processes: Radicals transformation and products formation. *J Clean Prod* 273, 123065. <https://doi.org/10.1016/J.JCLEPRO.2020.123065>
- Xiang, W., Xu, F., Wan, D., Wang, X., Luo, F., Chen, Y., 2023. Mechanistic investigation of direct photodegradation of chloroquine phosphate under simulated sunlight. *Chemosphere* 335, 139093. <https://doi.org/10.1016/J.CHEMOSPHERE.2023.139093>
- Xie, P., Chen, C., Zhang, C., Su, G., Ren, N., Ho, S.H., 2020. Revealing the role of adsorption in ciprofloxacin and sulfadiazine elimination routes in microalgae. *Water Res* 172, 115475. <https://doi.org/10.1016/J.WATRES.2020.115475>

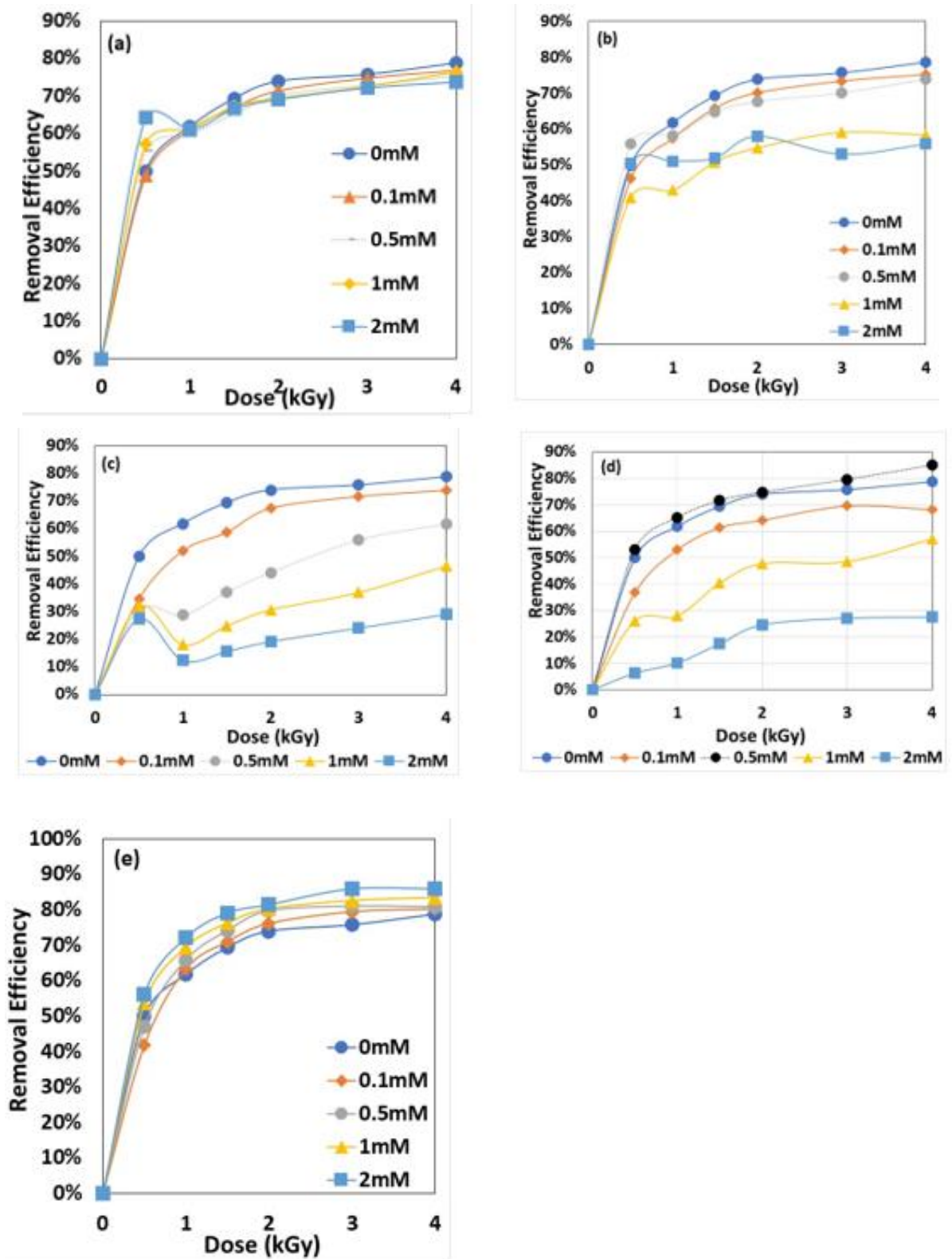
- Xu, D., Pan, F., Ruan, H., Sun, N., 2022. A study of impurities in the repurposed COVID-19 drug hydroxychloroquine sulfate using ultra-high-performance liquid chromatography-quadrupole/time-of-flight mass spectrometry and liquid chromatography-solid-phase extraction-nuclear magnetic resonance. *Rapid Communications in Mass Spectrometry* 36. <https://doi.org/10.1002/rcm.9358>
- Xu, J., Cooper, W.J., Song, W., 2014. Free radical destruction of haloacetamides in aqueous solution. *Water Sci Technol Water Supply* 14, 212–219. <https://doi.org/10.2166/ws.2013.184>
- Yamamoto, Y.I., Suzuki, T., 2020. Ultrafast Dynamics of Water Radiolysis: Hydrated Electron Formation, Solvation, Recombination, and Scavenging. *Journal of Physical Chemistry Letters* 11. <https://doi.org/10.1021/acs.jpcllett.0c01468>
- Yan, D., Sun, Z., Wang, J., Wang, L., Pan, R., Wu, Q., Liu, X., 2019. Enhanced coagulation with Mn(III) pre-oxidation for treatment of micro-polluted raw water. *Water (Switzerland)* 11. <https://doi.org/10.3390/w11112302>
- Yang, R., Wang, M., Shen, Z., Wang, W., Ma, H., Gu, J., 2007. The degradation and mineralization of 4-chlorophenol in aqueous solutions by electron beam irradiation in the presence of TiO₂ nanoparticles. *Radiation Physics and Chemistry* 76, 1122–1125. <https://doi.org/10.1016/J.RADPHYSICHEM.2006.10.008>
- Yao, Y., Volchek, K., Brown, C.E., Robinson, A., Obal, T., 2014. Comparative study on adsorption of perfluorooctane sulfonate (PFOS) and perfluorooctanoate (PFOA) by different adsorbents in water. *Water Science and Technology* 70. <https://doi.org/10.2166/wst.2014.445>
- Yi, X.H., Ji, H., Wang, C.C., Li, Y., Li, Y.H., Zhao, C., Wang, A., Fu, H., Wang, P., Zhao, X., Liu, W., 2021. Photocatalysis-activated SR-AOP over PDINH/MIL-88A(Fe) composites for boosted chloroquine phosphate degradation: Performance, mechanism, pathway and DFT calculations. *Appl Catal B* 293, 120229. <https://doi.org/10.1016/J.APCATB.2021.120229>
- Yoon, Y.J., Jung, Y.J., Han, B.S., Kang, J.W., 2009. Performance of electron beam irradiation for treatment of groundwater contaminated with acetone. *Water Science and Technology* 59, 2475–2483. <https://doi.org/10.2166/wst.2009.234>
- Yoshinaga, T., Ohta, K., 1990. Spectrophotometric Determination of Chloride Ion Using Mercury Thiocyanate and Iron Alum. *analytical sciences* 6. <https://doi.org/10.2116/analsci.6.57>
- Youssef, S.A., Bashour, I.I., 2017. Uptake of Antibiotics by Plants 221–237. https://doi.org/10.1007/978-3-319-66260-2_12
- Yu, S., Choi, D., Lee, M., 2008. Kinetic and modeling of radiolytic decomposition of antibiotics. *WIT Transactions on Ecology and the Environment* 109. <https://doi.org/10.2495/WM080051>
- Yu, Y., Chen, L., fang, Y., Jia, X., Chen, J., 2019. High temperatures can effectively degrade residual tetracyclines in chicken manure through composting. *J Hazard Mater* 380, 120862. <https://doi.org/10.1016/J.JHAZMAT.2019.120862>
- Yuri Kim, Ponomarev, A. v., Ershov, B.G., 2020. Electron-Beam Water Cleaning from 2,4,6-Trinitrotoluene and Hexahydro-1,3,5-Trinitro-1,3,5-Triazine. *High Energy Chemistry* 54, 358–362. <https://doi.org/10.1134/S0018143920050094>
- Zaouak, A., Jebali, S., Chouchane, H., Jelassi, H., 2022. Impact of gamma-irradiation on the degradation and mineralization of hydroxychloroquine aqueous solutions. *International Journal*

of Environmental Science and Technology 1–10. <https://doi.org/10.1007/S13762-022-04360-Z/TABLES/2>

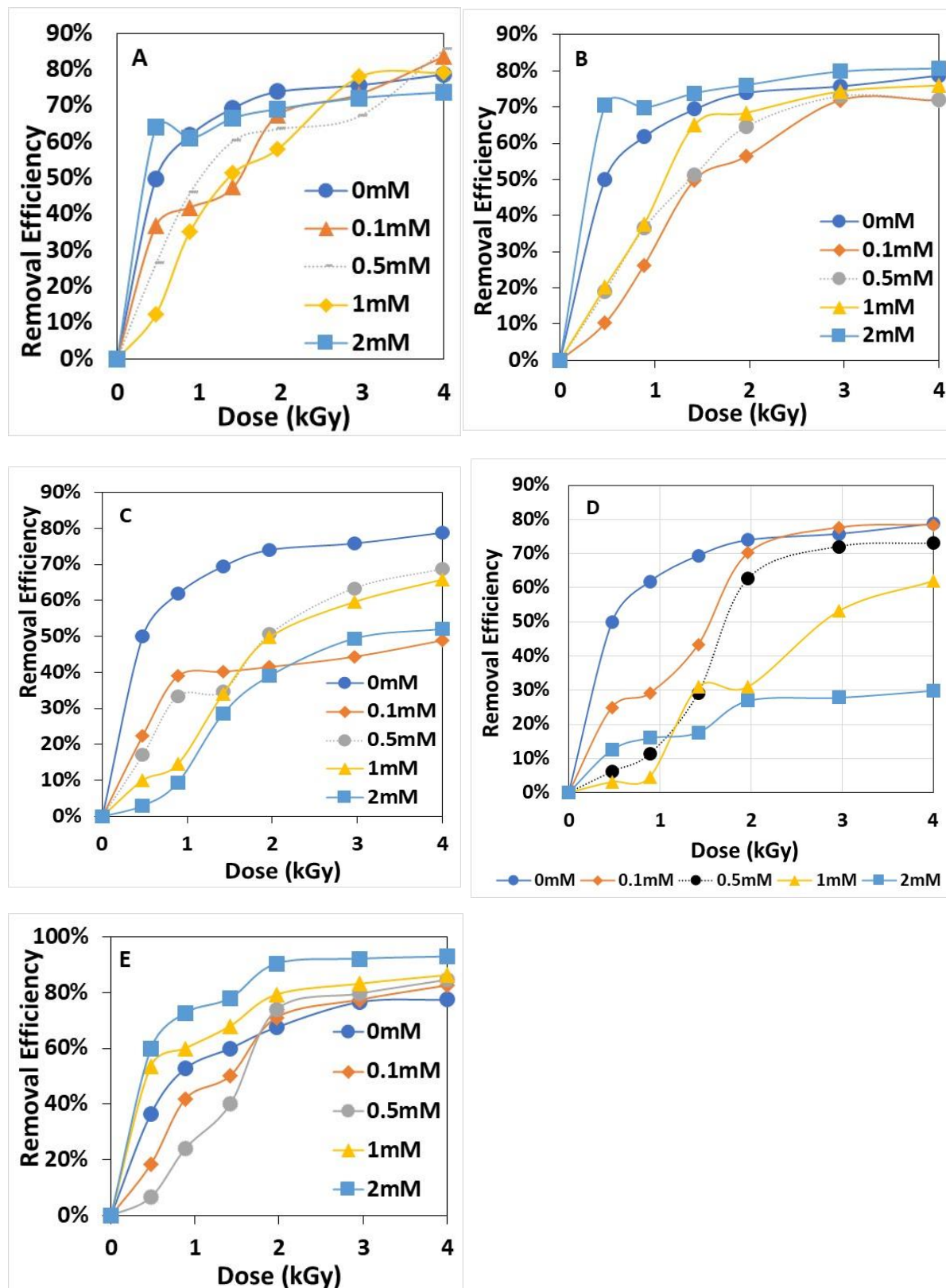
- Zaouak, A., Noomen, A., Jelassi, H., 2021. Degradation mechanism of losartan in aqueous solutions under the effect of gamma radiation. *Radiation Physics and Chemistry* 184. <https://doi.org/10.1016/j.radphyschem.2021.109435>
- Zaouak, A., Noomen, A., Jelassi, H., 2018. Gamma-radiation induced decolorization and degradation on aqueous solutions of Indigo Carmine dye. *J Radioanal Nucl Chem* 317. <https://doi.org/10.1007/s10967-018-5835-z>
- Zbigniew Zimek, 2018. PRE-FEASIBILITY STUDY OF SETTING UP AN ELECTRON BEAM R&D FACILITY. Warsaw.
- Zhang, H., Hu, X., Li, T., Zhang, Y., Xu, H., Sun, Y., Gu, X., Gu, C., Luo, J., Gao, B., 2022. MIL series of metal organic frameworks (MOFs) as novel adsorbents for heavy metals in water: A review. *J Hazard Mater* 429, 128271. <https://doi.org/10.1016/J.JHAZMAT.2022.128271>
- Zhao, N.N., Ding, L., Bei, H.F., Zheng, S.Y., Han, B., 2018. The role of dissolved oxygen in Fenton system, in: *IOP Conference Series: Earth and Environmental Science*. <https://doi.org/10.1088/1755-1315/191/1/012084>
- Zhen, G., Pan, Y., Lu, X., Li, Y.Y., Zhang, Z., Niu, C., Kumar, G., Kobayashi, T., Zhao, Y., Xu, K., 2019. Anaerobic membrane bioreactor towards biowaste biorefinery and chemical energy harvest: Recent progress, membrane fouling and future perspectives. *Renewable and Sustainable Energy Reviews* 115, 109392. <https://doi.org/10.1016/J.RSER.2019.109392>
- Zheng, B.G., Zheng, Z., Zhang, J.B., Luo, X.Z., Wang, J.Q., Liu, Q., Wang, L.H., 2011. Degradation of the emerging contaminant ibuprofen in aqueous solution by gamma irradiation. *Desalination* 276, 379–385. <https://doi.org/10.1016/J.DESAL.2011.03.078>
- Zheng, H., Bao, J., Huang, Y., Xiang, L., Faheem, Ren, B., Du, J., Nadagouda, M.N., Dionysiou, D.D., 2019. Efficient degradation of atrazine with porous sulfurized Fe₂O₃ as catalyst for peroxydisulfate activation. *Appl Catal B* 259, 118056. <https://doi.org/10.1016/J.APCATB.2019.118056>
- Zheng, M., Bao, Y., Huang, Z., Qiu, W., Xu, G., Wang, Z., 2020. Radiolysis of carbamazepine by electron beam: Roles of transient reactive species and biotoxicity of final reaction solutions on rotifer *Philodina* sp. *Science of The Total Environment* 703, 135013. <https://doi.org/10.1016/J.SCITOTENV.2019.135013>
- Zhou, Y., Cao, S., Xi, C., Li, X., Zhang, L., Wang, G., Chen, Z., 2019. A novel Fe₃O₄/graphene oxide/citrus peel-derived bio-char based nanocomposite with enhanced adsorption affinity and sensitivity of ciprofloxacin and sparfloxacin. *Bioresour Technol* 292, 121951. <https://doi.org/10.1016/J.BIORTECH.2019.121951>
- Zhuan, R., Wang, J., 2020. Degradation of diclofenac in aqueous solution by ionizing radiation in the presence of humic acid. *Sep Purif Technol* 234, 116079. <https://doi.org/10.1016/j.seppur.2019.116079>
- Zhuan, R., Wang, J., 2019. Degradation of sulfamethoxazole by ionizing radiation: Kinetics and implications of additives. *Science of The Total Environment* 668, 67–73. <https://doi.org/10.1016/J.SCITOTENV.2019.03.027>

APPENDICES

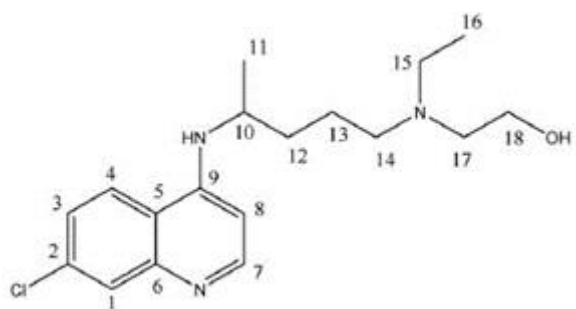
Appendix 1 The effect of (a) HCO_3^- , (b) CO_3^{2-} , (c) NO_3^- , (d) humic acid, and (e) SO_4^{2-} on CQ removal efficiency under electron beam irradiation



Appendix 2 The effect of (a) HCO_3^- , (b) CO_3^{2-} , (c) NO_3^- , (d) humic acid, and (e) SO_4^{2-} on HCQ removal efficiency under electron beam irradiation



Appendix 3 Proposed •OH radical addition and hydrogen atom transfer reactions



Carbon Number	•OH addition to the aromatic ring kcal mol ⁻¹	Hydrogen atom transfer to •OH kcal mol ⁻¹
C10		$\Delta G^\circ = -18.37$ $E_0 = 2.80$
C1	$\Delta G = -19.01$ $E_0 = -4.21$	$\Delta G^\circ = 2.93$ $E_0 = -18.86$
C4	$\Delta G = -17.93$ $E_0 = 9.19$	$\Delta G^\circ = -1.05$ $E_0 = 4.94$
C2	$\Delta G = -15.96$ $E_0 = 1.13$	
C9	$\Delta G^\circ = -11.21$ $E_0 = 13.97$	

Appendix 4 Reactions for the simulated degradation of CQ and HCQ using CHEMSIMUL

Number	Chemical reactions	K = M ⁻¹ s ⁻¹
RE1	H ⁺ +OH ⁻ =H ₂ O	A=1.4E11
RE2	H ₂ O=H ⁺ +OH ⁻	A=1.4E01
RE3	H ₂ O ₂ =H ⁺ +HO ₂ ⁻	A=1.17E01
RE4	H ⁺ +HO ₂ ⁻ =H ₂ O ₂	A=5.0E10
RE5	H ₂ O ₂ +OH ⁻ =HO ₂ ⁻ +H ₂ O	A=1.3E10
RE6	HO ₂ ⁻ +H ₂ O=H ₂ O ₂ +OH ⁻	A=1.17E01
RE7	e ⁻ +H ₂ O=H+OH ⁻	A=1.90E-01
RE8	H+OH ⁻ =E ⁻ +H ₂ O	A=2.2E07
RE9	H=E ⁻ +H ⁺	A=9.77
RE10	e ⁻ +H ⁺ =H	A=2.30E10
RE11	OH+OH ⁻ =O ⁻ +H ₂ O	A=1.30E10
RE12	O ⁻ +H ₂ O=OH+OH ⁻	A=1.19E01
RE13	OH=O ⁻ +H ⁺	A=11.9
RE14	O ⁻ +H ⁺ =OH	A=1.00E11
RE15	HO ₂ =O ₂ ⁻ +H ⁺	A=4.57
RE16	O ₂ ⁻ +H ⁺ =HO ₂	A=5.00E10
RE17	HO ₂ +OH ⁻ =O ₂ ⁻ +H ₂ O	A=5.00E10
RE18	O ₂ ⁻ +H ₂ O=HO ₂ +OH ⁻	A=4.57
RE19	e ⁻ +OH=OH ⁻	A=3.00E10
RE20	e ⁻ +H ₂ O ₂ =OH+OH ⁻	A=1.10E10
RE21	e ⁻ +HO ₂ =HO ₂ ⁻	A=2.00E10
RE22	e ⁻ +O ₂ =O ₂ ⁻	A=1.90E10
RE23	e ⁻ +HO ₂ ⁻ =O ⁻ +OH ⁻	A=3.50E09
RE24	H+H ₂ O=H ₂ +OH	A=1.10E01
RE25	H+O ⁻ =OH ⁻	A=1.00E10
RE26	H+HO ₂ ⁻ =OH+OH ⁻	A=9.00E07
RE27	H+H=H ₂	A=7.80E09
RE28	H+OH=H ₂ O	A=7.00E09
RE29	H+H ₂ O ₂ =OH+H ₂ O	A=9.00E07
RE30	H+O ₂ =HO ₂	A=2.10E10
RE31	H+HO ₂ =H ₂ O ₂	A=1.80E10
RE32	H+O ₂ ⁻ =HO ₂ ⁻	A=1.80E10
RE33	2*OH=H ₂ O ₂	A=3.6E10
RE34	OH+HO ₂ =H ₂ O+O ₂	A=6.00E09
RE35	OH+O ₂ ⁻ =OH ⁻ +O ₂	A=8.20E09
RE36	OH+H ₂ =H+H ₂ O	A=4.30E07
RE37	OH+H ₂ O ₂ =HO ₂ +H ₂ O	A=2.70E07
RE38	OH+O ⁻ =HO ₂ ⁻	A=2.50E10
RE39	OH+HO ₂ ⁻ =HO ₂ +OH ⁻	A=7.50E09
RE40	HO ₂ +O ₂ ⁻ =HO ₂ ⁻ +O ₂	A=8.00E07
RE41	2*HO ₂ =H ₂ O ₂ +O ₂	A=7.00E05
RE42	HO ₂ +O ⁻ =O ₂ +OH ⁻	A=6.00E09
RE43	HO ₂ +H ₂ O ₂ =OH+O ₂ +H ₂ O	A=5.00E-01

Number	Chemical reactions	$K = M^{-1}s^{-1}$
RE44	$HO_2+HO_2^-=OH+O_2+OH^-$	A=5.00E-01
RE45	$O_2^-+H_2O_2=OH+O_2+OH^-$	A=1.30E-01
RE46	$O_2^-+HO_2^-=O^-+O_2+OH^-$	A=1.30E-01
RE47	$O^-+H_2=H+OH^-$	A=8.00E07
RE48	$O^-+H_2O_2=O_2^-+H_2O$	A=5.00E08
RE49	$O^-+HO_2^-=O_2^-+OH^-$	A=4.00E08
RE50	$H_2O_2=H_2O+O$	A=1.00E-03
RE51	$O+O=O_2$	A=1.00E09
RE52	$OH+Cl^-=ClOH^-$	A=4.300E+09
RE53	$OH+HClO=ClO+H_2O$	A=9.000E+09
RE54	$e^-+Cl=Cl^-$	A=1.000E+10
RE55	$e^-+Cl_2^-=Cl^-+Cl^-$	A=1.000E+10
RE56	$e^-+ClOH^-=Cl^-+OH^-$	A=1.000E+10
RE57	$e^-+HClO=ClOH^-$	A=5.300E+10
RE58	$e^-+Cl_2=Cl_2^-$	A=1.000E+10
RE59	$H+Cl=Cl^-+H^+$	A=1.000E+10
RE60	$H+Cl_2^-=Cl^-+HCl$	A=8.000E+09
RE61	$H+ClOH^-=Cl^-+H_2O$	A=1.000E+10
RE62	$H+Cl_2=Cl_2^-+H^+$	A=7.000E+09
RE63	$H+HClO=ClOH^-+H^+$	A=1.000E+10
RE64	$H+Cl_3^-=Cl_2^-+HCl$	A=1.000E+10
RE65	$HO_2+Cl_2^-=Cl^-+HCl+O_2$	A=4.000E+09
RE66	$HCl=Cl^-+H^+$	A=5.000E+05
RE67	$HO_2+Cl_2=Cl_2^-+H^++O_2$	A=1.000E+09
RE68	$HO_2+Cl_3^-=Cl_2^-+HCl+O_2$	A=1.000E+09
RE69	$O_2^-+Cl_2^-=Cl^-+Cl^-+O_2$	A=1.200E+10
RE70	$O_2^-+HClO=ClOH^-+O_2$	A=7.500E+06
RE71	$H_2O_2+Cl_2^-=HCl+HCl+O_2^-$	A=1.400E+05
RE72	$H_2O_2+Cl_2=HO_2+Cl_2^-+H^+$	A=1.900E+02
RE73	$H_2O_2+HClO=HCl+H_2O+O_2$	A=1.700E+05
RE74	$OH^-+Cl_2^-=ClOH^-+Cl^-$	A=7.300E+06
RE75	$OH^-+Cl_2=HClO+Cl^-$	A=1.000E+10
RE76	$H^++ClOH^-=Cl+H_2O$	A=2.100E+10
RE77	$H_2O+Cl_2O_2=HClO+ClO_2^-+H^+$	A=2.000E+02
RE78	$H_2O+Cl_2O_2=O_2+HClO+HCl$	A=0.000E+00
RE79	$H_2O+Cl_2O=HClO+HClO$	A=1.000E+02
RE80	$H_2O+Cl_2O_4=ClO_2^-+ClO_3^-+H^++H^+$	A=1.000E+02
RE81	$H_2O+Cl_2O_4=HClO+HCl+O_4$	A=1.000E+02
RE82	$O_4=O_2+O_2$	A=1.000E+05
RE83	$Cl^-+Cl=Cl_2^-$	A=2.100E+10
RE84	$Cl^-+ClOH^-=Cl_2^-+OH^-$	A=9.000E+04
RE85	$Cl^-+HClO=Cl_2+OH^-$	A=6.000E-02
RE86	$Cl^-+Cl_2=Cl_3^-$	A=1.000E+04
RE87	$ClOH^-=OH+Cl^-$	A=6.100E+09
RE88	$Cl_2^-=Cl+Cl^-$	A=1.100E+05

Number	Chemical reactions	K = M ⁻¹ s ⁻¹
RE89	Cl ₂ ⁻ +Cl ₂ ⁻ =Cl ₃ ⁻ +Cl ⁻	A=7.000E+09
RE90	Cl ₃ ⁻ =Cl ₂ +Cl ⁻	A=5.000E+04
RE91	ClO+ClO=Cl ₂ O ₂	A=1.500E+10
RE92	ClO ₂ +ClO ₂ =Cl ₂ O ₄	A=1.000E+02
RE93	Cl ₂ O ₂ +ClO ₂ ⁻ =ClO ₃ ⁻ +Cl ₂ O	A=1.000E+02
RE94	HClO+HClO=Cl ⁻ +ClO ₂ ⁻ +H ⁺ +H ⁺	A=6.000E-09
RE95	ClO ₂ ⁻ +HClO=Cl ⁻ +ClO ₃ ⁻ +H ⁺	A=9.000E-07
RE96	HClO+HClO=O ₂ +HCl+HCl	A=3.000E-10
RE97	Fe ²⁺ +OH=Fe ³⁺ +OH ⁻	A=4.300E+08
RE98	Fe ²⁺ +Cl=Fe ³⁺ +Cl ⁻	A=1.300E+10
RE99	Fe ²⁺ +Cl ₂ ⁻ =Fe ³⁺ +Cl ⁻ +Cl ⁻	A=3.100E+07
RE100	Fe ²⁺ +ClO ₂ =ClO ₂ ⁻ +Fe ³⁺	A=3.000E+03
RE101	Fe ³⁺ +HO ₂ =Fe ²⁺ +H ⁺ +O ₂	A=3.100E+05
RE102	Fe ³⁺ +E ⁻ =Fe ²⁺	A=6.000E+10
RE103	Fe ³⁺ +H=Fe ²⁺ +H ⁺	A=1.200E+09
RE104	Fe ²⁺ +H ₂ O ₂ =Fe ³⁺ +OH+OH ⁻	A=7.000E+01
RE105	OH+HClO ₂ =ClO ₂ +H ₂ O	A=6.3E09
RE106	e ⁻ +HClO ₂ =ClO+OH ⁻	A=4.5E10
RE107	e ⁻ +HClO ₃ =ClO ₂ +OH ⁻	A=4.0E6
RE108	H ₂ O+Cl ₂ O ₂ =HClO+HClO ₂	A=2.0E02
RE109	H ₂ O+Cl ₂ O ₄ =HClO ₂ +HClO ₃	A=1.0E2
RE110	Cl ₂ O ₂ +HClO ₂ =HClO ₃ +Cl ₂ O	A=1.0E2
RE111	H ⁺ +CO ₃ ²⁻ =HCO ₃ ⁻	A=5.00E10
RE112	CO ₂ +H ₂ O=H ⁺ +HCO ₃ ⁻	A=7.00E01
RE113	H ⁺ +HCO ₃ ⁻ =CO ₂ +H ₂ O	A=1.00E10
RE114	HCO ₃ ⁻ =CO ₃ ²⁻ +H ⁺	A=2.00E00
RE115	CO ₂ +e ⁻ =CO ₂ ⁻	A=7.70E09
RE116	HCO ₃ ⁻ +OH=CO ₃ ⁻ +H ₂ O	A=8.50E06
RE117	CO ₃ ²⁻ +OH=CO ₃ ⁻ +OH ⁻	A=3.90E08
RE118	HCO ₃ ⁻ +H=H ₂ +CO ₃ ⁻	A=4.4E04
RE119	CO ₃ ²⁻ +e ⁻ =CO ₂ ⁻ +2OH ⁻ +H ₂ O	A=3.90E05
RE120	2CO ₃ ⁻ =C ₂ O ₆ ²⁻	A=1.40E07
RE121	2CO ₃ ⁻ =CO ₂ +CO ₄ ²⁻	A=7.00E06
RE122	CO ₃ ⁻ +H ₂ O ₂ =CO ₃ ²⁻ +O ₂ ⁻ +2H ⁺	A=9.80E05
RE123	CO ₃ ⁻ +HO ₂ ⁻ =CO ₃ ²⁻ +O ₂ ⁻ +H ⁺	A=1.00E07
RE124	CO ₃ ⁻ +O ₂ ⁻ =CO ₃ ²⁻ +O ₂	A=4.00E08
RE125	CO ₃ ⁻ +CO ₂ ⁻ =CO ₃ ²⁻ +CO ₂	A=3.00E08
RE126	CO ₂ ⁻ +e ⁻ =HCO ₂ ⁻ +OH ⁻ +H ₂ O	A=1.00E09
RE127	CO ₂ ⁻ +CO ₂ ⁻ =C ₂ O ₄ ²⁻	A=6.50E08
RE128	CO ₂ ⁻ +O ₂ =CO ₂ +O ₂ ⁻	A=2.00E09
RE129	CO ₂ ⁻ +H ₂ O ₂ =CO ₂ +OH ⁻ +OH	A=7.30E05
RE130	CO ₂ ⁻ +HCO ₃ ⁻ =HCO ₂ ⁻ +CO ₃ ⁻	A=1.00E03
RE131	C ₂ O ₆ ²⁻ =C ₂ O ₄ ²⁻ +O ₂	A=1.00E00
RE132	C ₂ O ₆ ²⁻ =HO ₂ ⁻ +OH ⁻ +2CO ₂ +H ₂ O	A=2.00E02
RE133	CO ₃ ⁻ +C ₂ O ₄ ²⁻ =C ₂ O ₄ ⁻ +CO ₃ ²⁻	A=3.00E03

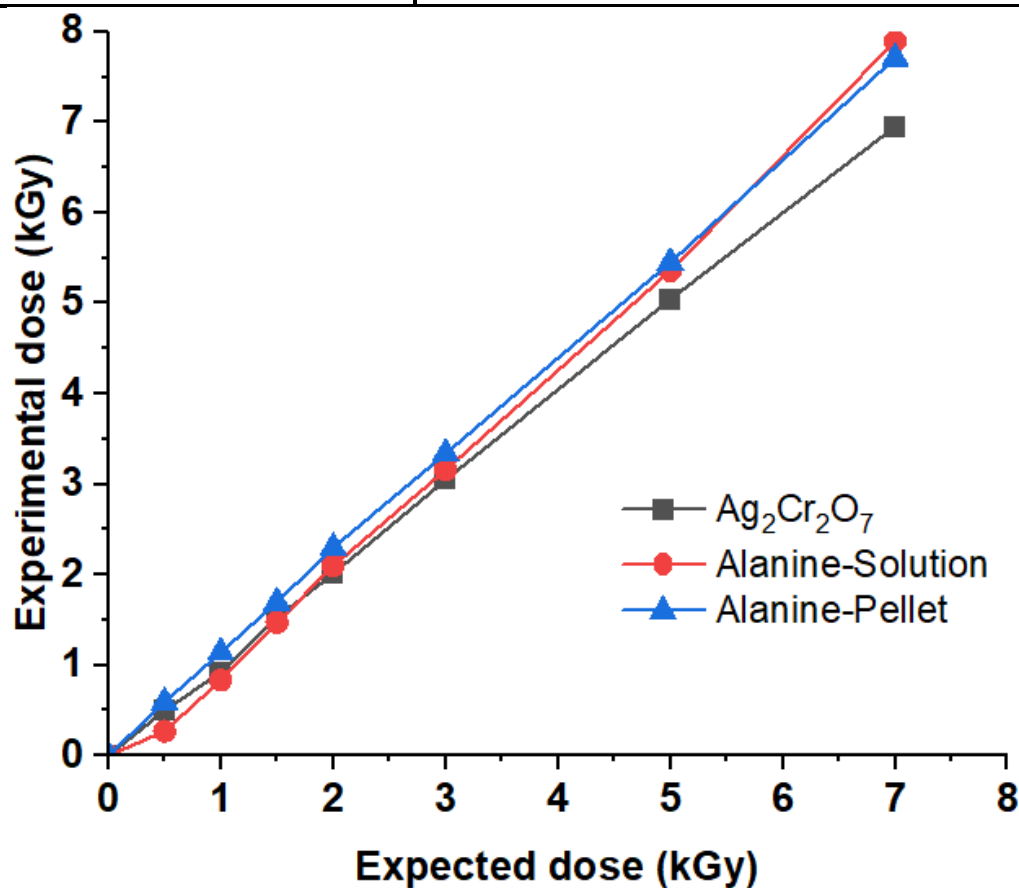
Number	Chemical reactions	K = M ⁻¹ s ⁻¹
RE134	$C_2O_4^{2-} + e^- = C_2O_4^{3-}$	A=3.10E07
RE135	$C_2O_4^{2-} + OH^- = C_2O_4^- + OH^-$	A=7.70E06
RE136	$C_2O_4^- + C_2O_4^- = C_2O_4^{2-} + 2CO_2$	A=4.80E08
RE137	$C_2O_4^- + O_2 = O_2^- + 2CO_2$	A=5.00E09
RE138	$C_2O_4^- = CO_2 + CO_2^-$	A=0
RE139	$CO_3^- + HCO_2^- = HCO_3^- + CO_2^-$	A=1.5E05
RE140	$HCO_2^- + OH^- = H_2O + CO_2^-$	A=3.2E09
RE141	$HCO_2^- + H = H_2 + CO_2^-$	A=2.10E08
RE142	$OH^- + HCO_3^- = CO_3^{2-} + H_2O$	A=1.00E09
RE143	$CO_3^{2-} + H_2O = OH^- + HCO_3^-$	A=3.60E03
RE144	$CO_3^- + CO_3^- = CO_4^{2-} + CO_2$	A=7.00E06
RE145	$H_2O + CO_4^{2-} = HO_2^- + CO_2 + OH^-$	A=2.00E-01

Appendix 5 Statistical Analysis of Removal Efficiency

Dose (kGy)	CQ		HCQ		CQ	HCQ	EB	EB-F
	EB	EB-F	EB	EB-F	EB - EBF	EB - EBF	CQ - HCQ	CQ - HCQ
0	0.00	0.00	0.00	0.00	0.00	0.00	0.00	0.00
0.50	40.17	70.13	34.18	74.94	29.96	5.99	4.81	40.75
0.92	58.88	82.32	51.29	81.57	23.44	7.59	-0.75	30.28
1.52	67.03	85.04	58.19	84.07	18.01	8.84	-0.97	25.88
2.01	71.60	86.52	66.21	85.44	14.92	5.39	-1.08	19.23
3.05	74.96	87.34	72.99	94.26	12.38	1.97	6.92	21.27
5.04	78.59	89.73	75.90	94.81	11.13	2.69	5.08	18.91
6.95	82.01	91.00	79.73	94.89	8.99	2.28	3.89	15.16
			sum		118.84	34.75	17.90	171.48
			\bar{d}		14.85	4.34	2.24	21.44
			SD		9.16	3.07	3.26	11.84
			v		83.83	9.43	10.66	140.18
			α		0.05	0.05	0.05	0.05
			df		7.00	7.00	7.00	7.00
			cv		1.895	1.895	1.895	1.895
			t		4.589	4.001	1.938	5.121
					significant difference	significant difference	significant difference	significant difference

Appendix 6 Statistical analysis of dosimetry using silver dichromate, alanine pellets, and alanine solution

Dose (kGy)	Ag ₂ Cr ₂ O ₇ (kGy)	A-Sol (kGy)	A-Pell (kGy)						
d1	d2	d3	d4	d1-d2	d1-d3	d1-d4	d2-d3	d2-d4	d3-d4
0	0.000	0.000	0.000	0.000	0.000	0.000	0.000	0.000	0.000
0.5	0.500	0.269	0.590	0.000	0.231	-0.090	0.231	-0.090	-0.321
1	0.922	0.833	1.140	0.078	0.167	-0.140	0.089	-0.218	-0.307
1.5	1.524	1.471	1.695	-0.024	0.029	-0.195	0.053	-0.171	-0.224
2	2.013	2.099	2.300	-0.013	-0.099	-0.300	-0.086	-0.287	-0.201
3	3.048	3.157	3.340	-0.048	-0.157	-0.340	-0.110	-0.292	-0.183
5	5.044	5.359	5.450	-0.044	-0.359	-0.450	-0.315	-0.406	-0.091
7	6.953	7.895	7.710	0.047	-0.895	-0.710	-0.942	-0.757	0.185
			sum	-0.005	-1.084	-2.225	-1.079	-2.220	-1.141
			\bar{d}	-0.001	-0.135	-0.278	-0.135	-0.278	-0.143
			SD	0.043	0.358	0.226	0.363	0.231	0.169
			v	0.002	1.156	4.383	1.151	4.367	1.168
			α	0.050	0.050	0.050	0.050	0.050	0.050
			df	7.000	7.000	7.000	7.000	7.000	7.000
			cv	1.895	1.895	1.895	1.895	1.895	1.895
			t	-0.034	-0.926	-3.008	-0.910	-2.942	-2.064



Appendix 7 Statistical analysis of removal efficiency with regard to the initial concentration of CQ

	25 mg/L	50 mg/L	75 mg/L	100 mg/L	125 mg/L										
Dose (kGy)	d1	d2	d3	d4	d5	d1-d2	d1-d3	d1-d4	d1-d5	d2-d3	d2-d4	d2-d5	d3-d4	d3-d5	d4-d5
0.00	0.00	0.00	0.00	0.00	0.00	0.00	0.00	0.00	0.00	0.00	0.00	0.00	0.00	0.00	0.00
0.50	77.82	63.10	59.91	51.59	47.97	14.73	17.91	26.23	29.85	3.18	11.50	15.13	8.32	11.95	3.62
0.92	84.68	75.99	71.57	65.75	59.55	8.69	13.11	18.93	25.13	4.43	10.24	16.45	5.82	12.02	6.20
2.01	94.35	84.72	77.26	75.40	73.63	9.63	17.09	18.95	20.73	7.46	9.32	11.09	1.86	3.63	1.77
4.01	95.97	91.67	88.40	83.37	78.39	4.30	7.57	12.59	17.58	3.27	8.29	13.28	5.03	10.01	4.99
6.95	99.19	94.44	92.67	87.32	84.47	4.75	6.53	11.88	14.73	1.78	7.13	9.98	5.35	8.20	2.85
					sum	42.10	62.21	88.58	108.02	20.11	46.49	65.92	26.38	45.81	19.43
					\bar{d}	7.02	10.37	14.76	18.00	3.35	7.75	10.99	4.40	7.64	3.24
					SD	5.12	6.92	8.91	10.33	2.52	4.09	5.90	2.98	4.86	2.23
					v	26.17	47.94	79.48	106.73	6.36	16.70	34.79	8.90	23.62	24.78
					α	0.05	0.05	0.05	0.05	0.05	0.05	0.05	0.05	0.05	0.05
					df	5.00	5.00	5.00	5.00	5.00	5.00	5.00	5.00	5.00	5.00
					cv	2.01	2.01	2.01	2.01	2.01	2.01	2.01	2.01	2.01	2.01
					t	3.36	3.67	4.06	4.27	3.26	4.64	4.56	3.61	3.85	3.56

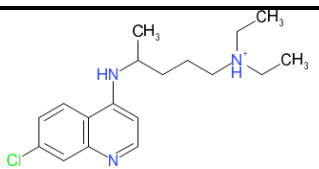
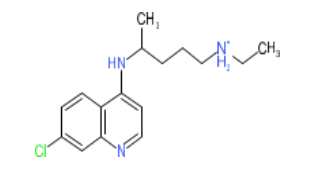
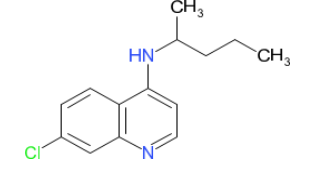
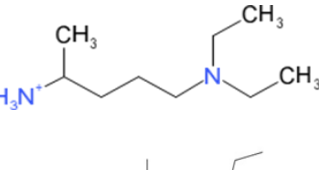
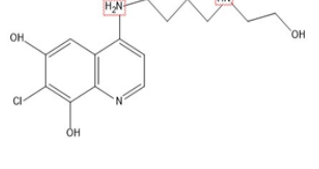
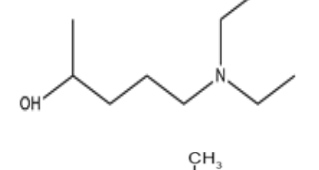
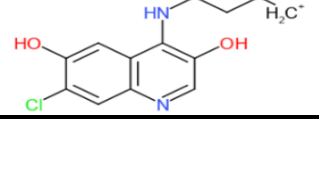
Appendix 8 Statistical analysis of removal efficiency with regard to the initial concentration of HCQ

	25 mg/L	50 mg/L	75 mg/L	100 mg/L	125 mg/L										
Dose (kGy)	d1	d2	d3	d4	d5	d1-d2	d1-d3	d1-d4	d1-d5	d2-d3	d2-d4	d2-d5	d3-d4	d3-d5	d4-d5
0.00	0.00	0.00	0.00	0.00	0.00	0.00	0.00	0.00	0.00	0.00	0.00	0.00	0.00	0.00	0.00
0.50	68.02	50.10	39.28	45.60	43.82	17.92	28.74	22.42	24.20	10.82	4.50	6.28	-6.32	-4.54	1.78
0.92	78.95	70.42	61.57	56.73	57.49	8.52	17.38	22.21	21.45	8.85	13.69	12.93	4.84	4.08	-0.76
2.01	90.28	77.87	77.86	76.01	72.51	12.42	12.42	14.27	17.77	0.01	1.85	5.36	1.84	5.35	3.51
4.01	93.93	85.31	80.67	78.10	74.43	8.62	13.26	15.83	19.49	4.65	7.21	10.88	2.57	6.23	3.67
6.95	92.71	89.94	86.27	83.00	79.21	2.77	6.45	9.71	13.51	3.67	6.94	10.73	3.27	7.06	3.79
					sum	50.24	78.25	84.44	96.42	28.00	34.20	46.18	6.20	18.18	11.98
					\bar{d}	8.37	13.04	14.07	16.07	4.67	5.70	7.70	1.03	3.03	2.00
					SD	6.46	9.79	8.44	8.65	4.47	4.82	4.76	3.94	4.46	2.00
					v	41.79	95.83	71.22	74.90	19.97	23.27	22.69	15.51	19.89	-19.92
					α	0.05	0.05	0.05	0.05	0.05	0.05	0.05	0.05	0.05	0.05
					df	5.00	5.00	5.00	5.00	5.00	5.00	5.00	5.00	5.00	5.00
					cv	2.02	2.02	2.02	2.02	2.02	2.02	2.02	2.02	2.02	2.02
					t	3.17	3.26	4.08	4.55	2.56	2.89	3.96	0.64	1.66	2.45

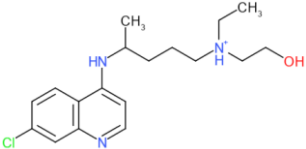
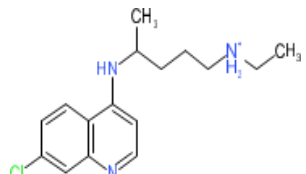
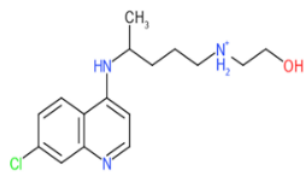
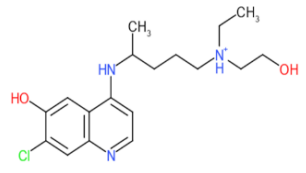
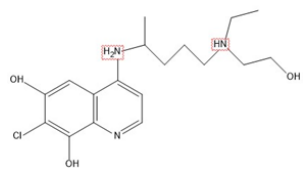
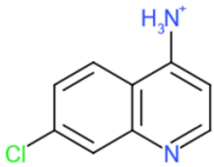
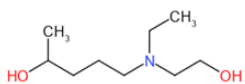
Appendix 9 Statistical analysis of removal efficiency with regard to COD, TOC, chloride, and nitrogen

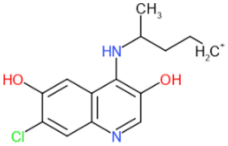
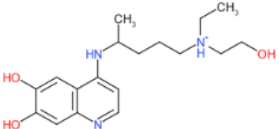
Dose (kGy)	COD		TOC		NH₄⁺		Cl	
	CQ (d)	HCQ (d)	CQ (d)	HCQ (d)	CQ (d)	HCQ (d)	CQ (d)	HCQ (d)
0.00	0.00	0.00	0.00	0.00	0.00	0.00	0.00	0.00
0.50	9.67	33.67	0.50	5.75	2.33	1.80	0.10	1.50
0.92	17.33	37.00	6.50	6.67	2.48	2.24	1.10	1.50
2.01	16.67	29.33	5.50	6.38	2.64	2.19	1.60	1.70
4.01	17.00	31.00	11.00	9.30	2.33	2.17	-	-
6.95	17.33	33.33	9.50	9.25	1.95	1.74	-	-
sum	78.00	164.33	33.00	37.34	11.72	10.14	2.80	4.70
\bar{d}	13.00	27.39	5.50	6.22	1.95	1.69	0.70	1.18
SD	7.03	13.67	4.53	3.40	0.98	0.85	0.78	0.79
v	49.42	186.82	20.50	11.56	0.97	0.73	0.56	0.93
α	0.05	0.05	0.05	0.05	0.05	0.05	0.05	0.05
df	5.00	5.00	5.00	5.00	5.00	5.00	4.00	4.00
cv	2.02	2.02	2.02	2.02	2.02	2.02	2.13	2.13
t	4.53	4.91	2.98	4.48	4.86	4.85	2.20	3.65

Appendix 10 Toxicity analysis of CQ and degradations products

m/z	chemical structure	Organism	Acute toxicity			Chronic toxicity		
			Fish	Daphnia	Green Algae	Fish	Daphnia	Green Algae
			Duration	End Pt				
			96-hr	48-hr	96-hr	ChV	ChV	ChV
m/z	chemical structure	Class	mg/L	mg/L	mg/L	mg/L	mg/L	mg/L
320		Aliphatic Amines	1.41	0.224	0.104	0.034	0.024	0.043
292		Aliphatic Amines	3.71	0.545	0.298	0.114	0.055	0.115
247		Aliphatic Amines	1.73	1.21	2.18	0.217	0.214	0.919
158		Aliphatic Amines	70.9	7.92	7.43	5.03	0.61	2.35
370		Aliphatic Amines	63.4	7.62	6.19	3.6	0.631	2.07
159		Aliphatic Amines	70.6	7.9	7.4	5	0.609	2.34
279		Aliphatic Amines	14.2	9.13	11.4	1.61	1.26	3.93

Appendix 11 Toxicity analysis of HCQ and degradation products

			Acute toxicity			Chronic toxicity			
m/z	chemical structure	Organism	Fish	Daphnia	Green Algae	Fish	Daphnia	Green Algae	
			Duration	96-hr	48-hr	96-hr			
			End Pt	LC50	LC50	EC50	ChV	ChV	ChV
m/z	chemical structure	Class	mg/L	mg/L	mg/L	mg/L	mg/L	mg/L	
336		Aliphatic Amines	13.5	1.82	1.18	0.547	0.168	0.429	
292		Aliphatic Amines	3.71	0.545	0.298	0.114	0.055	0.115	
308		Aliphatic Amines	35.9	4.45	3.4	1.86	0.379	1.16	
352		Aliphatic Amines	29.3	3.73	2.71	1.41	0.326	0.942	
370		Aliphatic Amines	63.4	7.62	6.19	3.6	0.631	2.07	
179		Aliphatic Amines	192	108	76.3	18.5	10.2	19.5	
175		Neutral Organics	385	38.1	45.5	39.7	2.61	13.2	

			Acute toxicity			Chronic toxicity			
m/z	chemical structure	Organism	Fish	Daphnia	Green Algae	Fish	Daphnia	Green Algae	
			Duration	96-hr	48-hr	96-hr			
			End Pt	LC50	LC50	EC50	ChV	ChV	ChV
m/z	chemical structure	Class	mg/L	mg/L	mg/L	mg/L	mg/L	mg/L	
279		Aliphatic Amines	14.2	9.13	11.4	1.61	1.26	3.93	
334		Aliphatic Amines	152	17	16	10.9	1.31	5.06	

Appendix 12 Data sheet of properties of CQ and HCQ

	CQ	HCQ
Molecular weight (g/mol)	320	336
Chemical formula	C ₁₈ H ₂₆ ClN ₃	C ₁₈ H ₂₆ ClN ₃ O
IUPAC name	7-chloro-N-[5-(diethylamino)pentan-2-yl]quinolin-4-amine	2-({4-[(7-chloroquinolin-4-yl)amino]pentyl}(ethyl)amino)ethan-1-ol
Solubility	Freely soluble in water as phosphate and sulfate form	2.61.10 ⁻² g L ⁻¹ (in water as sulfate salt)
pKa	4.0, 8.4 and 10.2	<4.0, 8.3 and 9.7
Log P	3.85 (experimental) 4.12 (calculated from Clog P)	4.72 (experimental) 5.06 (calculated from Clog P)
Absorption	89 ± 16% (oral, fasting subjects)	74 ± 13% (oral, fasting subjects)
Bioavailability	52– 102% (mean 78%) as 300 mg oral solution form 67–114% (mean 89%) as 300 mg tablets form	Relative bioavailability was 109.5% (according to AUC _{0–60d}) and 110.7% (according to AUC _{0–∞}) (0.2 g HCQS tablets)
C _{max}	122.10– 733.52 ng mL ⁻¹ (oral 150 mg CQ tablets)	135–422 ng mL ⁻¹ (oral 200 mg HCQS tablets)
t _{max}	14.0–28.0 days (oral 150 mg CQ tablets)	1.5–7.0 h (oral 200 mg HCQS tablets)
Volume of distribution	65,000 L	47,257 L
Protein Binding	33–70% (plasma)	33–70% (plasma)
Terminal elimination half-life	20–60 days	~40 days
Excretion	40– 60% unchanged or metabolized drug through kidneys 8–25% unchanged or changed for in feces 5% sloughed off through skin 25–45% stored long-term in lean body tissues	40–60% unchanged or metabolized drug through kidneys 8–25% unchanged or changed for in feces 5% sloughed off through skin 25–45% stored long-term in lean body tissues
Clearance	0.10 L h ⁻¹ kg ⁻¹ from whole blood and 0.7 to 1 L h ⁻¹ kg ⁻¹ from plasma	15.5 L h ⁻¹ from blood

